

University of Southampton Research Repository ePrints Soton

Copyright © and Moral Rights for this thesis are retained by the author and/or other copyright owners. A copy can be downloaded for personal non-commercial research or study, without prior permission or charge. This thesis cannot be reproduced or quoted extensively from without first obtaining permission in writing from the copyright holder/s. The content must not be changed in any way or sold commercially in any format or medium without the formal permission of the copyright holders.

When referring to this work, full bibliographic details including the author, title, awarding institution and date of the thesis must be given e.g.

AUTHOR (year of submission) "Full thesis title", University of Southampton, name of the University School or Department, PhD Thesis, pagination

UNIVERSITY OF SOUTHAMPTON
FACULTY OF MEDICINE, HEALTH AND LIFE SCIENCES

School of Biological Sciences

The structure of a voltage gated potassium channel

by

Nik Rogers

Thesis for the degree of Doctor of Philosophy

September 2010

University of Southampton

ABSTRACT

FACULTY OF MEDICINE, HEALTH AND LIFE SCIENCES

SCHOOL OF BIOLOGICAL SCIENCES

Doctor of Philosophy

STRUCTURE OF A VOLTAGE GATED POTASSIUM CHANNEL

By Nik Rogers

Voltage gated potassium channels (Kv channels) are tetrameric ion channels, responsible for regulating the potassium component of the membrane potential in a large range of cell types ranging from mammalian excitable cells to bacteria. Attempts have been made to elucidate the structure of voltage gated potassium channels using X-ray crystallography, however due to the inherent flexibility of the voltage sensors, removal of the channels from their native lipid environment causes distortion of the channels, and as a result much controversy remains over their exact structure. KvAP is a voltage gated potassium channel from the thermophilic archaea *Aeropyrum pernix* which contains a single cysteine residue, which can be removed by site directed mutagenesis to give a template for cysteine scanning mutagenesis. Fluorescence spectroscopy utilising cysteine reactive probes can be used to probe the membrane topology of proteins in the context of a lipid bilayer. Single cysteine mutants within the pore domain outer helix (S5 helix) of KvAP were generated and labelled with thiol reactive fluorescent probes. These probes were used to report on the polarity of the surrounding environment using a combination of the environmental sensitivity of the probes and fluorescence quenching from both aqueous and lipid phases. Fluorescence results fit well to a hypothetical model describing a trough like variation in dielectric constant of the membrane, allowing the determination of the position of the hydrophobic interface of the membrane at each end of the helix. A mutant of KvAP with no voltage sensing domains was also generated and subjected to cysteine scanning mutagenesis of the S5 helix. Again results fitted well to a hypothetical profile of the dielectric constant of the membrane, and the shift in fluorescence properties at some positions within the helix in the absence of the voltage sensor shows the residues of the pore domain which are in close contact with the voltage sensor.

Contents

1	Chapter 1: Introduction	4
1.1	Biological membranes.....	4
1.2	Lipids	4
1.2.2	Glycerophospholipids	6
1.2.3	Sphingolipids	6
1.2.4	Glycolipids.....	7
1.2.5	Sterols	7
1.2.6	Archebacterial lipids	10
1.3	Physical properties of lipids.....	10
1.3.1	Lipid polymorphism	10
1.3.2	Lateral pressure profile	12
1.3.3	Gel to liquid crystalline phase transition of a lipid bilayer.....	12
1.4	Membrane proteins	13
1.4.1	Peripheral membrane proteins	16
1.4.2	Integral membrane proteins	16
1.4.3	The transmembrane regions of membrane proteins.....	17
1.5	Protein lipid interactions	18
1.6	Potassium Channels	20
1.6.1	Identification of potassium channels	20
1.6.2	Potassium channel pore domain	20
1.6.3	Conduction of potassium ions	21

1.6.4	Potassium channel gating	33
1.6.5	Voltage gated potassium channels.....	35
1.6.6	Mechanism of voltage gating.....	49
1.7	Aims and objectives	52
2	Chapter 2: Materials and Methods	56
2.1	Materials.....	56
2.2	Methods.....	56
2.2.1	Microbiological techniques	56
2.2.2	Molecular Biology	58
2.2.3	Expression and Purification of KvAP.....	69
2.2.4	Reconstitution of purified KvAP mutants	73
2.2.5	Functional assays of KvAP and its mutants.	76
2.2.6	Fluorescence measurements	77
3	Chapter 3: Mutagenesis of KvAP.....	82
3.1	Introduction.....	82
3.2	Methods.....	83
3.2.1	Generation of single cysteine mutants of KvAP.....	83
3.2.2	Transformation, expression and purification of KvAP.....	90
3.2.3	Growth curve analysis of KvAP mutants	90
3.3	Results.....	91
3.3.1	QuikChange site directed mutagenesis of KvAP.....	91
3.3.2	Two stitch PCR to generate a pore domain only mutant	92

3.4	Discussion	98
3.4.1	Generation of cysteine free and single cysteine mutants of KvAP ...	98
3.4.2	Generation of the pore domain only mutant	98
3.4.3	Generation of single cysteine mutants of the pore domain only mutant	98
4	Chapter 4: Characterisation and reconstitution of wild type and mutant KvAP	99
4.1	Introduction	99
4.1.1	Detergents	99
4.1.2	Solubilisation	100
4.1.3	Reconstitution	100
4.2	Methods.....	102
4.2.1	Reconstitution of KvAP.....	102
4.2.2	Characterisation of reconstituted sample on a sucrose density gradient	103
4.2.3	Solubility of KvAP in detergent solutions.....	103
4.2.4	Functional assays of KvAP and its mutants.	103
4.3	Results.....	104
4.3.1	Characterisation of KvAP.....	104
4.3.2	Reconstitution of KvAP and mutants	111
4.3.3	Activity of KvAP.....	113
4.4	Discussion	120
4.4.1	Expression of KvAP and single cysteine mutants	120

4.4.2	Solubility of KvAP	121
4.4.3	Reconstitution of KvAP.....	123
4.4.4	Function of wild type KvAP and single cysteine mutants.....	125
5	Chapter 5: Determining the structure of KvAP using IANBD fluorescence .	127
5.1	Introduction	127
5.1.1	Fluorescence	127
5.1.2	Using NBD to study the membrane topology of KvAP	134
5.2	Materials and Methods	135
5.2.1	Materials	135
5.2.2	Methods	135
5.3	Results	137
5.3.1	Fluorescence results	137
5.3.2	NBD labelling of single cysteine mutants of full length KvAP	137
5.3.3	NBD labelling of single cysteine mutants of the KvAP pore only mutant	151
5.4	Discussion	166
5.4.1	The ends of the helices	167
5.4.2	Position of the voltage sensor	173
5.4.3	General analysis of quenching data.	190
6	Chapter six: Exploring the topology of KvAP using N-(1-Pyrenyl) maleimide	191
6.1	Introduction	191
6.1.1	Pyrene fluorescence	191

6.1.2	N-(1-Pyrenyl) maleimide	191
6.1.3	Environmental sensitivity of pyrene	192
6.2	Materials and methods	196
6.2.1	Methods	196
6.3	Results	198
6.3.1	Single cysteine mutants of full length KvAP	198
6.3.2	KvAP pore domain only mutant	206
6.4	Discussion	212
6.4.1	The ends of the S5 helix	212
6.4.2	Position of the voltage sensor	212
7	Chapter 7: General discussion	214
7.1	Mechanism of voltage sensor movement	214
7.2	Exposure of the S5 helix to the lipid bilayer	216
	218
7.3	Proximity of the voltage sensor to the S5 helix	220
7.4	Bilayer thickness around the S5 helix	220
7.5	General conclusions and further work	224

Acknowledgements

Firstly I would like to thank my supervisor Professor Tony Lee for all the help and support he has given me over the last four years. Words cannot describe how valuable his unfaltering patience and guidance have been; without him I could not have done it.

I would also like to thank my second supervisor Dr. Malcolm East for all of his help and support throughout my PhD, not least with his guidance on the 'black art' that is molecular biology, and for the numbers of hours we spent trying to get a hairpin out of a primer. I honestly could not have asked for a better pair of supervisors. A special thank you also goes to Neville Wright, who could always be relied on to find you the chemical you needed, fix the machine you have just broken, or just be there for a good chat.

A huge vote of thanks goes to all members of the lab, past and present. Firstly, to those who have now moved onwards and upwards; Andy, Jo and Jeab, all of whom taught me so much in the short time that we worked together, for which I will always be grateful. A huge thank you also goes to Phedra, who took me under her wing when I first started, and never really let go; I have never known such a kind and supportive person. Of course I have to thank all of the more recent members of the lab: John, Helen, Juan, Natalie and honorary lab member Mike, for providing both help in the lab, and being some of the best friends you could ask for!

I also have to say a big thank you to all of those who supported me away from Boldrewood. Thanks has to go to my mum; it is the drive, determination, and stubbornness which I have inherited, that has got me through the last four years. Thank you to my dad, for always being there to talk to about anything that isn't science and offering assistance and words of encouragement. Finally big thank you goes to the Southampton University Swimming Club and 622 Volunter Gliding Squadron ; over the last few years you have provided both support and entertainment; it would not have been the same without any you.

Abbreviations

APS	- Ammonium persulphate
Bp	- Base pair
CMC	- Critical micelle concentration
DDM	- <i>n</i> -dodecyl β , D-maltopyranoside
di(18:1)PC	- Dioleylphosphatidylcholine
di(Br ₂ C18:0)PC	- Brominated dioleylphosphatidylcholine
DM	- <i>n</i> -decyl β , D maltopyranoside
EGTA	- Ethylene glycol tetraacetic acid)
HEPES	- 4-(2-hydroxyethyl)-1-piperazineethanesulfonic acid
IANBD	- <i>N</i> -((2-(iodoacetoxy)ethyl)- <i>N</i> -methyl)amino-7-nitrobenz-2-oxa-1,3-diazole
IPTG	- Isopropyl β -D-1-thiogalactopyranoside
Kb	- Kilobase
kDa	- Kilodalton
KcsA	- Potassium channel from <i>Streptomyces lividans</i>
KvAP	- Voltage gated potassium channel from <i>Aeropyrum Pernix</i>
OG	- <i>n</i> -Octyl β , D-glucopyranoside
PA	- Phosphatidic acid
PAGE	-Polyacrylamide gel electrophoresis

PBS	- Phosphate buffered saline
PC	- Phosphatidylcholine
PCR	- Polymerase chain reaction
PE	- Phosphatidylethanolamine
NBD	- <i>N</i> -((2-(iodoacetoxy)ethyl)- <i>N</i> -methyl)amino-7-nitrobenz-2-oxa-1,3-diazole
NPM	- N-(1-Pyrenyl) maleimide
SDS	- Sodium dodecyl sulphate
TAE	- Tris-acetate ethylenediamine tetraacetic acid
TEMED	- N, N, N', N'-tetramethylethylenediamine
TM	- Transmembrane
TRIS	- Tris(hydroxymethyl)aminomethane
VSD	- Voltage sensing domain

1 Chapter 1: Introduction

1.1 Biological membranes

Biological membranes play a central role in all living organisms, delineating cells and forming an effective barrier between the internal components of the cell and the extracellular environment, as well as forming boundaries between the cytoplasm and intracellular compartments of membrane bound organelles such as the endoplasmic reticulum and Golgi apparatus (De Matteis and Luini 2008).

Membranes are complex structures primarily composed of lipids and proteins, with a smaller contribution to total membrane mass from lipid bound carbohydrates (Lotan and Nicholson 1981); these components are arranged to form an asymmetric biomembrane about 60 Å thick (Singer and Nicolson 1972). A central property of biological membranes is that they are impermeable to charged species, preventing the contents of membrane bound compartments being released into the cells, or the contents of cells being released into the surrounding environment.

Despite the diversity in organisation and compositions of membranes from different organisms, all membranes are fluid structures under physiological conditions with a hydrophobic core and hydrophilic surfaces, allowing rapid lateral diffusion of lipids and membrane proteins, as shown in Figure 1.1 (O'Leary 2010). It is the fluid nature of biological membranes that allows the cell membrane, and the components thereof to adapt to the immediate environment of a cell allowing all living organisms to reside in such a diverse range of environments.

1.2 Lipids

Lipids are amphipathic in nature; it is this property which causes hydrated lipids to form the bilayer structure which is typically associated with biological membranes (Gorter and Grendel 1925). In all living organisms, lipid bilayers consist of a number of different lipid species which can be classified by their different structural characteristics. There are four major classes of lipid found in the biological membranes of most living organisms: glycerophospholipids, sphingolipids, sterols and glycolipids (Fahy et al. 2005).

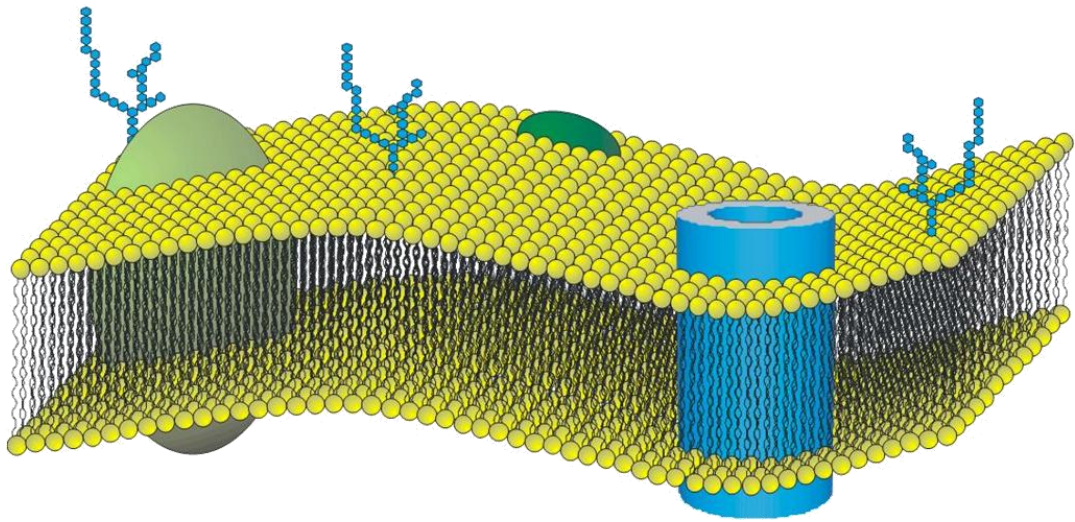


Figure 1.1: Representation of the fluid mosaic model of the lipid bilayer showing integral membrane proteins (light green, blue), peripheral membrane proteins (dark green), and carbohydrate moieties attached to membrane lipids (glycolipids).

1.2.1 Glycerophospholipids

Glycerophospholipids are the most common class of lipids found in eukaryotic and eubacterial biological membranes. Glycerophospholipids consist of four components, two acyl chains, a glycerol moiety, a phosphate group and an alcohol. These components can be grouped into two structural segments separated by a glycerol 'backbone'. The alcohol and phosphate groups together form the hydrophilic head group of the lipid, the phosphate group being attached to the glycerol moiety at the *sn*-3 position. Two fatty acyl chains form the hydrophobic 'tails' of the glycerophospholipids, and are esterified to the *sn*-1 and *sn*-2 positions of the glycerol moiety (Berg et al. 2002). These hydrocarbon tails vary in length and saturation but most acyl chains attached to glycerophospholipids contain an even number of carbon atoms, with 16 and 18 carbon chains occurring at the highest frequency in biological membranes. The majority of glycerophospholipids contain one saturated and one unsaturated hydrocarbon chain; the double bonds in unsaturated fatty acids can exist in either the *cis* or *trans* configuration but in biological membranes the double bonds in unsaturated acyl chains are almost exclusively in the *cis* configuration (Vance and Vance 2002). The simplest glycerophospholipid is phosphatidic acid, which consists of two acyl chains esterified to the glycerol moiety at the *sn*-1 and *sn*-2 positions, and a phosphate group attached at the *sn*-3 position; phosphatidic acid is a key intermediate in the biosynthesis of glycerophospholipids. Other glycerophospholipids contain alcohols such as serine, choline, ethanolamine, glycerol and inositol esterified to the phosphate group of phosphatidic acid; examples of lipids containing these alcohols can be seen in Figure 1.2.

1.2.2 Sphingolipids

Sphingolipids are a complex family of lipids, which rather than containing a glycerol moiety contain sphingosine, which is synthesised from a serine residue and a fatty acyl CoA molecule (Figure 1.3). Sphingosine is then used by the cell to synthesise ceramide, which is akin to phosphatidic acid in that it is the simplest biological sphingolipid, consisting of sphingosine with a single amide linked, unsaturated acyl chain attached to the sphingosine backbone, resulting in a head group of a single hydrogen atom (Merrill 2002; Guan et al. 2009). Ceramide, the

precursor to all sphingolipids, is esterified to a number of headgroups such as sugars or the same phosphoryl alcohols which are found in the glycerophospholipids described above. It has been suggested that sphingolipids interact with sterols to form membrane structures known as lipid rafts; these structures are distinguishable from the bulk glycerophospholipids of the bilayer due to their reduced solubility in detergents at low temperatures.

1.2.3 Glycolipids

Glycolipids are sugar-containing lipids that are generally found in the outer leaflet of the eukaryotic bilayer, although there is some evidence to suggest that they may occasionally occur in some intracellular membranes. Glycolipids can be synthesised from glycerophospholipid and sphingolipid precursors, hence can have either a glycerol or sphingosine backbone. In the case of glycosphingolipids and glycoglycerophospholipids, rather than containing a phosphoryl alcohol esterified to the primary hydroxyl group of the sphingosine or glycerol moiety respective, a sugar is attached by a β -glycosidic bond.

1.2.4 Sterols

Sterols are a group of lipids with an extensive range of biological functions; this class of lipid is closely linked to steroid hormones which are known to have a wide range of homeostatic roles (Accad 1998). The hydrophobic region of sterols consists of four linked carbon rings attached to an aliphatic chain as seen in Figure 1.3, whereas the hydrophilic region consists of a single hydroxyl group attached to the carbon ring distal to the aliphatic chain. Sterols are not able to form bilayers on their own but, in eukaryotic membranes, sterols, and in particular cholesterol, can compose up to 50 mole % of the membrane lipids (Alberts et al. 2007) . Cholesterol reduces the fluidity of lipids in the fluid, liquid crystalline phase, and has also been suggested to be important in the formation of rafts.

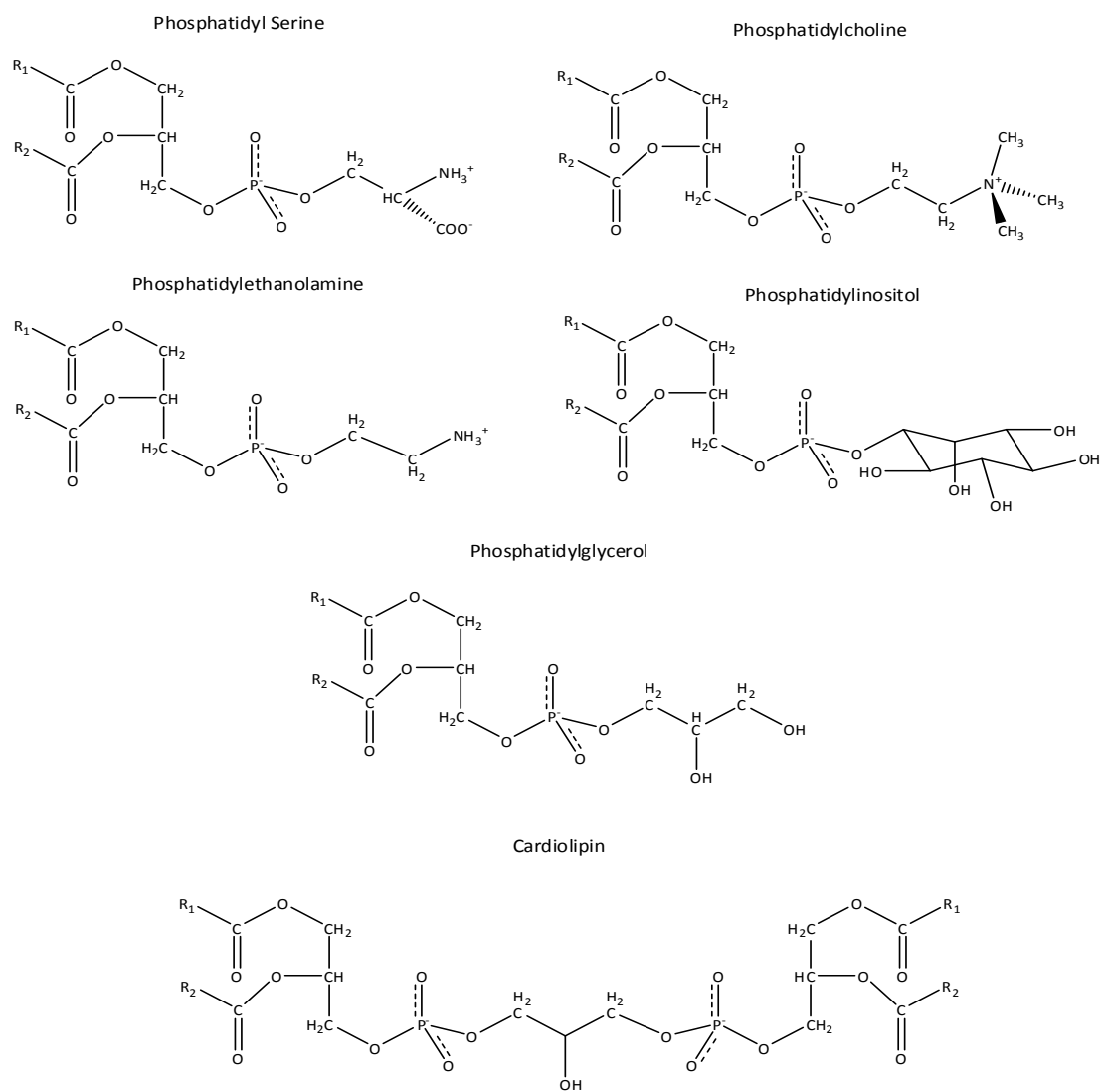


Figure 1.2: Structures of the most common phospholipids in eukaryotes. Fatty acyl chains R1 and R2 (indicated) are attached at the *sn*1 and *sn*2 positions respectively

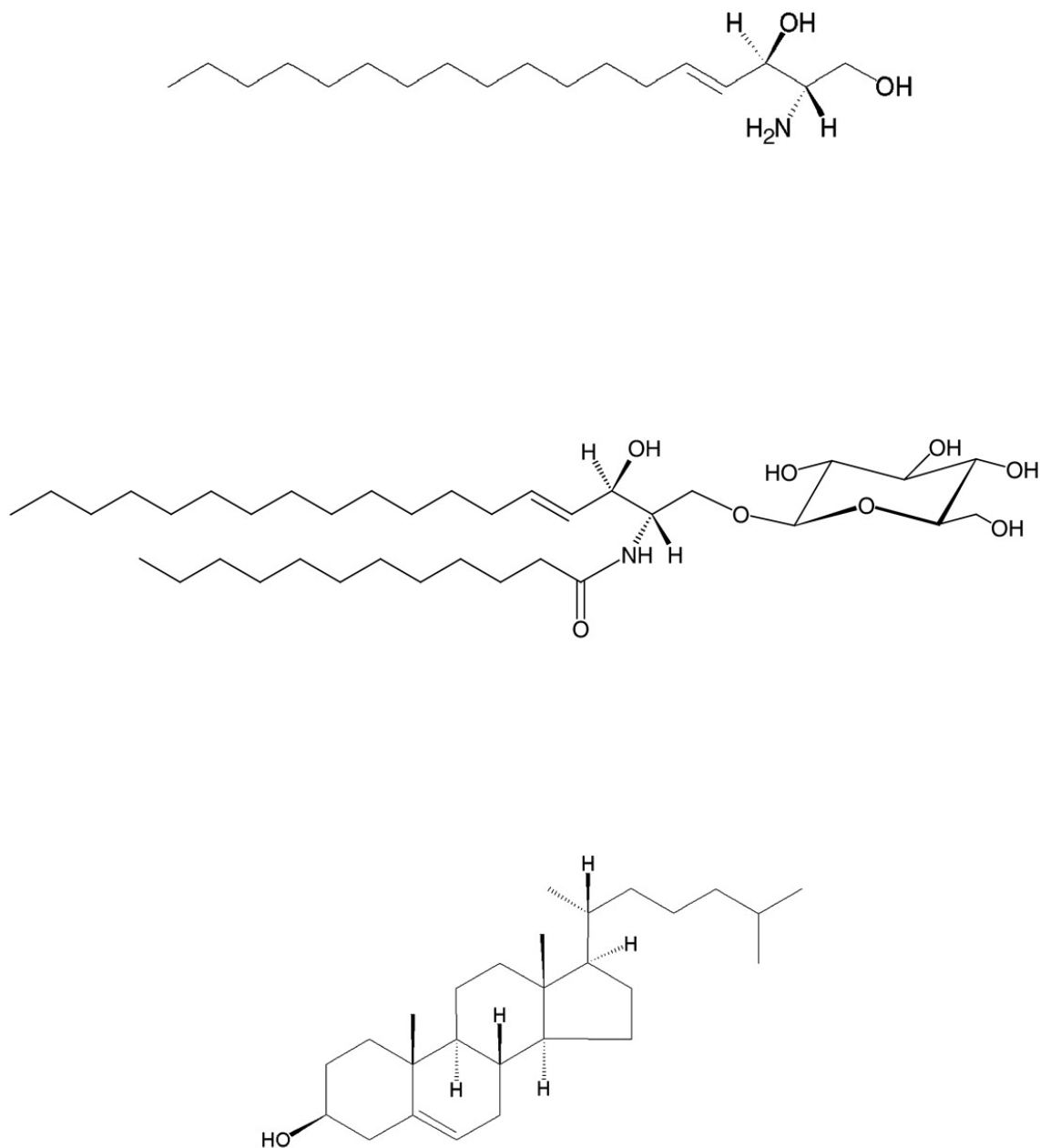


Figure 1.3: Representative structures of three common membrane lipid classes: **(a)** sphingolipids (sphingosine), **(b)** glycosphingolipids (Glc β -cer [d18:1/12:0]) **(c)** Sterols (cholesterol) Adapted from Fahy et al. 2005

1.2.5 Archebacterial lipids

Achaebacteria often inhabit environments in which extremes of temperature, pH and salinity are common, hence it would follow that the cell membranes, amongst other components of such organisms should differ from the majority of organisms which inhabit environments exhibiting less challenging conditions.

Glycerophospholipids in archebacterial membranes differ markedly from those in eubacterial and eukaryotic membranes. Primarily, the phosphoryl alcohol headgroups of archebacterial glycerophospholipids connect to the glycerol backbone of the lipid by an ether bond at the *sn*-1 position as opposed to an ester bond at the *sn*-3 position (De Rosa et al. 1986). The ether bond is considerably more stable than an ester bond, and much less likely to undergo degradation in the extreme environments which many archaea inhabit (Albers et al. 2000). The hydrophobic region of archaeal lipids is based on isoprenoid chains, resulting in multiple branches which can include cycloalkane ring structures, which are believed to prevent cell membranes becoming leaky at high temperatures (Damste et al. 2002; Koga and Morii 2005). A small number of archaea are able to fuse the ends of the isoprenoid tails distal to the head group to those of another ether lipid forming a molecule with two polar head groups and a hydrophobic core; these lipids form a monolayer which is much more rigid than a bilayer, assisting the organisms to survive in high temperatures and at low pH (Hanford and Peebles 2002).

1.3 Physical properties of lipids

1.3.1 Lipid polymorphism

Lipids tend to self associate in aqueous environments due to the high energy cost of exposing the hydrophobic acyl tails to water. These lipids will spontaneously adopt one of a number of distinct structures, the properties of which depend on the structural and chemical compositions of the lipids involved; these structures are known as lipid phases (Merrill 2002; Vance and Vance 2002). This behaviour is driven by the energetic penalty of having hydrophobic acyl chains exposed to a polar environment, and as such these structures act to sequester the hydrophobic

regions of lipids away from the bulk water so that just the polar headgroups of the lipids are in contact with the surrounding aqueous environment (Tanford 1980)

The shape of individual lipid molecules directs the phase which a collection of lipids will form when hydrated; the 'shape' of a lipid describes the sum of the effects of the polar and apolar regions of a lipid, and the charge density of the headgroup, as summarised in Figure 1.4 (Epand 1998; Lee 2000).

Both phosphatidylcholine (PC) and phosphatidic acid (PA) can be described as cylindrical. For PC the headgroup size is comparable to the cross sectional area of the two fatty acyl chains and although the physical cross sectional area of the headgroup of PA is less than that of PC, PA has a high charge density at physiological pH, charge repulsion then causing the PA headgroup to occupy a large surface area (Raja 2010). Conversely, phosphatidylethanolamine (PE) is described as having a cone shape, as the phosphoryl ethanolamine headgroup is much smaller than the cross sectional area of the hydrophobic tail region (Minones et al. 1981). Detergents and lysophospholipids are described as an inverted cone, as they have only one hydrophobic chain, and hence a comparatively large head group; the shapes of common glycerophospholipids are shown in Figure 1.4 (Dickey and Faller 2008).

Figure 1.4 shows the phases which single species of hydrated lipids form; the simplest micellar phase is formed when detergents or lysolipids are hydrated, due to the inverted cone shape of the molecules. Bilayers are formed by cylindrical lipids, such as phosphatidylcholine and many other common lipids detailed in Figure 1.2, at physiological temperature and pH. Cone shaped lipids such as phosphatidylethanolamine, when in an aqueous environment will form the more complicated, hexagonal H_{II} phase; the structural basis of this phase is that the lipid molecules arrange with the polar head groups assembled together to form 'rods' with a central aqueous pore with the hydrophobic tails facing outwards from the pore; packing of these rods forms the hexagonal H_{II} phase. Other more complex phases can also be formed by lipids, such as the cubic phase, which itself can exist in two forms: the micellar cubic phase and the bicontinuous cubic phase (Landau and Rosenbusch 1996). In the micellar cubic phase, the lipids form micelles arranged into a cubic lattice, whereas in the bicontinuous cubic phase, lipids form a

curved bilayer, extending in three dimensions, with numerous interconnecting aqueous channels running throughout the matrix (Epad 1998).

1.3.2 Lateral pressure profile

In a homogeneous lipid bilayer of lipids that favour the lamellar phase, the net lateral pressure forces acting over the bilayer are close to zero but the pressure profile across the span of the membrane is non-uniform, with particularly high local pressures near the glycerol backbone region (Cantor 1997a). Although the lipids are present as bilayers in biological membranes, membranes do contain lipids which have a propensity to form the hexagonal H_{II} phase (Cantor 1999). Lipids which do not natively form bilayers are stabilised in the lamellar phase by the bilayer forming lipids; up to 75 % of the biological membranes of some organisms can consist of lipids which, on their own, favour the hexagonal H_{II} phase (Vance and Vance 2002). The adoption of a planar bilayer structure by non bilayer forming lipids results in a curvature strain within the membrane (Cantor 1997b). It has been suggested that the lateral pressure profile in the vicinity of a given integral membrane protein and the curvature strain in a membrane could influence the conformation of the protein and therefore have a significant effect on its function (Cantor 1997b) but there is no direct evidence for this (Lee 2006; Van Voorst and De Kruijff 2000).

1.3.3 Gel to liquid crystalline phase transition of a lipid bilayer

Under physiological conditions, it is important that the bulk of the lipids exist as a fluid bilayer structure within which it is possible for the lipids and proteins to undergo rapid lateral diffusion; this fluid state is the liquid crystalline (L_α) phase, characterised by the lipid fatty acyl chains oriented normal to the bilayer surface but in an unordered and fluid state. At low temperatures, however, bilayer forming lipids can exist in a solid state, in which the lateral diffusion of lipids in the plane of the membrane is highly restricted and the lipid acyl chains are highly ordered; this state is known as the gel (L_β) phase (Chapman 1975).

A bilayer containing a single species of lipid will have a well defined transition temperature (T_C) at which the bilayer changes between the L_α and L_β phases; this transition can be monitored using a number of different methods including nuclear

magnetic resonance, electron spin resonance, fluorescence and differential scanning calorimetry (Caffrey et al. 1991). Of the many factors which influence the transition temperature of a bilayer; the length and degree of unsaturation of the acyl chains of the lipids is most important; the longer the acyl chain of the lipid, the higher the T_c of the bilayer, as can be seen in Table 1.1. Where a bilayer contains lipids with unsaturated acyl chains, the *cis* double bonds act to disrupt the packing of the lipids and so reduce the T_c of the bilayer markedly.

1.4 Membrane proteins

Genome wide statistical analyses have shown that around 30 % of all open reading frames encode integral membranes proteins (Bane et al. 2007; Grishammer and Tate 2003; O'Connor et al. 2009); this is particularly significant since over 70 % of all pharmacological targets are integral membrane proteins (Byrne and Iwata 2002). Despite their importance, membrane proteins make up only 0.3 % of all crystal structures listed in the protein data bank, generally due to their relative difficulty of expression and purification.

Up to 50 % of the mass of biological membranes can consist of membrane proteins, and this percentage may be much higher in localised micro domains (Muller et al. 2008). Membrane proteins can associate with the membrane in a number of ways; integral membrane proteins fully transverse the bilayer due to large hydrophobic stretches in their tertiary structures, and peripheral membrane proteins can associate with the membrane through charge interactions or hydrophobic interactions resulting from either post translational modifications to the protein or amphipathic helices interacting with the lipid bilayer at the region of the glycerol backbone, as described in the following section (Alberts et al. 2007).

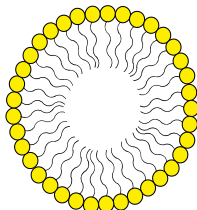
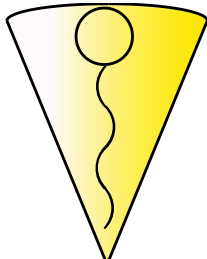
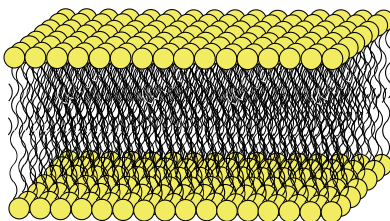
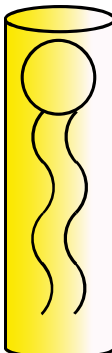
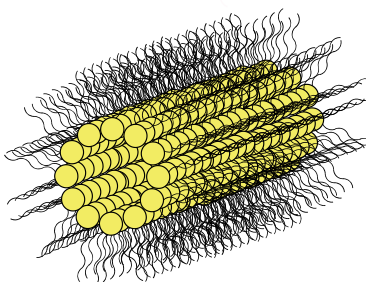
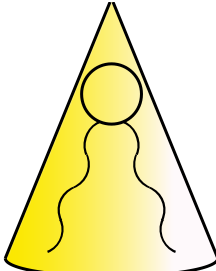
Lipid	Phase	Molecular shape	
Lysophospholipids Detergents	Micellar		
Phosphatidylcholine Sphingomyelin Phosphatidylserine Phosphatidylinositol Phosphatidylglycerol Phosphatidic acid Cardiolipin	Bilayer		
Phosphatidylethanolamine Phosphatidic Acid (pH <3.0) Phosphatidylserine (pH <4.0)	Hexagonal H _{II}		

Figure 1.4: The structures commonly adopted by hydrated lipids: The phase which any particular species of lipid forms is dependent on the overall shape of the lipid molecule. Shape does not depend just on physical size but also on the charge density of the headgroup. Lipids such as di(C18:1)PC with a cylindrical overall shape form a planar bilayer, whereas lipids such as di(C18:1)PE with an overall conical shape favour hexagonal H_{II} phases. Adapted from Vance and Vance (2002)

Lipid species	Headgroup	T _c (°C)
12:0/12:0	PC	-1
14:0/14:0	PC	23
16:0/16:0	PC	41
16:1/16:1	PC	-5
16:0/18:1	PC	-36
18:0/18:0	PC	54
18:1/18:1	PC	-20
16:0/16:0	PE	63
16:0/16:0	PS	55
16:0/16:0	PG	41
16:0/16:0	PA	67

Table 1.1: Phase transition temperatures (T_c) of pure bilayers consisting of lipids with a range of phosphoryl alcohol headgroups and acyl chains of varied length and saturation. Increasing the length of the acyl chain increases the T_c of the bilayer, whereas introducing *cis* double bonds into the lipid chains introduces disorder to the bilayer, consequently lowering the T_c of the bilayer. PC, PE, PS, PG and PA are phosphatidylcholine, phosphatidylethanolamine, phosphatidylserine, phosphatidylglycerol and phosphatidic acid respectively. The fatty acyl chains at the sn-1 and sn-2 positions are given as the number of carbon atoms in the chain followed by the number of *cis* double bonds. Adapted from Vance & Vance.

1.4.1 Peripheral membrane proteins

Peripheral membrane proteins are located at the surface of the membrane, and can be associated with the bilayer in a number of ways. Many peripheral membrane proteins interact with the membrane through structural motifs within the protein: some have stretches of positively charged amino acids which associated with the lipid head groups (Johnson and Cornell 1999), and others such as the annexins undergo conformational changes upon calcium binding to expose residues such as tryptophan which interact with the membrane (Concha et al. 1993). Amphipathic helices and small hydrophobic loops play an important part in membrane association of some peripheral membrane proteins, interacting with the glycerol backbone and headgroup regions of the lipids (Hanakam et al. 1996). Some peripheral membrane proteins are post-translationally modified, and have fatty acyl chains of up to 20 carbon atoms covalently bound to one or more cysteine residues, anchoring them to the membrane (Maurer-Stroh and Eisenhaber 2005). Peripheral membrane proteins can be freed from their interactions with the membrane through mild treatments such as change in pH or ionic conditions, and mild detergents at concentrations that do not significantly disrupt the membrane (Alberts et al. 2007).

1.4.2 Integral membrane proteins

Integral membrane proteins are distinct from peripheral membrane proteins as isolation of these proteins from their native membrane requires treatment with detergents which completely disrupt the bilayer and solvate the protein, replacing membrane lipids (Garavito and Ferguson-Miller 2001). Most integral membrane proteins transverse the bilayer completely, and contain both hydrophilic and hydrophobic regions. Logically, the hydrophilic regions reside either side of the hydrophobic core of the lipid bilayer, and the hydrophobic regions transverse the core of the lipid bilayer. The hydrophilic domains on either side of the membrane act to anchor integral membrane proteins into the lipid bilayer. Integral membrane proteins interact with the lipids in the bilayer as intimately as soluble proteins with water; the hydrophobic regions in the proteins form good van der Waals contacts with the membrane lipids, and lipids are occasionally found tightly bound to crevices in the surface of the protein in which particular lipids are energetically favoured (Lee 2003; Lee 2004). Interactions of integral membrane proteins with

lipids can show specificity particularly where charged interactions between anionic lipids and positively charged residues in the membrane protein are involved (Marius et al. 2005).

Membrane proteins traverse the lipid bilayer as either one or more α -helices or as β -barrels; β -barrel proteins such as the porins are often found in the outer membranes of prokaryotes, mitochondria and plastids (Wimley 2003). As well as the requirement for an abundance of hydrophobic amino acids in the transmembrane region of a protein, the polypeptide backbone must also be satisfied, as the energetic cost of moving a non-hydrogen bonded peptide bond from water to a hydrophobic environment is around 25 kJ mol^{-1} as opposed to 2.5 kJ mol^{-1} for a hydrogen bonded peptide bond (Roseman 1988); in an α -helix, the backbone nitrogen donates a hydrogen bond to the carbonyl oxygen of the peptide bond four residues upstream. Residues in a transmembrane α -helix exposed to the lipid bilayer can be expected to be predominantly hydrophobic, but residues involved in helix-helix contact could be polar or charged. As a result of the β -sheet secondary structure, β -barrels have residues alternating between polar and non polar, with polar residues within the barrel structure and non polar residues projecting into the lipid bilayer (Murzin et al. 1994).

1.4.3 The transmembrane regions of membrane proteins

The structure and orientation adopted by a membrane protein within a lipid bilayer is highly dependent on physical properties of the bilayer such as the thickness of the hydrophobic core of the bilayer (von Heijne 1996). The average thickness of the hydrophobic core of a typical membrane is 30 \AA , and the distance between two $\text{C}\alpha$ atoms in an α -helix is 1.5 \AA ; therefore a typical non-polar region of a transmembrane α -helix will be 20 amino acids long if it lies along the membrane normal. Many membrane proteins contain transmembrane α -helices which are tilted within the bilayer, and this will require a longer stretch of hydrophobic residues. The distance between the $\text{C}\alpha$ atoms of two consecutive amino acids in a β -sheet is 3.5 \AA , therefore for a β -barrel the number of residues required to transverse the hydrophobic core is about 10 amino acids (White and Wimley 2003).

1.5 Protein lipid interactions

Membrane proteins operate in the environment provided by the lipid bilayer and so lipids and membrane proteins must have co-evolved to form functioning membranes. (Mulkidjanian et al. 2009). Details of how lipids interact with membrane proteins are often unclear as lipids are usually not seen in X-ray crystal structures of membrane proteins; lipids are often lost during crystallization from detergent and any remaining lipids will only be resolved in the crystal structure if they are well ordered. This results in very few crystal structures of membrane proteins containing lipids; structures which have been resolved with lipid bound to the protein often correspond to lipid molecules at protein-protein interfaces as in the case of bacteriorhodopsin and may not be typical of 'normal' bound lipids (Lee 2003). It is therefore often unclear where the membrane interface lies on a membrane protein, and in turn which parts of a protein molecule are accessible to bulk water and which parts are accessible to lipid (Victor K.G, 2001).

In much the same way that water molecules surround a soluble protein, lipid molecules must pack tightly around a membrane protein in order to prevent unwanted holes in the membrane which would result in leak through the bilayer. Crystal structures of many membrane proteins have shown that the transmembrane regions of the proteins are rough and irregular, so that lipid molecules packed closely to the surface of membrane proteins will be disordered (Lee 2003). Such lipids would have a lesser degree of mobility when compared to membrane lipids in the bulk phase. This phenomenon can be examined using electron spin resonance (ESR) using lipid molecules with fatty acyl chains containing nitroxide spin labels at different positions in the acyl chains. ESR studies have shown the presence of a ring, or annulus, of lipid molecules with restricted motion around membrane proteins, referred to as annular lipids; the annular lipids are considerably less mobile than the bulk lipids as their movement is impeded by the presence of the protein (Watts et al. 1981; Lee 2003). However, the interaction between the annular lipids and the protein surface is 'non-sticky', the annular lipids being in fast exchange with the normal bulk lipid (Lee 2003). In addition to annular lipid molecules, lipids have been found tightly bound to proteins, often between α -helices or between subunits of multi-subunit membrane proteins (Ernst et al. 2010;

Simmonds et al. 1982; Valiyaveetil et al. 2002); these lipids, referred to as non-annular lipids, are bound much more tightly than annular lipids and are, in fact, resolved in a limited number of crystal structures (Lee 2003). Figure 1.5 shows a crystal structure of the potassium channel KcsA with one lipid molecule resolved at each protein-protein interface in the homotetrameric structure. The lipid molecule was modelled as a diacylglycerol molecule as no density was resolved in the crystal structure for the lipid headgroup, but chemical analysis shows that the lipid is actually a phosphatidylglycerol. Particular lipid molecules bound to non-annular sites in some proteins have been shown to be important modulators of protein activity (Lee 2004; Marius et al. 2005) and as such are sometimes known as cofactor lipids.

Biological membranes exist in the liquid crystalline phase under physiological conditions and therefore the lipid and protein molecules have a significant amount of vertical and lateral mobility within the membrane. Figure 1.6 shows the structure of a bilayer of dioleoylphosphatidylcholine (DOPC); the positions of the peaks show the locations of the lipid components along the membrane normal, and the width of the peaks shows the extent of motion of each component. It is obvious from this that the glycerol backbone shows the least mobility of any of the parts of the lipid molecule, and is therefore useful to use as a datum when talking about the position of a protein within the bilayer.

The structure of a membrane protein has a sizable effect on its interactions with the lipid molecules in a membrane system, and are therefore very important for the positioning of a protein within the membrane. It is common to find both positively and negatively charged amino acids at the ends of a transmembrane helix. (Ganapathiraju et al. 2008). These charged residues are able to interact with the headgroup region of the lipid bilayer through electrostatic charge interactions, stabilising the vertical position of the protein within the bilayer. Some charged residues such as arginine or lysine may have their α carbons within the membrane, but due to the length of their side groups, with the charged region of the amino acid ‘snorkeling’ into the headgroup regions of the bilayer (Strandberg and Killian 2003). Identifying the charged residues at either end of a transmembrane α -helix in the crystal structure of a membrane protein therefore helps to identify the likely

location of that helix with respect to the lipid bilayer that will surround the protein in a native membrane. In much the same way that charged residues can be used to predict the length of the transmembrane region of an α -helix, the presence of tryptophan and tyrosine residues often mark the ends of a transmembrane α -helix because the amphipathic nature of these residues means that they have a tendency to locate in the glycerol backbone region of the bilayer (Yau et al. 1998b).

1.6 Potassium Channels

Ion channels are a group of multi-pass membrane proteins which control a large number of physiological processes, from the regulation of muscle contraction, hormone and neurotransmitter release, to transpiration in plants (Tombola et al. 2006). Potassium channels are able to conduct potassium ions across bilayers at diffusion limited rates, and are found in nearly every type of organism (Miller 2003).

1.6.1 Identification of potassium channels

Common to all potassium channels is a highly conserved signature sequence of five amino acids with the sequence TVGYG, which can be used by genome analysis tools to identify potassium channels in all organisms. This high level of sequence conservation arises because the amino acid sequence forms a highly conserved structural feature of all potassium channels, central to the high selectivity of the channels for potassium ions whilst maintaining conduction at diffusion limited rates.

1.6.2 Potassium channel pore domain

The pore domain of all potassium channels is highly structurally conserved (MacKinnon et al. 1998), with the pore domain showing a high sequence conservation throughout a range of organisms, and a significant conservation with sodium and calcium channels (Doyle et al. 1998; Tombola et al. 2006; Zhou et al. 2001). With the exception of the K2P family, all potassium channels are tetramers that surround the ion conduction pore with fourfold symmetry as shown in Figure 1.7. Each subunit contributes two transmembrane helices to the central pore, termed the inner and outer helices, the inner helix being closest to the ion

conduction pathway, and the outer helix residing closest to the hydrophobic core of the bilayer (Uysal et al. 2009). Each subunit also contributes a shorter, tilted hydrophilic helix to the central pore termed the pore helix, the axes of the four pore helices pointing to the centre of the pore (Alagem et al. 2003). Following each pore helix in the sequence is the potassium channel signature sequence; the four signature sequences project outwards into the central pore forming the selectivity filter which is the fundamental structural feature of potassium channels which underpins selective ion conduction.

1.6.3 Conduction of potassium ions

Potassium channels are over 10,000 times more permeable to potassium ions than to sodium ions (MacKinnon 2003), which is surprising considering the atomic radius of a potassium ion is 1.33 Å whereas that of sodium is considerably smaller at 0.95 Å. What is more surprising is that despite the selectivity for potassium exhibited by these channels, the rate of conduction of potassium ions through the pore is around 10^8 ions per second, approaching the limit of diffusion (Tombola et al. 2006). The mechanism by which potassium ions pass through a potassium channel have been extensively studied in the potassium channel KcsA from the bacterium *Streptomyces lividans*, and the structural conservation found in the pore domain of all potassium channels which have crystal structures available indicates that the mechanism of potassium conduction is also highly conserved.

1.6.3.1 Intracellular gate

In order for potassium ions to flow through a potassium channel unhindered, the pore forming helices must open wide enough to allow potassium ions to pass through the channel. The mechanism of opening and closing the pore has recently become a topic of debate due to the increasing knowledge of channel structure.

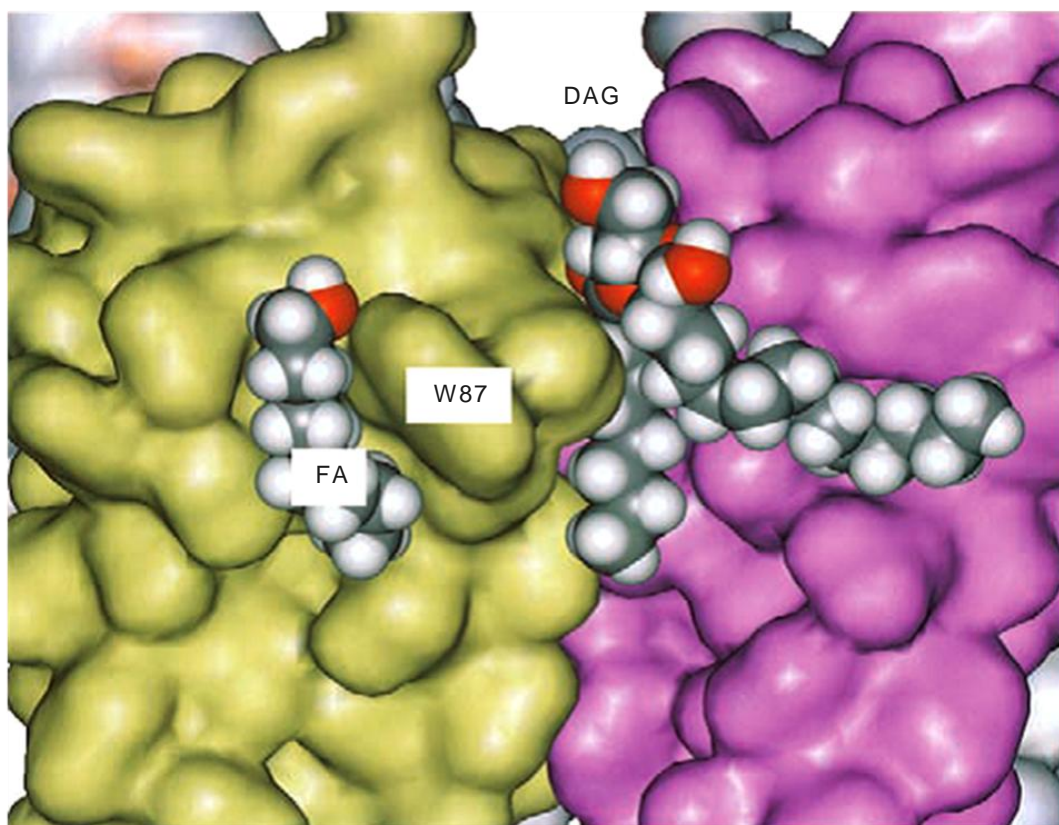


Figure 1.5: Interactions of membrane lipids with membrane proteins. The surface of the KcsA channel nearest the extracellular side of the membrane is shown, with two partial lipid molecules, a DAG molecule and a fatty alcohol (FA), bound to crevices on the protein surface close to W87. The DAG molecule binds at the interface between two monomers, shown in yellow and purple. The diacylglycerol molecule represents the position of a molecule of phosphatidylglycerol. The headgroup of this lipid was not resolved in the crystal structure. Adapted from Lee (2003), rendered with WebLab ViewerPro (Molecular Systems Inc.); PDP file 1K4C.

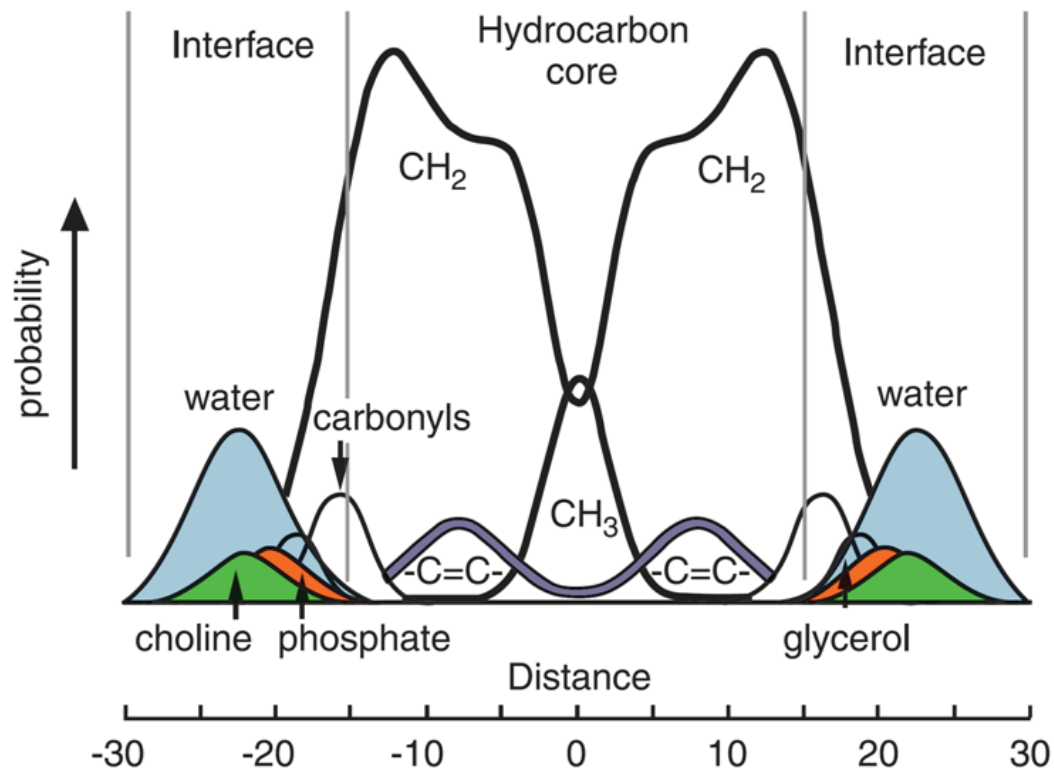


Figure 1.6: The structure of a bilayer of DOPC at 23 °C at low hydration (5.4 waters/lipid) determined by joint refinement of x-ray and neutron diffraction data. The figure shows the distribution of structural groups within the bilayer averaged over time, highlighting the fluid nature of the bilayer. Blue regions indicate water molecules, green – choline and orange - phosphate. Adapted from Lee (2003)

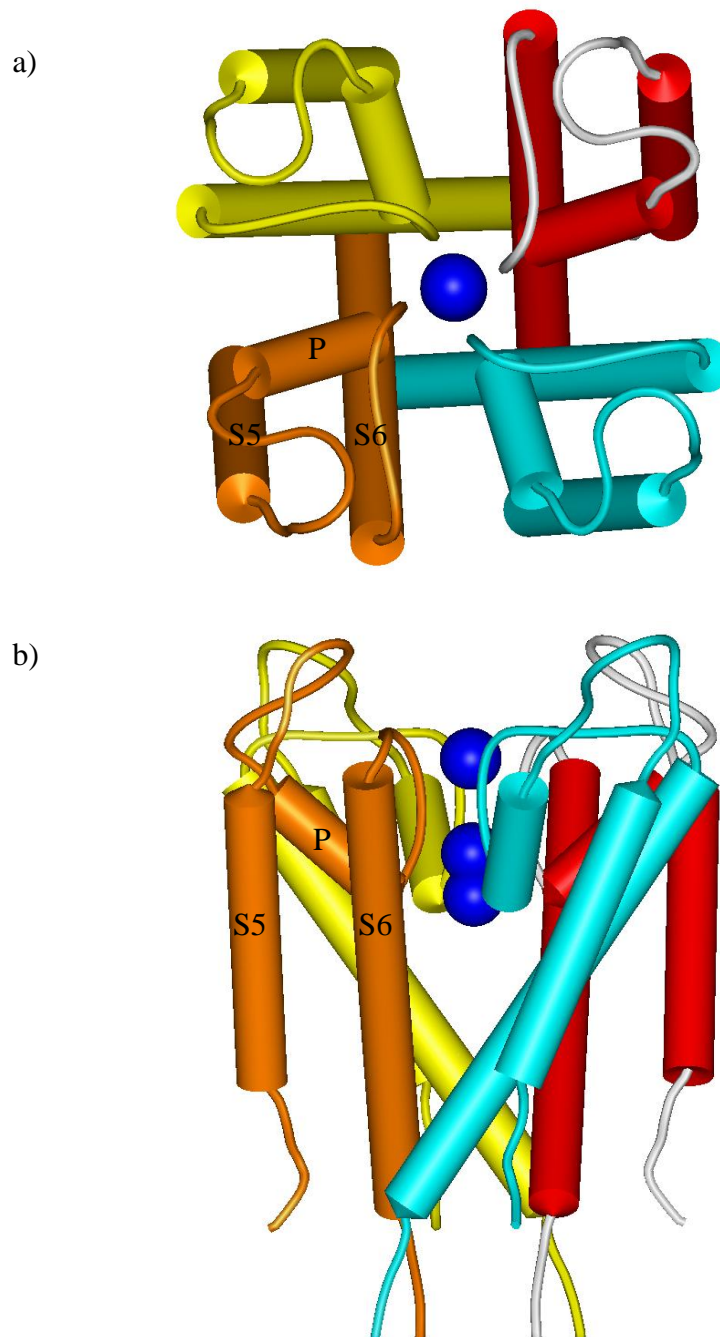


Figure 1.7: The structure of the potassium channel KcsA with each subunit shown in a different colour. The two transmembrane helices of each KcsA monomer correspond to helices S5 and S6 of a voltage gated potassium channel, separated by the P helix; these are marked. Potassium ions in the ion conduction pathway are shown in blue. **(a)** shows the channel from the extracellular side of the membrane, and **(b)** the channel from the plane of the membrane, with the extracellular side at the top and the intracellular side at the bottom, modelled using Weblab ViewerPro (Molecular systems Inc.), PBD ID: 1BL8.

1.6.3.2 The glycine bend model

Crystallographic and, more recently, nuclear magnetic resonance studies of KcsA and the calcium gated potassium channel MthK have identified mechanisms by which conformational changes can occur to open the channel. The closed state of the pore domain of a potassium channel is exemplified by the KcsA crystal structure shown in Figure 1.8; the inner helices of the channel form a bundle in the centre of the pore, preventing potassium ions transiting through the pore. The crystal structures of MthK and KvAP (Jiang et al. 2002a; Jiang et al. 2003a) however are examples of the pore domain of a potassium channel in the open conformation; as shown in Figure 1.8 the inner helices now have a much wider opening at the intracellular entrance to the channel because the inner helices are bent outwards from the centre of the pore. This bend occurs at a hinge consisting of three non- consecutive residues in the inner helices, highly conserved in a range of potassium channels opening in response to a range of different stimuli, as shown in Figure 1.9, indicating a conserved method of opening the channel. The first key residue implicated is a highly conserved glycine (Magidovich and Yifrach 2004) near the centre of the helix which forms the point at which the helix bends to open the channel (Jiang et al. 2002b; Perozo et al. 1999). The side chain of the residue five amino acids downstream of the hinge glycine protrudes directly into the centre of the pore; at this position potassium channels have an amino acid with a small side chain to prevent blockage of the pore when the pore is in the open state (Jiang et al. 2002b). The final important amino acid is a bulky hydrophobic residue near the C terminus of the inner helices; in the closed state of the channel, the proximity of these residues from the four inner helices form a hydrophobic gate, blocking the channel from the intracellular side.

1.6.3.3 The PVP bend model

Functional studies with the Shaker potassium channel using channel blockers of various sizes to protect against thiol modification of cysteine residues introduced into the internal vestibule of the channel showed that the S6 helices bent outwards nearer the end of the helix at a proline-valine-proline motif that is highly conserved in eukaryotes (del Camino et al. 2000). Subsequent studies utilising further cysteine mutagenesis and metal bridge formation within the pore showed that the bend was

present in both closed and open states of the channel (del Camino and Yellen 2001), and that the lengths of the metal bridges were too short to block the pore if the width of the pore was as predicted by the glycine bend model. This, combined with functional data and molecular dynamics simulations of anaesthetic binding at a PVP motif in human Kv 1.5 and Kv1.2 channels (Luzhkov et al. 2003; Nilsson et al. 2003) and the crystal structures of Kv 1.2 and the Kv 1.2/2.1 chimera, lead to the conclusion that eukaryotic Kv channels may be gated by a PVP motif rather than a glycine hinge (Swartz 2004). A difference in gating mechanism in which an open eukaryotic Kv channel has a smaller opening than a prokaryotic Kv channel would explain the smaller single channel conductance of the Shaker potassium channel than of the MthK and KvAP channels (Webster et al. 2004), but, nevertheless, involvement of the glycine hinge in opening of the eukaryotic channel seems likely as the glycine residue is conserved in eukaryotic channels.

1.6.3.4 Central cavity

Potassium conduction can occur in either direction across the membrane, depending on the electrochemical gradient of potassium, but flux will normally be out of the cell given the high internal concentration of potassium in the cell. In this case, translocation of a potassium ion through a potassium channel will begin when the ion enters the inner vestibule of the potassium channel, coordinated by eight water molecules. The ion enters a water filled cavity near the centre of the membrane (Figure 1.10), formed by the inner helices of the channel and with a diameter of around 10-12 Å when the channel is in the open state (Jogini and Roux 2005; Miloshevsky and Jordan 2007). The cavity is nearly completely lined with hydrophobic residues which is thought to aid potassium conduction by preventing any extensive interactions between potassium ions and the walls of the cavity (Armstrong 1966). The position and size of the water filled cavity are the key factors allowing potassium ions to begin their journey across the bilayer; the energetic cost of moving a cation into the middle of the membrane in the absence of coordination by water molecules would be ca 60 kcal mol⁻¹ compared to ca 6.3 kcal mol⁻¹ to move a cation into an aqueous environment the size and shape of the cavity (Roux and MacKinnon 1999). The radius of the cavity is also important as electrostatic calculations show that as an ion crosses a membrane in a pore, the

energy barrier that it has to overcome increases to a maximum in the centre of the bilayer, but that this energy barrier reduces as the radius of the pore increases (Parsegian 1976).

The dipole moments of the four pore helices, arising from the sum of the dipole moments of each peptide bond in the helix, is also important; this gives rise to the equivalent of a small negative charge at the C terminal end of the helix (Sengupta et al. 2005). In potassium channels this helix dipole is utilized to stabilise a potassium ion in the cavity at the point of entry into the selectivity filter (Doyle et al. 1998). The positioning of the pore helices is paramount, as the axes of the four pore helices point directly towards the centre of the cavity, with the C terminal ends of the helices proximal to the potassium ion. The ends of the helices are positioned around 8 Å away from the cavity centre, but the sum of the electrostatic effects of the helix dipoles reduces the energy required for a potassium ion to reside in the centre of the cavity to $-4.5 \text{ kcal mol}^{-1}$ (Roux and MacKinnon 1999). The actual transfer free energy of a potassium ion entering the central cavity of the potassium channel KcsA when the electrostatic effect of the entire protein is taken into account is around $-8.5 \text{ kcal mol}^{-1}$. This explains the selectivity of the pore for potassium over divalent cations such as calcium as the transfer free energy for a divalent cation reaching the centre of the cavity of a potassium channel is $-4.6 \text{ kcal mol}^{-1}$, despite the structural similarity of the calcium channel pore domain to that of a potassium channel mentioned above (Roux and MacKinnon 1999).

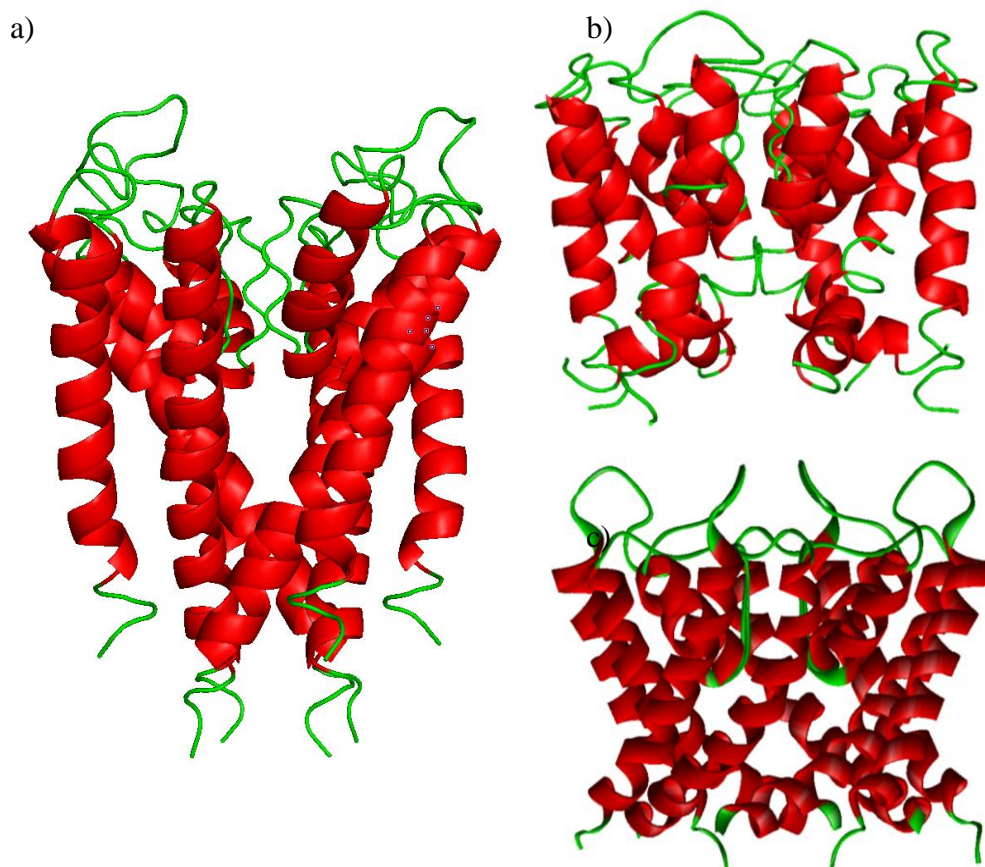


Figure 1.8: Open and closed pore structures of potassium channels, all with the extracellular face of the channel at the top. **(a)** KcsA (PDB ID:1BL8) crystallised in the closed conformation. **(b)** the potassium channel MthK (PDB ID: 1LNQ) crystallised in the open conformation; the helices appear bent outwards from the potassium conduction pore. **(c)** the crystal structure of the voltage gated potassium channel KvAP (PDB ID: 2A0L), again showing the pore in the open conformation with the S6 helices bent outwards from the centre of the channel. Weblab ViewerPro (Molecular systems Inc.),

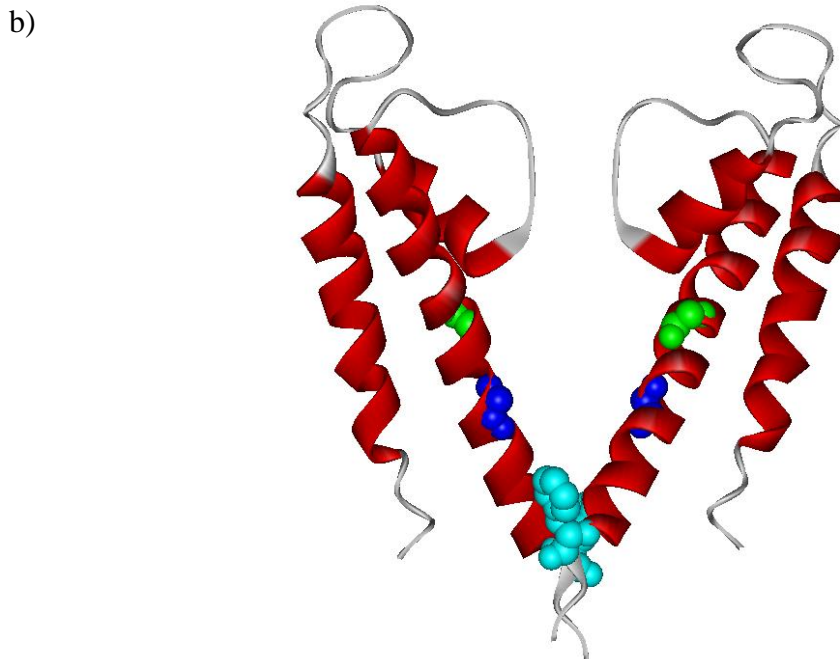
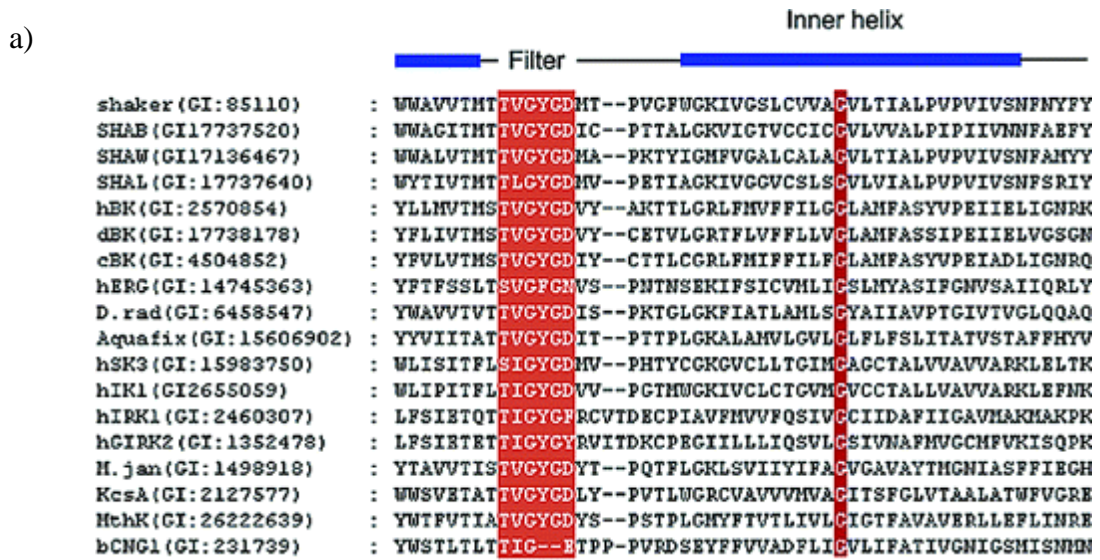


Figure 1.9: (a) Alignment of potassium channels from eukaryotic and prokaryotic organisms showing conservation in the selectivity filter (TVGYGD) and at the glycine hinge region of the inner (S6) helix. (adapted from Magidovic et al. 2004) (b) The crystal structure of KcsA (PDB accession code 1BL8) with conserved gating residues highlighted. Two subunits of the KcsA tetramer have been removed in this image. In green is the gating hinge glycine residue (KcsA Gly99), in blue is the conserved small residue (KcsA Gly104), and in cyan spacefill is a phenylalanine residue which contributes to the hydrophobic gate. Modelled using Weblab ViewerPro (Molecular systems Inc.),

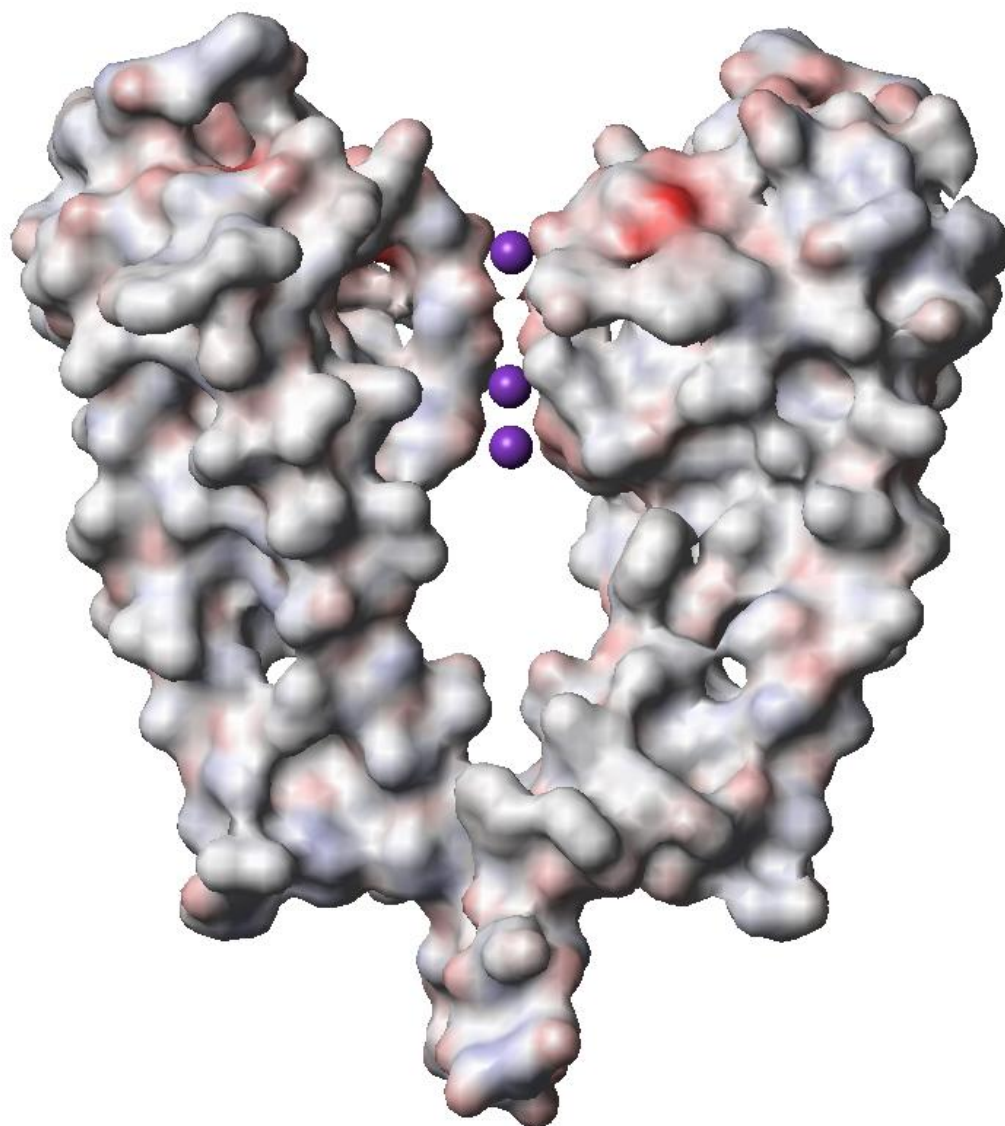


Figure 1.10: The internal cavity of a potassium channel. A cross section of KcsA is shown. The extracellular side of the channel is at the top of the page. A solvent accessible surface has been added and coloured according to electrostatic potential. potassium ions in the selectivity filter are shown in purple. The central cavity of the channel is evident at the centre of the structure. Modelled using Weblab ViewerPro (Molecular systems Inc.), PDB accession code 1BL8.

1.6.3.5 Selectivity filter

The selectivity filter is constructed from the tetrameric assembly of the potassium channel signature sequences from each subunit, forming a constriction 12 Å long containing four distinct binding sites for potassium ions, numbered S1 to S4, S4 being closest to the central cavity, and S1 being the most extracellular, as illustrated in Figure 1.11. Each potassium ion binding site is surrounded by eight oxygen atoms, which are utilised by the channel to coordinate a dehydrated potassium ion, so overcoming the energetic cost of dehydration when the potassium ion sheds its water shell to enter the filter. The oxygen atoms which create the potassium binding sites S1 to S3 are contributed by carbonyl backbone oxygens of the Thr-Val-Gly-Tyr-Gly sequence from each subunit whereas the oxygen atoms which coordinate a potassium ion in the S4 site are contributed by the hydroxyl oxygen of the threonine residue preceding the above sequence, and the carbonyl oxygen of the valine residue, as shown in Figure 1.11.

Potassium channels discriminate highly for potassium over all other monovalent cations and the selectivity filter achieves this feat in a number of ways (Doyle et al. 1998). This discrimination is easy to explain for Rb^+ , and Cs^+ , as these ions are larger than the potassium ion, and therefore simply cannot pass through the selectivity filter. More difficult to explain is why a Na^+ ion, which is smaller than a potassium ion by 0.38 Å, passes through the channel so much more slowly than the potassium ion. In fact it is the smaller size of the Na^+ ion that prevents it passing through the selectivity filter under physiological conditions. A dehydrated potassium ion is coordinated well by the oxygen atoms at each binding site, whereas the smaller Na^+ ion is only weakly coordinated, increasing the energy required for the ion to enter the selectivity filter since the water hydration shell of the ion is not mimicked by the oxygen atoms provided by the protein.

An important characteristic of the selectivity filter is that of the four potassium ion binding sites, two are always occupied by potassium ions (Shrivastava et al. 2002) with two possible configurations for the ions, either in sites S1 and S3 (the 1, 3 configuration) or in sites S2 and S4 (the 2, 4 configuration); in each case a water molecule occupies the empty potassium ion binding sites (Cordero-Morales et al. 2006; Morais-Cabral et al. 2001). A potassium ion in the centre of the aqueous

cavity will enter the selectivity filter when the potassium occupancy is in the 1, 3 configuration; the entry of this ion into the S4 site will of course cause electrostatic repulsion between that ion and the ion in the S3 site, resulting in the transition of the ion in the S3 site to the S2 site, and the simultaneous exit of the potassium ion at the S1 site into the extracellular medium, leaving the selectivity filter in the 2,4 configuration (Zhou et al. 2001). The electrochemical gradient of potassium ions drives another potassium into the central cavity, allowing the cycle of potassium conduction to restart (Berneche and Roux 2003), resulting in translocation across the membrane at diffusion limited rates. At low potassium concentrations, the selectivity filter adopts a flexible, non conducting conformation containing only one potassium ion, and the channel is effectively blocked until the potassium concentration is high enough for a potassium ion to enter the selectivity filter and return the channel to the conductive state. Therefore, some of the energy of potassium ion binding to the selectivity filter must be used to change the structure of the filter, which in turn means that the ions bind less tightly to the filter than they would to a conformationally stable structure; coupled with electrostatic repulsion from other potassium ions occupying the filter, this explains the high throughput of potassium ions despite the high selectivity of the filter (MacKinnon 2003).

1.6.3.6 Inactivation of potassium channels

After a period of prolonged activity, potassium channels spontaneously close, regardless of whether or not the stimulus which caused the opening of the channel is still being applied (Loots and Isacoff 1998); in some cases the inactivation is coupled to the initial activation (Olcese et al. 1997). There are two molecular processes by which potassium channels can self-inactivate, N type inactivation and C type inactivation. N type inactivation is a rapid event in which the N terminal region of the protein binds the open pore, preventing ion conduction (Hoshi et al. 1990), and C type inactivation is generally a slower process occurring at the selectivity filter, and is modulated by the ions in the pore and other exogenous pore blocking molecules (Choi et al. 1991; Hoshi et al. 1991).

1.6.4 Potassium channel gating

Potassium channels fulfil a number of roles in nature, enabling the passage of potassium across a membrane in response to a wide range of stimuli, and can be broadly classified into four main types: calcium gated, voltage gated, inward rectifier and leak (2P) channels (Korn and Trapani 2005).

1.6.4.1 Calcium gated potassium channels

During an action potential in mammals, calcium channels open in the cell membrane to allow calcium into the cell. The increase in intracellular calcium results in potassium channels opening and allowing potassium ions to flow out of the cell, returning the voltage across the membrane towards the resting potential. Mammalian calcium gated channels can be split into two categories: large conductance (BK) and small conductance (SK) channels. Prokaryotic calcium gated potassium channels are generally classified as small conductance channels, as the cells of origin are not excitable, but their pore and calcium binding domains are similar in sequence to human BK channels (Zadek 2000)

1.6.4.1.1 SK channels

SK channels are purely calcium gated channels, and their function is to aid in the repolarisation of the cell following the action potential, maintaining the cell in a hyperpolarised state until the intracellular levels of calcium drop, preventing repeat depolarisations (Stackman et al. 2002). SK channels are tetramers and have the same pore domain structure as the potassium channels described above. However, the topology of SK channels is similar to that of voltage gated potassium channels in that the SK channel monomer has 6 transmembrane α -helices, the last two of which constitute the pore domain (Xia et al. 1998). Sequence analysis of SK channels show no calcium binding motifs, but it has been shown that calmodulin constitutively interacts with SK channels via the region immediately C terminal to the inner helix of the pore (Schumacher et al. 2001). Calcium binding to the calmodulin domain causes conformational changes in the channel to allow the intracellular gate to open (Maylie et al. 2004).

1.6.4.1.2 BK channels

BK channels are potassium channels which are activated by both calcium and changes in transmembrane voltage; their physiological purpose is to exert a negative feedback effect on transmembrane voltage and to modulate potassium efflux from the cell in response to increases in intracellular calcium concentration and as such control cell excitability (Magleby 2003). It follows that the structure of these channels is rather complex, in that the BK channels have the same transmembrane topology as the voltage gated channels discussed below, but also have an 800 amino acid intracellular regulatory domain (Shipston 2001). The RCK domain of BK channels is similar to that of prokaryotic channels such as MthK and contains a Rossman fold motif near the C terminus of the channel where calcium can bind and initiate the chemomechanical gating of the channel (Jiang et al. 2002a).

1.6.4.2 Inward rectifier potassium channels.

Inward rectifier potassium channels are essential in maintaining the resting potential of cells and vary in the strength of the inward rectification, which is linked to the physiological process controlled by the channel. Strong inward rectifiers are important in skeletal muscle and in neurons, and are important for the stabilisation of the resting potential of cardiac tissue. Such channels have very low conductance at positive membrane potentials, but at around -40 mV they start to become conductive, letting potassium ions into the cell to maintain the resting potential; since they are essentially inactive at positive membrane potentials they do not interfere with the action potential (Nichols and Lopatin 1997). Other inward rectifier potassium channels include the K_{ATP} channels which regulate the secretion of insulin in the pancreas, and are present in the brain and muscle cells. These channels however only provide a weak inward rectification current and allow the passage of potassium ions at positive membrane potentials (Nichols and Lederer 1991). The brain contains a large number of inward rectifier channels which have functional properties somewhere between those already discussed. These are usually ligand gated channels which are activated by G-proteins or by intracellular second messengers (Breitwieser 1991; Doupnik et al. 1995; Hartzell 1988). Under certain physiological conditions, such as a high extracellular

potassium concentration, voltage gated potassium channels can show a weak inward rectifier action, but this activity is usually blocked by sodium ions that can cause the selectivity filter to adopt its collapsed conformation (Nichols and Lopatin 1997).

1.6.4.3 Leak (2P) channels

Leak channels conduct background potassium currents in order to assist in the maintenance of the resting potential of excitable cells (Honore 2007). A large range of stimuli are known to affect the function of this family of potassium channels such as mechanical stretch, pH, temperature and cyclic nucleotides, although little is known about the channels and the exact conformational changes which occur upon activation (Cohen et al. 2009). Leak channels differ from the other potassium channels described in that the pore region of each subunit of these channels contains four transmembrane α -helices instead of the conventional two (Goldstein et al. 2001) and these extra helices confer on each subunit two pore forming domains, hence the channels are often referred to as two pore channels (Choe 2002)

1.6.5 Voltage gated potassium channels

The voltage gated potassium channel (Kv channel) family is responsible for regulating the potassium component of the membrane potential in a large range of cell types (Li and Gallin 2004). In excitable cells, Kv channels cause the repolarisation of the cell following an action potential, allowing potassium ions out of the cell down their electrochemical gradient (Hodgkin and Huxley 1952) and they are also found in most mammalian non excitable cells. Prokaryotic organisms have a highly controlled potassium flux system, and some bacteria will accumulate an intracellular concentration of potassium of nearly five hundred millimolar (Stumpe et al. 1996) but it is still surprising that voltage gated potassium channels have been discovered in nearly every sequenced prokaryotic genome (Derst and Karschin 1998). Little is known about their function other than to suggest that the channels have an emergency function to maintain membrane potential during cell stress and cell growth (Ungar et al. 2001).

1.6.5.1 Structure of voltage gated potassium channels

Nearly all voltage gated potassium channels are homotetramers, although some mammalian channels are able to function as either homotetramers or heterotetramers (Grunnet et al. 2003). Each subunit consists of six transmembrane α -helices that are named S1 to S6 and a short hydrophilic helix between S5 and S6 called the P helix as shown in Figure 1.12. Helices S5 and S6 along with the P helix from each subunit assemble with fourfold symmetry to form the pore domain, a conserved feature in all potassium channels containing the potassium conduction pathway and gating regions discussed earlier. The S1 to S4 helices of each subunit form the four independent voltage sensing domains which control the gating of the channel. Within the S4 helix of Kv channels are a number of highly conserved arginine residues, giving a pattern of positive charges every three amino acids in the helix. The number of arginine residues in the S4 helix ranges from three to five depending on the channel (Chakrapani et al. 2008), and the conservation is not limited to Kv channels, as the same pattern of positively charged amino acids can be found in sodium channels, calcium channels, proton channels and voltage dependent phosphatases (Nelson R.D. et al. 1999). Eukaryotic Kv channels also contain an N terminal cytoplasmic tetramerisation domain not found in any bacterial channels discovered to date (Bixby et al. 1999); this domain also operates as a scaffold for binding accessory subunits which modulate the sensitivity of the channels (Li et al. 2006). There is general agreement that the pore domains in Kv have structures comparable to those in all other potassium channels (Doyle et al. 1998; Jiang et al. 2003a; Tombola et al. 2006). However, the structures of the voltage sensing domains of Kv channels have been the subject of considerably more debate.

1.6.5.2 Conservation of voltage sensing domains

The blocking of potassium channels from both prokaryotes and eukaryotes by toxins that bind with a 4:1 stoichiometry (i.e. one per voltage sensor (Ruta and MacKinnon 2004)), has led to the conclusion that the structure and function of the voltage sensing domain is evolutionarily conserved, in structure if not in sequence (Swartz and MacKinnon 1997a; Swartz and MacKinnon 1997b). This has been confirmed by experiments such as the construction of chimeric Kv channels in

which the C terminal half of the S3 helix and the entire S4 helix have been transferred from rat Kv2.1 to rat Kv1.2 to form a fully functional channel (Long et al. 2007). The modular nature of the voltage sensors has been further demonstrated by the construction of chimeric channels containing the pore domain of rat Kv1.2 and the paddle motif of either the proton channel Hv1 or the voltage dependent phosphatase Ci-VSP; the chimeras had gating properties similar to those of full length Kv1.2 (Alabi et al. 2007).

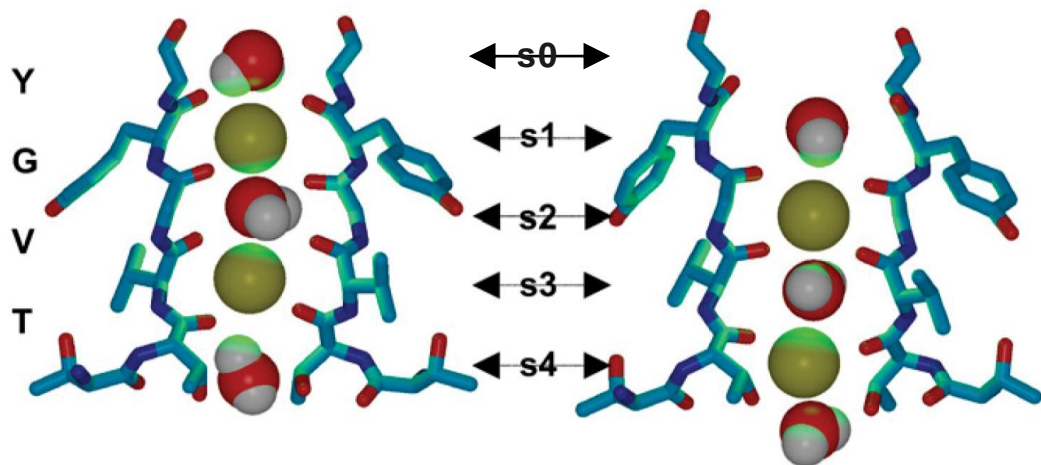


Figure 1.11: Selectivity filter of the potassium channel KcsA in two conduction states. The selectivity filter cycles between these two states thousands of times per second to pass potassium ions through the membrane at diffusion limited rates. The potassium ion binding sites are labelled S1 to S4, and at the top, S0 is a potassium ion (green spheres) in the extracellular solution, partially hydrated by water (red spheres) and partially coordinated by carbonyl oxygen from a glycine residue. S1 to S4 are binding sites created by three other carbonyl oxygens and one carboxyl oxygen of the selectivity filter amino acids. Adapted from Shrivastava et al. 2002

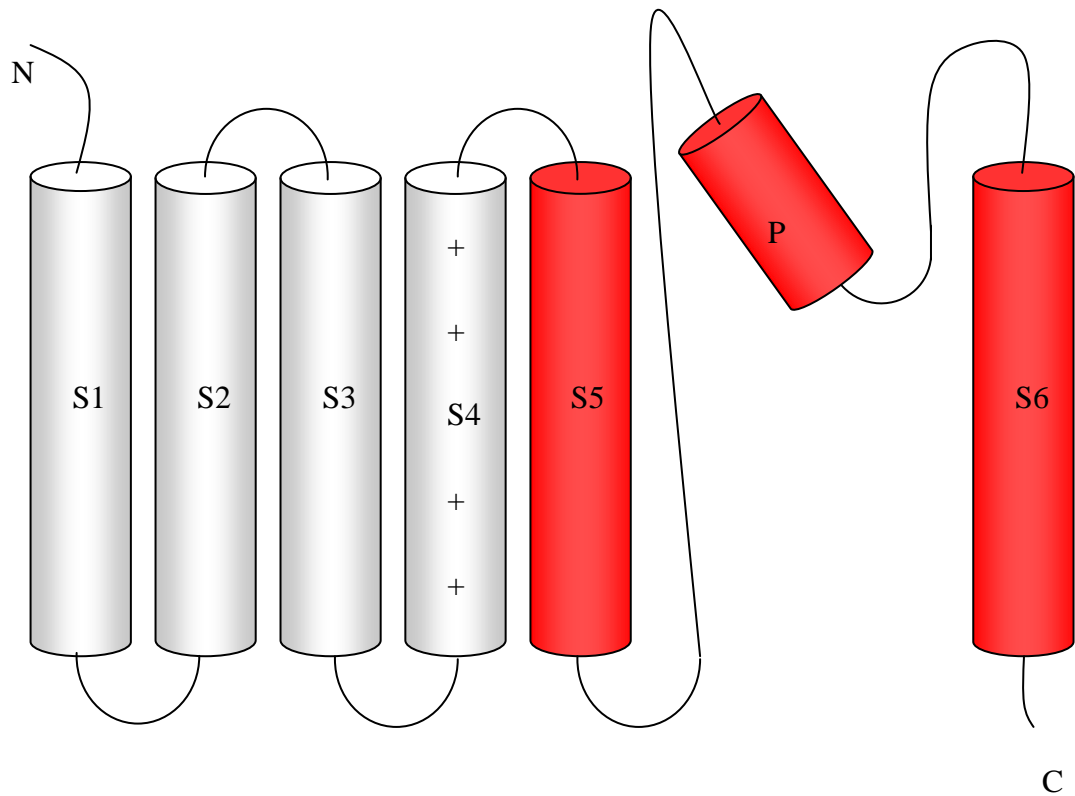


Figure 1.12: Topology of the voltage gated potassium channel. The figure shows the voltage sensing domain consisting of helices S1-S4 with helices S5 and S6 together with the pore helix (P) forming the pore domain. The positive charges carried by arginine residues in the S4 helix are shown in black.

1.6.5.3 Structure of voltage sensing domains

The principle of voltage gating in a Kv channel is that a change in membrane voltage must cause a conformational change in the protein resulting in the transition of the channel into a state in which it can conduct potassium ions across the membrane. It is therefore reasonable to expect the components of the protein that move in response to a change in membrane voltage to be highly flexible domains, and it is this flexibility that has made it so difficult to determine the structure of these voltage sensing domains and their orientation relative to the channel pore (Jiang et al. 2003a; Long et al. 2005b).

Crystal structures for three voltage gated potassium channels have been reported. The first of these, KvAP, was from the thermophilic archaea *Aeropyrum pernix* (Jiang et al. 2003a); this structure, shown in Figure 1.13 shows the voltage sensing domains (S1-S4) of the protein to be very loosely attached to the pore domain of the protein, and outside the plane of the membrane, contrary to the expectation that helices S1-S6 would span the lipid bilayer in the usual manner. (Broomand and Elinder 2008). It was therefore suggested that the crystal structure shows a distorted structure, distortion arising from the use of a large Fab fragments to stabilise the voltage sensing domain and prevent aggregation during crystallisation; subsequent crystal structures in which smaller Fv fragments were used to bind the voltage sensors showed the voltage sensors within the plane of the membrane, although the helices did not adopt a fully transmembrane orientation (Lee et al. 2005). Subsequent studies suggested that the absence of lipid could also have been important in distortion of the structure (Long et al. 2005a; Long et al. 2007).

The second reported structure was of rat Kv1.2 (Figure 1.14). This showed the S1-S4 helices as a fully transmembrane cluster, and as in the KvAP structure, the voltage sensing domains were only loosely attached to the pore domain (Long et al. 2005a). Comparison of the Kv1.2 voltage sensing domains with those of KvAP showed that a consistent structural feature of the voltage sensing domains was a kink in S3, breaking the helix into two parts, denoted S3a and S3b, as shown in Figure 1.15 (Long et al. 2005b). Unfortunately the Kv1.2 structure exhibited poor electron density around the voltage sensors, so that the side chains of many of the residues, including those of the voltage sensing arginines, were poorly resolved. A

rigid structural unit consisting of a helix turn helix arrangement of the S3b and S4 helices (Figure 1.15) was observed in both of these structures and was termed the paddle motif; this motif contains the positively charged arginine residues implicated in voltage sensing.

Finally, the structure of a chimeric construct of Kv1.2 with the paddle motif Kv2.1 was determined in the presence of added lipid and shows a structure which is thought to be most similar to that of a Kv channel in the native membrane (Long et al. 2007). The crystal structure, shown in Figure 1.16, confirms the conserved structure of KvAP and the eukaryotic Kv channels. Figure 1.17 shows an alignment of the structure of the chimera with the voltage sensors of Kv1.2 and KvAP. It is clear that there is a high level of homology in the voltage sensors, with the charged amino acids almost superimposing in the structures. Further, the paddle motifs from the chimera and KvAP can be superimposed with good agreement indicating that the paddle motifs of both prokaryotic and eukaryotic Kv channels adopt a common structure, possibly with a large degree of mobility with respect to the S1 and S2 helices (Long et al. 2005a).

An interesting feature of the current structures of voltage gated potassium channels is that without exception, the voltage sensing domain of each subunit lies between the hydrophobic core of the membrane, and the pore domain of the neighbouring subunit (Figure 1.16). From the available crystal structures there appears to be little free space between the voltage sensing domain and the S5 helix and it has been suggested that the S4 and S5 helices of Kv channels show direct interactions (Neale et al. 2003; Soler-Llavina et al. 2006). It has, however, also been suggested that lipid could separate the voltage sensor from the pore, increasing the mobility of the sensor itself (Neale et al. 2007).

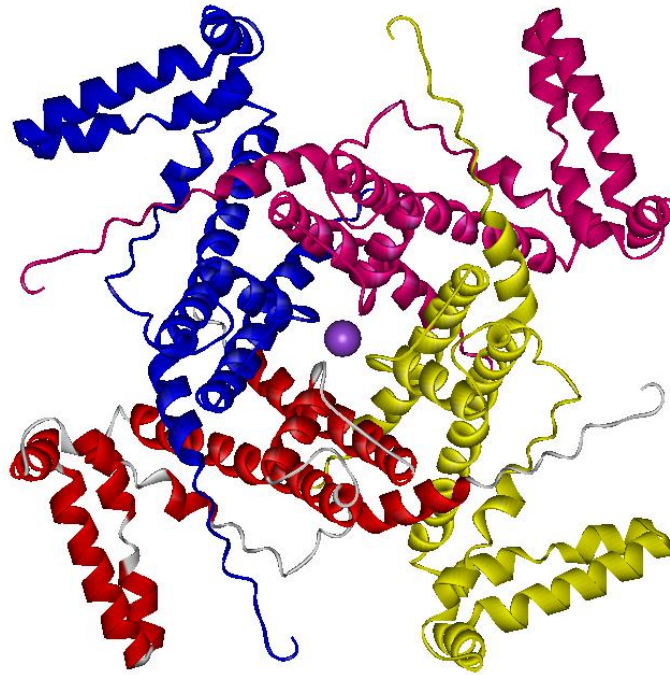
The available crystal structures of the voltage sensing domain allow a number of conclusions to be drawn about the structure of the voltage sensing domain of voltage gated potassium channels. The structure of the domain is evolutionarily conserved between prokaryotes and eukaryotes and there are very few structural differences between these domains from a variety of proteins (Lee et al. 2005), a conclusion confirmed by functional studies with chimeras. It is also evident that the voltage sensing domains form a four helix transmembrane cluster that is very

loosely attached to the pore domain, although conserved protein-protein contacts between the S4-S5 linker and the N terminus of S6 and between S1 and the pore helix have been suggested to be functionally important (Lee et al. 2009).

Basic biochemistry dictates that it is highly energetically unfavourable for charged groups such as the arginine residues in the S4 helix to reside within the hydrophobic core of a lipid bilayer. The location of the voltage sensing domains with respect to the lipid bilayer and to the pore domain is therefore a critical piece of information as this shows the extent of exposure of the voltage sensing arginines to the membrane. The structure of the chimera shows, in fact, that the Arg residues are not exposed to the lipid bilayer, but are either located in aqueous clefts or are in contact with negatively charged residues in the other helices (Figure 1.19). Importantly, the C terminal half of S4, which carries two of the gating charges, forms a 3_{10} helix, which means that all of the gating charges appear on one face of the helix (Long et al. 2007). The first two voltage sensing arginines of the S4 helix are in a position where they could interact with the lipid phosphodiester headgroup region (Lee et al. 2005; Long et al. 2007). The structure also shows two clusters of negatively charged amino acids from the S1 and S2 helices separated by a phenylalanine residue, projecting towards the S4 helix (Long et al. 2007); the second of the two voltage sensing arginine residues forms hydrogen bonds with the most extracellular of these negative clusters. The separation of the paddle motif from the S1 and S2 helices produces an aqueous crevice around the arginine residues which would allow water to penetrate up to 10 Å into the plane of the membrane within the voltage sensor; this is in agreement with prior work suggesting that the voltage sensing arginines faced a polar cleft in the voltage sensing domain (Cuello et al. 2005). Recent functional data and molecular simulations (Krepkiy et al. 2009a; Lu et al. 2002) have also shown that the electrostatic attraction of the most extracellular negative cluster, along with the presence of the aqueous crevice, allows the charged residues to be accommodated within the plane of the membrane in the closed state of the channel. Since the crystal structure corresponds to a situation with no membrane potential, it is thought that the crystal structure corresponds to the channel in an open, but probably inactivated state. Figure 1.19b shows a hypothetical closed state of the

channel, generated by a sliding downwards of helix S4 (Long et al 2007); this possible model for channel opening and closing is described below.

a)



b)

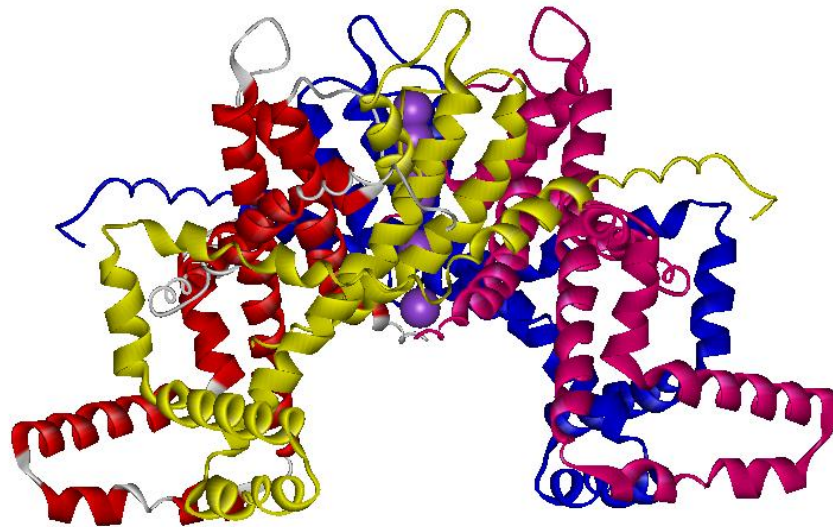


Figure 1.13: Crystal structure of the potassium channel KvAP **(a)** from the extracellular side with potassium ions shown in purple. Each subunit is shown as a distinct colour. The voltage sensing domains are loosely attached to the pore domain, and each voltage sensing domain makes contacts with the S5 helix of the neighbouring subunit. **(b)** KvAP from the plane of the membrane, showing that the voltage sensing domain helices S1-S4 are clearly not transmembranous modelled using Weblab ViewerPro (Molecular systems⁴⁴Inc.), PDB accession number 1ORQ.

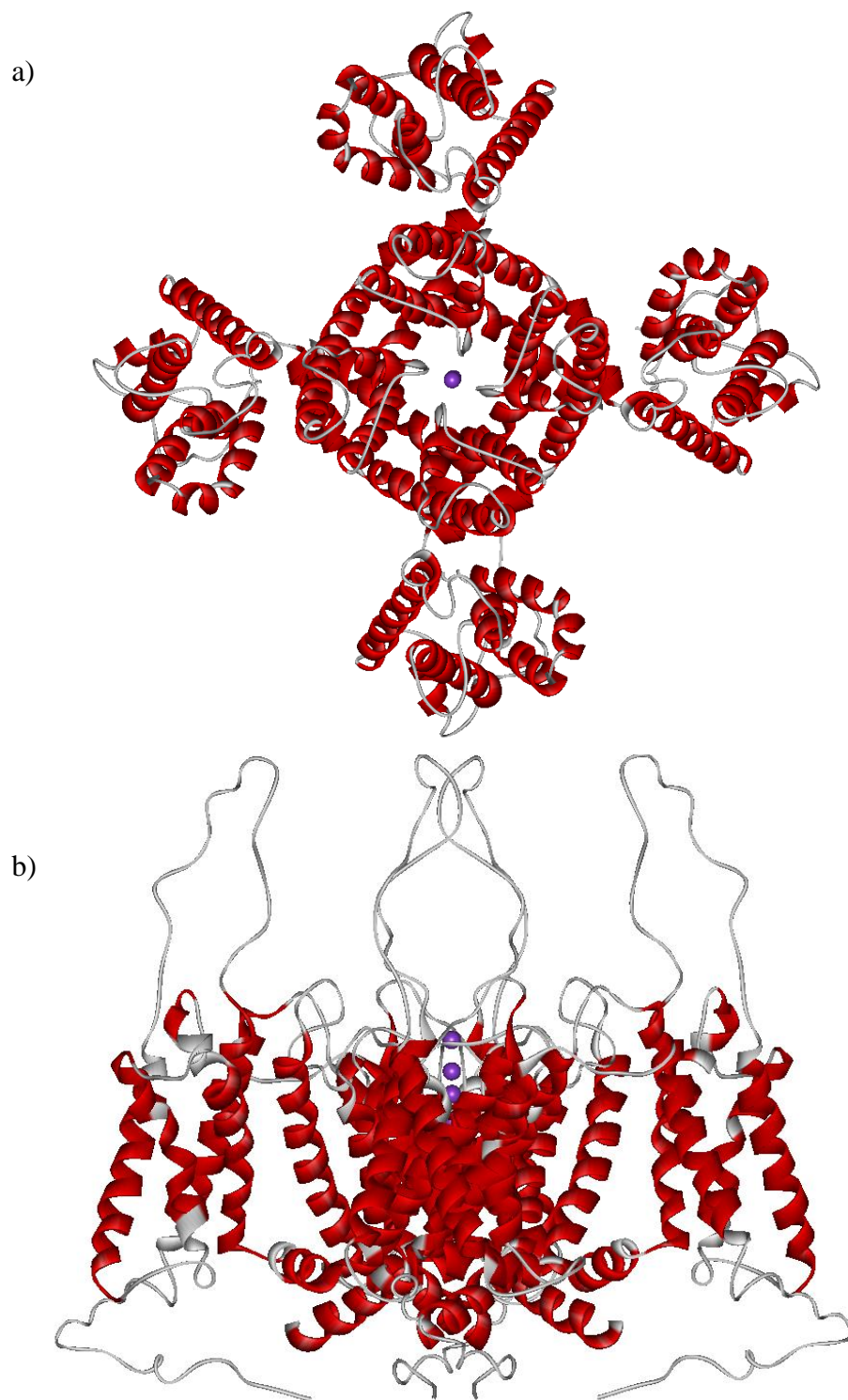


Figure 1.14: Crystal structure of rat Kv 1.2. **(a)** from the extracellular side and **(b)** a side view with the extracellular face on top. The voltage sensing domains appear fully transmembranous. Modelled using Weblab ViewerPro (Molecular systems Inc.) PDB accession code 3LUT

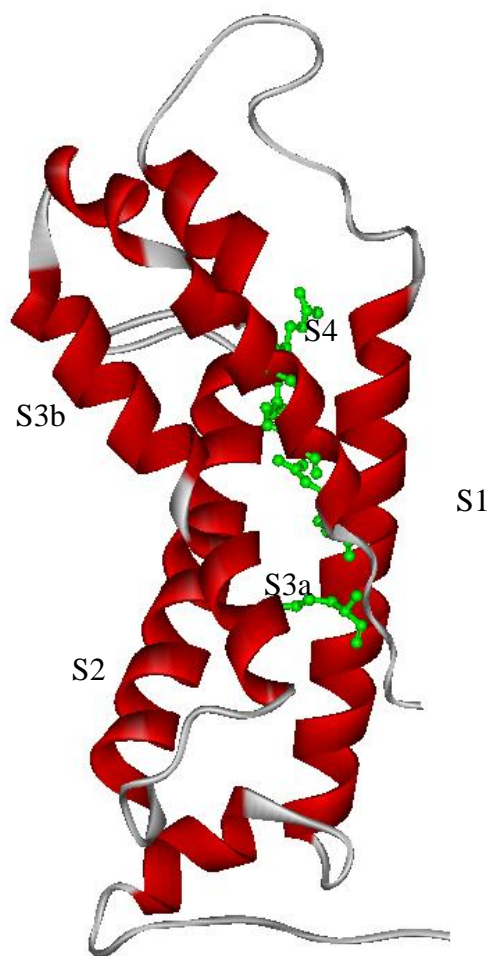


Figure 1.15: Voltage sensing domain of Kv 1.2-2.1 chimera. Gating charges are shown in green ball and stick format. The break in S3 is shown in grey and highlighted with an arrow. modelled using Weblab ViewerPro (Molecular systems Inc.), PDB accession number 3LUT

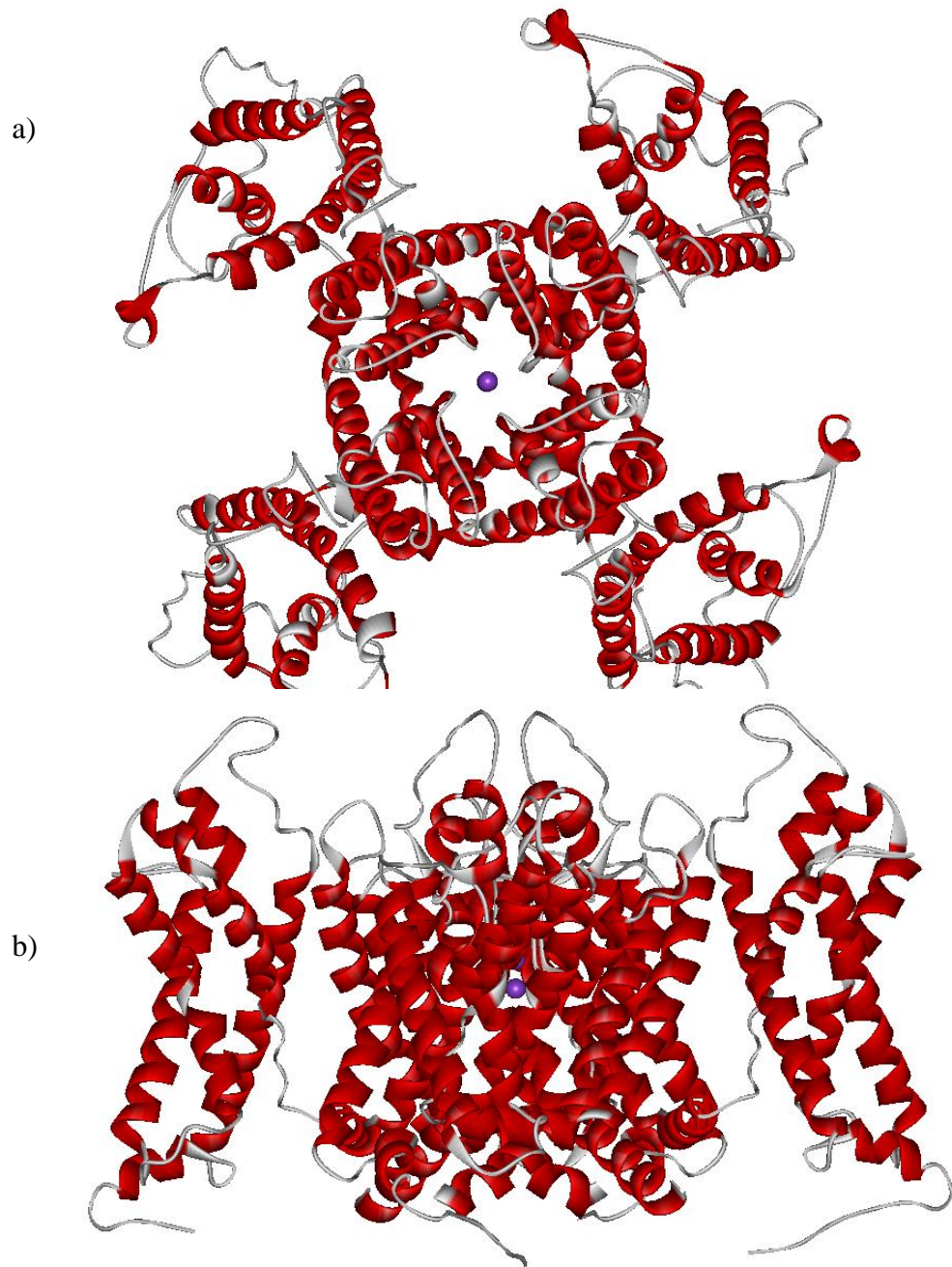


Figure 1.16: Structure of the rat Kv1.2 – 2.1 chimera. **(a)** From the extracellular side and **(b)** in the plane of the membrane with the extracellular face on top. The voltage sensing domains appear fully transmembranous, and match closely the structure of the voltage sensing domain of Kv 1.2. modelled using Weblab ViewerPro (Molecular systems Inc.) PDB accession number: 3LUT

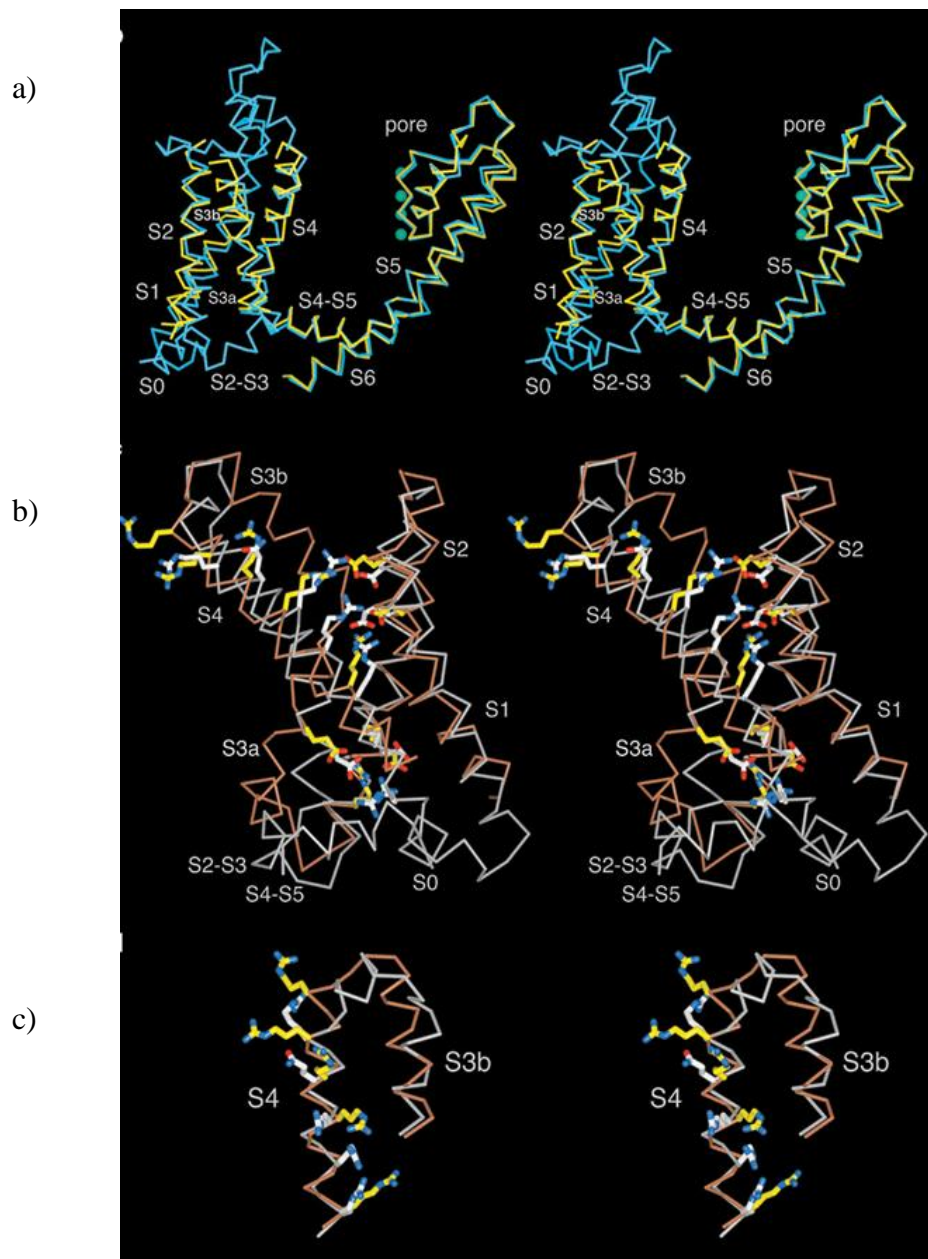


Figure 1.17: (a) Comparison of the chimera structure (blue, PDB ID: 2R9R) with the structure of Kv 1.2 (yellow, PDB ID: 2A79). The superposition of the structures shows a high level of agreement between the structures. (b) Superposition of the paddle chimera voltage sensor with the S1–S2 connecting loop removed (grey), and the isolated voltage sensor of KvAP (brown, PDB ID: 1ORS). Positively and negatively charged amino acids are shown in stick format (KvAP yellow, chimera, white). (c) Comparison of the S3b–S4 voltage sensor paddles from KvAP and the chimera paddle motif. From Long et al. 2007

1.6.6 Mechanism of voltage gating

Depolarisation of a membrane is detected by the voltage sensing domains of a voltage gated potassium channel leading to opening of the gate of the channel. As described above, crystal structures of Kv channels often show distorted structures because of the flexible attachment of the voltage sensor to the pore, so that techniques able to study Kv channels in native lipid bilayers are required to get a full picture of channel structure. There is also a problem as to the actual state of the channel in an X-ray crystal structure; as described above, the structure is likely to correspond to some kind of open state of the channel, so that again other techniques must be used to probe the structure of the closed state voltage sensor.

1.6.6.1 Gating current

In order to sense a change in membrane potential, a voltage sensor must contain charges in the electric field which are able to move upon a change in membrane potential (Hodgkin and Huxley 1952). The four conserved arginine residues in the S4 helix have been identified as the gating charges in voltage gated potassium channels (Aggarwal and MacKinnon 1996). The gating current is the current created when the gating charges move from one side of the membrane electric field to the other; however this current can be hard to measure as the gating current of a single channel is in the region of 10^{-15} A, around 100 times less than the current caused by the channel itself (Tombola et al. 2006). The gating current is transient, and can therefore only be accurately measured when there are a large number of channels in the membrane and the pore of the channel is blocked to eliminate the pore current (Bezanilla and Stefani 1998).

Gating current measured in this way can provide information about the total number of charges which move through the membrane in response to a change in membrane voltage. This has been calculated experimentally for the shaker potassium channel and a total of 13 charges per channel were found to cross the membrane electric field (Aggarwal and MacKinnon 1996; Schoppa et al. 1992; Seoh et al. 1996), equating to 3.25 charges per subunit per activation event crossing the membrane electric field. Molecular dynamic simulations have shown that the equivalent charge movement for Kv1.2 is very similar at 12.7 charges crossing the

membrane electric field (Khalili-Araghi et al. 2010) The voltage sensing arginines therefore must translocate from contact with the intracellular solution in the inactive conformation of the channel, to contact with extracellular solution in the active state of the channel (Miller 2003). However the mechanism by which the charges actually change their exposure from intracellular to extracellular solution is still a matter of active debate.

1.6.6.2 The Paddle Model

A number of mechanisms have been proposed by which the voltage sensor of a voltage gated potassium channel could react to a change in voltage and subsequently open the channel; these theories differ mainly in the extent of movement of the gating charges. The paddle model was initially proposed following the determination of the first crystal structure of KvAP (Jiang et al. 2003a). The paddle model involved a translocation of the gating charges by up to 20 Å with the paddle motif moving as a rigid structure through the hydrophobic core of the membrane. Not surprisingly, this theory met strong criticism because of the exposure of the gating charges to the hydrophobic core of the membrane (Cohen et al. 2003). The more recent crystal structures of Kv1.2 and of the Kv1.2-2.1 chimera have resulted in a considerable revision of the model (Figure 1.19) (Long et al. 2007), although the translocation of some of the gating charges through the membrane is still around 15 Å, about half the thickness of the hydrophobic core of a pure dioleoylphosphatidylcholine bilayer (King and White 1986). The proposed closed state structure of the voltage sensor is shown in Figure 1.19 in which the voltage sensing arginines are exposed to the intracellular solution, stabilised by the internal negative cluster mentioned above. The S4-S5 linker helix is in a lower position in the closed model than in the open structure; this in turn exerts a force on the pore domain, constricting the pore and closing it (Long et al. 2007). In response to a depolarisation of the membrane, the S1 and S2 helices remain stationary, the paddle motif bends outwards from the S1 and S2 helices and translocates 15 Å perpendicular to the membrane towards the extracellular solution (Long et al. 2007) into the open state described above. A large movement of arginine residues is supported by experiments involving cysteine scanning mutagenesis of KvAP voltage sensors combined with a tethered biotin-avidin

accessibility assay (Figure 1.19) (Ruta et al. 2005). It was found that biotin attached by a 10 Å linker to cysteine residues introduced next to the gating charges was able to bind avidin from the internal side of the membrane in the resting state but not the activated state (Figure 1.20). In the model, movement of the S4 helix towards the extracellular solution would move the S4-S5 linker, so that movement in the voltage sensor would exert a force on the S5 helix of the pore domain, releasing the constriction of the pore.

1.6.6.3 Helical Screw model

The helical screw model was initially proposed when it was found that mutation of some of the gating charges in potassium channels to His lead to the conduction of protons through the voltage sensor in a voltage dependent manner (Starace et al. 1997). When the C terminal gating charge of the S4 helix of the Shaker potassium channel was mutated to a histidine, each voltage sensor of the channel became a proton pore in the activated state, whereas changing the first gating charge to a histidine turned the voltage sensors into proton pores in the resting state (Starace and Bezánilla 2001). These findings suggested that there is an aqueous pore through which the arginine residues can translocate, consistent with the large proteinaceous crevices found in voltage sensors in the recent crystal structures. The presence of such crevices mean that the distance between the intracellular and extracellular solutions is much less than the thickness of the hydrophobic core of the bilayer, focussing the electric field of the membrane so that the gating charges do not have to move as far to change their exposure from intracellular to extracellular.

The helical screw model proposes a smaller translocation of the gating charges than the 15 Å movement proposed in the paddle model, and is supported by cysteine cross linking and metal bridge formation experiments defining the positions of the gating charges of S4 with relation to S1 and S2 in the closed state. The experiments suggest that the S4 helix undergoes a translation of just 6.5 Å from intracellular to extracellular solution (Campos et al. 2007). Fluorescence resonance energy transfer experiments have also suggested that movement of the S4 helix during voltage sensing is considerably less than that predicted by the paddle model (Cha et al. 1999; Glauner et al. 1999; Posson et al. 2005).

The helical screw model proposes a rotation of S4, concurrent with vertical translocation of the helix; without his rotation the proposed small translocation of S4 would not be enough to change the exposure of the gating charge from intracellular to extracellular. The S4 helix was suggested by Campos et al. (2007) to rotate by about 180° but other studies have suggested a smaller degree of rotation (Glauner et al. 1999; Posson et al. 2005).

1.7 Aims and objectives

It is evident that there is wealth of information relating to voltage gated potassium channels which has been gathered from a multitude of experimental techniques. Crystallography has been a hugely influential experimental technique in gathering huge amounts of data on voltage gated potassium channels. The original KcsA crystal structure (Doyle et al. 1996) has given us a datum structure for a general potassium channel pore domain, and subsequent structures of Kv channels have allowed us to probe the structure function relationship of such channels. The major disadvantage of this technique is that in order to crystallise the channels, they must be removed from their native membrane environment and immersed in detergent, which is regarded as a poor mimic for the lipid bilayer (Sonoda et al 2011). As such, experimental data for membrane proteins returned from crystallography bears the caveat that it is possible that the structure does not completely resemble that of the protein in the lipid bilayer, and it is therefore hard to accurately determine parameters such as the hydrophobic thickness of a protein. For a protein such as KvAP this is a particular problem; as described above, the flexible nature of the voltage sensors and their reliance on membrane structure for function means that the hydrophobic thickness of the protein in their vicinity, and the hydrophobic thickness of the surrounding bilayer are key to the function of the channel.

Electrophysiological data is a partial answer to the problems facing crystallography because electrophysiology requires a membrane protein to be reconstituted in a lipid bilayer if it is to record a channel is to functioning normally. Electrophysiology has been hugely useful in determining the nature of structural changes in channel proteins (Marius et al. 2005), and can to some extent, localise

those changes which lead to altered function, however, it is uncommon that such experimental procedures definitively pinpoint such changes on a molecular level.

Molecular dynamics simulations can be used to probe channel proteins such as KvAP at a molecular level, and can be used to determine a huge amount of data relating to a protein, such as the hydrophobic thickness around any area of a protein, and the strength of a membrane electric field acting on a voltage sensor. A number of considerations must be taken into account when examining data retrieved from molecular dynamics simulations. The inherent complexity and scale of membranes cannot yet be exactly modelled using molecular dynamics; simulations to date rely on large simplifications and assumptions, as well as occurring over microsecond timescales.

This work, therefore, aims to address some of the challenges of the above techniques using fluorescence spectroscopy. Like electrophysiology, fluorescence spectroscopy can be used to explore the properties of membrane proteins which have been reconstituted into a bilayer. With the aid of site directed mutagenesis and fluorescent molecules which are highly sensitive to the hydrophobicity of the local environment, fluorescence techniques are able to report on the environment surrounding individual amino acids. It should therefore be possible to describe the hydrophobicity profile of targeted regions of KvAP and relate these back to previously gathered data.

Since it has been previously established that there is considerable contacts of the pore domain with the voltage sensing domain (Ruta et al. 2004, Long et al. 2007), this work will focus on the outer pore helix, S5, and aim to probe the interactions of the voltage sensing domain with the S5 helix, and compare this to previously published crystallographic data through the removal of the voltage sensing domains of KvAP. As discussed above, the properties of the phospholipid bilayer surrounding KvAP are likely to have a large effect on both the structure and function of the protein, this work also aims to determine the thickness of the bilayer in the region of the S5 helix, and therefore, the voltage sensing domain.

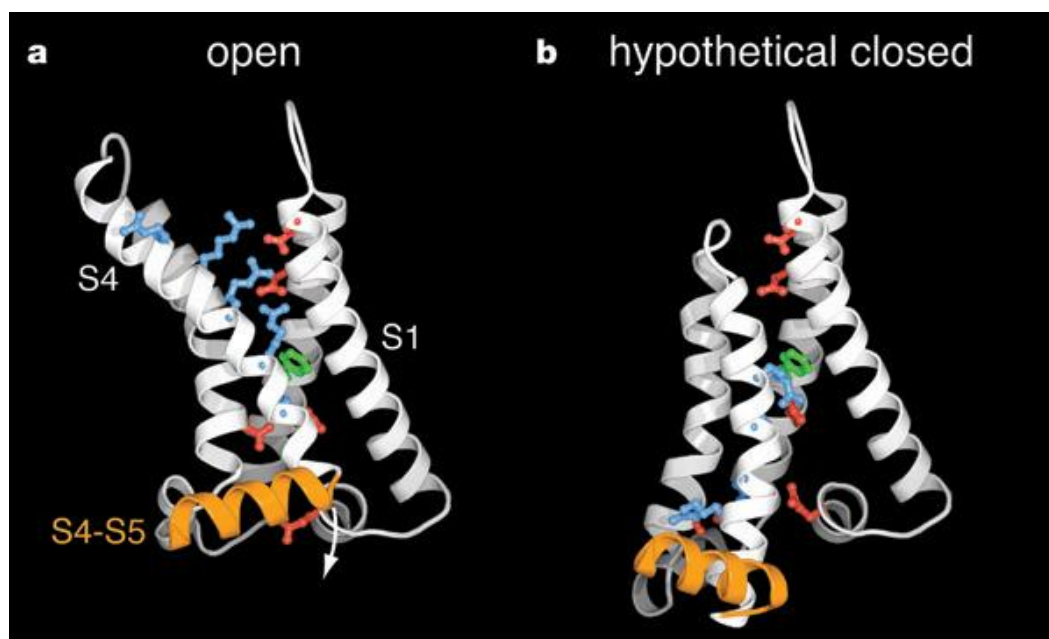


Figure 1.18: (a) Representation of the open structure of the voltage sensor of a voltage gated potassium channel from the chimera crystal structure viewed from the pore with the extracellular solution above and the intracellular solution below. The gating charges (R1 to K5) are shown as blue sticks. Negatively charged residues in the external and internal clusters are shown in red; the phenylalanine between the two clusters is green. The positively charged residues reach ‘outward’ towards the extracellular solution. (b) Depiction of a hypothetical closed state of the voltage sensor. The S1 and S2 helices have maintained their position, whereas the S3–S4 paddle moves inward. The positive charges on S4 now reach towards the intracellular solution, and are stabilized by the internal negative cluster. The α -carbon position of R1 is adjacent to the phenylalanine, representing a translation perpendicular to the plane of the membrane of approximately 15Å relative to the open structure. Adapted from Long et al. 2007.

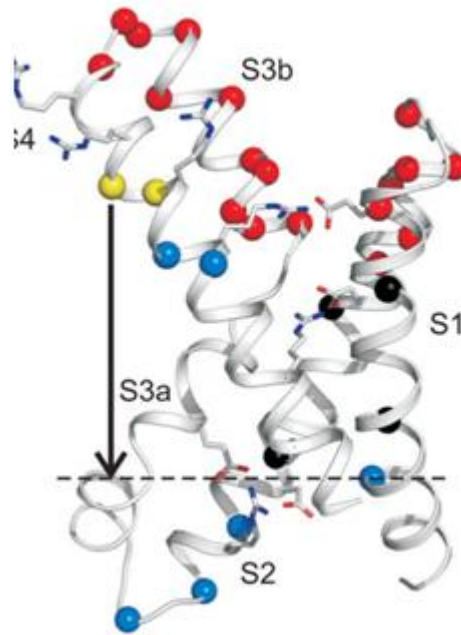


Figure 1.19: Ribbon diagram of the structure of the S1–S4 domain of KvAP, showing the accessibility of tethered biotinylated cysteines to avidin. Positions marked by red spheres are only accessible to external avidin, those marked by blue spheres are only accessible to internal avidin, and those marked by yellow spheres are accessible to both external and internal avidin. Black spheres show inaccessible positions. From Swartz (2008)

2 Chapter 2: Materials and Methods

2.1 Materials

All chemicals were supplied by Sigma Aldrich unless specified otherwise in the text.

2.2 Methods

2.2.1 Microbiological techniques

2.2.1.1 Sterilisation of materials

Utensils and solutions were autoclaved at 121 °C for 20 minutes at 15 lbs.sq.inch. Antibiotic solutions were sterilised by passing through a 0.22 µm filter.

2.2.1.2 Stock antibiotics

Ampicillin was dissolved in distilled water to a final concentration of 100 mg ml⁻¹. Tetracycline was dissolved in distilled water to a final concentration of 20 mg ml⁻¹ and sterilised as in section 2.2.1.1.

2.2.1.3 Luria Bertani (LB) Broth

Luria broth was made by adding 20.6 g of LB EZ mix per litre of distilled water and autoclaving as above. Once the temperature of the LB broth fell below 50 °C ampicillin was added to a final concentration of 100 µg ml⁻¹ unless otherwise stated.

2.2.1.4 Luria Bertani Agar

10 g of agar was added to 1 l of LB broth. The mixture was then sterilised as above. Once the temperature of the LB agar fell below 50 °C ampicillin was added to a final concentration of 100 µg ml⁻¹. LB agar was then poured into sterile 10 cm agar plates and left to set; plates were stored at 4 °C until use.

2.2.1.5 Escherichia coli strains

Escherichia coli strain XL-1 blue (Invitrogen) was used for all microbiological work. XL-1 blue cells have the genotype *recA1*, *endA1*, *gyrA96*, *thi-1*, *hsdR17*, *supE44*, *relA1*, *lac* [*F'* *proAB lacIqZΔM15*], and *Tn10*.

2.2.1.6 Vectors

The gene encoding KvAP inserted into the vector pQE60 (Qiagen) between *Bgl*II and *Nco*I restriction sites was kindly donated by Professor R. MacKinnon. The resulting gene, when expressed, encodes KvAP with a C terminal hexahistidine tag.

2.2.1.7 Seed cultures

10 ml of LB broth containing ampicillin was poured into a sterile universal tube and inoculated with a bacterial colony from a LB agar plate containing the appropriate antibiotic. This was incubated for 18 hours at 37 °C.

2.2.1.8 Glycerol stocks

0.75 ml of sterilised glycerol was mixed with 1 ml seed culture in a sterile cryotube (Greiner) and stored at -80 °C.

2.2.1.9 Preparation of heat shock competent cells

A seed culture of XL-1 blue cells containing 20 µg ml⁻¹ tetracycline was used to inoculate 1 l of LB broth in a conical flask containing 20 µg ml⁻¹ tetracycline. This was incubated at 37 °C until the culture reached an optical density at 600 nm (OD₆₀₀) of 0.5. The cells were then collected by spinning at 6000 rpm in a Beckman J20 XPI centrifuge for 15 minutes; the supernatant was discarded, and the cells resuspended in 100 ml ice cold sterile CaCl₂ and left on ice for 30 minutes. The cells were then collected by spinning at 3000 rpm in a Heraeus Labofuge 400e and resuspended in 20 ml ice cold sterile CaCl₂ containing 10 % glycerol. 200 µl aliquots were stored at -80 °C until use in 100 µl aliquots.

2.2.1.10 Transformation of plasmid DNA

Competent cells prepared as per section 2.1.1.9 were thawed on ice and transferred to a sterile 15 ml centrifuge tube. 50 ng plasmid DNA was added to the cells, which were then incubated on ice for 30 minutes. The cells were transferred to a 42 °C water bath for 45 seconds and then returned to ice for two minutes. The cells were supplemented with 900 µl sterile LB broth and incubated for 1 hour at 37 °C, shaking at 200 rpm. Transformants were selected by spreading 200 µl of the transformed cells onto an LB agar plate containing ampicillin at 100 µg ml⁻¹.

2.2.2 Molecular Biology

2.2.2.1 Cloning of KvAP

The gene encoding KvAP in the pQE-60 vector was a kind gift from Professor R. MacKinnon. The vector is shown in Figure 3.1. The pQE-60 vector must be grown in cells which encode the *lac* repressor, such as the XL-*x* Blue series in order for protein expression to be inducible by isopropyl β-D-1-thiogalactopyranoside (IPTG). pQE-60 also carries a C terminal hexahistidine tag with a downstream trypsin cleavage sequence. This makes the protein product of the plasmid suitable for purification by NiNTA column affinity chromatography.

2.2.2.2 Agarose gel electrophoresis

2.2.2.2.1 50 x TAE Solution

Stock 50x TAE solution was made by dissolving 1.9 g Ethylenediaminetetraacetic acid disodium salt (Na EDTA) and 242.2 g tris(hydroxymethyl)aminomethane (TRIS) in 500 ml distilled water. 57.1 ml of Acetic Acid was added, and the pH adjusted to 8.0. The solution was made to 1 l with distilled water. 50x TAE buffer was diluted 1:50 with distilled water before use.

2.2.2.2.2 DNA gel loading buffer

30 mg of Bromophenol blue was mixed with 0.2 ml 50x TAE buffer and 3 ml sterile glycerol; the solution was made to 10ml with distilled water.

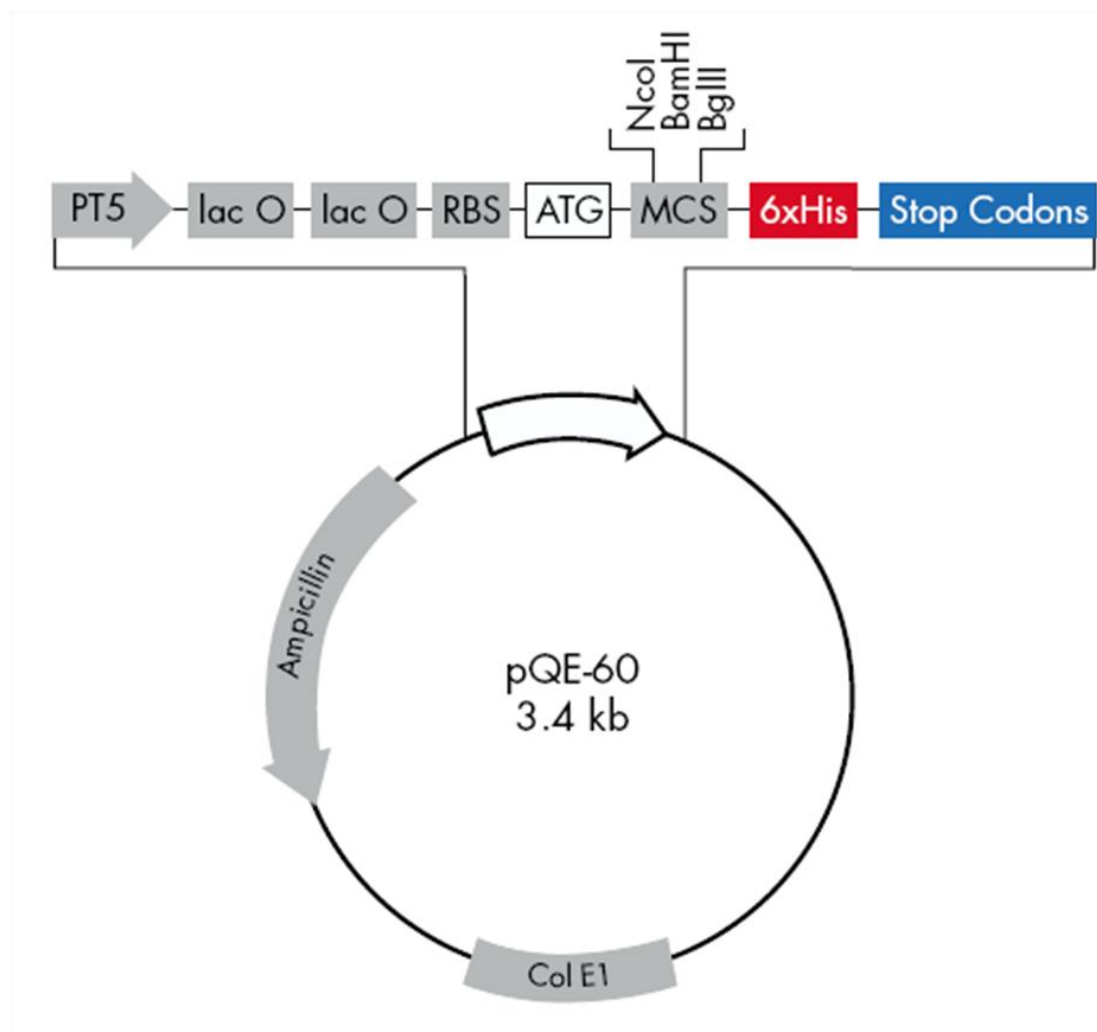


Figure 2.1: Vector map of the pQE-60 vector. The map shows the ampicillin resistance gene and the colicin resistance gene. The white arrow indicates the position of the inserted gene, KvAP in this case. Abbreviations shown represent: PT5 – PT5 promoter., lacO – Lac operon, RBS – Ribosome binding site, ATG – Start of transcription; MCS – multiple cloning site, 6xHis – Polyhistidine tag encoding sequence.

2.2.2.2.3 Ethidium Bromide solution

100 mg ethidium bromide was added to 10 ml analytical reagent grade water.

2.2.2.2.4 DNA electrophoresis

1 % agarose (w/v) was added to 100 ml 1 x TAE solution and heated until dissolved. Ethidium bromide solution made as per section 2.1.2.1.3 was added to a final concentration of $0.5 \mu\text{g ml}^{-1}$. The agarose solution was then poured into a horizontal gel tank and left to set at room temperature. DNA was mixed 4:1 with loading buffer before loading, and was run alongside 1 μl DNA ladder mixed 1:1 with DNA loading buffer. The gel was submerged in 1 % TAE solution and electrophoresis was carried out at 120 V for 30 minutes. DNA was subsequently visualised under ultraviolet light in a Gene Genius imaging system (Syngene).

2.2.2.3 Purification of plasmid DNA

Plasmid DNA was purified using a Promega *Wizard*® plasmid purification system. A seed culture was inoculated with a single colony containing the desired plasmid from a selective agar plate, and grown for 18 hours at 37 °C. Cells were harvested by centrifugation at 3000 rpm for 10 minutes in a Heraeus Labofuge 400e and plasmid DNA was extracted from the pellet as directed by the manufacturer's instructions, eluting the plasmid DNA in 50 μl sterile water into a sterile 1.5 ml microcentrifuge tube. Purity of plasmid DNA was assessed by running 3 μl of the plasmid DNA with 3 μl running buffer on a 1 % (w/v) agarose gel containing $0.5 \mu\text{g ml}^{-1}$ ethidium bromide, and the concentration determined by absorbance at 260 nm as per section 2.1.2.3.

2.2.2.4 DNA cleanup

DNA cleanup was undertaken using a Wizard PCR cleanup kit (Promega). A volume of Membrane Binding Solution equal to the volume of the PCR reaction was added to the PCR reaction microcentrifuge tube. One SV Minicolumn was placed in a collection tube and the PCR reaction/ membrane binding solution mixture was transferred to the SV Minicolumn assembly and incubated for 1 minute at room temperature. The SV Minicolumn assembly was centrifuged in a

tabletop microcentrifuge at $16,000 \times g$ (14,000 rpm) for 1 minute. The SV Minicolumn was removed from the spin column assembly and the liquid in the collection tube discarded. The SV Minicolumn was inserted into the collection tube. The column was washed by adding 700 μ l of Membrane Wash Solution, previously diluted with 95% ethanol and centrifuged for 1 minute as before. The collection tube was emptied as before and the SV Minicolumn placed back in the collection tube. This was repeated with 500 μ l of Membrane Wash Solution and the SV Minicolumn was centrifuged for 5 minutes at $16,000 \times g$. The SV Minicolumn assembly was removed from the centrifuge. The collection tube flow through was discarded and the column recentrifuged for 1 minute as before but with the lid open to allow evaporation of any residual ethanol. The SV Minicolumn was transferred to a clean 1.5 ml microcentrifuge tube and 50 μ l of nuclease free water was added directly to the centre of the column and the column was incubated at room temperature for 1 minute. The column was then centrifuged for 1 minute as before. The eluted DNA was stored at -20°C until use.

2.2.2.5 Gel extraction of DNA

Gel extraction is an efficient method of separating different size DNA fragments, for example, after digestion or ligation. DNA samples were run in separate lanes on an agarose gel, the gel was placed on a transilluminator to visualise the digested DNA. The region of the gel containing the cut plasmid was excised using a sterile scalpel blade and placed in a 0.5 ml microcentrifuge tube with a siliconised glass wool plug at the bottom. The tube was sealed and frozen in liquid nitrogen for 5 minutes. A hole was then pierced in the top and bottom of the microcentrifuge tube and it was placed inside a 1.9 ml microcentrifuge tube. The tube was then spun at 10,000 rpm in a tabletop microcentrifuge for four minutes. The flow through was kept and underwent a PCR cleanup as described in Section 2.2.2.4.

2.2.2.6 Measurement of DNA concentration

The absorbance at 260 nm of a 50 x dilution of plasmid DNA was measured on a Hitachi U-2001 spectrophotometer. DNA concentration was then calculated using a modified Beer-Lambert equation with an extinction coefficient for double stranded DNA of 50:

Equation 2.1

$$[\text{DNA}] (\text{ng } \mu\text{l}^{-1}) = A_{260} \times \delta \times \varepsilon$$

where δ is the dilution factor and ε is the extinction coefficient. The purity of the DNA was assessed by measuring the absorbance ratio of the solution at 260:280 nm.

2.2.2.7 Ethanol precipitation of plasmid DNA

Plasmid DNA purified as described in Section 2.2.2.3 was precipitated from solution for sending for sequencing. 10 μl of 3M sodium acetate was added for every 2.5 μg purified plasmid DNA in the solution calculated using the concentration determined as per section 2.1.2.3. 200 μl ice cold ethanol was added to the sample, and the mixture incubated on ice for 30 minutes. The mixture was then centrifuged at 14,000 x g for 20 minutes in an Eppendorf 5415C centrifuge. The supernatant was removed from the sample and replaced with 1 ml ice cold 70 % (v/v) ethanol. The sample was centrifuged for a further 10 minutes at 13,000 x g and the supernatant discarded. The microcentrifuge tubes were then covered with a dry paper towel and allowed to air dry at room temperature.

2.2.2.8 Restriction digests

Restriction digests were performed in sterile 0.5 ml microcentrifuge tubes with a total reaction volume of 200 μl . Digests contained 10 μl bovine serum albumin (1 mg ml^{-1}), 10 μl of each restriction enzyme used (10 U μl^{-1}), 1 μg DNA and sterile distilled water to a final volume of 200 μl . Digests were incubated at 37°C. Digest products were visualised using a 1 % agarose gel as described in Section 2.2.2.2.

2.2.2.9 Quikchange site directed mutagenesis

Site directed mutagenesis was performed using a modified Quikchange method (Stratagene) and is summarised in Figure 2.2. This method utilises the polymerase chain reaction to amplify the template DNA; the primers used to allow the

polymerase to elongate the new DNA chain contain mismatches to the template DNA which encode the required mutation. This allows the production of mutated, unmethylated ssDNA containing the required mutation. Reactions were performed in 0.5 ml microcentrifuge tubes in an MJ research PTC-200 thermal cycler. Reactions contained 1 µl template plasmid DNA (50 ng µl⁻¹), 1.5 µl forward primer (10 µM), 1.5 µl reverse primer (10 µM), 1 µl deoxyribonucleoside triphosphates (25 mM), 2 µl magnesium chloride (25 mM), 1 µl DMSO, 5 µl 10 x *Pfu* polymerase reaction and sterile distilled water to 50 µl.

The theoretical annealing temperature of each individual primer in each primer pair was calculated using Equation 2.2, and the lowest value calculated used as the annealing temperature for the reaction

Equation 2.2

$$\text{Annealing Temperature (}^{\circ}\text{C)} = 4 \times (C + G) + 2 \times (A + T) - 5$$

where A, T, C and G are the number of adenosine, thymine, cytosine and guanine bases of the primer 5' of the mismatch. Cycling conditions involved denaturation at 95 °C for 30 seconds, annealing at the calculated annealing temperature for 60 seconds and extension at 68 °C for 8 minutes 40 seconds (2 minutes kb⁻¹). This cycle was repeated 20 times and the temperature dropped to 4 °C. Samples were analysed on a 1 % (w/v) agarose gel as described in Section 2.2.2.2 to confirm the size and purity of the product.

Following mutagenesis, the methylated template DNA was digested using *dpnI*. 1 µl *dpnI* was added to the PCR reaction and incubated at 37 °C for 2 hours. The resulting DNA was transformed into competent XL-1 Blue cells as described in Section 2.2.1.10.

2.2.2.10 Two stitch PCR

Two stitch PCR can be used to excise region of DNA from a contiguous sequence, and the protocol for two stitch PCR is summarised in Figure 2.3

2.2.2.10.1 Two Stitch PCR Reaction 1

Reaction mixtures contained 2 μl Template KvAP DNA 50 ng μl^{-1} , 10 μl *pfu* polymerase 10x reaction buffer (Promega), 2.5 μl of forward primer (as shown in Table 3.2 (Reaction 1a – primer 1; reaction 1b – primer 2), 2.5 μl of forward primer (Reaction 1a – primer 2; reaction 1b – primer 4), 0.8 μl 10 mM dNTPs and sterile distilled water was added to 98 μl . 2 μl *pfu* polymerase (Promega) was added immediately before reaction.

The reaction was carried out in thick walled 500 μl microcentrifuge tubes with a final reaction volume of 50 μl . The reaction mixture was placed in a Peltier Thermal Cycler PTC-200 with the following conditions:

1. 95 °C for 45 seconds,
2. 95 °C for 45 seconds,
3. 55 °C for 45 seconds,
4. 72 °C for 1.5 minutes
5. Return to step 2 29 times
6. 72 °C for 10 minutes
7. 4 °C forever

The concentrations of the amplified products were determined by running on an agarose gel.

2.2.2.10.2 Two Stitch PCR Reaction 2

Reaction mixtures contained 6 μl of the product of reaction 1a, 4 μl of the product of reaction 1b, 10 μl *pfu* polymerase 10x reaction buffer (Promega), 1 μl 10 mM dNTPs and the mixtures were made to 98 μl with sterile distilled water. Immediately before reaction 2 μl *pfu* polymerase (Promega) was added.

The second reaction utilises the 3' overhangs generated by the 19bp primer mismatches of the primers in the first reaction. This causes the two products of the first reaction to act as primers for each other to create the full length product required. The two products from reactions 1a and 1b respectively were added to the PCR reaction at a 1:1 molar ratio. The reaction was carried out in thick walled 500 μl microcentrifuge tubes with a final reaction volume of 50 μl . The reaction

mixture was placed in a Peltier Thermal Cycler PTC-200 with the following conditions:

1. 95 °C for 45 seconds,
2. 95 °C for 45 seconds,
3. 65 °C for 45 seconds,
4. 72 °C for 1.5 minutes
5. Return to step 2 4 times
6. 4 °C forever

2.2.2.10.3 Two Stitch PCR Reaction 3

2.5 µl of primer 1 and 2 were then added to the two stitch PCR reaction described above and the reaction was continued under the following conditions:

1. 95 °C for 45 seconds,
2. 95 °C for 45 seconds,
3. 65 °C for 45 seconds,
4. 72 °C for 1.5 minutes
5. Return to step 2 29 times
6. 72 °C for 10 minutes
7. 4 °C forever

2.2.2.11 Sequencing of plasmid DNA

A seed culture was inoculated with a bacterial colony grown on a selective media plate containing the plasmid to be sequenced and incubated overnight at 37 °C with shaking. DNA was extracted from the seed culture as described in Section 2.2.2.3 and ethanol precipitated as described in Section 2.2.2.7 and sent to Eurofins MWG Operon for automated sequencing.

2.2.2.11.1 Quality assurance of sequencing data

Sequencing of cysteine mutants of KvAP occurred at MWG Operon. Resultant sequences were assessed for mutations and for quality. Sequencing from this source has a high quality read length of 1100 bases, the full length KvAP sequence from the initiator ATG to the end of the polyhistidine tag is 991 bases, therefore

sequencing was only undertaken in one direction. Where sequencing data confirmed the presence of the correct mutation, sequencing data underwent quality assurance to ensure that the sequencing data were correct. NCBI BLAST was used to compare the returned sequence to the wild type sequence with polyhistidine tag attached in order to confirm the presence of the desired mutation. In order for the cell line to progress to protein purification, the nucleotide sequence had to be 100% correct. MWG Operon provides an indication of sequencing quality with their results; each nucleotide is rated on a quality scale of 1 – 30 (1 - low quality, 30 - high quality). Only if the whole sequence was above a level of 20, and the nucleotide sequence correct, was the sequencing classed as successful. If sequencing was of good quality, but the sequence incorrect, the mutagenesis was repeated, however if the sequencing was of poor quality, the mutant was resequenced.

2.2.2.12 Ligation

Where it was necessary for an insert to be ligated into the vector as shown in Figure 2.3. A number of ligation reactions were undertaken with varying insert to vector ratios as seen in the following Table

<i>Reaction number Reagent</i>	<i>1 (μl)</i>	<i>2 (μl)</i>	<i>3 (μl)</i>	<i>4 [control] (μl)</i>
Vector	4	4	4	4
Insert	12	6	3	0
Sterile Water	0	6	9	14
T4 Buffer	2	2	2	2
T4 Ligase	2	2	2	2

The reaction was left for 24 hours at 16 °C and frozen until use.

2.2.2.12.1 Dialysis of ligation mixture

20 µl of the DNA solution from the ligation in section 3.2.4.9 was placed on a nitrocellulose filter which was subsequently floated on 200 ml 10% glycerol solution stirring gently for 20 minutes. 5 µl of the remaining solution was removed after 20 minutes and placed in a 500 µl microcentrifuge tube at -20 °C until needed.

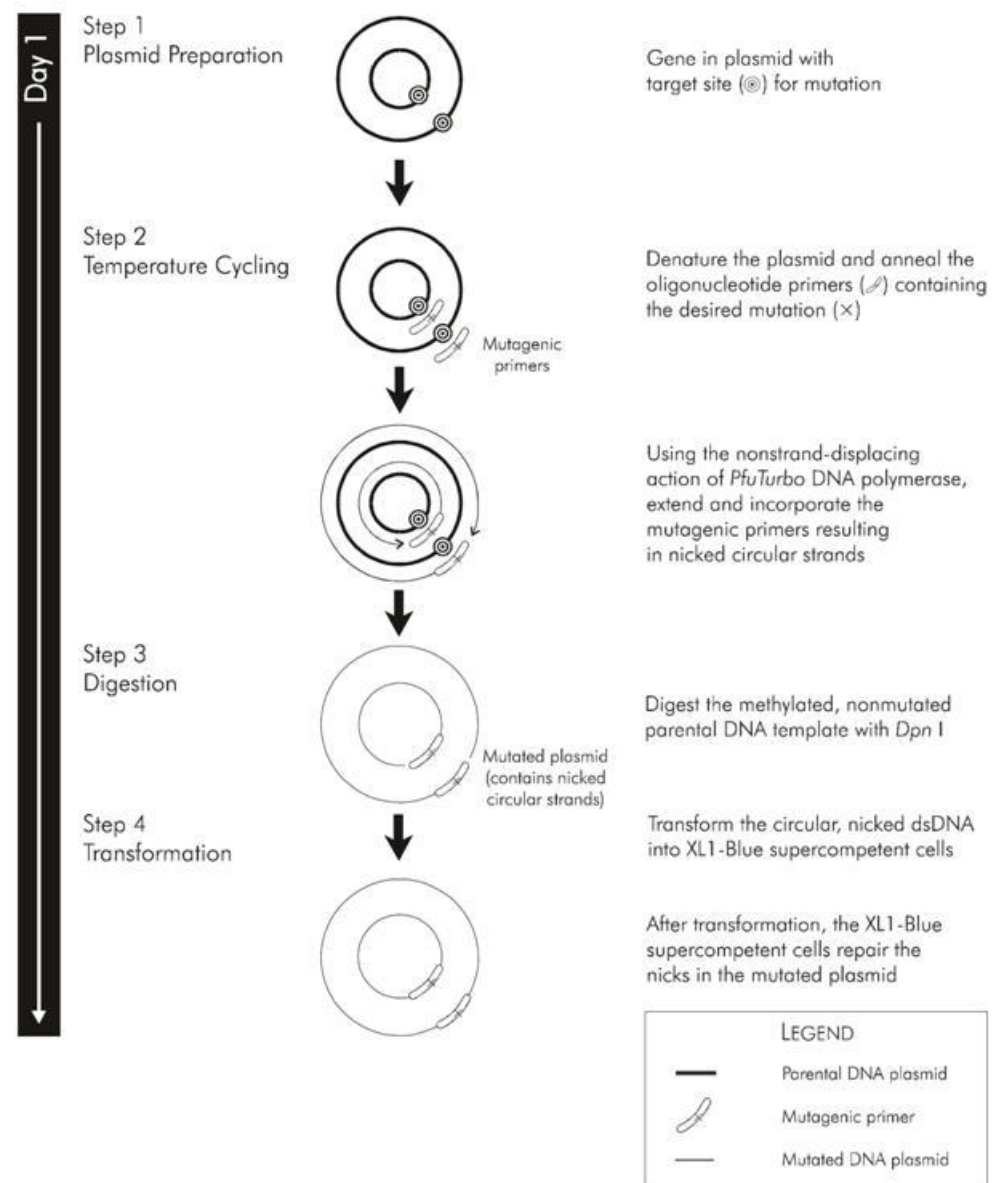


FIGURE 1 Overview of the QuikChange® site-directed mutagenesis method.

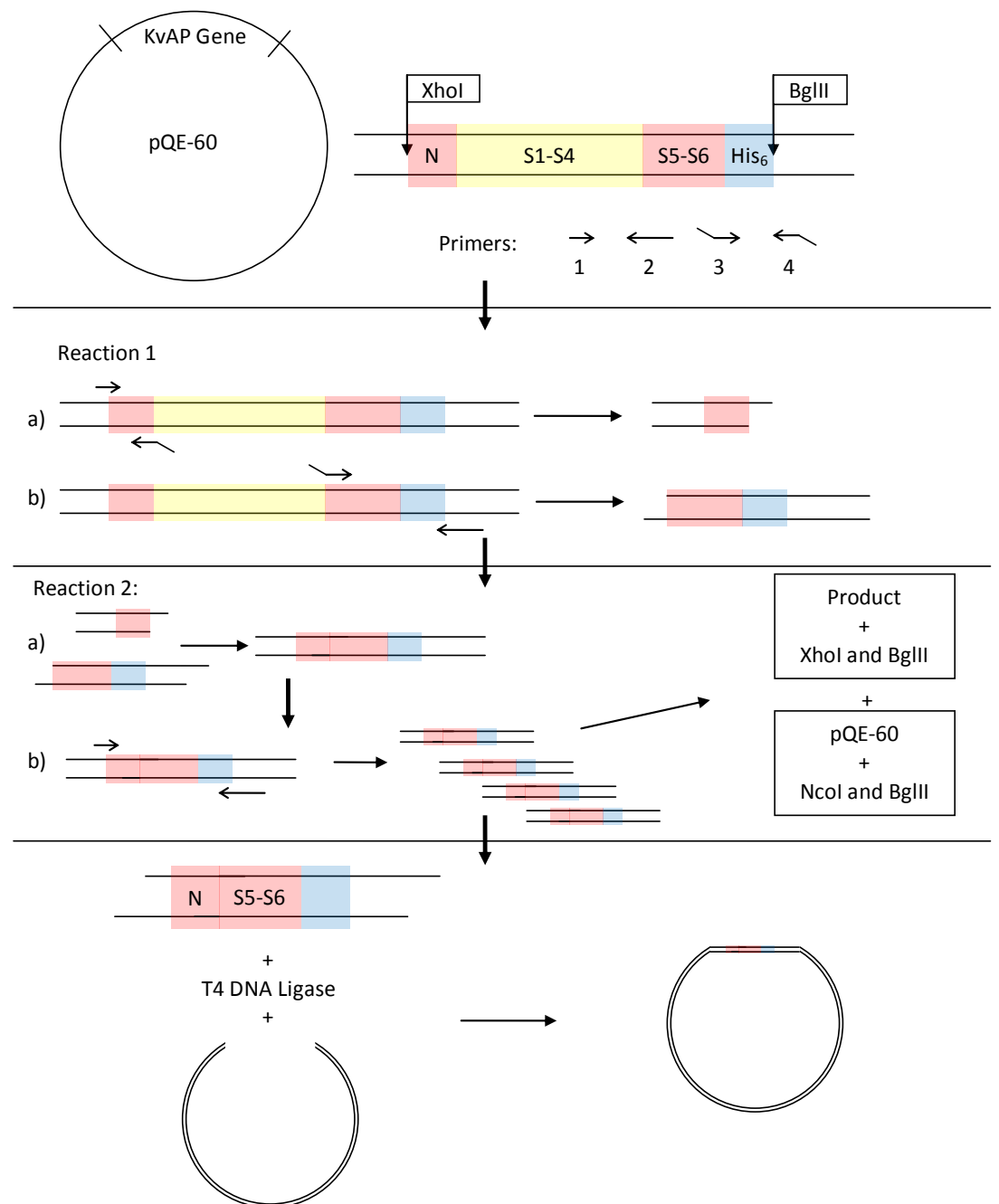


Figure 2.3: Protocol for two stitch PCR reaction of KvAP to generate pore domain only mutant

2.2.3 Expression and Purification of KvAP

2.2.3.1 Growth of cells containing the KvAP construct

All mutants of KvAP were expressed and purified under identical conditions. Six seed cultures were inoculated with a colony from a selective media plate and grown as described in Section 2.2.1.7. Each seed culture was used to inoculate 1 l sterile LB broth containing 100 $\mu\text{g ml}^{-1}$ ampicillin and 20 $\mu\text{g ml}^{-1}$ tetracycline which had been pre-warmed to 37 °C. The 1 l culture was incubated at 37 °C with shaking at 200 rpm in an orbital shaker (New Brunswick) until the culture reached an OD₆₀₀ of 0.6. Protein expression was then induced by addition of 1 ml 0.4 mM isopropyl β , D-thiogalactopyranoside per 1 l culture; flasks were incubated for a further 4 hours at 37 °C. Bacterial cells were then harvested by centrifugation at 15900 x g for 20 minutes in a Beckman Avanti J-20 XPI centrifuge at 4 °C; the cell pellet was stored at -20°C until use.

2.2.3.2 Purification of KvAP

2.2.3.2.1 Preparation on Phosphate Buffered Saline (PBS)

8.18 g NaCl, 2.01 g KCl, 1.42 g Na₂HPO₄, and 0.244g KH₂PO₄ was dissolved in 900 ml distilled water. The pH was adjusted to pH 7.4 and the distilled water added to 1 l.

2.2.3.2.2 Purification

Cell pellets were thawed and resuspended in 1 x PBS to a final volume of 70 ml containing 1 ml protease inhibitor solution for histidine tagged proteins (Sigma) and transferred to a sonication vial suspended in a sodium chloride ice slurry. Cells were lysed by sonication for a total pulse time of 5 minutes (20 second pulses separated by 15 seconds) with a Misonix XL-2020 probe sonicator. The lysate was then centrifuged at 110000 x g rpm for 40 minutes at 4 °C in a TFT 49.54 rotor in a Beckman L7 Ultracentrifuge. The supernatant was discarded and the pellet was resuspended in 100 ml 1 x PBS containing 40 mM n-decyl- β -D-maltopyranoside and left for 4 hours at 4 °C with constant stirring. Insoluble material was removed from solution by centrifugation at 16750 x g for 20 minutes at 4 °C in a Beckman

J2-HS centrifuge. The supernatant was filtered through a 0.22 μm filter and imidazole (Calbiochem) was added to the solution to a final concentration of 20 mM. A 1 ml HisTrap Column (GE Healthcare) was equilibrated by running 20 ml wash buffer through the column using a Gilson MiniPlus 2 peristaltic pump at a flow rate of 0.5 ml min⁻¹. Imidazole was added to the sample to a final concentration of 20 mM; the sample was then loaded onto the column at a flow rate of 0.5 ml min⁻¹. Columns were then washed with 50 ml of wash buffer or until the OD₂₈₀ of the flow through reached a value of 0. Protein was eluted from the column with elution buffer and collected in 500 μl fractions. Fractions were assayed for protein concentration by absorbance of the protein sample at 280 nm on a Thermo Scientific Nanodrop 2000 spectrophotometer and for protein purity using SDS-PAGE as detailed in Section 2.2.3.3. Fractions containing pure KvAP were pooled, aliquoted and flash frozen in liquid nitrogen. Aliquots were stored at -80 °C until use.

2.2.3.3 Sodium dodecyl sulphate polyacrylamide gel electrophoresis (SDS PAGE)

2.2.3.3.1 Resolving gel (12 %)

BioRad Protean II spaced glass plates were secured onto a BioRad Protean II casting rack. Resolving gel was made by adding 3.5 ml Protogel (National Diagnostics), 2.4 ml 1.5 M TRIS pH 8.8, 60 μl 10% Sodium dodecyl sulphate, and 30 μl 25% ammonium persulphate to 3.13 ml distilled water. Finally 10 μl Tetramethylethylenediamine (TEMED) was added to the mixture before setting.

2.2.3.3.2 Stacking Gel

After the resolving gel had set, stacking gel was made by mixing 1.7 ml sterile distilled water, 600 μl Protogel, 1.6 ml 3.6M TRIS pH 9.3, 20 μl 25% APS and 40 μl 10% SDS. Finally 4 μl TEMED was added to the solution before setting.

2.2.3.3.3 SDS Sample Buffer

1 ml 0.625M TRIS pH 6.8 was mixed with 2 ml 10% SDS, 1 ml Glycerol and 0.5 ml sterile distilled water. Bromophenol blue was added to a final concentration of 2.5%.

2.2.3.3.4 5x SDS Running Buffer (5L)

75.7 g TRIS, 360.3 g of glycine and 20 g SDS were dissolved in distilled water, and the solution made to 5 l.

2.2.3.3.5 Stain Solution

450 ml Methanol was mixed with 460 ml distilled water and 90 ml Acetic Acid. Coomassie brilliant blue was added to 0.025 % (w/v)

2.2.3.3.6 Destain solution

1 l methanol was mixed with 375 ml Glacial acetic acid and 3.625 l distilled water.

2.2.3.3.7 SDS PAGE

SDS-PAGE was carried out using a modified Laemmli method. 12 % polyacrylamide gels were used to assess the purity of KvAP eluted from the nickel columns. Gels were set and run using a BioRad mini Protean II system. 2.5 μ l of protein sample was added to 2.5 μ l SDS Sample Buffer and 5 μ l sterile distilled water. Samples were then loaded onto the gel. Novex Sharp® molecular weight marker (Invitrogen) was used to assess the mass of the purified protein unless otherwise stated. Gels were run at a constant voltage of 120 V and a maximum current of 40 mA for 60 minutes. Gels were stained with Coomassie Brilliant blue using stain solution and destained in destain solution and imaged using a Syngene gel imaging system.

2.2.3.4 Determination of protein concentration

The concentration of protein in eluted samples was determined by measuring the OD₂₈₀ of 20 μ l of the solution diluted in 980 μ l of 1% SDS solution in a 1 ml quartz cuvette blanked against 980 μ l 1% SDS and 20 μ l elution buffer. Using the molar extinction coefficient of KvAP of 35110 M⁻¹ cm⁻¹ (calculated by ExPASy

ProtParam) and the molecular weights of each mutant, the concentration of the protein in the sample was calculated.

2.2.3.5 Western Blot analysis

2.2.3.5.1 PBS-TWEEN

PBS-TWEEN solution was made by dissolving 0.5 ml TWEEN-20 and 100 ml 10x PBS buffer (in 899.5 ml distilled water

2.2.3.5.2 Transfer Buffer

6.04 g TRIS and 28.8 g Glycine were mixed with 200 ml AR grade methanol and distilled water added to 1 l.

2.2.3.5.3 Western blot transfer

For characterisation by Western blot analysis, protein samples were run on an SDS PAGE gel as described in Section 2.2.3.3 but with SeeBlue Plus2 Marker (Invitrogen) as a protein size ladder. Rather than staining with Coomassie brilliant blue, the gel was removed from the running buffer and applied to a pre cut portion of nitrocellulose membrane. This was then placed between two pieces of filter paper in a transfer apparatus. The apparatus was then filled with transfer buffer and was run at a current of 500 mA at a voltage of 100 V for 2 hours to transfer the protein from the gel to the filter paper. The nitrocellulose membrane was then blocked against non-specific antibody binding by incubating at room temperature for a minimum of 2 hours with 1g Marvel milk powder dissolved in 20 ml 1 x PBS supplemented with 0.05% TWEEN-20 (Sigma). Following blocking, the membrane was washed with PBS-TWEEN for 20 minutes with a total of four changes of buffer. The nitrocellulose membrane was then incubated at room temperature for one hour in PBS-TWEEN containing a monoclonal anti-polyhistidine antibody conjugated to horseradish peroxidase (Sigma) produced in mouse. The membrane was then washed for 20 minutes as before and transferred to a Versadoc imaging machine. The membrane was developed using SuperSignal horseradish peroxidase developing kit (Pierce) and images were recorded every 3 minutes for 18 minutes using a gain of 1.

2.2.3.6 Analysis of pore domain only mutant by native PAGE

To confirm the oligomeric state of the pore domain only mutant, the protein was analysed on a NativePage™ precast 4-16 % non denaturing gel. 5 µl nickel column eluate containing KvAP as determined by SDS PAGE was mixed with 2.5 µl distilled water and 2.5 µl NativePage™ loading buffer. The gel was placed in an Invitrogen SureLock Mini cell gel tank and 600 ml 1 x NativePage™ running buffer was added to the anode compartment. 400 ml 1 x NativePage™ running buffer containing 0.025 % Coomassie brilliant blue G-250 was added to the cathode compartment and the gel was run for 2 hours at a constant voltage of 150 V. The pore domain only mutant was run alongside KcsA for size comparison of the tetramer and NativeMark™ unstained protein marker for size analysis.

2.2.4 Reconstitution of purified KvAP mutants

2.2.4.1 Preparation of potassium cholate

Potassium cholate was prepared by dissolving equimolar quantities of potassium hydroxide and cholic acid in a minimal volume of methanol. The resulting potassium cholate was then precipitated from the methanol by adding an excess of diethyl ether and leaving at 4°C overnight. The product was removed by filtration and dried under a vacuum for 12 hours. Potassium cholate solutions were made to a concentration of 8.6 mg ml⁻¹ in 20 mM Hepes solution (20 mM Hepes, 150 mM KCl, 1mM EGTA, pH 7.2 KOH)

2.2.4.2 Preparation of stock lipid

Lipid stock of phosphatidylcholine was prepared at a concentration of 20 mg ml⁻¹ by dissolving 100 mg of lipid in 5 ml of ice cold chloroform.

2.2.4.3 Preparation of stock brominated lipid

A solution of lipid in chloroform was made as described in section 4.2.1.5 and brominated by drop-wise addition of bromine until a pale yellow colour could be seen. Chloroform and excess bromine were then evaporated using a nitrogen stream followed by drying under vacuum. The dried lipid was then reweighed and redissolved in chloroform to 20 mg ml⁻¹; stock lipid was stored at -20 °C until use.

2.2.4.4 Reconstitution of KvAP by the dilution method

2 μ mol DOPC was dried onto the walls of a glass scintillation vial under a nitrogen stream and placed in a vacuum dessicator for a minimum of 15 minutes. 1.6 ml cholate solution (Section 4.2.1.4) was then added to the lipid and mixed until cloudy. The solution was then sonicated to clarity in a Ultrawave bath sonicator. KvAP was then added to give a molar ratio of 100:1 lipid:KvAP monomer. The sample was left at room temperature for 20 minutes at 25 °C. 100 μ l of the sample was then added to 2.9 ml 20 mM Hepes solution containing 150 mM potassium chloride and 1 mM EGTA to dilute the potassium cholate below the CMC and induce the formation of bilayer fragments.

2.2.4.5 Reconstitution by the dialysis method

Purified KvAP was added to lipid in potassium cholate as described in Section 2.2.4.1. After 20 minutes of incubation at 25 °C the sample was transferred to a dialysis tube with a molecular weight cut off of 7 kDa. The sample was dialysed against 500 ml 20 mM Hepes solution containing 150 mM potassium chloride and 1 mM EGTA for 5 hours at room temperature with three changes of buffer.

2.2.4.6 Preparation of BioBeads SM2

BioBeads were dehydrated by adding 300 ml methanol to 10 g BioBeads SM2 and stirring gently for 1 hour. The methanol was then removed using a Buchner funnel and the BioBeads washed on the Buchner funnel three times with 500 ml 20 mM Hepes solution containing 150 mM potassium chloride and 1 mM EGTA. The BioBeads were then placed in a glass column and continuously washed for 3 hours with Hepes buffer at a flow rate of 2 ml min⁻¹. The BioBeads were then stored in Hepes buffer at 4 °C until use with a maximum storage time of 5 days.

2.2.4.7 Reconstitution using BioBeads SM2

2 μ mol lipid was dried onto the walls of a glass scintillation vial under a nitrogen stream and placed in a vacuum dessicator for a minimum of 15 minutes. 1.6 ml 40 mM OG solution in Hepes solution (20 mM Hepes, 150 mM KCl, 1mM EGTA, pH 7.2 KOH) was added to the lipid and was then added to the lipid and mixed until

cloudy; the solution was then sonicated to clarity in a Ultrawave bath sonicator. Purified KvAP was added at the desired concentration and the mixture was incubated at 25 °C for 20 minutes. 80 mg of BioBeads prepared as described above were added to the sample and left for 1 hour at 25 °C. Another 80 mg of BioBeads were then added and the sample left for a further 1 hour at 25 °C. The sample was then removed from the BioBeads using a thin tipped Pasteur pipette so as not to disturb the BioBeads.

2.2.4.8 Sucrose density gradient

Sucrose density centrifugation was used to characterise the reconstituted KvAP. 1.8 μ mol di(C18:1)PC was mixed with 94 nmol rhodamine labelled di(C18:1)PE (19:1 molar ratio of PC to rhodamine labelled PE) and dried onto the walls of a glass scintillation vial as described above. This was then solubilised in 1.6 ml cholate solution prepared as described above and sonicated to clarity. KvAP was then added to a molar ratio of 100:1 lipid to KvAP monomer and the mixture incubated for 20 minutes at 25 °C. Detergent was then removed from the sample using Biobeads SM2 as described in section 2.2.4.7 for 5 hours at 25 °C. Discontinuous sucrose gradients were made using the following concentrations of sucrose (w/w) in 20mM Hepes solution containing 150 mM potassium chloride and 1 mM EGTA: 2.5 %, 5 %, 10 %, 15 %, 20 %, 30 %. Samples were then placed on the top of the gradient and spun at 80,000 g (24,000 rpm) for 18 hours at 4°C in a Beckman Ultracentrifuge in a SW18 rotor. 1ml fractions were taken from the gradients following centrifugation and analysed for lipid and protein by absorbance at 570 nm and absorbance at 270nm, using extinction coefficients of 70,000 M⁻¹ cm⁻¹ (figure from Invitrogen Molecular probes) and 35,110 respectively (determined using ExPASy protparam). Identical gradients were loaded with samples containing protein only, lipid only, and reconstituted pore domain only mutant.

2.2.4.9 Solubility of KvAP in detergent solutions

The solubility of 100 μ g KvAP in 2.5 ml filtered Hepes solution (20 mM Hepes, 1 mM EGTA, 100 mM KCl, pH 7.2 KOH), was determined at 25 °C using an SLM Aminco 8000c fluorimeter with excitation and emission wavelengths both set at 500 nm with excitation and emission slit widths of 4 nm. Solutions of different

concentrations of four detergents were prepared : n-octyl- β -D-maltopyranoside (OG), potassium cholate, n-dodecyl- β -D-maltopyranoside (DDM) and *n*-decyl- β -D-maltopyranoside (DM). KvAP was added to the detergent solutions in a quartz cuvette before light scatter measurement and results were corrected for background light scatter by the subtraction of the light scatter of an identical sample in the absence of KvAP.

2.2.5 Functional assays of KvAP and its mutants.

The activity of KvAP and mutants was assessed using single channel electrophysiology. Single channel recordings were made using standard planar bilayer recordings. For reconstitution, stock solutions of 20 mg ml⁻¹ 1-palmitoyl-2-oleoyl phosphatidylethanolamine (POPE) and 1-palmitoyl-2-oleoyl phosphatidylglycerol (POPG) were mixed to yield 20 mg total lipid at a molar ratio of POPG:POPE of 1:3 and then dried onto the walls of a thin glass vial. 1 ml 10 mM Hepes solution containing 150 mM KCl and 40 mM β -D-octyl glucoside was added and the sample was sonicated to clarity in a bath sonicator (Ultrawave). KvAP (40 μ g) was then added to give a molar ratio of lipid:KvAP tetramer of 20000:1. Detergent was removed using BioBeads as described above. For forming the bilayer lipid membrane (BLM), stock solutions of POPG and POPE were mixed to give 20 mg lipid at a molar ratio of POPG:POPE of 1:3. The mixture was then dried onto the wall of a glass scintillation vial and resuspended in 1 ml decane; this was painted over a 150 μ m aperture in the planar bilayer assembly and allowed to dry. 1 ml of the 10 mM HEPES solution (20 mM Hepes, 1 mM EGTA, 100 mM KCl, pH 7.2 KOH) above was then added to both the *cis* and *trans* compartments of the bilayer system; Lipid in decane was added until a bilayer of capacitance greater than 60 pF was formed. 1-5 μ l of the vesicle suspension was then added to the *cis* chamber of the planar bilayer and the bilayer was then broken and immediately reformed in the presence of the vesicles. The membrane was then polarised to -100 mV for 2 minutes and depolarised to +100 mV to determine if there was active KvAP in the bilayer. If no activity was seen, the bilayer was broken and reformed, adding additional vesicles if necessary, until activity was observed. Single channel currents were recorded with a ID562 amplifier. The electrode in the *cis* chamber was connected to the input of the amplifier headstage.

The bias voltage was applied to the *trans* chamber electrode. All measurements were performed at room temperature and data were sampled at 5 kHz.

2.2.5.1 Current-Voltage curves

After activity was confirmed, current-voltage curves were recorded by depolarising the bilayer from -100 mV to potential differences of between 0 mV and 100 mV at intervals of 10 mV and current flowing through the channel was measured.

2.2.6 Fluorescence measurements

2.2.6.1 Preparation of Hepes buffer

Hepes buffer was prepared by making a 20 mM Hepes solution (20 mM Hepes, 150 mM KCl, 1 mM EGTA pH 7.2 KOH) and filtering the solution through a 0.22 μ m filter (Sartorius).

2.2.6.2 Preparation of Sephadex

Sephadex G-50 was used to remove free dye from the purified KvAP. 10 g of Sephadex G-50 was placed in a 200 ml conical flask and hydrated overnight at 4 °C with 100 ml Hepes buffer containing 5 mM DM and kept at 4 °C until required.

2.2.6.3 Labelling of KvAP and mutants with IANBD

A stock solution of IANBD was made by dissolving 1 mg of IANBD in 100 μ l molecular biology grade DMSO. Purified KvAP was taken from storage at -80 °C and defrosted in sufficient quantity to provide 5 nmol of KvAP for each fluorescence experiment. Where required the KvAP concentration was adjusted to 10 mg ml⁻¹ by dilution in elution buffer (140 mM NaCl, 27 mM KCl 10 mM Na₂HPO₄, 1.8 mM KH₂PO₄ pH 7.2 KOH), to ensure that the required amount of IANBD could be added without the concentration of DMSO rising above 10 %. IANBD was added at a 5x molar excess to KvAP and left to incubate for 60 minutes at room temperature wrapped in foil. Following incubation, free IANBD was removed from the solution by passing through two Sephadex G-50 columns. 700 μ l of hydrated Sephadex G-50 was placed in a number of E-Z-Spin columns (Pierce) and centrifuged at 2000 rpm for 1 minute in a bench top centrifuge to

remove excess fluid. 50 μ l of labelled protein was loaded onto each column and the column was placed in a 1.5 ml microcentrifuge tube and spun at 2000 rpm for 2 minutes. The elutate was then collected and run again in 50 μ l fractions on fresh Sephadex columns prepared as before. The second elutate was then collected and pooled. All mutants of KvAP and of the KvAP pore domain were labelled using this method.

2.2.6.4 Determination of IANBD labelling ratio

The molar ratio of labelling by NBD (Invitrogen Molecular Probes) was determined by running an absorbance scan from 270 nm to 500 nm on a Hitachi U2001 spectrophotometer. The absorbances at 478 nm (NBD) and 280 nm (KvAP) were recorded and, using the molar extinction coefficients of the two substances (35110 $M^{-1} cm^{-1}$ (determined by ExPASy ProtParam) and 14000 $M^{-1} cm^{-1}$ (as per Manufacturers information) respectively), the concentrations of each were determined and used to calculate the labelling ratio.

2.2.6.5 Labelling of KvAP and mutants with NPM

A stock solution of NPM was made by dissolving 1 mg of NPM in 100 μ l molecular biology grade DMSO. Purified KvAP was taken from storage at -80 $^{\circ}C$ and defrosted in sufficient quantity to provide 5 nmol of KvAP for each fluorescence trace. Where required the KvAP concentration was adjusted to 10 mg ml^{-1} by dilution in elution buffer (140 mM NaCl, 27 mM KCl, 10 mM Na_2HPO_4 , 1.8 mM KH_2PO_4 , 5 mM DM, pH 7.2 KOH), to ensure that the required amount of NPM could be added without the concentration of DMSO rising above 10 %. NPM was added at a 5x molar excess to KvAP and left to incubate for 60 minutes at room temperature wrapped in foil. Following incubation, free NPM was removed from the sample by passing through two Sephadex G-50 columns. 700 μ l of hydrated Sephadex G-50 was placed in a number of E-Z-Spin columns (Pierce) and centrifuged at 2000 rpm for 1 minute in a bench top centrifuge to remove excess fluid. 50 μ l of labelled protein was loaded onto each column and the column was placed in a 1.5 ml microcentrifuge tube and spun at 2000 rpm for 2 minutes. The elutate was then collected and run again in 50 μ l fractions on fresh Sephadex

columns prepared as before. The second elutate was then collected and pooled. All mutants of KvAP and the KvAP pore domain were labelled using this method.

2.2.6.6 Determination of NPM labelling ratio

The molar ratio of labelling by NPM was determined by running an absorbance scan from 270 nm to 500 nm on a Hitachi U2001 spectrophotometer. The absorbances at 340 nm (NPM) and 280 nm (KvAP) were recorded and using the molar extinction coefficients of $35110 \text{ M}^{-1} \text{ cm}^{-1}$ and $40000 \text{ M}^{-1} \text{ cm}^{-1}$ for pyrene and KvAP respectively (Patel et al. 2010), the concentrations of each were determined and used to calculate the labelling ratio.

2.2.6.7 Fluorescence measurements of KvAP-NBD

NBD fluorescence was excited at 478 nm using an SLM-Aminco 8000C fluorimeter. 4 nm excitation slits were used in all measurements with the emission slit set to 8 nm. Emission spectra were recorded between 490 nm and 590 nm. To obtain accurate measurements of fluorescence emission maxima, the spectra were fitted to a skewed Gaussian distribution:

Equation 2.3

$$F = F_{\max} \times \left(-\ln 2 \left(\frac{\ln(1 + 2b(\lambda - \lambda_{\max}))}{\frac{w_{\lambda}}{b}} \right) \right)$$

Here F and F_{\max} are the fluorescence intensities at λ and λ_{\max} respectively, b is the skew parameter and w_{λ} is the width of the peak at half height.

2.2.6.8 Fluorescence measurements of NPM-labelled KvAP

NPM fluorescence was excited at 338 nm using an SLM-Aminco 8000C fluorimeter. 4 nm slits were used in all measurements for both emission and excitation monochromators. Emission spectra were recorded between 350 nm and 450 nm.

2.2.6.9 Fluorescence quenching with iodide

A 1 M stock solution of sodium iodide was prepared in 20 mM Hepes buffer containing 100 mM potassium thiosulphate and 1 mM EGTA. Sodium iodide was used in preference to potassium iodide in case a large concentration of potassium ions altered the conformation of the channel. For fluorescence quenching experiments this was added to a 3 ml sample of Hepes buffer containing 1 M sodium chloride and 100 mM sodium thiosulphate in 20 mM Hepes to achieve a final concentration of sodium of 0.91 M and a final iodide concentration of 0.45 M. The corresponding fluorescence intensity in the absence of iodide was determined in 20 mM Hepes buffer containing 1M NaCl, 100 mM Na₂S₂O₃ and 1 mM EGTA, pH 7.2.

2.2.6.10 Fluorescence quenching with TEMPO

A stock solution of 10 mM 2,2,6,6-tetramethylpiperidine-1-oxyl (TEMPO) in Hepes buffer (20 mM Hepes, 150 mM KCl, 1 mM EGTA pH 7.2) was made by dissolving Tempo in the buffer with gentle heating. Aliquots of the stock solution were added to labelled KvAP in Hepes buffer to a final concentration of 2 mM.

2.2.6.11 Quenching of fluorescence with 16-doxyl stearic acid

16-Doxyl stearic acid was dissolved in methanol to a final concentration of 1.92 mg ml⁻¹ prior to use. 50 µl of the stock solution was then added to a fluorescence cuvette containing reconstituted fluorescently labelled KvAP mutants as described in Section 5.2.2.8. so that the 16-doxyl stearic acid constituted 33% of the total lipid in the sample. To correct for the dilution effect of adding 50 µl methanol to the cuvette, an identical sample was prepared and 50 µl methanol added without 16-doxyl stearic acid, and the spectra corrected accordingly.

2.2.6.12 Quenching of NPM-labelled KvAP fluorescence with brominated lipid

NPM-labelled KvAP was prepared as described in section 6.2.1.6 and reconstituted into brominated phosphatidylcholine as described in 5.2.2.8 taking into account the higher molecular weight of the brominated lipid. Fluorescence was then recorded as described in section 6.2.1.9. Levels of quenching were calculated as F/F_0 at 386

nm and were plotted as a function of residue number, where F is fluorescence intensity when NPM labelled KvAP is reconstituted into bominated phosphatidylcholine and F_0 is the fluorescence intensity in di(18:1)PC.

3 Chapter 3: Mutagenesis of KvAP

3.1 Introduction

Although there are a number of crystal structures for KvAP and other voltage gated potassium channels, a definitive structure for this family of proteins in a membrane has not been agreed on, as described in Chapter 1. Much of the disagreement over the structure of KvAP results from the positioning of the voltage sensing domains with respect to the pore domain, which is known to be structurally conserved. The positions of the voltage sensing domains relative to the pore domain has significant implications for the mechanism of voltage gated potassium channels and is in part the cause of the controversy over how the voltage sensing domains of these channels carry out their function (see Chapter 1). Further, since voltage sensing by the voltage sensing domain is believed to involve some movement across the membrane, it is important to know exactly how KvAP sits in the surrounding lipid bilayer. In order to determine both the position of the voltage sensing domain in relation to the pore domain and the position of the hydrophobic interface of KvAP, the S5 helix which is the outer helix of the pore domain has been chosen for study. In order to carry out fluorescence studies of KvAP using cysteine reactive probes, it is necessary to first create a cysteine free mutant of KvAP into which single cysteine residues can be introduced at positions of interest.

In order to determine the residues of S5 which contact the voltage sensing domain of KvAP, it is also helpful to compare fluorescence data for the full length channel with that of the isolated pore domain. Until now the only domain of KvAP that has been isolated and expressed on its own is the voltage sensing domain. The pore domain of KvAP is very similar to that of KcsA and since there are no highly charged amino acids in the face of the KvAP S5 helix which is likely to be exposed to the voltage sensing domain, it should be possible for the pore domain to integrate into a lipid bilayer in the absence of the voltage sensing domains.

3.2 Methods

All molecular biological techniques were carried out as detailed in Chapter 2

3.2.1 Generation of single cysteine mutants of KvAP

Site directed mutagenesis of KvAP was performed using the QuikChange® site directed mutagenesis protocol as described in Section 2.2.2.9. The sequence of KvAP is given in Figure 3.3. Table 3.1 shows the primers used to create the mutants which have been successfully expressed are shown in Table 3.1.

3.2.1.1 Transformation of mutant DNA into XL1-blue cells

Mutated DNA was transformed into XL1-blue cells (Stratagene) as described in section 2.2.1.10. An overnight culture was then made of a single colony of XL1-blue cells from a selective media plate as described in section 2.2.1.7 and DNA was then harvested from these cells as outlined in Section 2.2.2.7, and sent to MWG biotech for sequencing to confirm the presence of the desired mutation.

3.2.1.2 Generation of Pore domain only mutant using two stitch PCR

In order to create a pore domain only mutant, the polymerase chain reaction was again utilised; two stitch PCR was used to generate a KvAP mutant which contained only the pore domain of the protein, as described in section 2.2.2.10..

3.2.1.2.1 Two stitch Primer design

Four primers were required, shown in Table 3.2 and the sequence of the construct and comparison to the full length structure are seen in Figure 3.1 and Figure 3.2.. Primer 1 was designed to be complementary to the sense strand of the KvAP gene 5' to the NcoI restriction site, resulting in elongation 5' to 3' from the beginning of the gene. Primer 2 was designed to bind the antisense strand resulting in elongation towards the beginning of the gene from the end. The 5' most 20 bases of primer 3 are complementary to the sense strand at the beginning of the S5-S6 segment (see Figure 2.3) of the KvAP gene and the 3'- most 19 bases are complementary to the end of the N terminal section and therefore has a mismatch to the last 19 bases of the S1-S4 segment indicated by the angled primer in Figure 3.5. Primer 4 is

essentially the reverse of primer 3 with the 5'-most 19 bases of primer 3 being complementary to the antisense strand at the end of the N terminal region of the KvAP gene and the 3'-most 19 bases being complementary to the beginning of the S5-S6 segment and therefore has a mismatch to the first 19 bases of the S1-S4 segment. Two separate PCR reactions (1a and 1b) were undertaken to amplify the two regions of the KvAP gene either side of the S1-S4 segment as shown in Figure 2.3.

151C	Forward	CTG CGG ACA AAA TAA GAT TCT GTC ACC TCT TTG GCG CCG
	Reverse	GCG CCA AAG AGG TGA CAGAAT CTT ATT TTG TCC GCA G
152C	Forward	GGA CAA AAT AAG ATT CTA CTG TCT CTT TGG CGC CGT AAT G
	Reverse	ACG GCG CCA AAG AGA CAG TAG AAT CTT ATT TTG TCC GCA G
153C	Forward	CAA AAT AAG ATT CTA CCA CTG CTT TGG CGC CGT AAT GCT G
	Reverse	CAG CAT TAC GGC GCC AAA GCA GTG GTA GAA TCT TAT TTT GTC C
154C	Forward	GAT TCT ACC ACC TCT GCG GCG CCG TAA TGC TGA CC
	Reverse	GGT CAG CAT TAC GGC GCC GCA GAG GTG GTA GAA TCT TAT TTT G
155C	Forward	TAA GAT TCT ACC ACC TCT TTT GCG CCG TAA TGC TGA CCG TC
	Reverse	GAC GGT CAG CAT TAC GGC GCA AAA GAG GTG GTA GAA TCT TAT TT
156C	Forward	CTA CCA CCT CTT TGG CTG TGT AAT GCT GAC CGT CCT CTA CG
	Reverse	GAG GAC GGT CAG CAT TAC ACA GCC AAA GAG GTG GTA GAA TC
157C	Forward	CTA CCA CCT CTT TGG CGC CTG TAT GCT GAC CGT CCT CTA CG
	Reverse	CGT ACA GGA CGG TCA GCA TAC AGG CGC CAA AGA GGT GGT AG
158C	Forward	CAC CTC TTT GGC GCC GTA TGT TCT GAC CGT CCT CTA CG
	Reverse	CGT AGA GGA CGG TCA GAC ATA CGG CGC CAA AGA GGT G
159C	Forward	CTT TGG CGC AGT GAT GTG CAC AGT CCT CTA CGG AGC CTT C
	Reverse	GTA GAG GAC TGT GCA CAT CAC TGC GCC AAA GAG GTG GTA G
160C	Forward	CTT TGG CGC AGT GAT GCT GTG TGT CCT CTA CGG AGC CTT C
	Reverse	GTA GAG GAC ACA CAG CAT CAC TGC GCC AAA GAG GTG GTA G
161C	Forward	CTT TGG CGC AGT GAT GCT GAC ATG CCT CTA CGG AGC CTT CGC C
	Reverse	GTA GAG GCA TGT CAG CAT CAC TGC GCC AAA GAG GTG GTA G
162C	Forward	GGC GCA GTG ATG CTG ACA GTC TGT TAC GGA GCC TTC GCC ATC
	Reverse	CCG TAA CAG ACT GTC AGC ATC ACT GCG CCA AAG AGG TGG TAG
163C	Forward	GTA ATG CTG ACC GTC CTC TGT GGA GCC TTC GCC ATC TAC
	Reverse	GTA GAT GGC GAA GGC TCC ACA GAG GAC GGT CAG CAT TAC
164C	Forward	GCT GAC CGT CCT CTA CTG TGC CTT CGC CAT CTA CAT AG
	Reverse	CTA TGT AGA TGG CGA AGG CAC AGT AGA GGA CGG TCA GCA TTA C
165C	Forward	CGT CCT CTA TGG ATC TTT CGC AAT CTA CAT AGT GGA GTA TCC GG
	Reverse	GAT TGC GAA ACA TCC ATA GAG GAC GGT CAG CAT TAC GGC G
166C	Forward	CGT CCT CTA CGG AGC CTG CGC CAT CTA CAT AGT G
	Reverse	CAC TAT GTA GAT GGC GCA GGC TCC GTA GAG GAC G
167C	Forward	CTC TAC GGA GCC TTC TGT ATC TAC ATA GTG GAG TAT CCG G
	Reverse	ATA CTC CAC TAT GTA GAT ACA GAA GGC TCC GTA GAG GAC G
168C	Forward	TAC GGA GCC TTC GCC TGT TAC ATA GTG GAG TAT CCG GAT C
	Reverse	CCG GAT ACT CCA CTA TGT AAC AGG CGA AGG CTC CGT AGA G
169C	Forward	GGA GCC TTC GCC ATC TGT ATA GTG GAG TAT CCG GAT CC
	Reverse	GGA TAC TCC ACT ATA CAG ATG GCG AAG GCT CCG TAG
170C	Forward	GAG CCT TCG CCA TCT ACT GTG TGG AGT ATC CGG ATC CG
	Reverse	GAT CCG GAT ACT CCA CAC AGT AGA TGG CGA AGG CTC C
171C	Forward	GCC ATC TAC ATA TGT GAG TAT CCG GAT CCG AAC AGC
	Reverse	TGT TCG GAT CCG GAT ACT CAC ATA TGT AGA TGG CGA AGG
172C	Forward	CGC CAT CTA CAT AGT GTG CTA TCC GGA TCC GAA CAG
	Reverse	GCT GTT CGG ATC CGG ATA GCA CAC TAT GTA GAT GGC G
173C	Forward	CCA TCT ACA TAG TGG AGT GTC CGG ATC CGA ACA GCA GTA TC
	Reverse	CTG CTG TTC GGA TCC GGA CAC TCC ACT ATG TAG ATG GCG
174C	Forward	CTA CAT AGT GGA GTA TTG TGA TCC GAA CAG CAG TAT CAA G
	Reverse	GAT ACT GCT GTT CGG ATC ACA ATA CTC CAC TAT GTA GAT GGC G
175C	Forward	CTA CAT AGT GGA GTA TCC GTG TCC GAA CAG CAG TAT CAA G
	Reverse	GAT ACT GCT GTT CGG ATC CGT GTA CTC CAC TAT GTA GAT GGC G

Table 3.1: Primers directed to the S5 helix used to create single cysteine mutants of KvAP

Primer 1	CGT CTT CAC CTC GAG AAA TC
Primer 2	GAT GGT GAT GAG ATC TAG ATC CAC GCG GAA CTA ATT TC
Primer 3	CTC GGC GGT AGG GTC AGG AAC ATA GCG GAT GCT GCG GAC
Primer 4	GTC CGC AGC ATC CGC TAT GTT CCT GAC CCT ACC GCC GAG

Table 3.2: Primers used to generate the pore only mutant of KvAP

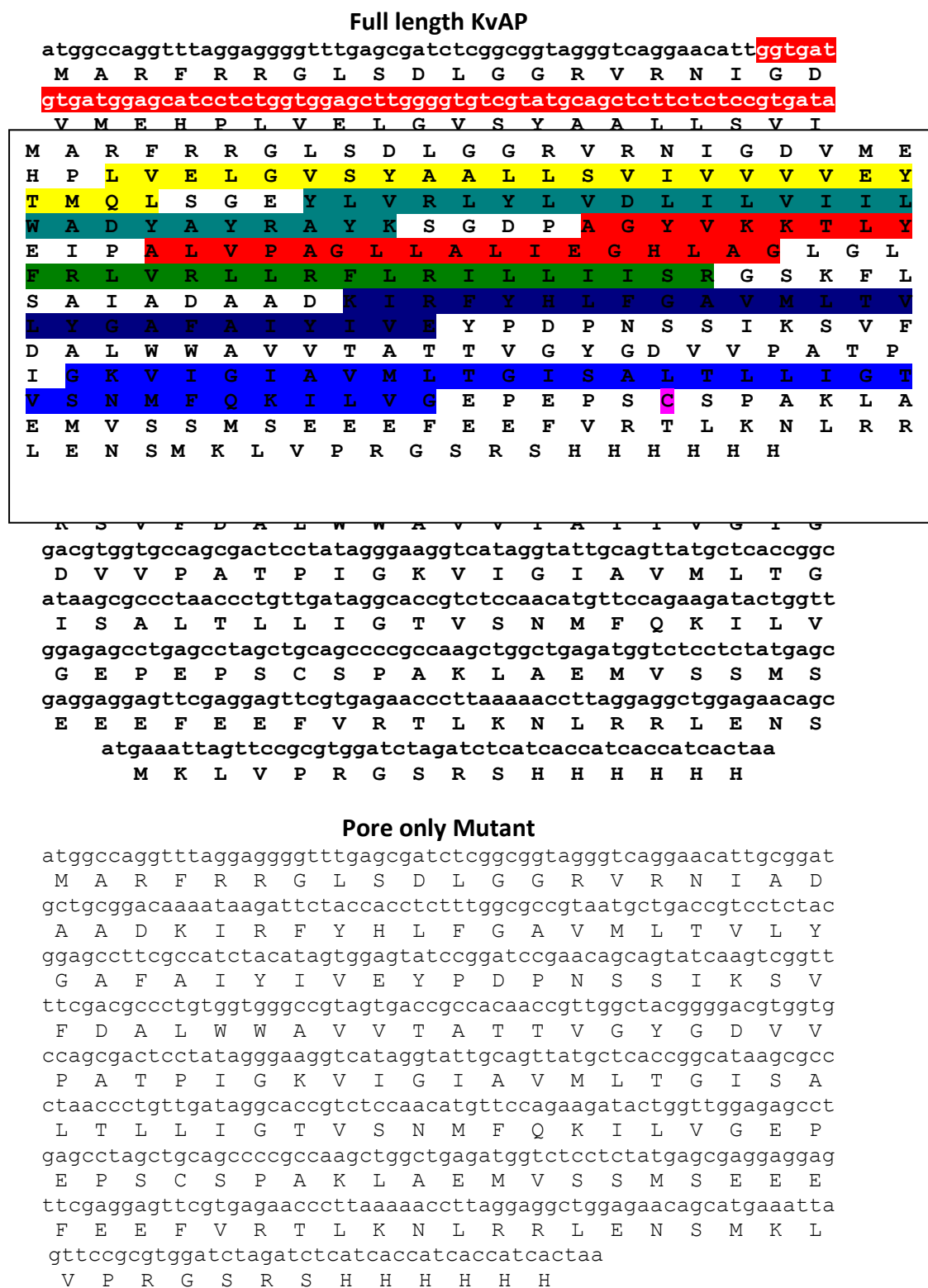


Figure 3.1: Comparison between full length KvAP and the pore only mutant. Full length KvAP is shown with the region to be excised by two stitch PCR shown in red. The residue at which the excision occurs is an isoleucine on both the N and C terminal end of the excised region. This was chosen in order to reduce disruption of the tertiary structure of the beginning of the S5 helix. The isoleucine residue at the C terminus of the S1-S4 region was removed.

```

atg gcc agg ttt agg agg ggt ttg agc gat ctc ggc ggt agg gtc agg aac att ggt gat
met ala arg phe arg arg gly leu ser asp leu gly gly arg val arg asn ile gly asp
gtg atg gag cat cct ctg gtg gag ctt ggg gtg tcg tat gca gct ctt ctc tcc gtg ata
val met glu his pro leu val glu leu gly val ser tyr ala ala leu leu ser val ile
gtc gtt gtc gtc gaa tat acc atg cag ctt agc gga gag tac ctt gta aga ctc tat ctt
val val val val glu tyr thr met gln leu ser gly glu tyr leu val arg leu tyr leu
gtc gac ctt att ctc gtc atc atc ctg tgg gcc gac tat gca tac cgc gcc tac aag agc
val asp leu ile leu val ile ile leu trp ala asp tyr ala tyr arg ala tyr lys ser
ggg gat ccg gcg ggt tat gtt aag aag acg ctc tac gag atc cca gcc ctc gta cca gcg
gly asp pro ala gly tyr val lys lys thr leu tyr glu ile pro ala leu val pro ala
ggt cta ctg gcc ctc ata gag ggc cat ctg gcc ggt ctc ggg ctc ttc agg ctc gtg agg
gly leu leu ala leu ile glu gly his leu ala gly leu gly leu phe arg leu val arg
Ctt ctc agg ttc ctc agg atc cta ctc atc ata tcg agg ggc agc aag ttc ctc tca gcc
leu leu arg phe leu arg ile leu leu ile ile ser arg gly ser lys phe leu ser ala
ata gcg gat gct gcg gac aaa ata aga ttc tac cac ctc ttt ggc gcc gta atg ctg acc
ile ala asp ala ala asp lys ile arg phe tyr his leu phe gly ala val met leu thr
gtc ctc tac gga gcc ttc gcc atc tac ata gtg gag tat ccg gat ccg aac agc agt atc
val leu tyr gly ala phe ala ile tyr ile val glu tyr pro asp pro asn ser ser ile
aag tcg gtt ttc gac gcc ctg tgg tgg gcc gta gtg acc gcc aca acc gtt ggc tac ggg
lys ser val phe asp ala leu trp trp ala val val thr ala thr thr val gly tyr gly
gac gtg gtg cca gcg act cct ata ggg aag gtc ata ggt att gca gtt atg ctc acc ggc
asp val val pro ala thr pro ile gly lys val ile gly ile ala val met leu thr gly
ata agc gcc cta acc ctg ttg ata ggc acc gtc tcc aac atg ttc cag aag ata ctg gtt
ile ser ala leu thr leu leu ile gly thr val ser asn met phe gln lys ile leu val
gga gag cct gag cct agc tgc agc ccc gcc aag ctg gct gag atg gtc tcc tct atg agc
gly glu pro glu pro ser cys ser pro ala lys leu ala glu met val ser ser met ser
gag gag gag ttc gag gag ttc gtg aga acc ctt aaa aac ctt agg agg ctg gag aac agc
glu glu glu phe glu glu phe val arg thr leu lys asn leu arg arg leu glu asn ser
atg aaa tta gtt ccg cgt gga tct aga tct cat cac cat cac cat cac taa
met lys leu val pro arg gly ser arg ser his his his his his his STOP

```

Figure 3.2: Amino acid sequence of wild type KvAP. (top) Wild type amino acid sequence of KvAP. All transmembrane helices are coloured. S1 – yellow, S2 – teal, S3a/b – red, S4 – green, S5 – dark blue, S6 – blue. C247 is labelled in pink. **(Bottom)** In frame nucleotide sequence of KvAP with translated amino acids below in three letter code in blue

3.2.1.3 PCR cleanup of two stitch PCR reaction

Products of Two stitch PCR reactions were transferred to distilled water using PCR cleanup kits as detailed in section 2.2.2.4.

3.2.1.4 Large scale digestion of pQE-60 vector

Restriction digests of the pQE 60 vector were undertaken as per section 2.2.2.8. 20 μ l Gel Loading buffer were then added to the reaction and the reaction was loaded into a single well on an agarose gel and run as described in Section 2.2.2.4.

3.2.1.5 Large scale digestion of two stitch PCR product

Digestion of the PCR reaction having undergone the PCR cleanup was performed as outlined in Section 2.1.2.5, and run in a single well on an agarose gel.

3.2.1.6 Gel extractions

Following digestion of pQE-60 and two stitch PCR products, the reaction mixtures were run in separate lanes on an agarose gel and underwent gel extraction as described in 2.2.2.5. The flow through was kept and underwent a PCR cleanup as described in Section 2.2.2.4.

3.2.1.7 Ligation of the pore domain only mutant into pQE-60

The insert was ligated into the vector as described in section 2.2.2.12 and the product dialysed as described in section

3.2.1.8 Transformation of construct into competent cells

Competent XL1-blue cells were prepared as described in Section 2.2.1.9 and the DNA transformed into the cells as described in Section 2.2.1.10. The cells were plated onto agar plates supplemented with 100 μ g ml^{-1} ampicillin and left overnight at 37°C.

3.2.1.9 Selection of colonies and sequencing

Colonies from the plates were picked and used to inoculate LB containing 100 μ g ml^{-1} ampicillin. These were left to grow for 16 hours at 37 °C and DNA harvested

from the cells as described in Section 2.2.2.3. The DNA was then ethanol precipitated and sent to MWG Biotech for sequencing.

3.2.2 Transformation, expression and purification of KvAP

When a successful mutant had been confirmed by sequencing, transformation and expression were undertaken as described in sections 2.2.1.10 and 0 respectively.

3.2.3 Growth curve analysis of KvAP mutants

XL-1 blue cells containing mutants of KvAP were grown in 1 l flasks as described in section 2.2.3.1. The optical density of 1 ml of the culture was measured every 15 minutes with a Hitachi U2001 spectrophotometer blanked with sterile LB.

3.3 Results

3.3.1 QuikChange site directed mutagenesis of KvAP

3.3.1.1 Generation of a single cysteine mutant

Site directed mutagenesis was undertaken as per the QuikChange protocol using the primers shown in Table 3.1. A cysteine free mutant was created by the substitution of Cysteine 247 with a Serine residue. Serine was chosen as a conservative mutation, and because the same mutant had already been shown to be active by MacKinnon et al. (Ruta et al. 2005).

3.3.1.2 Growth of cysteine mutants of KvAP

The optical density at 600 nm of XL1-blue cells of the C247S mutant, and further mutants thereof were monitored throughout their growth. Figure 3.3 shows a growth curve of the C247S mutant and of the C247S/Y151C mutant, which is representative of all double mutants of KvAP and of all cysteine mutants of the pore domain only mutant. It is evident that double mutants of KvAP grow significantly slower than the C247S mutant; this results in the time taken to reach an optical density of 0.6 at 600 nm for the double mutants being around an hour longer than for C247S.

3.3.1.3 Generation of single cysteine mutants of KvAP.

The cysteine free mutant was then used as the template for all other mutagenic PCR reactions where a single cysteine was substituted into the gene. Following mutagenic PCR the presence of an amplified product was confirmed by running 10% of the final volume of the PCR reaction on a 1% agarose gel. The results of a typical gel of this kind is seen in Figure 3.4 Following confirmation of the presence of the desired mutation the DNA was transformed into XL1-Blue cells, a miniprep carried out and the DNA ethanol precipitated and sent for sequencing.

3.3.2 Two stitch PCR to generate a pore domain only mutant

3.3.2.1 Amplification of N and C terminal regions to the VSD

The N and C terminal regions of the KvAP gene flanking the voltage sensing domain were amplified using the primers shown in Table 3.1 using the polymerase chain reaction. To analyse the product 5 µl of the completed reaction was run on a 1% agarose gel. Figure 3.5a shows the product of these reactions. Lane 2 shows the N terminal flanking region corresponding to the yellow sequence in Figure 3.6. On the 1% gel this runs at well under 500 bases consistent with the predicted length of this region of 187 bases. Lane 3 shows the product of the reaction amplifying the C terminal region (blue in Figure 3.6). This runs on agarose gel at just under 500 bp, consistent with the predicted molecular weight of 471 bases.

3.3.2.2 Amplification of full length pore domain only mutant

The products of the two reactions in produced as described in Section 3.3.2.1 were used to amplify full length pore mutant before the addition of primers to complete this amplification. 5 µl of the PCR product was run on the 1% agarose gel seen in Figure 3.5b. This runs at a molecular weight of between 1 and 0.5 kb consistent with the calculated length of 658 bases.

3.3.2.3 Digestion of the pore domain only mutant and the pQE-60 vector

The pore domain only mutant and the pQE-60 vector were digested with XhoI and BglII to allow the subsequent ligation of these two DNA fragments. Figure 3.5c shows the digestion of pQE-60 containing full length KvAP, showing a band at 3.5 kb corresponding to pQE-60 and at just less than 1 kb corresponding to KvAP. The 3.5 kb band was excised from the gel and the DNA purified. This was subsequently used to ligate with the above PCR product following its digestion with the same enzymes to allow complementary 5' overhangs on the insert.

3.3.2.4 Insertion of pore only mutant into pQE-60

The pore domain only mutant was inserted into pQE-60 using T4 DNA ligase. This was transformed by heat shock into chemically competent cells which were subsequently plated out on agar plates containing 100 µg µl⁻¹ ampicillin. Colonies

were picked and used to inoculate overnight cultures. A miniprep was carried out on these overnight cultures, the results of which are seen in Figure 3.5d where the pore only mutant is run next to KvAP to show the difference in size of the plasmids. Some of the purified plasmid DNA was sent to MWG biotech for sequencing.

3.3.2.5 Generation of single cysteine mutants of the pore only mutant

The pore domain only mutant was generated from the C247S mutant that contains no cysteine residues. The pore domain only mutant was then used as the template for all other mutagenic PCR reactions where a single cysteine was substituted into the S5 helix at the same positions and using the same primers as full length KvAP. Following mutagenic PCR the presence of an amplified product was confirmed by running 10% of the final volume of the PCR reaction on a 1% agarose gel. Following confirmation of the presence of the desired mutation the DNA was transformed into XL1-Blue cells, a miniprep was carried out and the DNA ethanol precipitated and sent for sequencing.

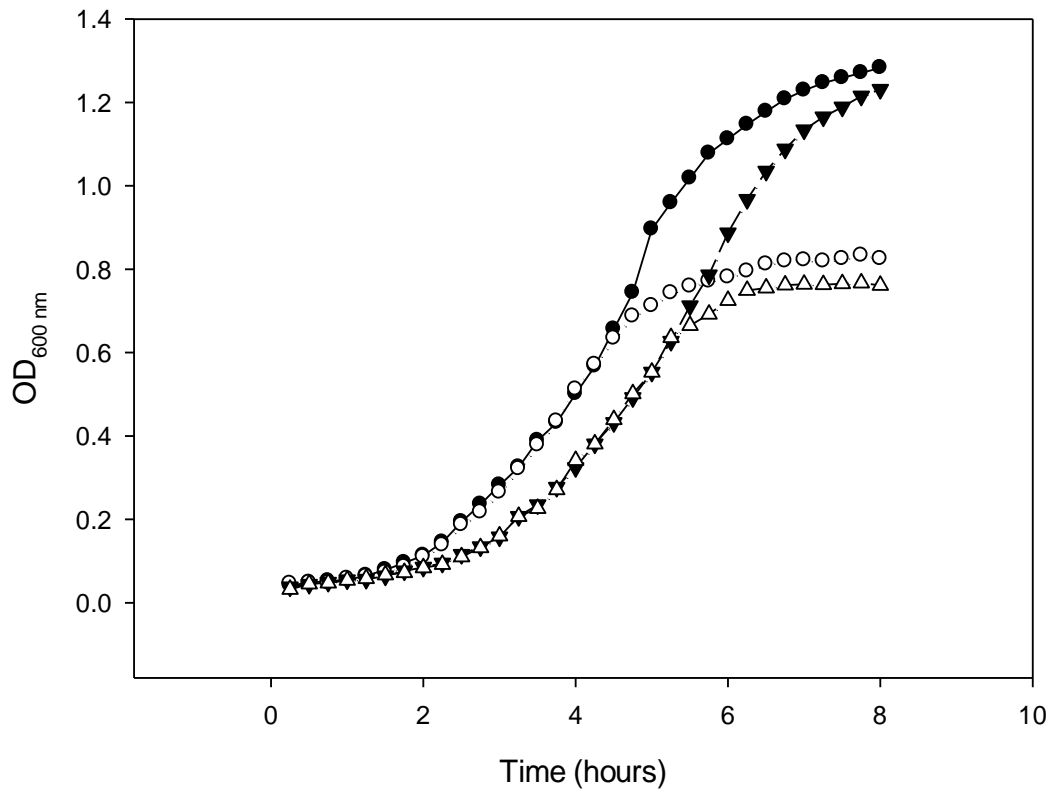


Figure 3.3: Growth curve of C247S mutant with (○) and without (●) IPTG induction with 400 mM IPTG compared with C247S/Y151C mutant with (△) and without (▼) induction with 400 mM IPTG at an optical density of 0.6 at 600 nm. The speed of growth of Y151C is representative of all double mutants of KvAP and the pore domain only mutant.

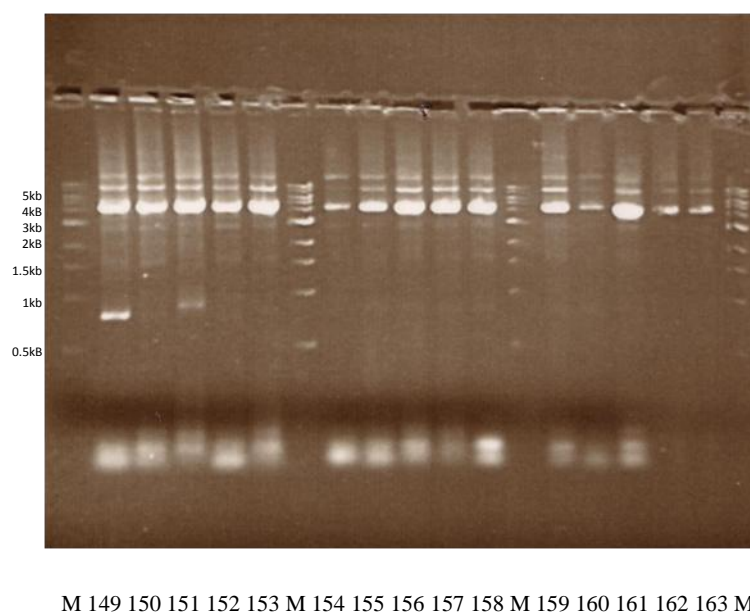


Figure 3.4: 1% agarose gel of S5 helix PCR reactions. This gel shows 5 μ l of PCR reactions for mutants at positions 149 -163 separated by 1kb ladder. The PCR products run at ca 4.5 kb in agreement with the size of the 981kb KvAP gene in a pQE-60 vector.

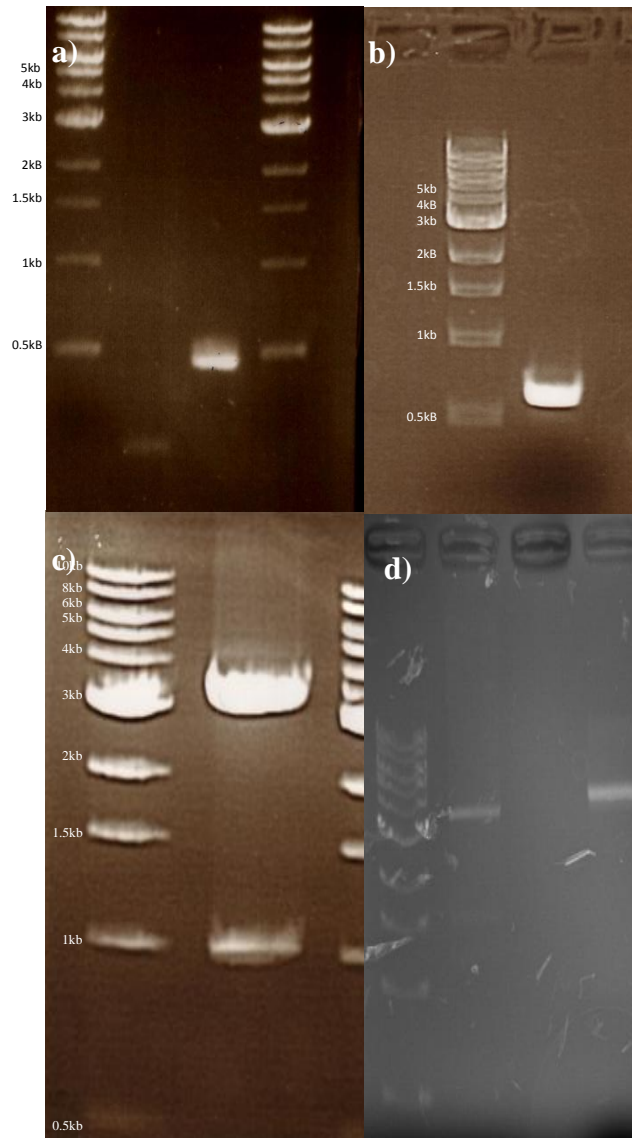


Figure 3.5: Two stitch PCR for removal of voltage sensing domains from KvAP, analysed by 1% agarose gel. **(a)** Reaction 1a+b. Lane 1 and 4 contain 1kb Ladder (NEB), Lane 2 contains reaction 1a, amplifying the N terminal 187 bases of KvAP to the voltage sensor, Lane 3 contains reaction 1b, amplifying the C terminal 471 bases of KvAP. **(b)** Lane 1 contains 1kb ladder, Lane 2 contains the product of reaction 2 showing a single band of between 500 and 100 kb(c) Lane 1 contains 1kb ladder, Lane 2 contains a test digest of pQE-60 vector containing KvAP with XhoI and BglII showing two bands, pQE 60 at 3.5kb and KvAP at 1kb **(d)** Lane 1 contains 1kb Ladder, Lane 2 contains pore only mutant in pQE-60, Lane 3 is empty and Lane 4 contains full length KvAP in pQE-60

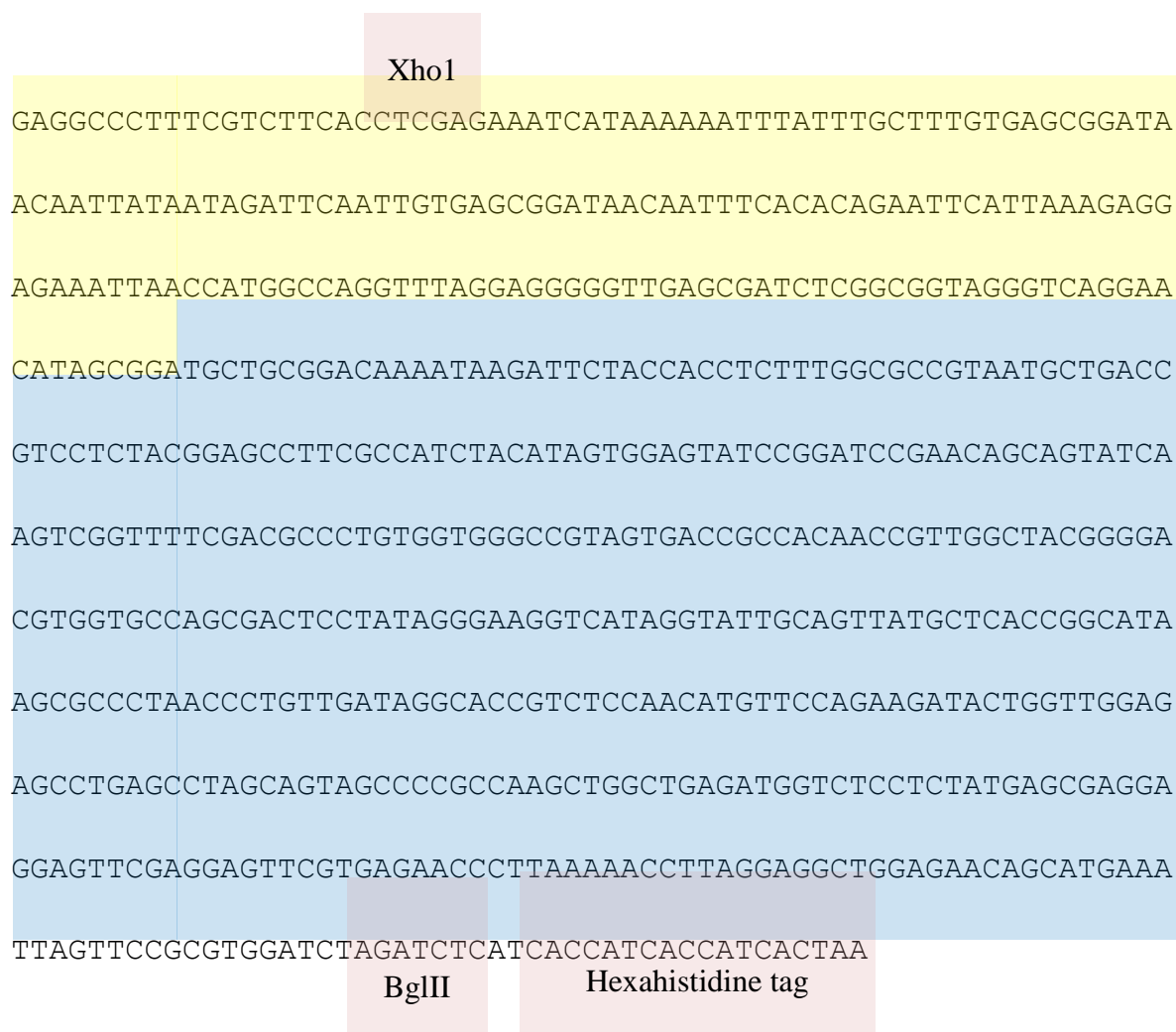


Figure 3.6: Sequence of pore domain only mutant showing the C and N terminal regions flanking the voltage sensing domains in blue and yellow respectively. Restriction enzyme sites for enzymes used and the sequence of the polyhistidine tag are overlaid with red transparencies.

3.4 Discussion

3.4.1 Generation of cysteine free and single cysteine mutants of KvAP

Single cysteine mutants of KvAP were generated at each position in the S5 helix, the outer helix of the KvAP pore domain. All mutants shown were produced successfully by PCR, and expressed at milligram quantities under the same expression conditions as for wild type KvAP. It was noted, however, that XL-1 blue cells containing the C247S KvAP mutant and another single cysteine substitution grew slower than cells containing the C247S mutant as is shown in Figure 3.3, resulting in the time taken to reach an O.D. of 0.6 at 600 nm being an hour longer for double mutants of KvAP.

3.4.2 Generation of the pore domain only mutant

A KvAP pore only mutant was produced by two stitch PCR. The reaction products of all PCR reactions were of the correct size for the segments of the KvAP gene which were being amplified. The digestion with XhoI and BglII (data not shown) was successful for both the pore only insert and for the pQE-60 vector. Ligation of the pore domain only mutant into cut pQE-60 was successful and the pore only mutant was successfully transformed into XL-1 Blue cells and expressed to the same level as wild type KvAP under the same expression conditions as KvAP.

3.4.3 Generation of single cysteine mutants of the pore domain only mutant

Single cysteine mutants of the KvAP pore domain only mutant were generated at each position in the S5 helices for KvAP itself. All the mutants shown were produced successfully by PCR as determined by nucleotide sequencing, and expressed at milligram quantities under the same expression conditions as the KvAP pore domain only mutant.

4 Chapter 4: Characterisation and reconstitution of wild type and mutant KvAP

4.1 Introduction

Biological membranes are highly diverse structures with many different components. This makes it difficult to study individual proteins under repeatable conditions. Model membrane systems allow the study of purified membrane proteins reconstituted into lipid bilayers of known composition, allowing the study of lipid-protein interactions.

4.1.1 Detergents

In order to study membrane proteins *in vitro* it is essential to have a method for isolating the protein from other components of the cell membrane without causing irreversible damage to the protein. Detergents provide an answer to this problem, as they are able to mimic the hydrophobic effects of a membrane on a protein for short periods of time, and can then be removed (DeGrip et al. 1998). If the detergent solution contains a mixture of lipid and protein, removal of the detergent will allow a lipid bilayer to form around the protein (Sonoda et al 2011). Detergents are amphipathic with a hydrocarbon nonpolar region and a polar region which may or may not be ionic. In aqueous solution it is energetically favourable for detergents to form micelles where the hydrophobic tails are sequestered from water and the hydrophilic head groups are exposed to water (Ludlum 1956). The formation of micelles only occurs once a certain concentration of detergent is reached, known as the critical micelle concentration (CMC). The more hydrophobic the non-polar region of a detergent is, the more readily it will form micelles and hence the lower the CMC will be. Detergents with high CMCs are therefore convenient for reconstitution experiments as it is then relatively easy to lower the concentration of the detergent below the CMC (for example, by dilution, dialysis or using absorbent beads) to reform membranes (Horigome 1983).

Different detergents have varying efficacy for solubilising membrane proteins and are generally classified into one of three groups – non-ionic detergents, ionic detergents and steroid based detergents. The headgroups of non-ionic detergents often consist of sugar molecules, as in n-decyl- β -D-maltopyranoside (DM) and n-

octyl- β -D-glucopyranoside (OG), which contain maltose and glucose headgroups respectively. These detergents are often used for solubilising membrane proteins due to their high critical micelle concentrations and weak denaturation properties. Ionic detergents consist of a hydrocarbon tail and a charged headgroup. Sodium dodecyl sulphate (SDS) is a much used ionic detergent but its strong protein denaturing properties mean that it is unsuitable for reconstitution experiments. Steroid based detergents such as cholate are rigid molecules based on a steroid nucleus with small hydrophilic regions and the high cmc for cholate again makes it a convenient detergent for reconstitution.

4.1.2 Solubilisation

Solubilisation is the process by which the lipid bilayer surrounding a membrane protein is replaced by detergent. Solubilisation has been described as having three phases – detergent entry into the lipid bilayer, an increase in the detergent levels within the bilayer, and finally disruption of the bilayers to form detergent-lipid-protein micelles when the concentration of detergent reaches its CMC (Pata et al. 2004). When a high concentration of detergent is added to a solution containing bilayers of any form, structural changes are immediately evident in the bilayers in the form of increased permeability as detergent molecules partition into the membrane. As the concentration of detergent in the membrane reaches the CMC the bilayers destabilise and become structurally unstable, leading to a transition to a mixed lipid-detergent-protein micellar phase. The final phase of membrane solubilisation involves the formation of detergent-lipid-protein micelles and the loss of the bilayer structure (Pata et al. 2004).

4.1.3 Reconstitution

As already described, detergents are able to keep membrane proteins in a soluble form for a limited period of time in the absence of lipid molecules. For the purification of a membrane protein a detergent must be chosen that does not denature the protein. However, the environment provided by even a mild detergent is likely to be significantly different to that provided by a lipid bilayer, hence proteins are often less stable in a detergent solution than in a lipid bilayer (Sonoda et al 2011). Further, it is known that the function of many membrane proteins in

lipid bilayers is very sensitive to the chemical structures and characteristics of membrane lipid (Lee 2003). In order to study the structure and function of a purified membrane protein it is therefore necessary to reconstitute the protein into a lipid bilayer. This can be achieved by mixing lipid and protein in a detergent solution and then removing the detergent to reform membranes. Detergent can be removed by simply diluting the detergent solution so that the concentration of detergent falls below its CMC (Rigaud et al. 1995), when it will no longer form micelles, allowing membranes to form. Detergent can also be removed by dialysis, or using absorbent beads such as BioBeads. Reforming membranes by dilution forms bilayer fragments or unsealed vesicles due to the rapidity of the dilution process, whereas dialysis and BioBeads remove the detergent more slowly resulting in the formation of sealed vesicles.

4.2 Methods

4.2.1 Reconstitution of KvAP

4.2.1.1 Purification of KvAP

Purification of KvAP was undertaken as detailed in section 0. SDS gels of all mutants were run to confirm the purity of KvAP. Western Blots were used as in section 2.2.3.5 to confirm the presence of His-Tagged KvAP.

4.2.1.2 Purification of KvAP pore domain only mutant

Purification of the KvAP pore was undertaken as KvAP, described in section 0.

4.2.1.3 Analysis of Pore domain only mutant by native PAGE

To confirm the oligomeric state of the pore domain only mutant, the protein was analysed on a native page gel, as described in section 2.2.3.6.

4.2.1.4 Preparation of potassium cholate

Potassium cholate was prepared as detailed in section 2.2.4.1.

4.2.1.5 Preparation of stock lipid

Stock DOPC was prepared as described in section 2.2.4.2.

4.2.1.6 Preparation of BioBeads SM2

BioBeads were used to remove detergent from a lipid-protein-detergent mixture before loading onto a sucrose density gradient, and were prepared as described in section 2.2.4.6.

4.2.1.7 Reconstitution using BioBeads

Where it was required for KvAP to be reconstituted into a bilayer with no increase in volume, BioBeads SM2 were used. Reconstitution with biobeads was performed as described in section 2.2.4.7.

4.2.2 Characterisation of reconstituted sample on a sucrose density gradient

A sucrose density gradient was used to show the successful reconstitution of KvAP and the pore domain only mutant into DOPC. The sucrose density gradient was prepared as described in section 2.2.4.7.

4.2.3 Solubility of KvAP in detergent solutions

In order to determine which detergents best solubilised KvAP and the pore domain only mutant, the proteins were solubilised in a range of detergents and the amount of light scatter measured, as described in section 2.2.4.9.

4.2.4 Functional assays of KvAP and its mutants.

In order to determine that KvAP had the same activity as reported by other groups, single channel recording were taken as described in section 2.2.5, current-voltage curves were then produced as described in section 2.2.5.1

4.3 Results

4.3.1 Characterisation of KvAP

4.3.1.1 Purification of KvAP and single cysteine mutants

Figure 4.1a shows a typical SDS PAGE gel of wild type KvAP; wild type KvAP and mutants thereof are seen to run at between the 28 kDa and 38 kDa standards on the SeeBlue Plus2 protein ladder, consistent with the molecular weight of a KvAP monomer with polyhistidine tag attached of 32535 Da. Higher molecular weight bands correspond to multimers and appear at the correct molecular weights. All single cysteine mutants of KvAP express to the same level or higher than the expression of wild type KvAP; a comparison of protein yields attained from the purification protocol for all mutants can be seen in Table 4.1. Figure 4.2 shows a merged representative gel with wild type and mutant proteins, each with 3 µl of eluate from the third 1 ml fraction collected from the His-trap column. The intensity of all bands on the gel indicate that the expression of all the mutants from the protocol is similar.

4.3.1.2 Western Blots of KvAP

Western blotting was used to confirm that the protein running at the correct molecular weight on the SDS PAGE gels was KvAP. The protein was detected using an antibody to the C terminal polyhistidine tag attached to KvAP so that only KvAP expressed to full length will be detected. Figure 4.1b shows a western blot of the SDS gel of wild type KvAP seen in Figure 4.1a. This shows the large band of protein running between the 28 kDa and 38 kDa bands to be KvAP monomer. Dimer, trimer and tetramer are seen next to the appropriate molecular weight bands.. The results show that KvAP runs predominantly as a monomer with some higher aggregates up to the tetramer, unlike KcsA which runs predominantly as a tetramer.

4.3.1.3 SDS Gels of KvAP pore domain only mutant

The calculated molecular weight of the pore domain only KvAP mutant with polyhistidine tag is 19002 Da. The SDS PAGE gel in Figure 4.3a shows a heavy

protein band running just above the 18 kDa molecular marker consistent with the molecular weight of the pore domain only mutant. Dimer and tetramer are also visible at the expected molecular weights.

4.3.1.4 Western Blots of Pore domain only mutant

The Western blot of an identical gel to that seen in Figure 4.3b using an antibody to the polyhistidine tag confirms the heavy band seen in the SDS PAGE in Figure 4.3a to be the monomer of the pore domain only mutant. Dimer and tetramer are visible, and correspond to bands visible with coomassie staining in Figure 4.3a.

4.3.1.5 KvAP pore domain only analysis by Native PAGE

The pore domain only mutant was analysed by native PAGE to determine whether the pore domain was capable of tetramerisation without the voltage sensing domain. Figure 4.4a shows two bands for the pore only domain, the major band running at ca 220 kDa with a smaller band at 140 kDa. These are higher than would be expected; the tetramer would be expected to run at 76.39 kDa and the monomer at 19.09 kDa. To check whether the protein runs as expected in native PAGE gels KcsA was run on an identical gel; KcsA is known to be stable in SDS and runs as a tetramer on a denaturing gel and so would be expected to run as a tetramer in a non-denaturing gel. As shown in Figure 3.3b, the major band for KcsA is at ca 190 kDa, much higher than expected for a tetramer. However, if the major band for KcsA at ca 190 kDa does indeed correspond to the tetramer, the results would suggest that the major band for the pore only mutant at ca 220 kDa is likely also to correspond to the tetramer. For KcsA bands are also seen at higher apparent molecular weights (Figure 3.3b) presumably corresponding to aggregates of KcsA.

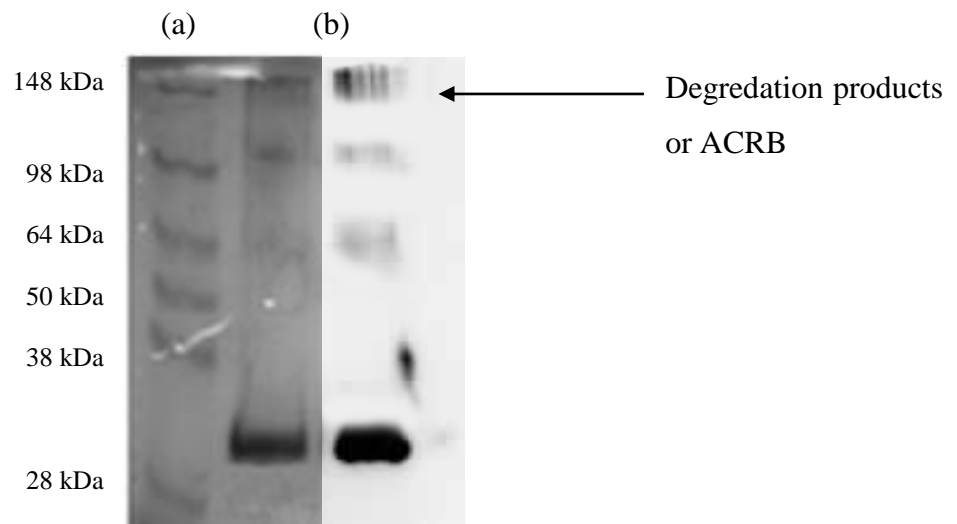


Figure 4.1. SDS analysis of wild type KvAP. **(a)** A typical SDS polyacrylamide gel showing purified KvAP immediately after elution from a nickel column with molecular weight markers on the left. **(b)** Western Blot of polyacrylamide gel identical to (a) loaded with the same sample. Dimer and trimer are visible at the correct molecular weights

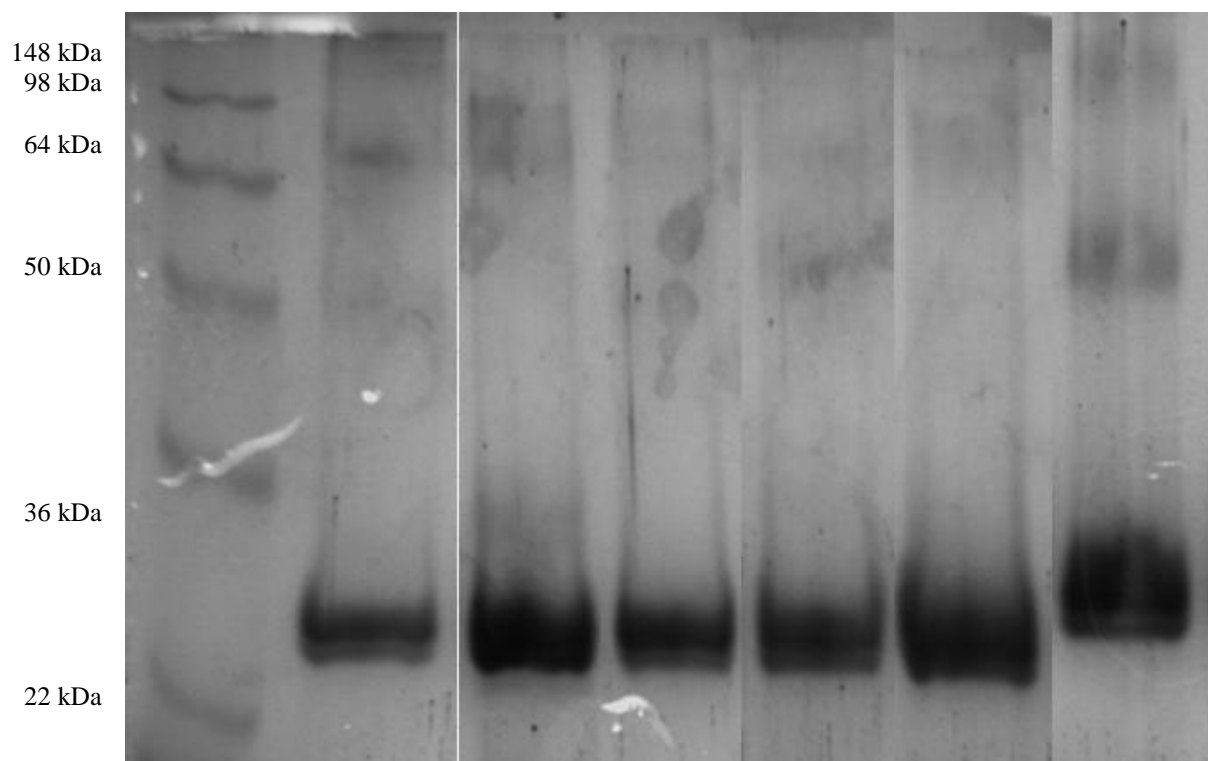


Figure 4.2. Merged representative gel of cysteine mutants of full length KvAP. Lanes left to right are SeeBlue Plus2 protein molecular weight marker 153C, 156C, 160C, 170C and 173C immediately after elution from a nickel column with molecular weight marker labelled in the first lane. Some extra bands are shown between dimer and tetramer (labelled) and are presumed to be multimers products.

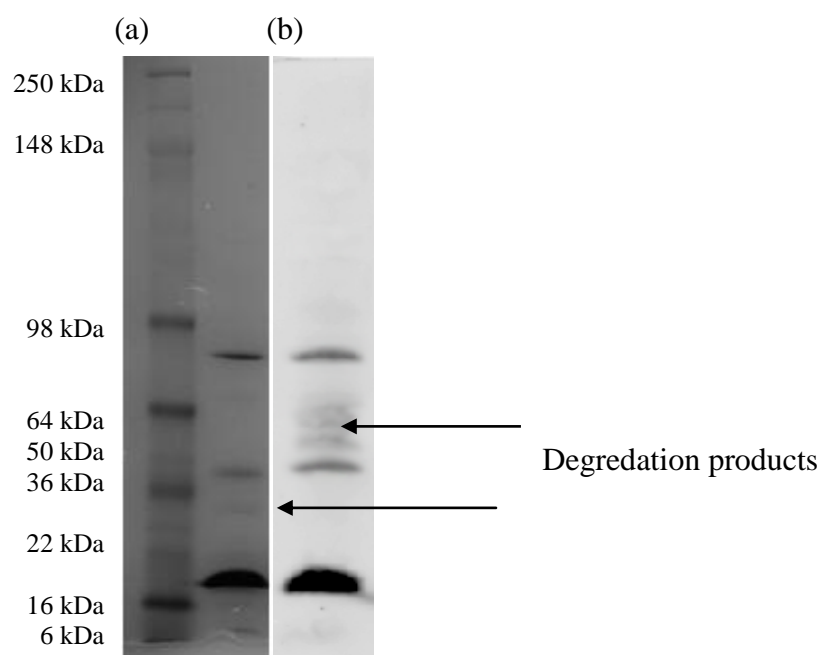


Figure 4.3. (a) Purified pore domain only mutant immediately after elution from a nickel column with molecular weight marker labelled in the first lane. (b) Western blot with antibody against the hexahistidine tag showing monomer, dimer and tetramer bands. Some extra bands are shown between dimer and tetramer (labelled) and are presumable degredation products. KvAP has a long C terminal tail, removal of which would allow tetramerisation, but reduce the molecular weight.

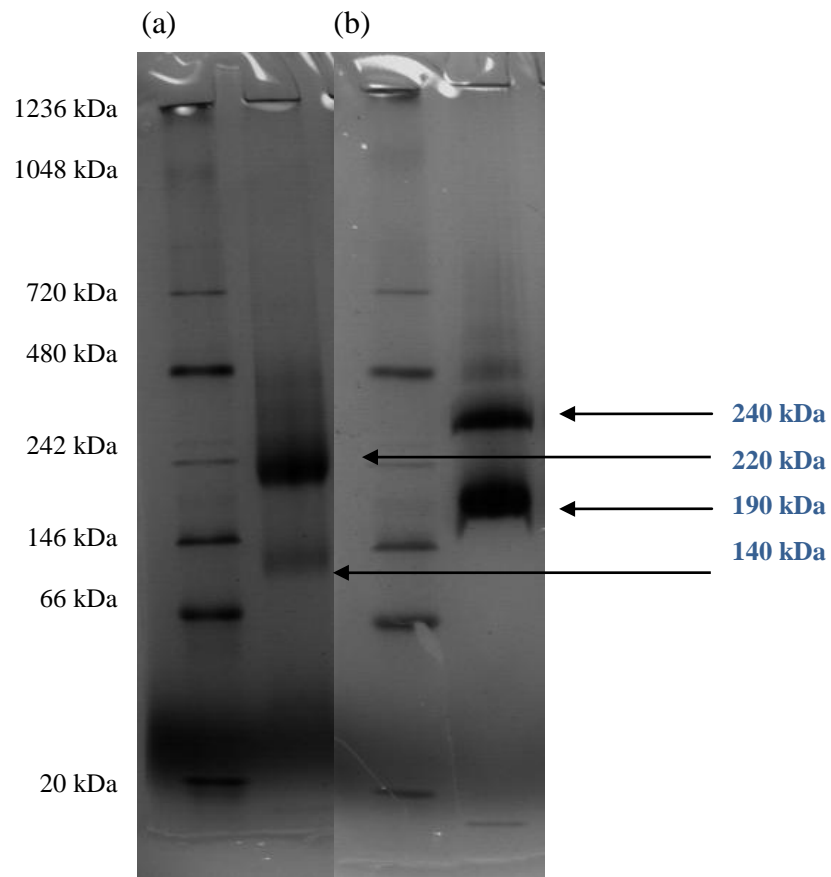


Figure 4.4. (a) Non denaturing gel of KvAP pore domain only mutant showing a dense band at ca 220 kDa with a lighter band at ca 140 kDa (b) Non denaturing gel of KcsA showing a dense band at ca 190 kDa and a higher molecular weight band at ca 300 kDa

Full length KvAP	Concentration (mg/ml)	Pore domain only mutant	Concentration mg/ml
Wild Type	6.45	Wild type	6.76
C247S	8.85	-	-
151	8.34	151	5.78
152	7.34	152	5.44
153	6.78	153	6.75
154	8.36	154	6.43
155	8.65	155	4.87
156	7.36	156	5.87
157	8.8	157	5.34
158	8.94	158	5.69
159	7.81	159	6.2
160	8.34	160	5.93
161	8.36	161	5.23
162	8.31	162	4.99
163	7.98	163	7.12
164	7.56	164	6.22
165	7.62	165	5.64
166	6.98	166	7.01
167	7.04	167	5.76
168	8.52	168	5.66
169	9.1	169	4.32
170	9.32	170	5.21
171	7.56	171	5.86
172	7.43	172	5.9
173	8.45	173	4.98
174	8.11	174	5.22
175	8.34	175	175

Table 4.1: Concentrations realised from purification protocols for all mutants. The concentration show is that of the third 1 ml fraction eluted from the His Trap column. All figures are the average of two purifications.

4.3.1.6 Solubility of KvAP

The solubility of KvAP was determined in a number of detergents, and the efficacy of each was assessed by the ability of the detergent to reduce light scatter caused by KvAP in Hepes buffer. The properties of the detergents used are shown in Table 4.2 and the results of the light scatter experiments are shown in Figure 4.5. OG is a non-ionic detergent with a relatively high CMC; Figure 4.5a shows that full solubilisation is achieved at around 27.5 mM OG, which is slightly higher than the published CMC for OG of 21 mM. Interestingly, Figure 4.5a indicates that potassium cholate does solubilise KvAP, but the sample never reaches complete solubilisation within the concentration range tested, which extends above the CMC of cholate of 13-15 mM. DM is a non-ionic detergent which has a relatively low CMC of 1.8 mM; Figure 4.5b shows that full solubilisation of KvAP is achieved near this value, at around 2.25 mM. Unless otherwise stated, in the following experiments DM is used to solubilise KvAP and all mutants at all stages of the purification process. DDM is seen to achieve full solubilisation of KvAP at around 0.225 mM, close to the CMC of 0.17 mM.

4.3.2 Reconstitution of KvAP and mutants

KvAP was reconstituted using the dialysis procedure described above to test the homogeneity of the sample; the samples were run on a discontinuous sucrose gradient, using rhodamine-labelled PE as a marker for the lipid component.

4.3.2.1 Sucrose density gradient of KvAP

KvAP reconstituted with di(18:1)PC and Lissamine Rhodamine B labelled di(18:1)PE at a 19:1 molar ratio was run on a discontinuous sucrose gradient. Unreconstituted KvAP was found at the 30% sucrose layer (Figure 4.6). For the reconstituted sample, all of the protein was observed in fraction numbers 14-18 (Figure 4.7), with no protein in the final fraction, showing that all the protein had reconstituted with lipid. Some lipid was also found at the top of the gradient in the 2.5% fraction indicating the presence of some lipid vesicles containing no protein.

4.3.2.2

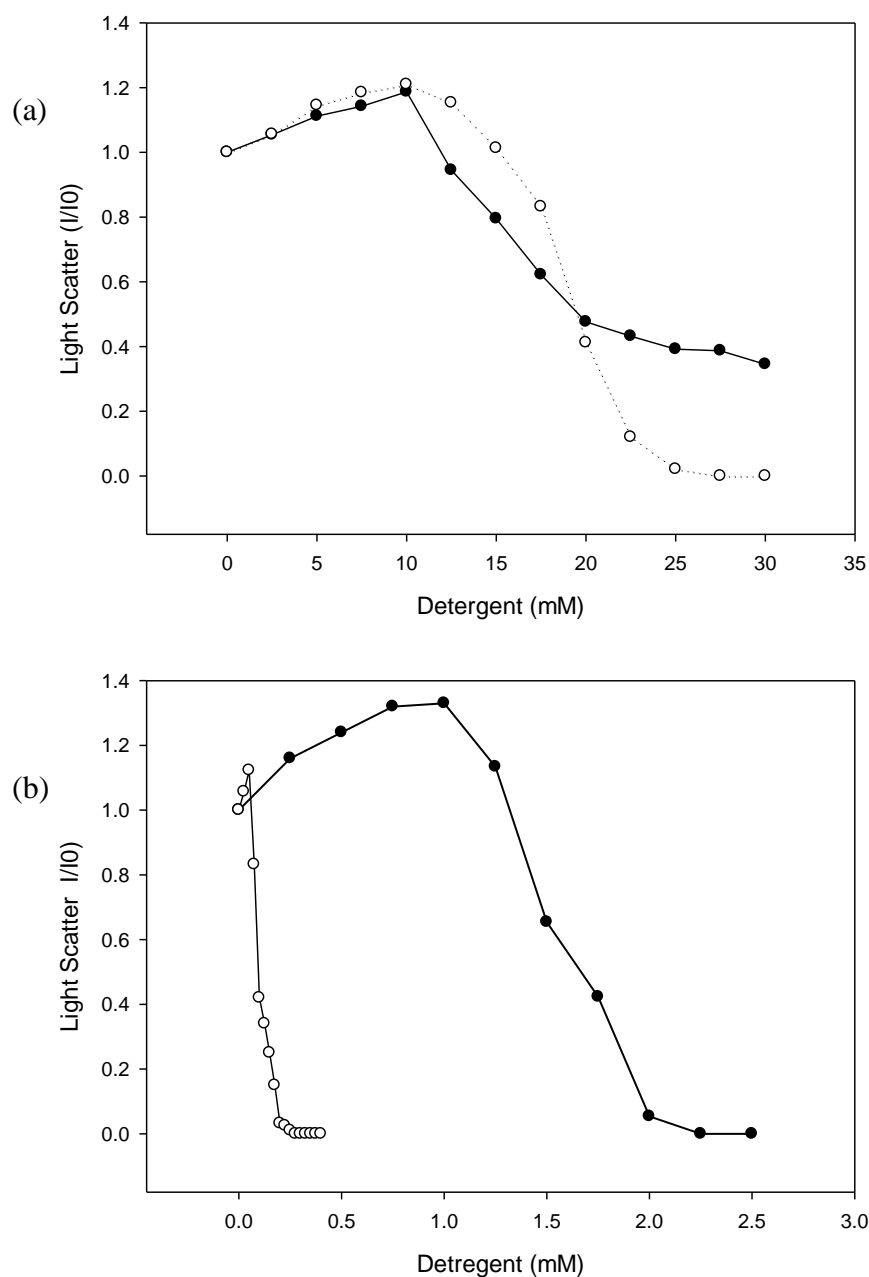


Figure 4.5. Solubility of KvAP in detergent solutions. Light scatter of KvAP (1.23 μ M) was measured as a function of increasing detergent concentration. (a) cholate (●) and OG (○) in Hepes buffer (20 mM Hepes, 1 mM EGTA, 100 mM KCl, pH 7.2). (b) DM (●) and DDM (○) Light scatter was recorded at 500 nm and expressed as I/I_0 where I is intensity in the presence of detergent and KvAP and I_0 is intensity in the absence of detergent.

4.3.2.3 Sucrose density gradient of KvAP pore domain only mutant

KvAP pore domain only mutant was reconstituted with di(18:1)PC and Lissamine Rhodamine B labelled di(18:1)PE at a 19:1 molar ratio and run on a discontinuous sucrose gradient. When run alone, the unreconstituted pore domain was found at the 30% sucrose layer (Figure 4.6). For the reconstituted sample, all of the protein and lipid was observed in fraction numbers 11-15 (Figure 4.8), with no protein in the final fraction, showing that all the protein had reconstituted with lipid. Again a small amount of lipid was found at the top of the gradient in the 2.5% fraction which had not reconstituted showing that similarly to the results with full length KvAP, there were some vesicles in the reconstituted sample which contained no protein.

4.3.3 Activity of KvAP

The function of KvAP was determined by reconstitution of KvAP into planar bilayers in an electrophysiology system. KvAP was reconstituted into a planar bilayer system and the bilayer polarised by applying -100 mV to the *trans* compartment of the bilayer system. The bilayer was then depolarised to +100 mV and the current passing through the bilayer measured. Recordings showed the appearance of single channel opening and closing with a single channel current flow of 25 pA at 100 mV (Figure 4.9). The single channel current varied linearly with voltage in the range 0 to +100 mV.

The activity of the mutant I168C of KvAP was examined as above to ensure that the mutation did not have an effect on the activity of the channel; Ile-168 is shown in the KvAP crystal structure (Griepner et al. 2010; Jiang et al. 2003a) to face both the S6 helix and the pore helix. The membrane was polarised to -100 mV as above and subsequently depolarised to voltages of between 0 mV and +100 mV. The average current for the open channel was taken and the resultant current was then plotted as a function of depolarising voltage as seen in Figure 4.9. This showed a proportional increase in current passage through a single KvAP channel in the planar bilayer up to a maximum of 25 pA when depolarised to +100 mV (Figure 4.9), as for wild type KvAP.

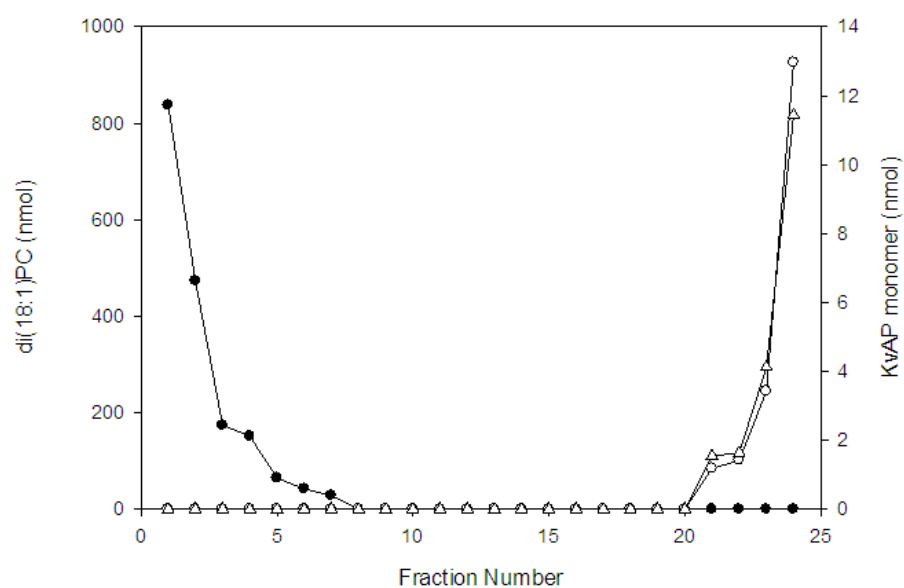


Figure 4.6. (a) Sucrose density gradient analysis. Lipid (●), KvAP (○), and KvAP pore domain only mutant (△) were run alone on separate sucrose density gradients. (b) Photograph of lipid alone after centrifugation at 80,000 g for 18 hours on the discontinuous sucrose density gradient

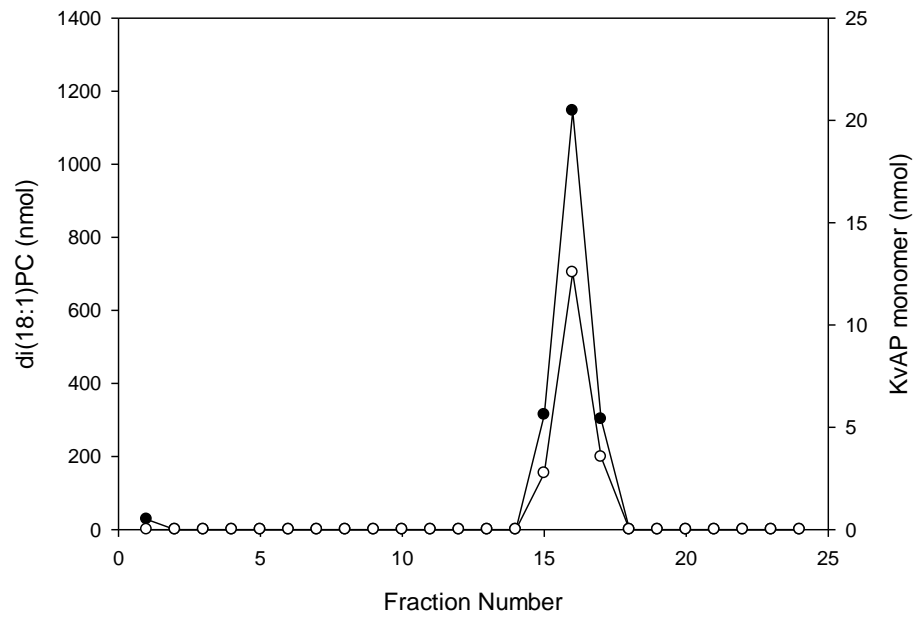


Figure 4.7. (a) Sucrose density gradient analysis of reconstituted wild type KvAP. 1.5 ml fractions were collected and assayed for lipid and protein by light absorption at 570 nm and 280 nm respectively. Amounts of lipid (●) and protein (○) are shown as a function of fraction number. **(b)** Photograph of gradient (a) after centrifugation.

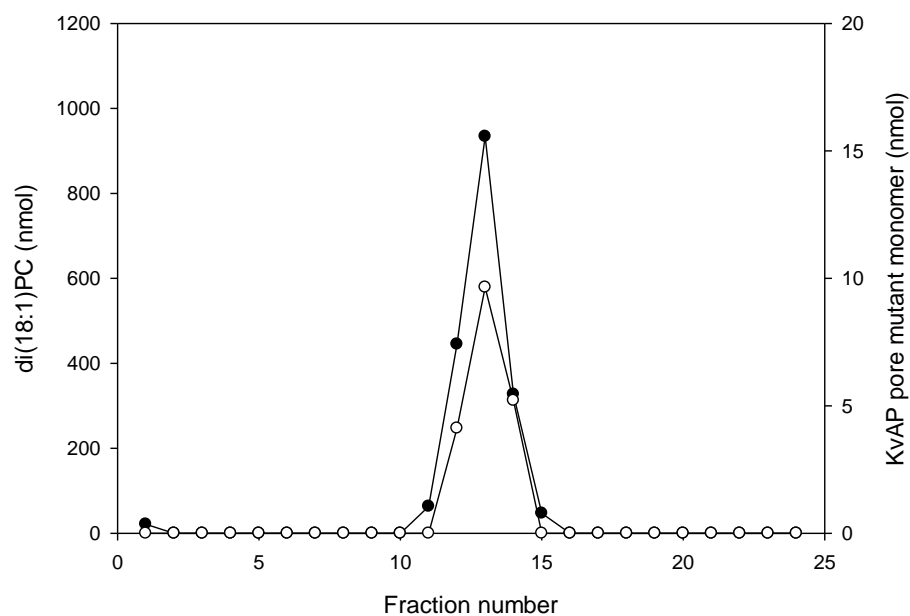


Figure 4.8. Sucrose density gradient analysis of reconstituted KvAP pore domain only mutant. 1.5 ml fractions were collected and assayed for lipid and protein by light absorption at 570 nm and 280 nm respectively. Amounts of lipid (●) and protein (○) are shown as a function of fraction number. **(b)** Photograph of gradient (a) after centrifugation..

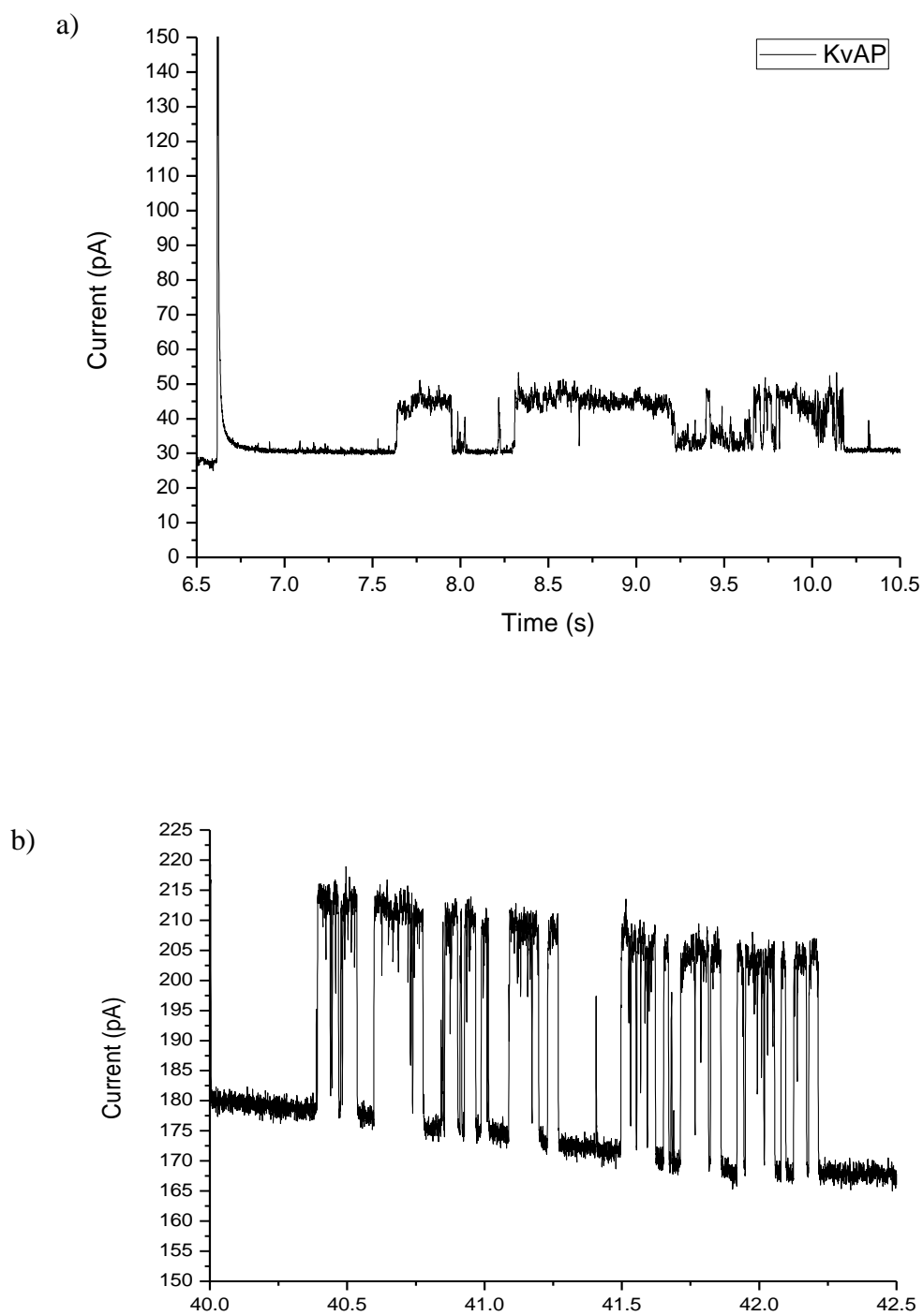


Figure 4.9. Activity of KvAP (a) Depolarisation from -100 mV to + 100 mV at 6.6 seconds resulted in single channel activity for mutant I168C (b) Depolarisation from -100 mV to + 100 mV at 6.6 seconds resulted in single channel activity for wild type KvAP.

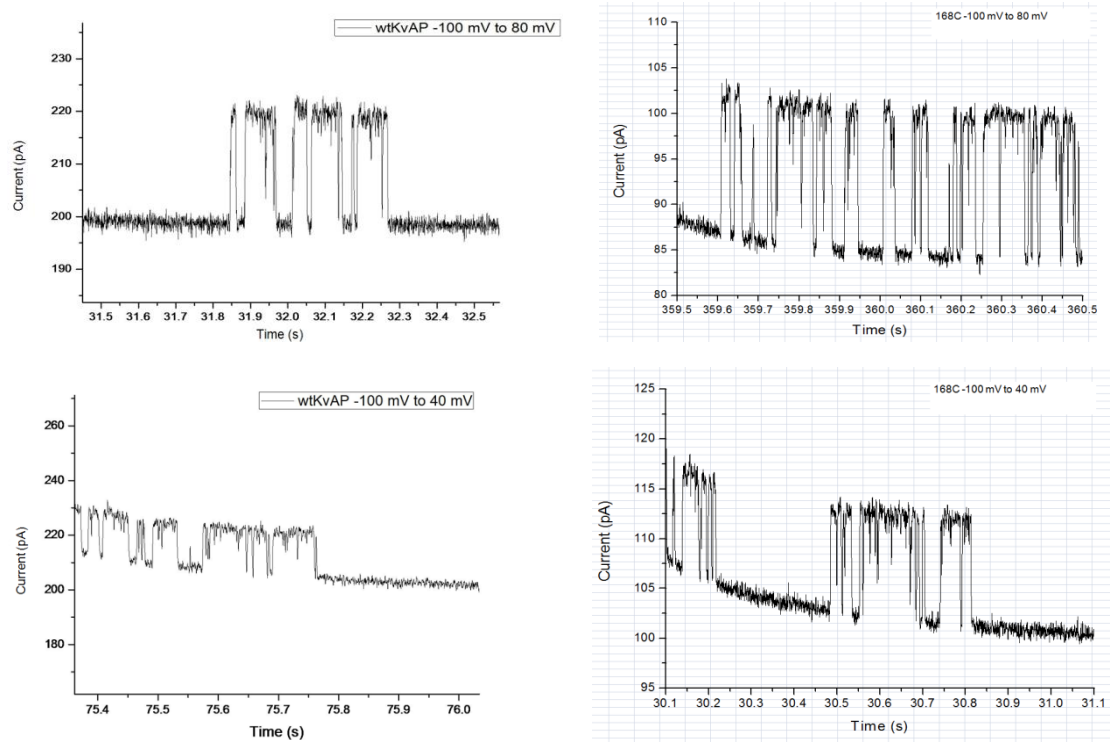


Figure 4.10: (a) Representative traces for wild type KvAP and the I168C mutant when depolarised from -100 mV to -80 mV and to -40 mV. Derived current-voltage plots can be seen in in figure 4.10

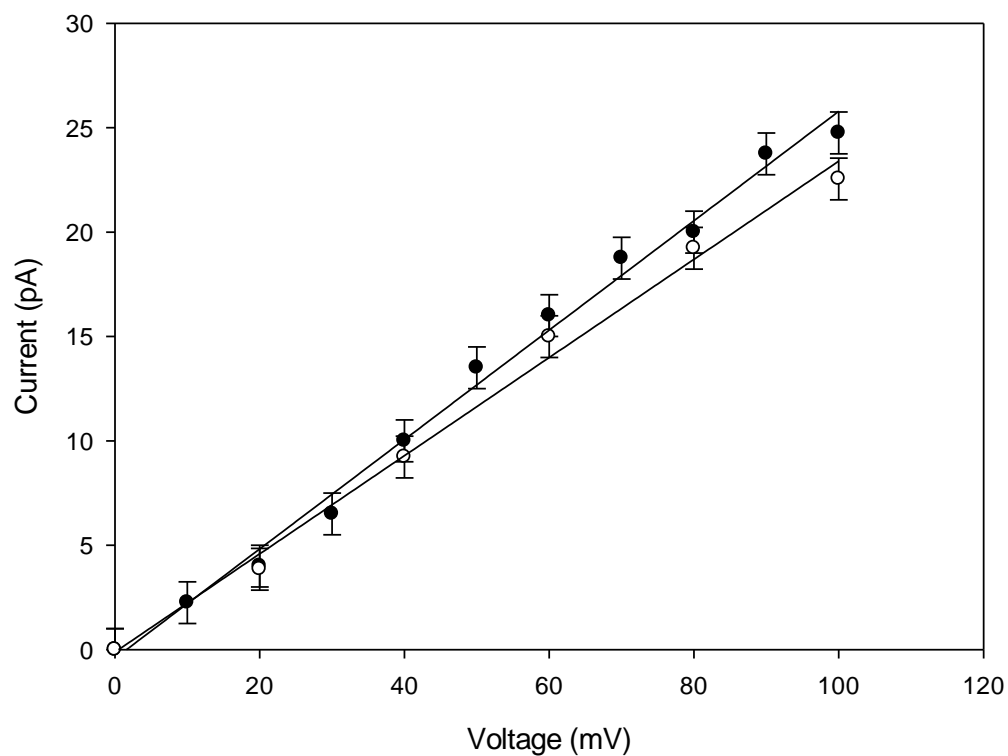


Figure 4.11: Current- Voltage graph for single cysteine mutant I168C (●) and for wild type KvAP (○). Average current observed plotted against applied membrane voltage. Data points are derived from a single recording and error bars are representative of the noise emanating from the recording equipment.

4.4 Discussion

4.4.1 Expression of KvAP and single cysteine mutants

4.4.1.1 Expression and purification of wild type KvAP

Wild type KvAP was expressed at milligram quantities under the control of an IPTG inducible expression vector. SDS polyacrylamide gels show a large band corresponding to KvAP monomer (Figure 4.1a) The protein appears to be pure, and western blot analysis with an antibody towards the hexahistidine tag shows that the protein detected on the gel is in fact His-tagged KvAP (Figure 4.1b). Lighter bands at higher molecular weights seen on the gel correspond to dimer, trimer, and tetramer, as confirmed by the western blot (Figure 4.1b).

4.4.1.2 Expression and purification of pore domain only mutant

The pore domain only mutant was successfully expressed and purified under the same conditions as wild type KvAP. The SDS PAGE gel shows that the pore domain is eluted from the column in a relatively pure state (Figure 4.3a), predominantly as monomer, with some dimer and tetramer as seen with KvAP, although no trimer was seen (Figure 4.3b)

On a non-denaturing polyacrylamide gel, the KvAP pore only mutant is seen at a much higher molecular weight than expected with a main band at ca 220 kDa compared to the 77 kDa expected for the tetramer (Figure 4.4a). For comparison, KcsA was therefore also run using the same non-denaturing gel system, and again ran at much higher molecular weight than expected (Figure 4.4b). It is possible that this band represents ACRB, a native e-coli protein which is well documented to co-purify with proteins bearing a polyhistidine tag, and would therefore be likely to appear in both the KcsA and KvAP pore mutant lanes. It is, however, more likely that this band represents aggregates of multimers, as in an SDS PAGE gel of KvAP pore domain purified with the same protocol (Figure 4.3), a band consistent with the molecular weight of ACRB (113.5 kDa) is not seen.

If the band at 220 kDa does indeed indicate the presence of ACRB, it is unlikely to affect fluorescence results, as the intensity of the band on the non denaturing gel is

significantly less than that of the KvAP pore domain mutant; as ACRB has one native cysteine, the huge excess of KvAP pore domain mutant over ACRB would result in the large majority of fluorescence signal emanating from KvAP bound fluorescence dye.

Since KcsA runs as a tetramer even in SDS PAGE gels it is likely that it also runs as a tetramer in non-denaturing gels; if the major band observed at 190 kDa for KcsA corresponds to tetramer then the major band for the pore only mutant at 220 kDa could also correspond to the tetramer. The fact that the pore only mutant reconstituted properly with lipid, as shown by the sucrose gradient experiments described later (Figure 4.8a) also argues that the mutant must have folded properly – denatured protein would not have reconstituted into a lipid bilayer.

4.4.2 Solubility of KvAP

The ability of a range of detergents to solubilise KvAP was investigated. All detergents produced a decrease in light scatter consistent with solubilisation of the protein, but varied in ability to completely solubilise the protein within the concentration range explored (Figure 4.5) DDM and DM completely solubilised KvAP at a concentration only slightly above the CMC of each lipid (Table 4.2) Cholate is not an appropriate detergent for complete solubilisation of KvAP, as although it could reduce light scatter, it did not completely solubilise KvAP even at concentrations well in excess of its CMC. OG was able to completely solubilise KvAP, but at a concentration in excess of the CMC. OG has a relatively high CMC which makes it a favourable lipid for reconstitution as the concentration of OG in solution is readily reduced below its CMC, but the superior solubilisation properties of DM mean that it was chosen as the detergent to be used in the purification of KvAP. Although cholate did not solubilise KvAP very well, it was used as a detergent for the solubilisation of lipid because of its high CMC; it has been used similarly in the reconstitution of a variety of other membrane proteins such as MscL, KcsA and diacylglycerol kinase (Carney et al. 2007; Cuello et al. 2004; Jittikoon et al. 2007; Marius et al. 2005; Powl et al. 2005)

<i>Detergent</i>	<i>Type</i>	<i>CMC (mM)</i>	<i>Monomer M_r</i>
OG	Non-ionic	20-25	292.4
Cholate	Anionic	13-15	431.0
DM	Non-ionic	1.8	492.6
DDM	Non-ionic	0.17	510.6

Table 4.2: Properties of detergents used to study KvAP solubility. Data from anatrace (<http://www.affymetrix.com>).

4.4.3 Reconstitution of KvAP

4.4.3.1 Sucrose density gradient of KvAP

A sucrose density gradient was run to determine the level of reconstitution of KvAP. KvAP was reconstituted into di(C18:1)PC doped with di(C18:1)PE labelled with rhodamine lissamine B at a 19:1 molar ratio PC:PE and a 100:1 molar ratio lipid: KvAP monomer. When KvAP was run on the gradient without lipid present it was found in the 30% sucrose region of the gradient, and lipid on its own was found in the 2.5% sucrose fraction of the gradient (Figure 4.6) When reconstituted KvAP was run on the gradient, KvAP was found between the 20 % and 25% fraction of the gradient with no protein in the 30% sucrose fractions, thus all the KvAP has reconstituted with lipid (Figure 4.7). The lipid:protein ratio of fractions which contained KvAP are shown in Table 4.3; the lipid:KvAP monomer ratios vary between 114:1 and 85:1 lipids per monomer in the fractions in which protein was detectable and very little lipid was unreconstituted. Unpublished studies by J. Bolivar Gonzalez with KcsA suggest that the presence of a small amount of protein-free lipid vesicles is associated with the use of dialysis to remove detergent and that with Biobeads no such protein-free vesicles are formed.

4.4.3.2 Sucrose density gradient of KvAP pore domain only mutant

The sucrose density gradient of KvAP pore domain only mutant largely reflects that of wild type KvAP, and is again consistent with a homogenous reconstitution of the protein at a molar ratio of lipid to protein monomer of ca 100:1 (Figure 4.8, Table 4.3) These experiments suggest that the pore domain cannot be present in a denatured, aggregated form, as this would not have reconstituted into a lipid bilayer. Given that the P-loops between helices S5 and S6 come together in the native structure to form the central, tetrameric selectivity filter, it is not unlikely that the pore domain will have adopted a tetrameric form in the reconstituted membranes, although there is no direct proof of this. However the presence of small quantities of tetramer on denaturing SDS PAGE discussed above also suggests that the pore forms stable tetramers in detergent.

(a)

<i>KvAP (wild type)</i>			
Fraction number	Lipid (nmol)	Protein (nmol monomer)	Ratio lipid:KvAP monomer
14	52	-	-
15	314	2.7	114
16	1146	12.5	91
17	302	3.5	85
18	34	-	-

(b)

<i>Pore domain only mutant</i>			
Fraction number	Lipid (nmol)	Protein (nmol monomer)	Ratio lipid:KvAP monomer
11	63.0	0.00	-
12	445	4.12	108
13	934	9.65	96
14	327	5.21	62
15	47	0.00	-

Table 4.3 (a) Sucrose density gradient results for fractions containing KvAP. Amounts of lipid and protein in each fraction were determined by absorbance at 570 nm and 280 nm respectively. **(b)** Sucrose density gradient results for fractions containing KvAP pore domain only mutant. Amounts of lipid and protein in each fraction were determined by absorbance at 570 nm and 280 nm respectively.

4.4.4 Function of wild type KvAP and single cysteine mutants

4.4.4.1 Wild type function

Function of wild type KvAP was measured by reconstituting KvAP into a BLM system and applying a constant hyperpolarising membrane voltage. The membrane was subsequently depolarised and the single channel activity was detected (Figure 4.9). KvAP was found to be active when reconstituted into 75% POPE/25% POPG. The single channel activity seen is similar to that reported by other groups for wild type KvAP (Griepnerau B 2010). The conductance for wild type KvAP and the mutant I168C channel were calculated using equation 4.1.

Equation 4.1

$$C = \frac{I}{V}$$

This gave conductance for wild type KvAP of 227.70 pS \pm 21.89 pS, and the mutant channel of 245.75 pS \pm 24.15 pS (error is standard deviation). Both of these values are higher than that of 150 pS which was experimentally determined by Griepnerau B (2010), but is closed to that calculated by Ruta et al. (2003) [supplemental data] of 187.5 (no error given). This supports the assumption made in the electrophysiological experiments that the recordings are of a single channel rather than multiple channels. This is further supported by the absence of double-stepped traces in any of the representative images.

4.4.4.2 Function of I168C mutant

The I168C mutant was reconstituted into vesicles and fused with planar bilayer as described. The membrane was held at a constant voltage and depolarised to a range of membrane potentials (Figure 4.11). A linear relationship was seen between voltage and current, increasing to 25 pA at 100 mV. A slightly higher current (by ca. 2.5 pA) was observed with I168C than for wild type KvAP. Mutant I168C was chosen for study because the crystal structure of KvAP shows Ile-168 in a particularly critical part of the structure, facing both the S6 helix and the pore helix.

The small increase in conductance as a result of the isoleucine to cysteine mutation could therefore reflect a small change in the pore structure. Perozo (Cuello et al. 2004) has prepared a large number of single Cys mutants of KvAP for study by EPR, and has also found no large effects of mutation on function.

5 Chapter 5: Determining the structure of KvAP using IANBD fluorescence

5.1 Introduction

Fluorescence is a highly sensitive method which can be used to study the structure and function of both water soluble and membrane proteins (Lakowicz 1999). Fluorescence has an advantage over many other analytical methods in that it can be used to study a protein in its native environment, as opposed to other techniques which require the protein of interest to be in a non-physiological environment to be studied (Lee 2003).

5.1.1 Fluorescence

Fluorescence usually arises from aromatic or polyunsaturated compounds and is the process in which photons are emitted from a molecule following excitation by light (Lakowicz 1999). Absorption of a photon of light leads to excitation to an energetically excited state on a timescale of 10^{-15} seconds as illustrated by the Jablonski diagram in Figure 5.1. After reaching the excited state, the electron returns to the lowest vibrational level of the excited state, S_1 , through a process known as internal conversion, which occurs within 10^{-12} seconds of excitation. Solvent relaxation around the excited state then results in a lowering of the energy of the excited state on a time scale which is dependent upon the rate of solvent motion, but is typically around 10^{-9} seconds (Figure 5.2). Finally the electron returns to the ground (S_0) energy level and energy is given out as a photon, of lower energy than that used to excite the molecule, so that the fluorescence emission is at a higher wavelength or a lower frequency than the excitation wavelength. This shift in wavelength between exciting and emitted light is known as the Stokes shift (Lakowicz 1999).

5.1.1.1 Fluorescence in proteins

Of the twenty amino acids, only three, phenylalanine, tyrosine and tryptophan, contribute to the inherent fluorescence of protein molecules and, in fact, fluorescence is predominantly due to the indole group of tryptophan. Tryptophan fluorescence is highly environmentally sensitive, and as such can be used to study the properties of membrane proteins. However, interpreting fluorescence data can

be difficult for proteins containing multiple tryptophan residues, and so the technique is most powerful for proteins where single tryptophan residues can be introduced into a region of interest. Alternatively, mutagenesis can be used to introduce residues such as Cys into a region of interest that can then be modified to introduce a chosen artificial fluorescence group (Lakowicz 1999).

5.1.1.2 Quantum yield and fluorescence lifetime

The quantum yield of a fluorophore is the ratio of the number of photons emitted to the number of photons absorbed, i.e. the probability that an electron will return to the ground state through the emission of a photon. The quantum yield can vary between 0 and 1, where a value of 0 means that the molecule is nonfluorescent and a value of 1 means that every time a molecule absorbs a photon of light it returns to the ground state by emitting a photon of light. The fluorescence lifetime is the average time that a fluorophore remains in the higher energy state once excited, and hence the amount of time a fluorophore has to undergo quenching and diffusion events.

5.1.1.3 Fluorescent probes

Fluorophores that can be used to study protein structure fall into two categories, natural fluorophores such as tryptophan, and artificial fluorophores. Artificial fluorophores are available with reactive groups that can react with groups such as the sulphhydryl or amine side chains in a protein, such as *N*-((2-(iodoacetoxy)ethyl)-*N*-methyl)amino-7-nitrobenz-2-oxa-1,3-diazole (IANBD) described below.

Environmental sensitivity often arises from solvent relaxation around the excited state fluorophore, which will have a different dipole moment to that of the ground state (Lakowicz 1999). Generally emission wavelength increases with increasing solvent polarity as shown for IANBD in Figure 5.3. Since the hydrophobic core of the membrane has a very low dielectric constant, whereas water has a high dielectric constant, fluorescence emission maxima can be used to report on the location of a group in a membrane protein relative to the surrounding lipid bilayer.

5.1.1.4 Fluorescence Quenching

Fluorescence quenching is an important property of fluorescence molecules, and arises through the deactivation of the excited state through mechanisms unrelated to radiative emission (Lakowicz 1999). There are three types of fluorescence quenching: static quenching, dynamic quenching and fluorescence energy transfer. Static quenching occurs due to the formation of nonfluorescent ground state complexes between the fluorophore and quencher molecules, which cause an immediate return to the ground state without photon emission on excitation of the complex. The level of quenching caused by such molecules depends on the concentration of the quencher and on the association constant of the quencher molecule with the fluorophore. Static quenching can be distinguished from other forms of quenching as it results in no reduction in fluorescence lifetime (Lakowicz 1999). Dynamic, or collisional quenching is caused by quencher molecules colliding with the fluorophore and the level of quenching of a given fluorophore can be described by the Stern Volmer Equation:

Equation 5.1

$$\frac{F_0}{F} = 1 + K_D[Q] = 1 + k_q\tau_0[Q]$$

where F_0 and F are the fluorescence intensities in the absence and presence of quencher respectively, K_D is the Stern Volmer quenching constant, k_q is the bimolecular quenching constant, τ_0 is the fluorescence lifetime of the fluorophore in the absence of quencher and $[Q]$ is the concentration of quencher (Lakowicz 1999). $k_q\tau_0$ gives the Stern Volmer constant. There are a number of usefull collisional quenchers available, such as molecular oxygen, many aromatic compounds, and halide ions. Quenching by halide ions such as iodide occurs through intersystem crossing to an excited triplet state, caused by spin orbit coupling of the fluorophore to the halide ion (Lakowicz 1999).

The final type for quenching is fluorescence energy transfer in which the emission spectrum of the fluorophore overlaps with the absorption spectrum of the quencher, leading to transfer of energy from the excited state of the fluorophore to the

quencher (Lakowicz 1999). Because of the spectral overlap between the emission spectrum of tryptophan and the absorbance spectra of many brominated molecules, it is possible that quenching of tryptophan fluorescence by brominated molecules occurs by a fluorescence energy transfer mechanism, as discussed later.

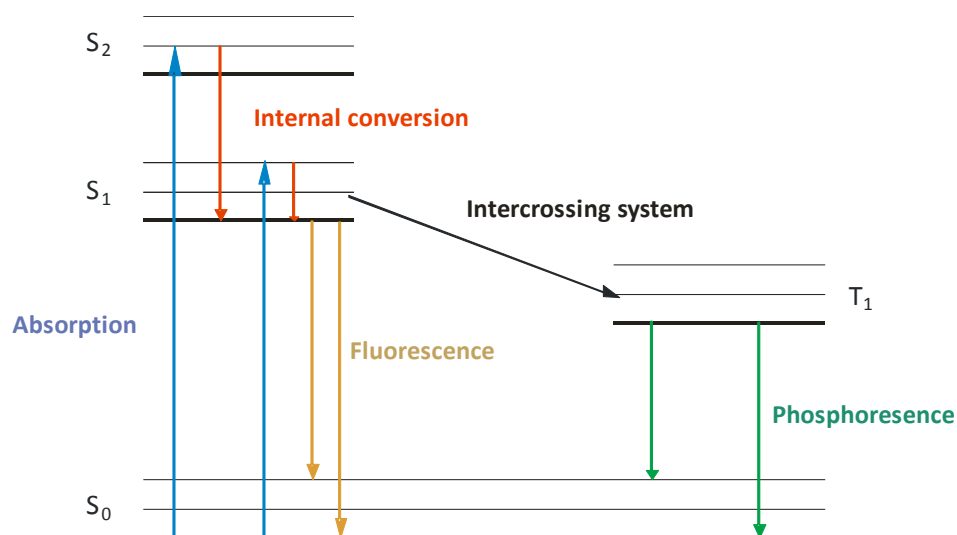


Figure 5.1: Jablonski diagram showing the phenomenon of fluorescence. Absorption of light can excite the molecule into the various singlet excited states S_1, S_2 etc. with their associated vibrational levels. Internal conversion results in the excited molecule falling into the lowest vibrational level of the S_1 state, from which fluorescence is emitted. Inter-system crossing into the triplet state T_1 is also possible, giving rise to phosphorescence. Adapted from Lakowicz 2006

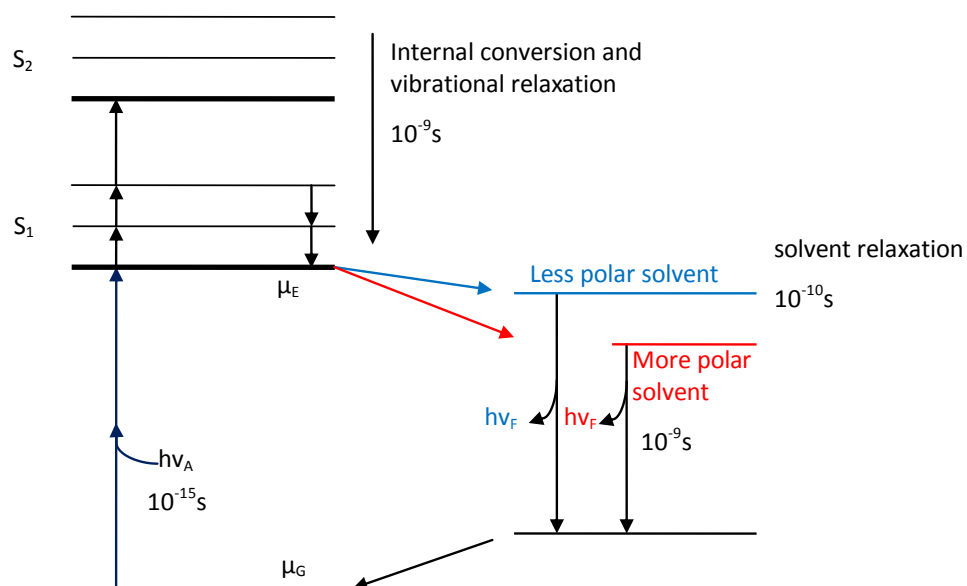


Figure 5.2: Jablonski diagram illustrating environmental sensitivity of fluorescence. The effects of solvent relaxation means that the emitted photon is of higher wavelength (lower energy) than the exciting photon.

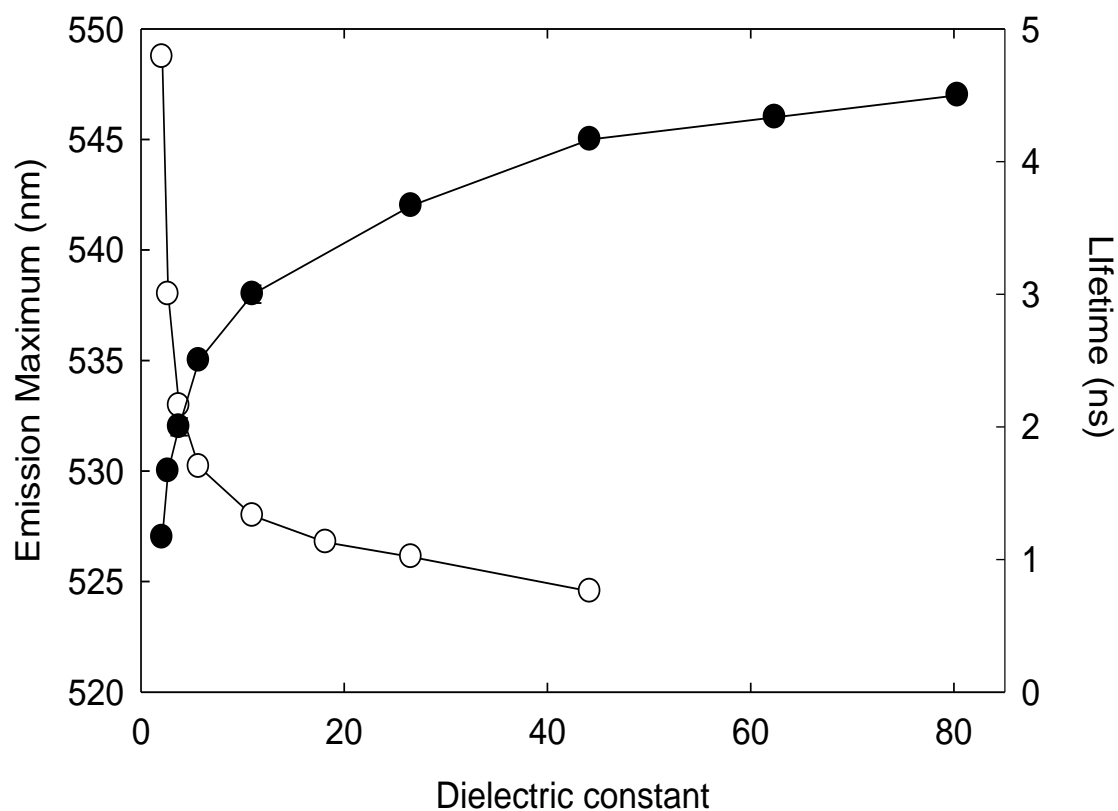


Figure 5.3: Fluorescence properties of IANBD in dioxane/water mixtures. Fluorescence emission maxima (●) and average fluorescence lifetimes (○) are plotted against dielectric constant for dioxane/water mixtures. The hydrophobic core of the membrane has a very low dielectric constant, whereas water has a very high dielectric constant. Adapted from Powl et al. (2005)

5.1.2 Using NBD to study the membrane topology of KvAP

Fluorescence has been used on many occasions to study the position of membrane proteins in a bilayer (Carney et al. 2007; Jittikoon et al. 2007; Powl et al. 2005). Often the fluorophore used is the naturally occurring tryptophan residue, which has been shown to be environmentally sensitive enough for such studies. In order to undertake such a task using tryptophan fluorescence, a protein devoid of tryptophan residues is required so that tryptophan can be substituted into points of interest in the protein and used to study the structure. Wild type KvAP contains three tryptophan residues; removal of these residues, although possible, might cause structural changes in the protein which would mean that the results obtained would not relate to the wild type protein. Cysteine reactive probes have also been used for the same type of studies; for studies involving cysteine reactive probes, a cysteine-less mutant is a requirement so that single cysteine residues can be introduced. Wild type KvAP contains only one cysteine residue which is C terminal to the end of the final transmembrane α -helix, which makes KvAP an ideal candidate for studies using cysteine reactive probes. IANBD is a cysteine reactive probe which has a molar extinction coefficient five times higher than that of tryptophan, and has a quantum yield in a hydrophobic environment which is higher than that of tryptophan (Wohland et al. 1999). NBD can be used to label cysteine residues which have been substituted into points of interest in a protein and report on the environment surrounding that amino acid. NBD has been used extensively to label proteins (Chattopadhyay 1990; Jittikoon et al. 2007; Powl et al. 2005) and lipid molecules (Mazeres et al. 1996). Emission wavelength can be used to determine the environment of NBD attached to cysteine residues, and a variety of fluorescence quenchers can be used to probe the availability of the NBD group to aqueous and membrane environments (Lakowicz 1999). NBD fluorescence can be quenched by aqueous quenchers such as cobalt ions and bromide ions, and lipid soluble quenchers such as spin labelled lipids and TEMPO, a free radical which partitions into hydrophobic areas when in aqueous solution.

5.2 Materials and Methods

5.2.1 Materials

All chemicals were obtained from Sigma Aldrich unless otherwise stated

5.2.2 Methods

5.2.2.1 Preparation of stock lipid

Stock DOPC (Avanti Polar Lipids) was produced as described in section 2.2.4.2

5.2.2.2 Preparation of stock Brominated lipid

Stock brominated dioleoylphosphatidylcholine was prepared from stock DOPC as described in section 2.2.4.3.

5.2.2.3 Preparation of Hepes buffer

Hepes buffer was prepared as described in section 2.2.6.1.

5.2.2.4 Preparation of Potassium cholate solution

Potassium cholate solution was prepared as described in section 2.2.4.1.

5.2.2.5 Preparation of Sephadex

Sephadex G-50 was used to remove free dye from the purified KvAP and was prepared as described in section 2.2.6.2.

5.2.2.6 Labelling of KvAP and mutants with NBD

Purified mutants of KvAP was labelled with the fluorescent dye IANBD as described in section 2.2.6.3..

5.2.2.7 Determination of labelling ratio

To determine what molar percentage of KvAP had been labelled, the labelling ratio of NBD to KvAP was determined as described in section 2.2.6.4.

5.2.2.8 Reconstitution of labelled KvAP into lipid bilayers by dilution

For IANBD fluorescence experiments, IANBD labelled KvAP was reconstituted into bilayers using the dilution method as described in section 2.2.4.4

5.2.2.9 Fluorescence measurements of KvAP-NBD

The fluorescence emission spectra of IANBD labelled mutants of KvAP were measured to determine the local environment of the fluorescent probe, as described in section 2.2.6.5.

5.2.2.10 Fluorescence quenching of NBD from the aqueous phase

Potassium Iodide solution was used to quench IANBD fluorescence where the NBD probe was accessible to the aqueous phase, as described in section 2.2.6.9.

5.2.2.11 Fluorescence quenching of NBD from the lipid phase

TEMPO and 16-doxyl stearic acid were used to quench IANBD fluorescence where the NBD probe was accessible to the lipid phase, as described in section 2.2.6.10 and 2.2.6.11 respectively

5.3 Results

5.3.1 Fluorescence results

Figure 5.4 shows representative spectra for KvAP and mutants 151C, 166C and 152C, as examples of cysteine bound NBD which exhibits a red shifted wavelength, a blue shifted wavelength, and a mutant which exhibits a fluorescence profile which was unexpected. All fluorescence data were recorded in triplicate, and in order to be selected had to have a peak 100 fold higher than the noise level of the instrument (14 units).

5.3.2 NBD labelling of single cysteine mutants of full length KvAP

5.3.2.1 Labelling ratios of single cysteine mutants of KvAP

Figure 5.5 shows the level of labelling of single cysteine mutants of both full length KvAP and the pore only mutant by IANBD. Each error bar is the average of three separate labelling reactions for each mutant. All mutants label to a high level, greater than 90 %. Since no mutants labelled in any labelling reaction above 100 %, this shows firstly that there is no free NBD present in solution after removal by sephadex, and secondly, that NBD effectively labels KvAP single cysteine mutants. The percentage of KvAP labelled varies little by position.

5.3.2.2 Fluorescence emission maxima

IANBD can be used to label proteins as it reacts with the sulphydryl group of cysteine residues in their reduced state. NBD labelled single cysteine mutants of KvAP were reconstituted into di(C18:1)PC and the fluorescence emission spectra were recorded upon excitation at 478 nm and fitted to a skewed Gaussian distribution to give an accurate value for the emission wavelength. NBD fluorescence is highly environmentally sensitive with an emission spectrum which peaks at 527 nm in a nonpolar environment with a low dielectric constant and at 547 nm in a polar environment with a high dielectric constant (Figure 5.3). Figure 5.6 shows the fluorescence emission maxima of NBD-labelled mutants in the S5 helix of KvAP plotted as a function of residue number.

If the S5 helix is a transmembrane α -helix lying perpendicular to the plane of the membrane, the hydrophobic core of the helix would contain around 20 amino acids. However, crystal structures of potassium channel pore domains have shown that the S5 helix is tilted away from the membrane normal (Doyle et al. 1998; Jiang et al. 2003a; Long et al. 2005a; Long et al. 2005b) and hence a longer stretch of hydrophobic amino acids are required to transverse the hydrophobic core; according to the crystal structure of KvAP (Jiang et al. 2003a) the hydrophobic transmembrane region is likely to correspond to ca residues R149 to D175 (see Table 5.1). However, tyrosine residues are often found close to the membrane interface and it is therefore possible that Y151 is the interfacial residue at the N-terminal end of the S5 helix rather than R149. Powl et al. (Powl et al. 2005), from studies with MscL, suggested that an NBD group located in the glycerol backbone region of a lipid bilayer would have an emission wavelength of 536 nm. The data shown in Figure 5.4 would then suggest that the interfacial residue is indeed Y151 on the intracellular side of the membrane; this would also be consistent with the marked decrease in emission wavelength from the position of Y151 to that of F154. At the C-terminal end of the S5 helix, the changes in emission maxima are somewhat more complex, rising from position 166 to position 174, but the emission maximum for NBD at position 174 corresponds to that expected for an interfacial residue, suggesting that P174 is the interfacial residue at the C-terminal end of S5.

The profile of NBD fluorescence emission against residue position for helix S5 shown in Figure 5.5 is generally similar to that determined by Jittikoon et al. (Jittikoon et al. 2007) in a study of the first TM α -helix of diacylglycerol kinase, also using NBD fluorescence, which showed a decrease in emission wavelength from 535 nm to 528 nm for the most central part of the helix, but with a decrease to 520 nm at the expected centre of the bilayer.

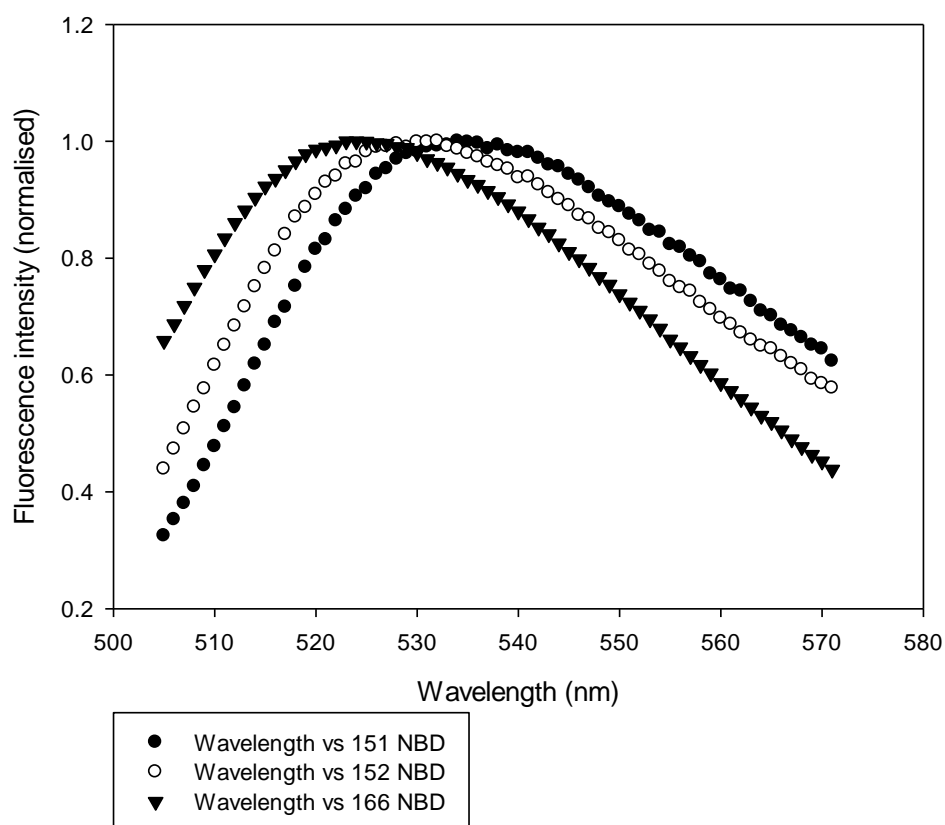


Figure 5.4: Representative fluorescence spectra of NBD bound at positions 151, 152 and 166 of full length KvAP labelled with IANBD, reconstituted into di(C18:1)PC, excited at 478 nm at 25°C in buffer (20 mM Hepes, 150 mM KCl, 1 mM EGTA, pH 7.2). Fluorescence data were recorded between 490 nm and 590 nm

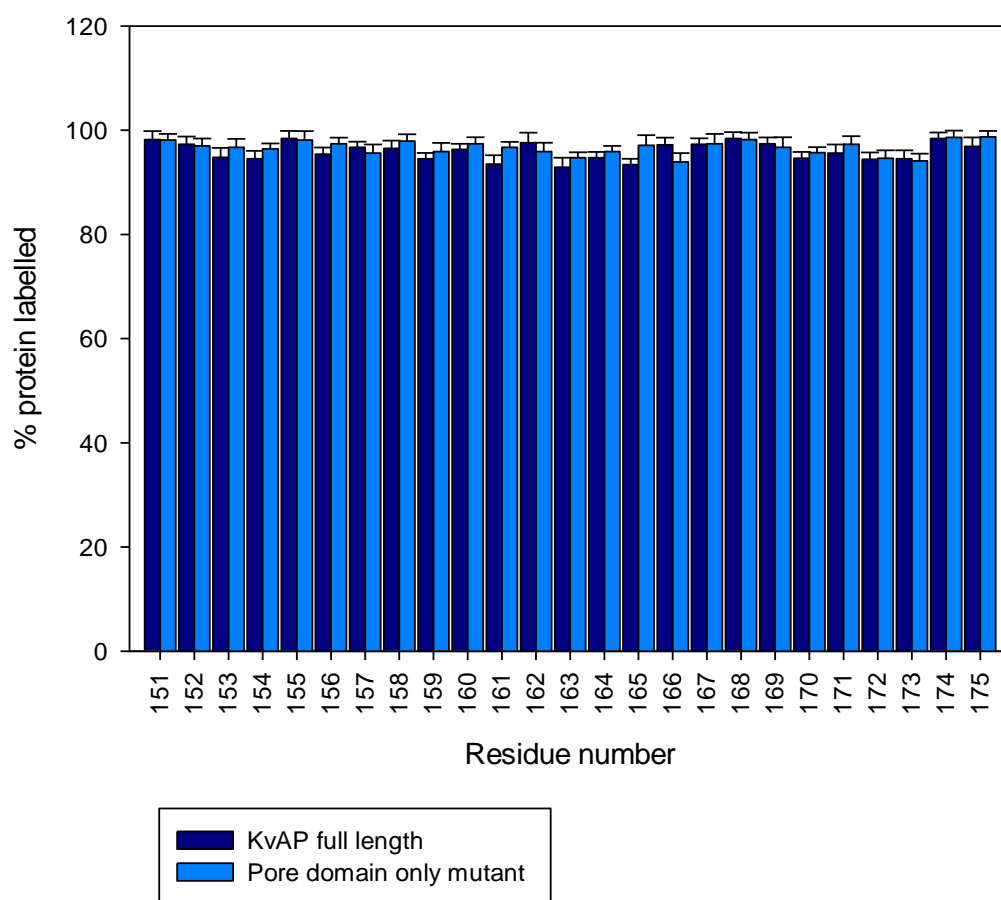


Figure 5.5: Labelling of single cysteine mutants of full length KvAP and the pore domain only mutant with IANBD. The bar chart shows the percentage of Cys residues labelled.

1.

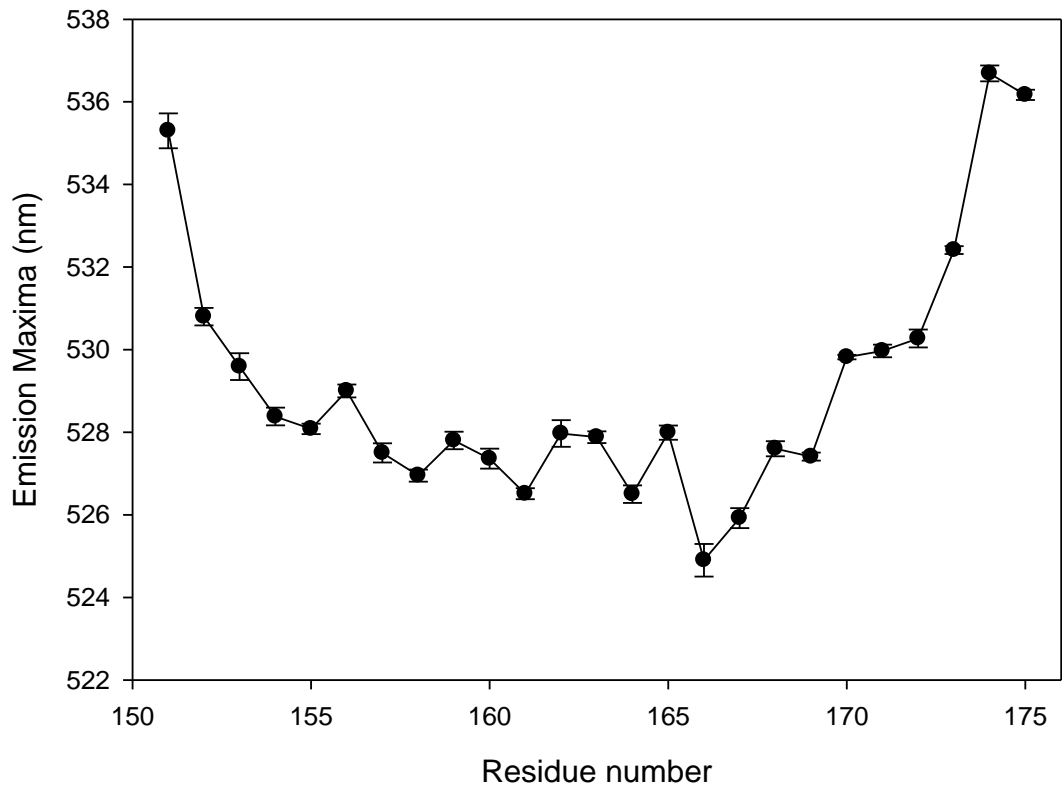


Figure 5.6: Emission maxima of single cysteine mutants of full length KvAP labelled with IANBD, reconstituted into di(C18:1)PC, excited at 478 nm at 25°C in buffer (20 mM Hepes, 150 mM KCl, 1 mM EGTA, pH 7.2). Fluorescence data were recorded between 490 nm and 590 nm and fitted to a skewed Gaussian distribution to obtain a value for the emission maximum. Error is standard deviation of measurements from three separate reconstitutions for each mutant.

<i>Residue Number</i>	<i>Resi</i>	<i>Exposure</i>
Y151 (KvAP) - G325 (chimera)	L	L
H152	VS + B	Aqueous
L153	B	B
F154	L	L
G155	VS+L	L
A156	VS+L	VS+L
V157	L	L
M158	VS+L	VS+L
L159	VS+L	VS+L
T160	B	B
V161	L	VS+L
L162	VS+L	VS+L
Y163	VS+L	VS+L
G164	B	B
A165	B	B
F166	VS+B	L
A167	VS+L	VS+L
I168	B	B
Y169	VS+B	L
I170	VS+B	VS+B
V171	B	B
E172	B	L
Y173	B	L
P174	VS+B	VS+B
D175 (KvAP) – E349 (chimera)	-	-

Table 5.1: Residue numbers of the S5 helix of KvAP and the equivalent residues in the Kv1.2 – 2.1 chimera and characterisation of the exposure of each residue. L – lipid exposed , B – buried in central pore structure, VS – in contact with voltage sensor domain (S1-S4), VS+L – in contact with the voltage sensor domain and lipid exposed, VS+B – in contact with the voltage sensor domain and with the central pore structure.

5.3.2.3 Sodium Iodide quenching

As shown in Figure 5.7, the extent of fluorescence quenching by sodium iodide clearly varies throughout S5. The highest level of quenching is observed at the position of Y151, the extent of quenching then decreasing markedly to position 157. This would be consistent with the suggestion that Y151 marks the interface at the N terminal end of the helix. Low levels of quenching by NaI would be expected for residues located toward the centre of the membrane, but the pattern of quenching shown in Figure 5.6 is clearly more complex than this simple picture. Minima in the levels of fluorescence quenching by NaI occur at positions 157, 162, 166, and 168. In the KvAP crystal structure (PDB accession number 2AOL), residues 157 and 161 point towards the centre of the pore but residues 162 and 166 face outwards from S5. The minima in NaI quenching (Figure 5.7) correspond closely to minima in emission wavelengths at positions 157, 166 and 168 (Figure 5.6), suggesting that these are buried residues. More surprising are positions within the membrane spanning region of S5 where quenching by NaI is almost as high as for positions close to the interface. Maxima in fluorescence quenching are observed at positions 159, 163, and 167 (Figure 5.6), positions similar to those showing maxima in fluorescence emission wavelengths, these occurring at positions 159, 162-163, and 168 (Figure 5.5). This suggests that these sites could be more polar and exposed than expected for sites in a membrane-buried helix. Residues 159, 163 and 167 lie along a distinct face of S5, pointing outwards towards the voltage sensing domain.

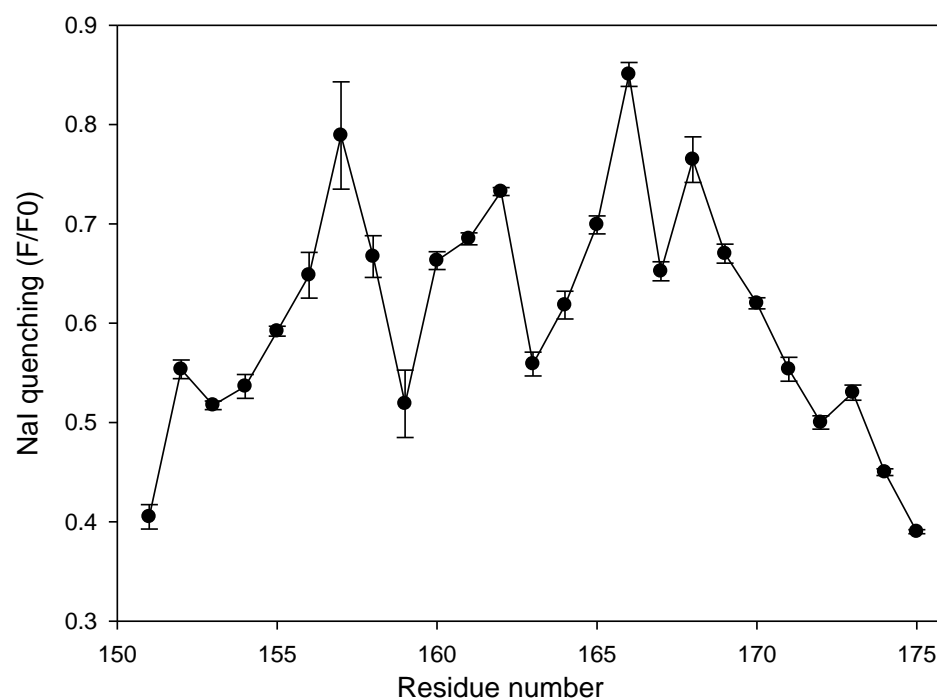


Figure 5.7: F/F_0 values for NaI quenching of NBD labelled single cysteine mutants of full length KvAP reconstituted into di(C18:1)PC, excited at 478 nm at 25°C in buffer (20 mM Hepes, 0.45 M NaI, 0.45M NaCl, 100 mM $K_2S_2O_3$, 1 mM EGTA pH 7.2). The value of F_0 is the fluorescence intensity in the absence of NaI, and F is the fluorescence intensity in the presence of 0.45 M NaI. Error is standard deviation of measurements from three separate reconstitutions for each mutant.

5.3.2.4 Tempo quenching

The spin label Tempo (2,2,6,6-tetramethylpiperidine-1-oxyl) can also be used as a quencher of NBD fluorescence, as seen in Figure 5.8. Tempo is a water soluble molecule which, due to its hydrophobic nature, can partition between water and a lipid bilayer. In a sample where the concentration of lipid is high, this will result in a high concentration of Tempo within the bilayer so that NBD fluorescence quenching will largely originate from Tempo in the bilayer phase. A low level of quenching for NBD-labelled KvAP is observed at positions around position 151 (Figure 5.7) consistent with Y151 being an interfacial residue. Quenching then increases towards position 157 and further increases towards the centre of the bilayer, with areas of local quenching minima around positions 158, 159 and 163. Quenching within the bilayer is at a maximum at positions 160 and 166 and there is a clear decrease in quenching from position 168 to position 175. The low quenching at positions beyond 172 would be consistent with these being interfacial residues.

If quenching by NaI represents quenching from the aqueous phase and quenching by Tempo represents quenching from the lipid phase, then an inverse relationship would be expected between the two. Figure 5.9a compares F_0/F values for NaI fluorescence quenching and F/F_0 values for Tempo quenching. There is a good general relationship between the two plots, with low NaI quenching corresponding to high Tempo quenching. The decrease in quenching by NaI from position 151 to 157 with an increase at position 158 is reflected in a rather similar increase in quenching by Tempo from position 151 to 157 with a decrease in Tempo quenching at position 158 and 159. In the middle of the helix the quenching patterns match quite well with minima in quenching by Tempo at positions 159 and 163, corresponding to maxima in quenching by NaI at these same positions, 159 and 163. At the C terminal end of the helix, quenching profiles again show good general agreement, with an increase in NaI quenching, and a decrease in Tempo quenching from position 166 to position 175. Maxima in Tempo quenching are observed at positions 157, 160, and 166 suggesting that these residues are exposed to the hydrophobic core of the bilayer. Interestingly, positions 157 and 166 correspond to the positions showing very low fluorescence emission maxima

(Figure 5.5). In the crystal structure, both residues 156 and 166 are outward facing in S5.

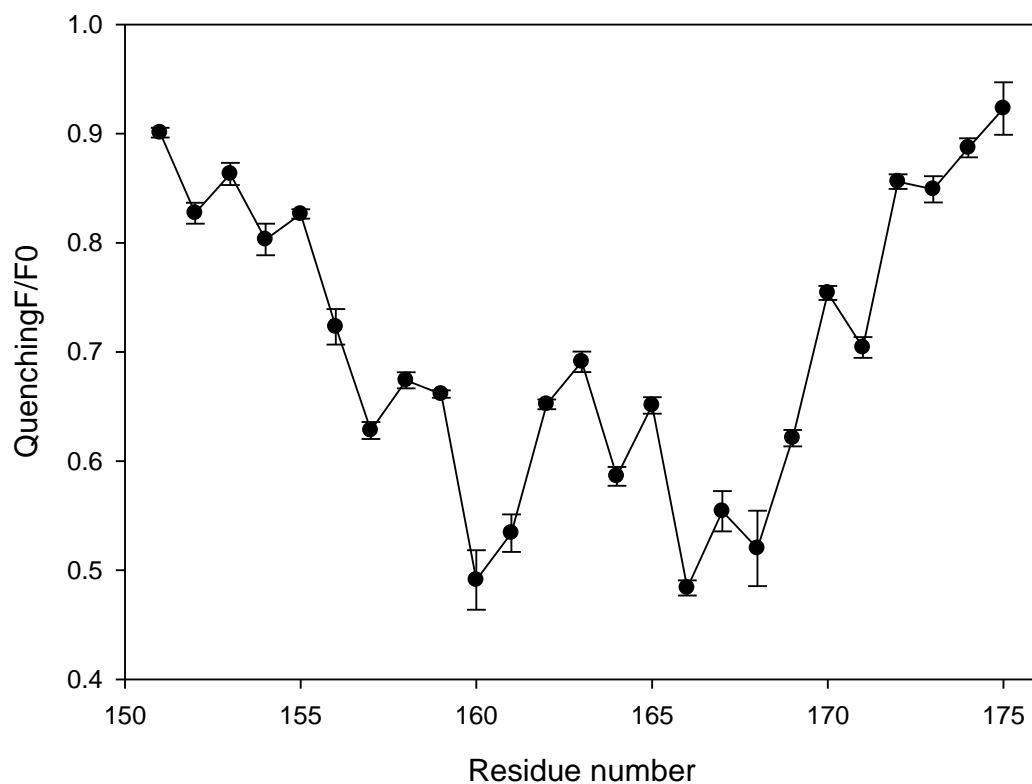


Figure 5.8: F/F_0 values for Tempo quenching of NBD labelled single cysteine mutants of full length KvAP reconstituted into di(C18:1)PC, excited at 478 nm at 25°C in buffer (20 mM Hepes, 150 mM KCl, 1 mM EGTA, pH 7.2, 2 mM TEMPO). The value of F_0 is the fluorescence intensity in the absence of Tempo and F is the fluorescence intensity in the presence of 2 mM Tempo. Error is standard deviation of measurements from three separate reconstitutions for each mutant.

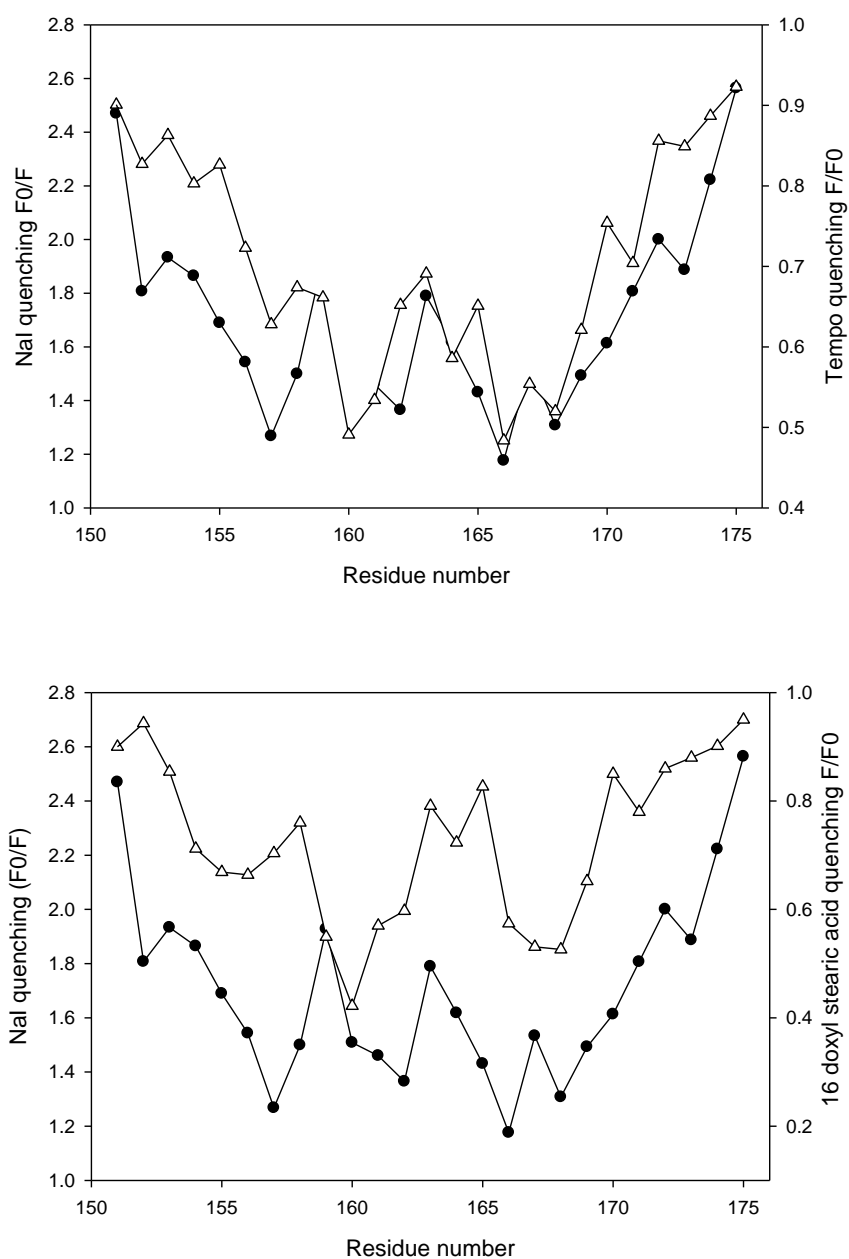


Figure 5.9 (a) A comparison of F/F_0 values for Tempo quenching (\triangle) of NBD labelled KvAP with F_0/F values for NaI quenching (\bullet), data taken from Figure 5.7 and Figure 5.8 **(b)** A comparison of F/F_0 values for 16-doxy stearic acid quenching (\triangle) of NBD labelled KvAP with F_0/F values for NaI quenching (\bullet), data taken from Figure 5.7 and Figure 5.10.

5.3.2.5 16-doxyl stearic acid quenching

NBD fluorescence is collisionally quenched by 16-doxyl stearic acid (Giddings et al. 2003); upon addition of this spin label to a solution containing bilayer fragments, the spin labelled fatty acid will partition into the bilayer phase and cause quenching of NBD exposed to the spin label at position 16 of the fatty acyl chain. Results would be broadly expected to match those of Tempo, although Tempo, as a smaller molecule, may be able to access small hydrophobic regions inaccessible to the larger 16-doxyl stearic acid molecule.

Figure 5.10 shows levels of quenching of NBD labelled single cysteine mutants of full length KvAP by 16-doxyl stearic acid. A low level of quenching is seen at positions 151 and 152, which is consistent with Y151 being an interfacial residue. Quenching then increases to position 160, with the exception of a local decrease in quenching around positions 157 and 158. Quenching maxima within the bilayer region are observed at positions 160, 166 and 167, and quenching minima at positions 163, 164, 165 and 170. In the KvAP crystal structure, residues 157, 158, 164 and 165 are on a distinct face of the S5 helix facing the pore, and 163 and 170 face outwards from the pore.

Figure 5.9b compares F_0/F values for NaI quenching with F/F_0 values for 16-doxyl stearic acid quenching; similarly to the relationship between Tempo and NaI quenching, an inverse relationship would be expected between 16-doxyl stearic acid and NaI quenching. As with Tempo quenching, there is good agreement between the two quenching profiles at the N terminus of the helix, with quenching by 16-doxyl stearic acid generally decreasing toward the middle of the helix and quenching by NaI decreasing. 16-doxyl stearic acid quenching decreases from positions 156 to 158 and NaI quenching increases from positions 157 to 159.

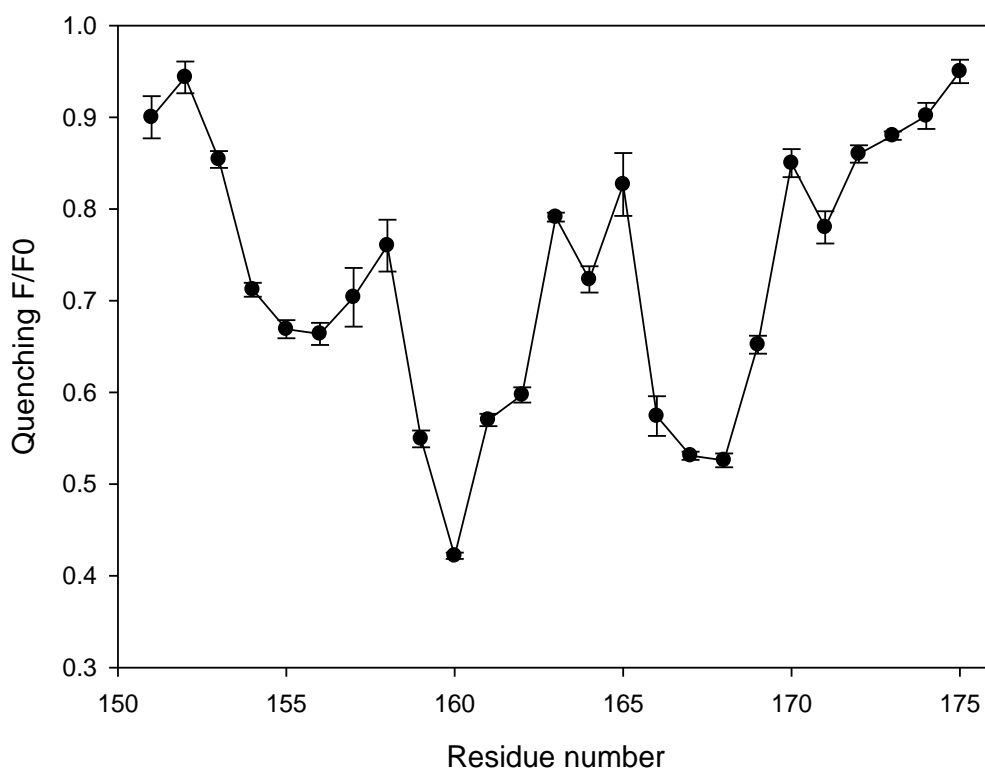


Figure 5.10 F/F_0 values for 16-doxyl stearic acid quenching of NBD labelled single cysteine mutants of full length KvAP reconstituted into di(C18:1)PC, excited at 478 nm at 25°C in buffer (20 mM Hepes, 150 mM KCl, 1 mM EGTA, pH 7.2) containing 86.6 μ M 16-doxyl stearic acid. The value of F_0 is the fluorescence intensity in the absence of 16-doxyl stearic acid and F is the fluorescence intensity in the presence of 16-doxyl stearic acid. Error is standard deviation of measurements from three separate reconstitutions for each mutant.

5.3.3 NBD labelling of single cysteine mutants of the KvAP pore only mutant

5.3.3.1 NBD Labelling efficiency of single cysteine mutants of the pore domain only mutant

The labelling efficiencies of NBD labelling of single cysteine mutants of the pore domain only mutant are all high, in excess of 90 %, as seen for single cysteine mutants of full length of KvAP (Table 5.2). Again, there is no evidence to show that free NBD may be present after spin column treatment.

5.3.3.2 Fluorescence emission maxima

Figure 5.11 shows fluorescence emission maxima for NBD labelled KvAP pore only mutant. The profile of fluorescence emission maxima for the pore only mutant is somewhat less complex than that of the full length protein, as may be expected since the potential protein interface of the voltage sensing domain has been removed. The emission maxima for NBD at positions 151 and 152 are consistent with those previously reported by Powl et al. (2005) for interfacial residues. There is then a steep drop in fluorescence emission maxima to position 159, with a local maximum in fluorescence emission maxima around residues 155 and 156. Position 165 shows a slightly high emission wavelength compared to the surrounding positions, the lowest observed for NBD in dioxane/water mixtures in Figure 5.3, There is a sharp increase in emission maxima from position 166 to position 174 which shows a fluorescence emission maximum similar to that of position 151 at the N terminus of the helix, consistent with the interfacial residues for helix S5 in the pore only mutant again being Y151 and P174.

Figure 5.11b shows a comparison of the emission wavelength profiles of NBD labelled single cysteine mutants of full length KvAP and the pore only mutant. The profiles are similar, but with noticeable shifts in the emission maxima at a few positions. The emission wavelength at position 152 has changed dramatically, by over 5 nm, indicating that the dielectric constant of the environment surrounding this residue has increased significantly in the pore only mutant; similarly, position 155 also shows an increase in emission maximum although much smaller than that observed at position 152. Positions 159, 162, 163 and 170 all show significant drops in the wavelengths of their emission maxima in the pore only mutant,

consistent with these residues being located in a region of lower dielectric constant following the removal of the voltage sensor. Interestingly positions 166, 167 and 175 all show an increase in emission wavelength maxima on removal of the voltage sensor. If the positions which have an altered NBD emission wavelength as a result of the removal of the voltage sensor are plotted on a helical wheel or helical net (Figure 5.12 and Figure 5.13 respectively), all of the residues with the exception D175 cluster on one face of the helix

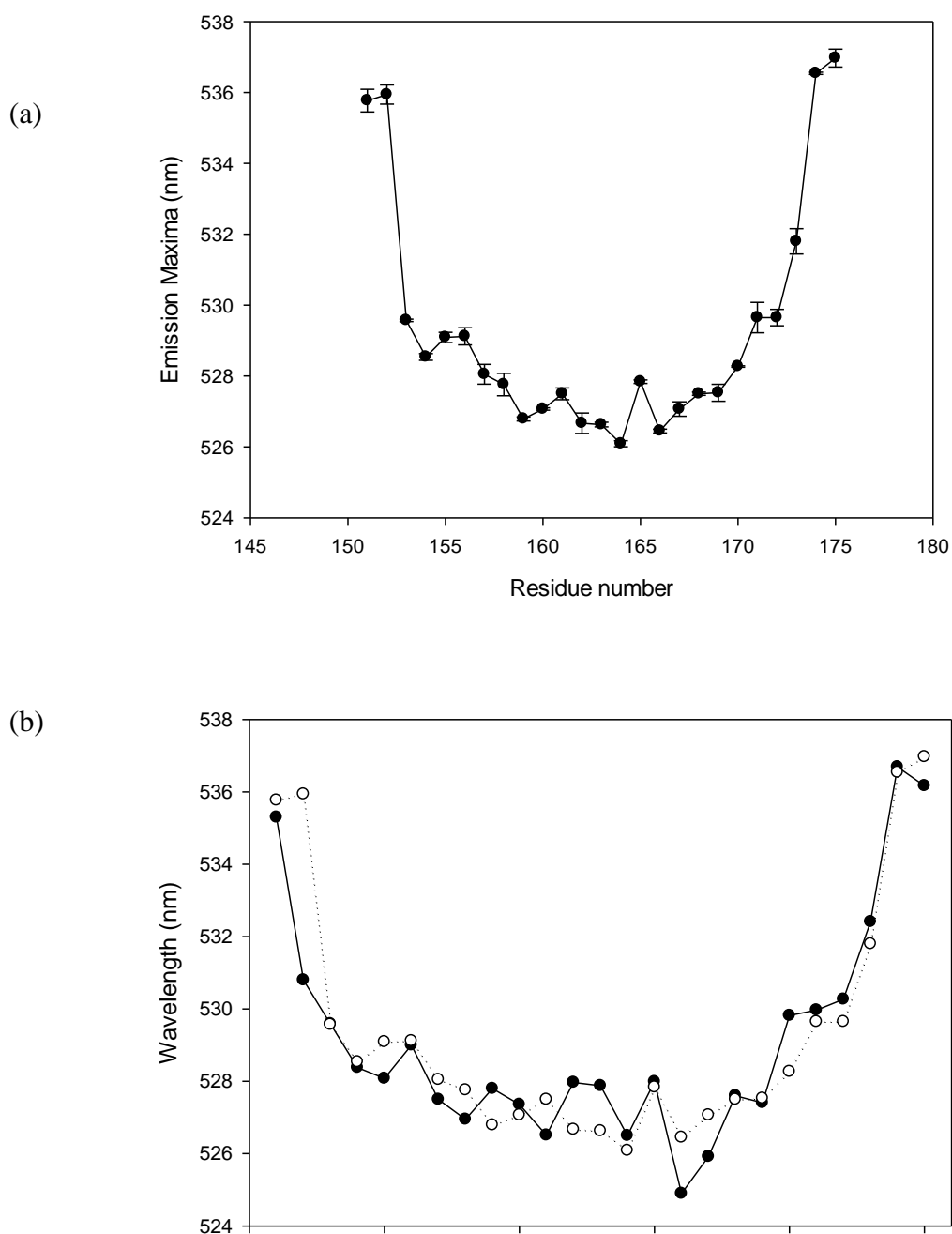


Figure 5.11: (a) Emission maxima of single cysteine mutants of the KvAP pore only mutant labelled with IANBD, reconstituted into di(C18:1)PC, excited at 478 nm at 25°C in buffer supplemented with 150 mM KCl. Fluorescence data were recorded between 490 and 590nm and fitted to a skewed Gaussian distribution to obtain a value for the emission maximum. Error is standard deviation of measurements from three separate reconstitutions for each mutant. (b) Comparison of emission maxima for NBD labelled cysteine mutants of full length KvAP (●) and pore only mutant (○). Error bars are omitted for clarity.

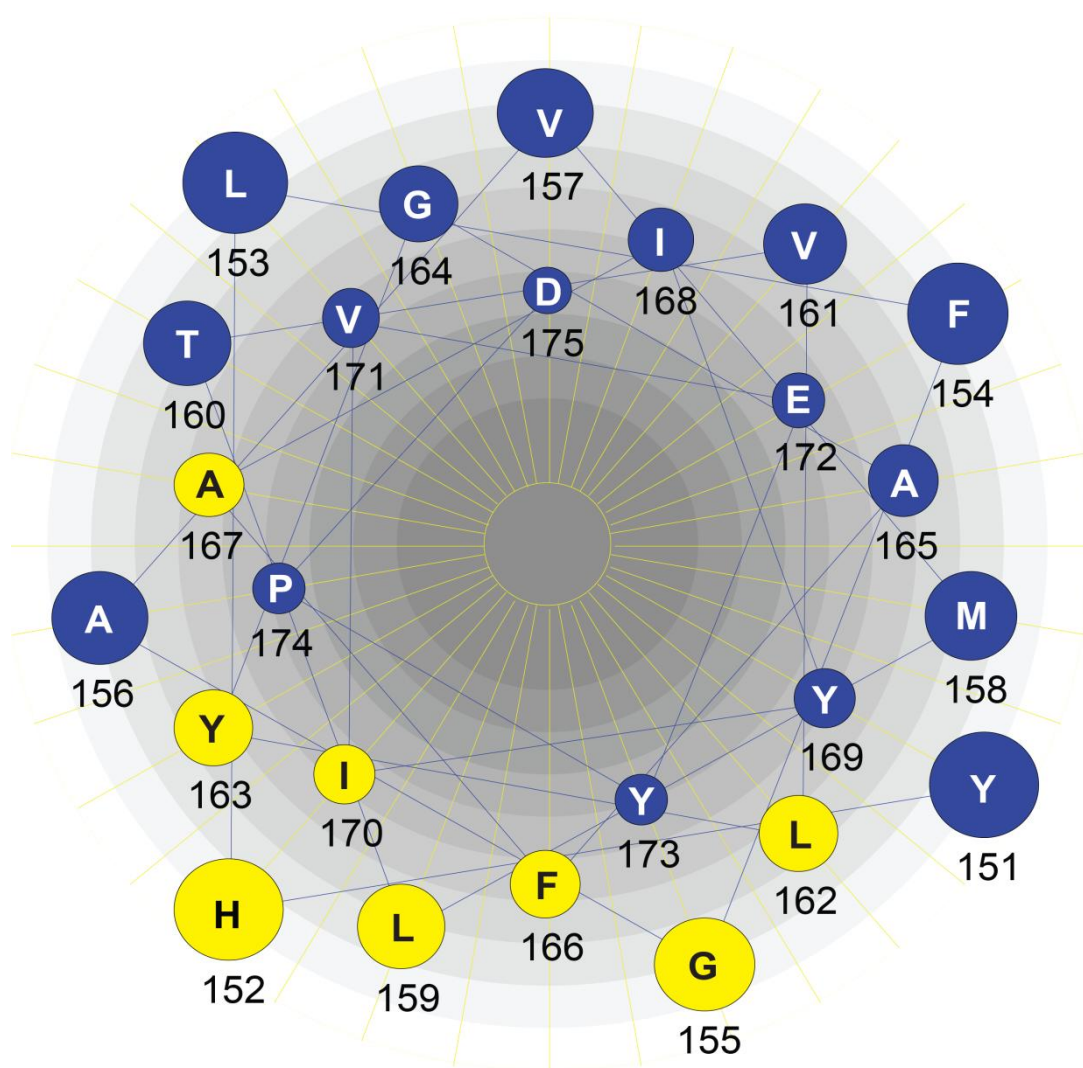


Figure 5.12: Helical wheel representation of the S5 helix of KvAP viewed from the N terminus of the helix. Positions exhibiting NBD emission maxima wavelengths differing by more than 0.75 nm between full length KvAP and the pore only mutant are shown in yellow; other residues are in blue. Map drawn using the Protean application in the Lasergene 8.0 suite.

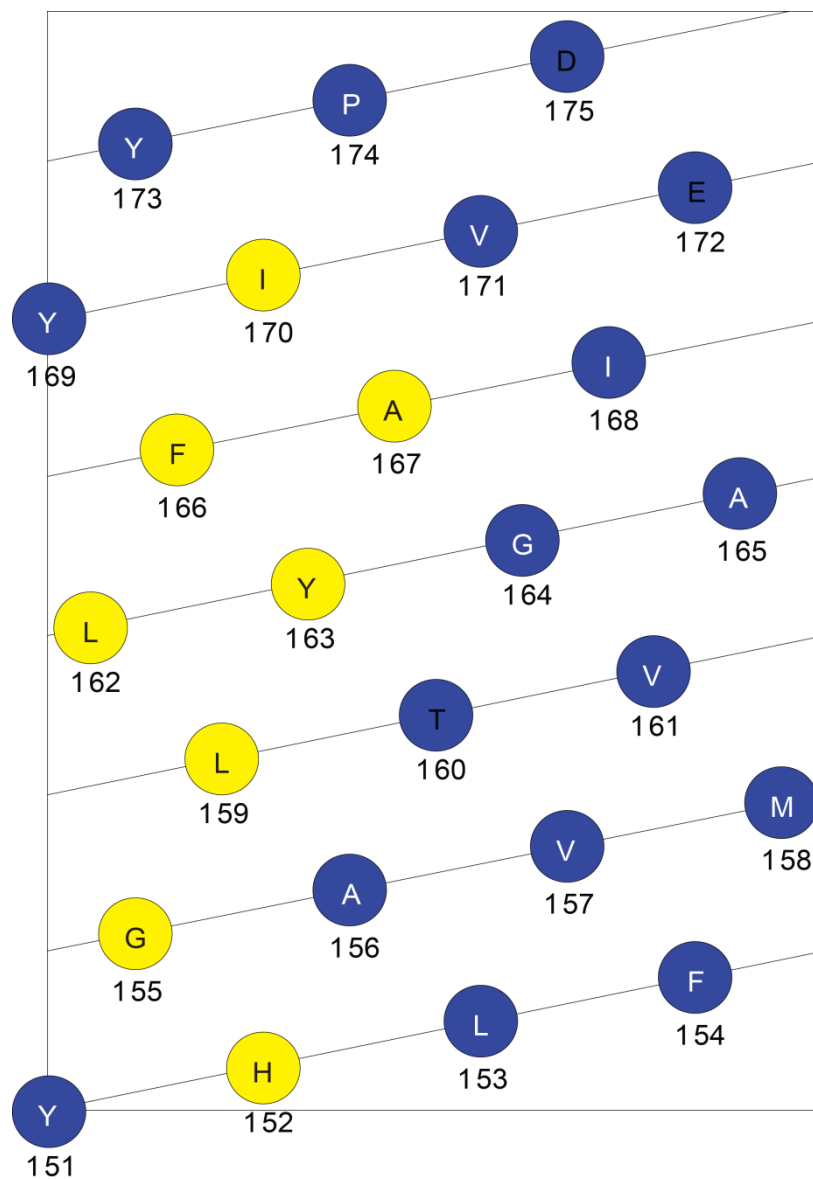


Figure 5.13: Helical net representation of the S5 helix of KvAP. Positions exhibiting NBD emission maxima wavelengths differing by more than 0.75 nm between full length KvAP and the pore only mutant are shown in yellow; other residues are in blue. Map drawn using the Protean application in the Lasergene 8.0 suite.

5.3.3.3 Sodium Iodide quenching

As shown in Figure 5.14, the extent of fluorescence quenching by NaI clearly varies throughout S5 in the pore only mutant, with a pattern very similar to that observed for the full length protein. As with full length KvAP the highest levels of quenching are observed at the positions of Y151, P174 and D175, consistent with Y151 and P174 being the interfacial residues on the N- and C- terminal ends of the helix, respectively.

Patterns of quenching by NaI are again slightly complex in the middle of the helix after position 157. Minima in the levels of fluorescence quenching occur at positions 157, 162 and 166, with maxima at positions 158 and 164a pattern very similar to that observed with full length KvAP (Figure 5.14b). The conclusion from these studies seems to be that removal of the voltage sensor has rather little effect on the environment of helix S5. Nevertheless, towards the middle of the helix (positions 159 to 164) quenching by NaI is slightly reduced in the pore only mutant, suggesting that the presence of the voltage sensors increases access of NaI to these positions. Positions 162 and 163 also show a decrease in fluorescence emission maxima on removal of the voltage sensor (Figure 5.11b) consistent with an increase in hydrophobicity on removal of the voltage sensor, presumably as protein-protein contacts are replaced by protein-lipid contacts.

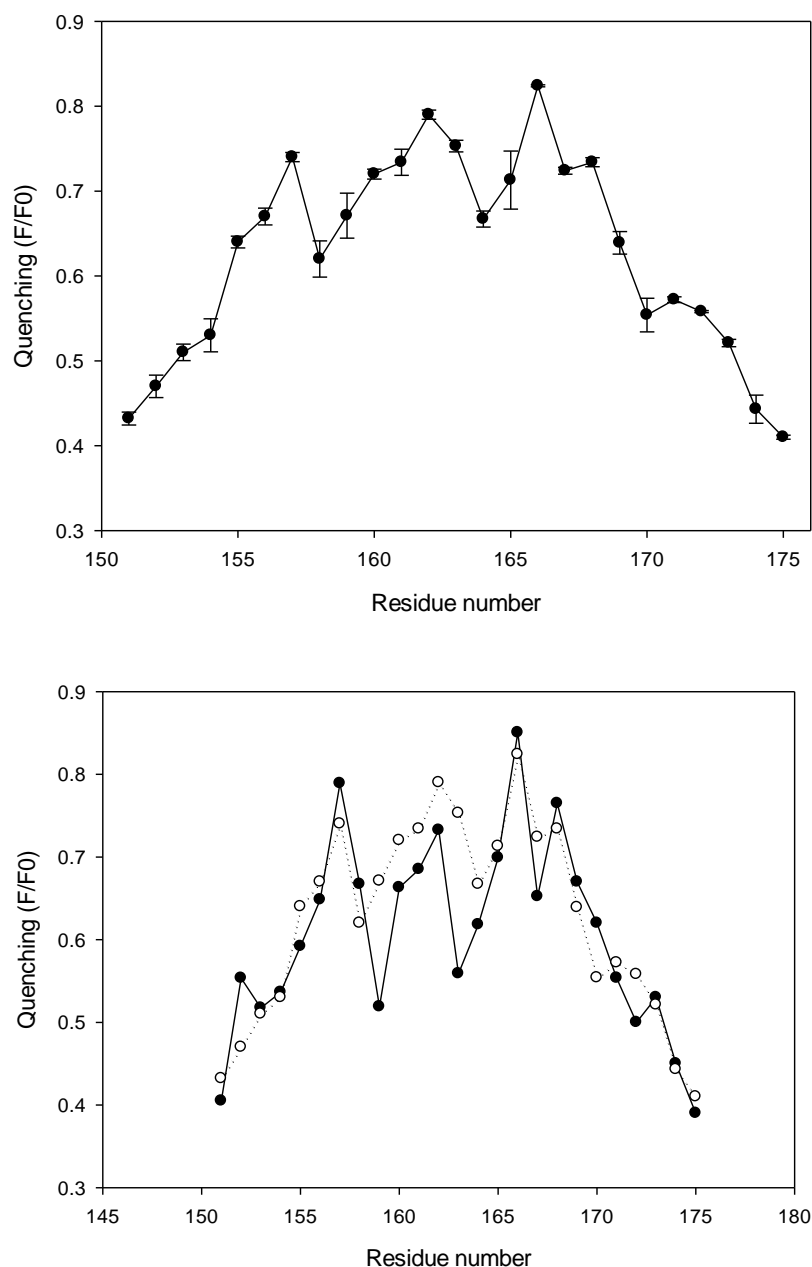


Figure 5.14: (a) F/F_0 values for NaI quenching of NBD single cysteine mutants of KvAP pore only mutant labelled with IANBD reconstituted into di(C18:1)PC, excited at 478 nm at 25°C in buffer (20 mM Hepes, 0.45 M NaI, 0.45M NaCl, 100 mM $K_2S_2O_3$, 1 mM EGTA pH 7.2). The value of F_0 is the fluorescence intensity in the absence of NaI and F is the fluorescence intensity in the presence of 0.45 M NaI. Error is standard deviation of measurements from three separate reconstitutions for each mutant. **(b)** Comparison of quenching by NaI for NBD labelled cysteine mutants of full length KvAP (●) and pore only mutant (○). Error bars are omitted for clarity.

5.3.3.4 Tempo quenching

Figure 5.15 shows measurements of Tempo quenching of single cysteine mutants of the KvAP pore only mutant. As would be expected there is a low level of quenching at the N and C terminal ends of the S5 helix, consistent with residues around positions 151 and 173 being interfacial. Again the pattern of quenching in the central region of the helix is somewhat complex. Quenching maxima within the helix exist at positions 157, 160-163, 166, and 168, with minima in quenching at positions 158 and 164-165. When the minima and maxima of tempo quenching are plotted on a helical wheel or helical net (Figure 5.17 and Figure 5.18 respectively) it is seen that the maxima in quenching are distributed around about two thirds of the circumference of the helix and that the minima in quenching are distributed on a face of the helix which accounts for about half of the circumference of the helix.

When the Tempo quenching profiles of the pore only mutant and of full length KvAP are compared, a number of residues are identified as undergoing a considerable change in the level of fluorescence quenching on removal of the voltage sensors (Figure 5.14b). Fluorescence quenching by Tempo of NBD at positions 155, 162, 163, 169 and 170 is considerably higher when no voltage sensor is present, consistent with an increase in lipid exposure for these residues when there is no voltage sensor present; all of these residues cluster on one face of the helix, and with the exception of F169 have been identified as undergoing an emission wavelength shift when the voltage sensor is removed (Figure 5.11).

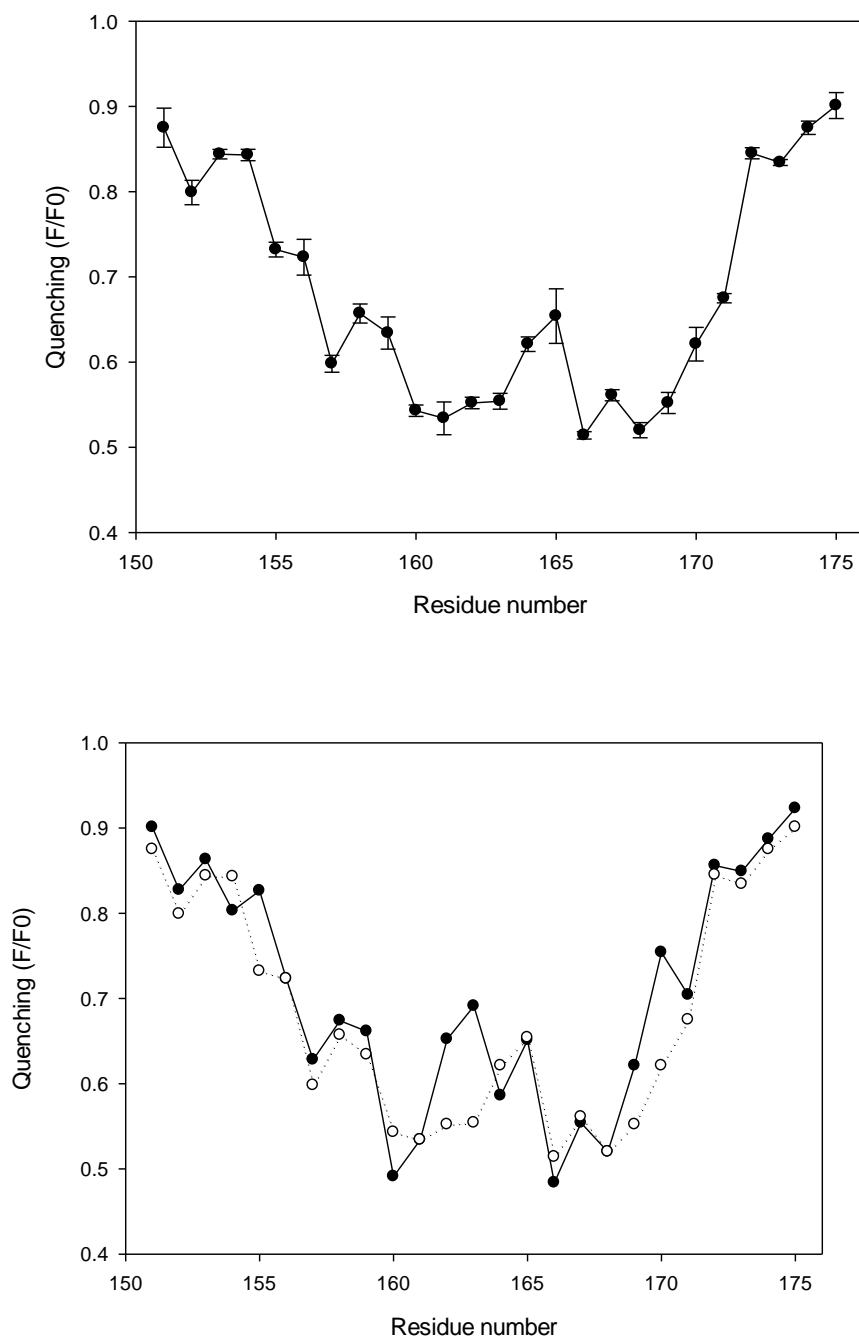


Figure 5.15: F/F_0 values for Tempo quenching of NBD labelled single cysteine mutants of KvAP pore only mutant labelled with IANBD reconstituted into di(C18:1)PC, excited at 478 nm at 25°C in buffer (20 mM Hepes, 150 mM KCl, 1 mM EGTA, pH 7.2, 2 mM TEMPO). The value of F_0 is the fluorescence intensity in the absence of Tempo and F is the fluorescence intensity in the presence of Tempo. **(b)** Comparison of quenching by Tempo for NBD labelled cysteine mutants of full length KvAP (●) and pore only mutant (○). Error bars are omitted for clarity.

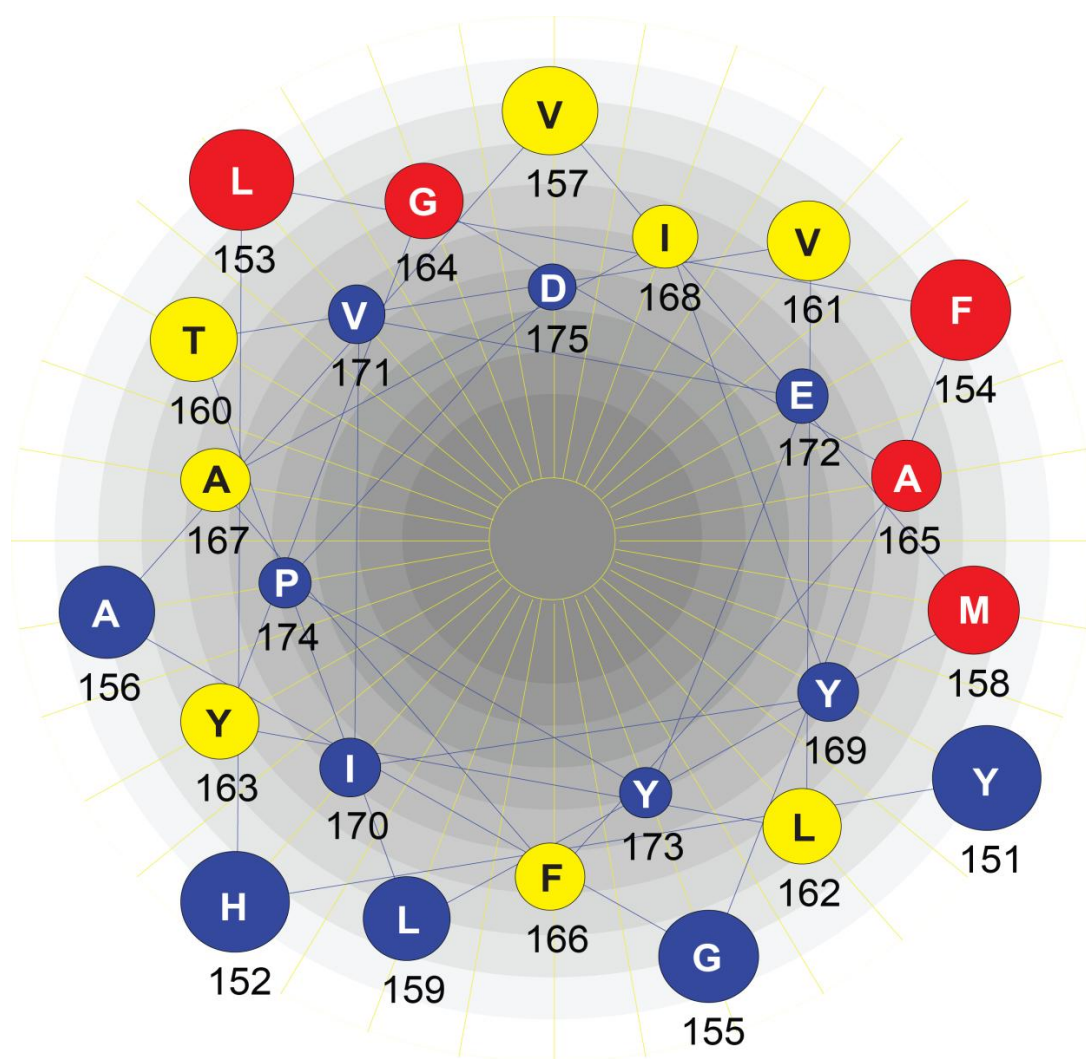


Figure 5.16: Helical wheel representation of the S5 helix of KvAP viewed from the N terminus of the helix. NBD labelled residues of the pore only mutant which exhibit a high level of Tempo quenching are shown in yellow, NBD labelled residues within the bilayer which exhibit low levels of Tempo quenching are shown in red and other residues in blue. Map drawn using the Protean application in the Lasergene 8.0 suite.

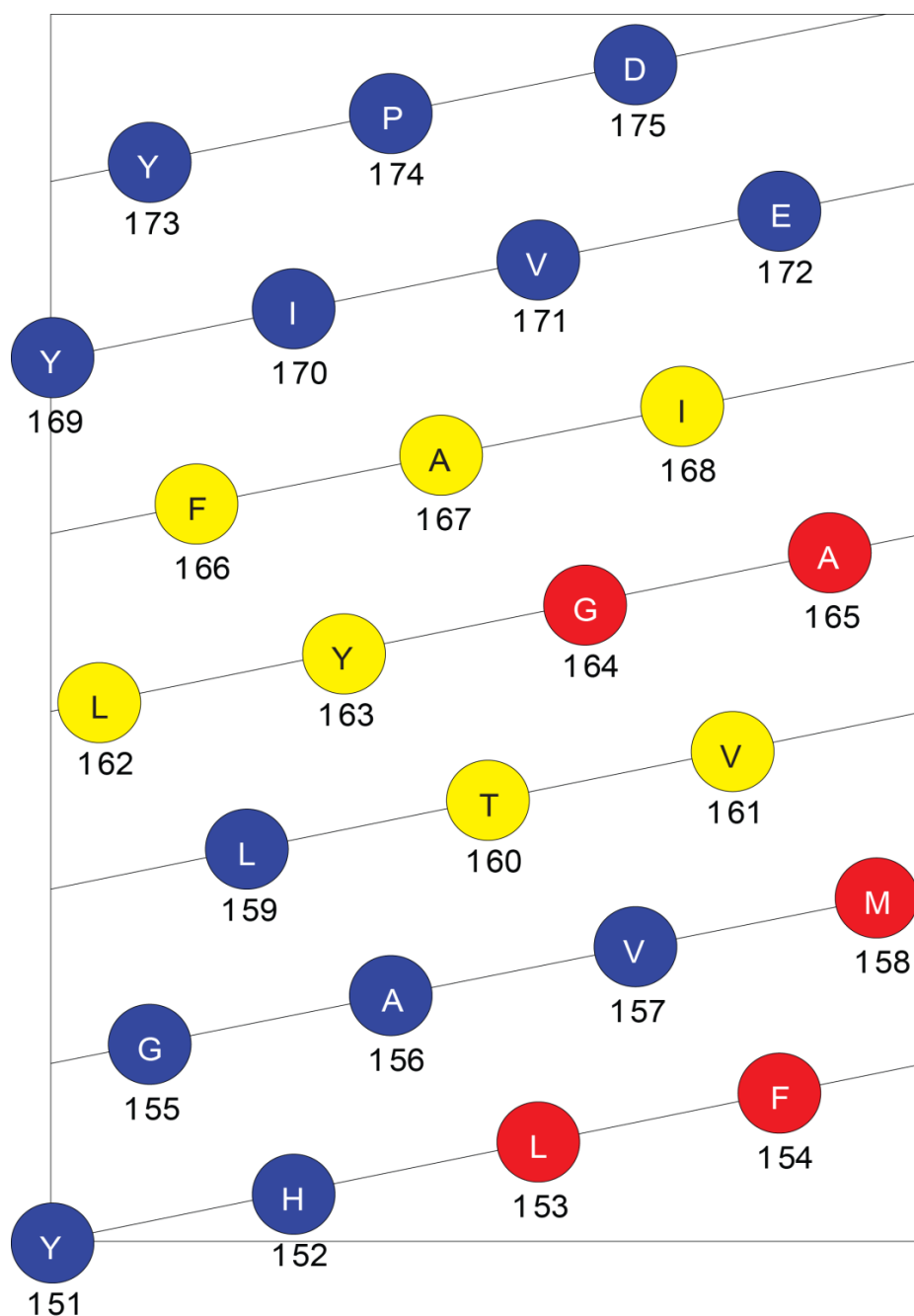


Figure 5.17: Helical net representation of the S5 helix of KvAP. NBD labelled residues of the pore only mutant that exhibit a high level of TempO quenching are shown in yellow, NBD labelled residues within the bilayer which exhibit low levels of TempO quenching are shown in red and other residues in blue. Map drawn using the Protean application in the Lasergene 8.0 suite.

5.3.3.5 16-doxyl stearic acid quenching

Figure 5.18a show levels of quenching of NBD labelled single cysteine mutants of the pore only mutant by 16-doxyl stearic acid. A low level of quenching is seen at positions 151 and 152, which is consistent with Y151 being an interfacial residue. Quenching then increases to position 160, with the exception of a local decrease in quenching around positions 157 and 158 as was observed with 16-doxyl stearic acid quenching of cysteine mutants of the full length channel (Figure 5.18b). At the C-terminus, there is a marked reduction in quenching from positions 169 to 175. The pattern of quenching within the bilayer is rather complex with a minimum in quenching level at positions 157-158, which should be within the hydrophobic core of the bilayer, with further minima at positions 161 and 164-165.

Figure 5.18b shows a comparison of quenching by 16-doxyl stearic acid for full length KvAP and for the pore only mutant. Again a number of positions show a large increase in the level of fluorescence quenching when there is no voltage sensing domain present. Positions 155-156, 159, 162-163 and 170 all exhibit an increase in quenching in the pore only mutant, consistent with an increase in lipid exposure when there is no voltage sensor present. All of these residues fall on one face of the S5 helix and also undergo a shift in emission wavelength when no voltage sensor is present (Figure 5.10). Figure 5.19 and Figure 5.20 show helical wheel and helical net diagrams respectively, with the cysteine mutants of the pore only mutant, showing the largest changes in NBD fluorescence quenching between full length KvAP and the pore only mutant marked in yellow and those showing a low level of quenching by Tempo Tempo in full length KvAP marked in red. It is evident that the residues which are resistant to quenching by 16-doxyl stearic acid in the presence of the voltage sensors are clustered on one face of the helix, suggesting that this face is involved in extensive protein-protein contacts, probably contacts between S5 and the S6 and P helices.

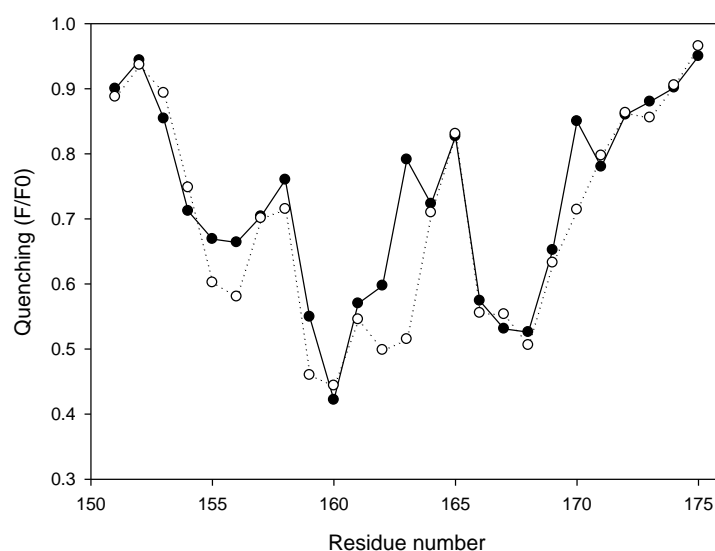
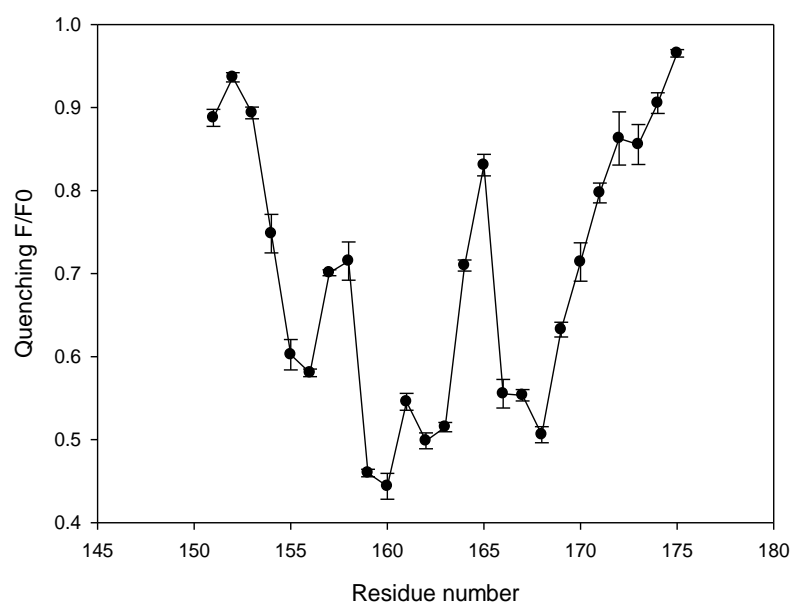


Figure 5.18: (a) F/F_0 values for 16-doxyl stearic acid quenching of NBD labelled single cysteine mutants of KvAP pore domain only mutant reconstituted into di(C18:1)PC, excited at 478 nm at 25°C in buffer (20 mM Hepes, 150 mM KCl, 1 mM EGTA, pH 7.2) containing 86.6 μ M 16-doxyl stearic acid. The value of F_0 is the fluorescence intensity in the absence of 16-doxyl stearic acid and F is the fluorescence intensity in the presence of 16-doxyl stearic acid. Error is standard deviation of measurements from three separate reconstitutions for each mutant. (b) Comparison of quenching by 16-doxyl stearic acid for NBD labelled cysteine mutants of full length KvAP (●) and pore only mutant (○). Error bars are omitted for clarity.

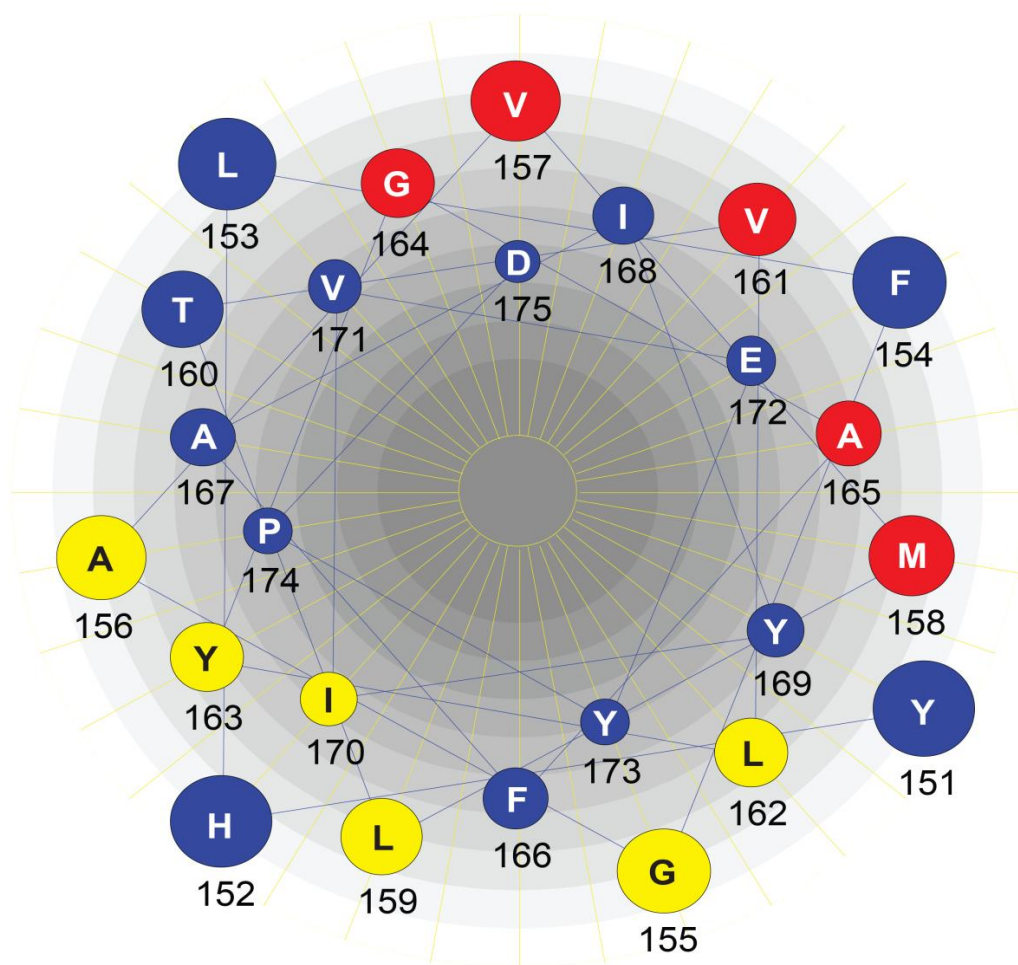


Figure 5.19: Helical wheel representation of the S5 helix of KvAP viewed from the N terminus of the helix. NBD labelled residues which show a difference in the level of quenching by 16-doxyl stearic acid between the full length KvAP channel and the pore only mutant are shown in yellow, NBD labelled residues in full length KvAP that exhibit low levels of Tempo quenching are shown in red and other residues in blue. Map drawn using the Protean application of in the Lasergene 8.0 suite

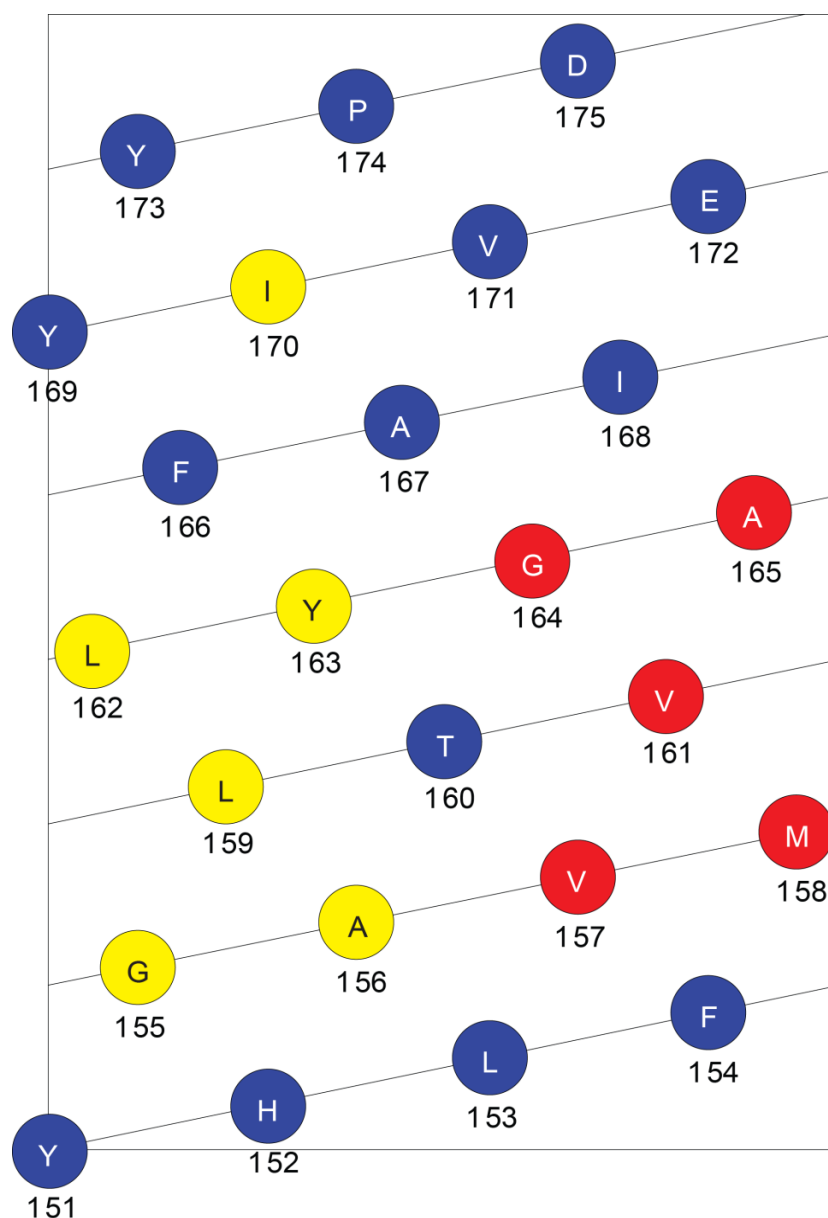


Figure 5.20: Helical net representation of the S5 helix of KvAP. NBD labelled residues which show a difference in the level of quenching by 16-doxyl stearic acid between the full length KvAP channel and the pore only mutant are shown in yellow, NBD labelled residues in full length KvAP that exhibit low levels of Tempo quenching are shown in red and other residues in blue. Map drawn using the Protean application in the Lasergene 8.0 suite

5.4 Discussion

The available crystal structures for voltage gated potassium channels stress the extent to which TM α -helices S1-S4, the voltage sensor, are independent of the final two helices S5 and S6 that make up the transmembrane pore in the tetrameric structure. The relatively weak contacts between the voltage sensor and the pore mean that the structure is easily distorted, explaining the significant differences between the available crystal structures. The presence of an antibody binding to the voltage sensor in some structures could distort the structure, as could the absence of lipid in most of the structures (Cohen et al. 2003; Jiang et al. 2003a). The most recent structure of a chimeric voltage gated channel was derived from a crystal grown in the presence of added phospholipid and is likely to represent the most undistorted of all the structures (Long et al. 2007).

The mechanism of action of the voltage gated ion channels involves the movement of at least TM α -helix S4 with respect to the membrane surface, and so it is important to know where the surface of the lipid bilayer is around the protein. Equally, in order to understand how the voltage sensing domain moves relative to the pore domain upon activation, it is important to know the topology of the voltage sensing domains in relation to the pore. For the voltage gated ion channels this may be complicated because it has been suggested that some of the positively charged residues in S4 might be located within aqueous pores penetrating into the bilayer surface (Long et al. 2005a; Long et al. 2005b). Crystal structures for membrane proteins generally contain few if any lipid molecules (Lee 2003) so that the position of the lipid bilayer around a membrane protein cannot usually be determined directly from the crystal structure. Clues as to the probable location of the hydrophobic core of the bilayer around a membrane protein are provided by the location of charged residues and Trp and Tyr residues within the TM α -helices. Residues such as Lys may be buried within the hydrophobic core of a lipid bilayer, ‘snorkelling’ to the surface to locate the charged NH_3^+ group in the glycerol backbone or lipid headgroup regions whereas Trp and Tyr residues are often found in the glycerol backbone region because of their amphipathic character (Petersen et al. 2005; Yau et al. 1998; Yuen et al. 2000). The hydrophobic region of S5 of KvAP is likely to stretch from Arg-149 or Tyr-151 on the intracellular side to Glu-

172 or Tyr-173 on the periplasmic side. Some residues within this helix will point inwards towards S6, some will point out towards the voltage sensor, S1-S4, and some could be exposed to the lipid bilayer or to water. The experiments described here with NBD-labelled KvAP will be interpreted in terms of the published crystal structure for KvAP (PDB file: 2A0L). In this structure, the central pore helices (helices S5 and S6) are probably distorted little, since their structure is very similar to that of KcsA (Jiang et al. 2003a). However, the voltage sensor is clearly distorted in this structure, so that the structure provides little information about the interaction of S5 with the neighbouring voltage sensor as it would be in a lipid bilayer. In contrast, the reported crystal structure of the chimeric Kv1.2-2.1 channel (PDB accession number 2R9R) appears to be less distorted, and probably gives a better picture of the relationship between S5 and the voltage sensor. Use will also be made therefore of the Kv1.2-2.1 structure. To compare the two structures it is necessary to know the alignment of the S5 helices in the two structures; the alignment suggested by Long et al. (2007) is shown in Table 5.1. Table 5.1 also classifies the exposure of the residues in S5, taken from the Kv1.2-2.1 structure, into lipid exposed, buried in the central pore structure, in contact with the voltage sensor domain, in contact with the voltage sensor domain and lipid exposed, and in contact with the voltage sensor domain and with the central pore structure.

5.4.1 The ends of the helices

As shown in Figure 5.6, the relationship between NBD fluorescence emission maxima and residue position in full length KvAP is rather complex. Previous studies (Powl et al. 2005) suggested that an NBD group located in the glycerol backbone region of a lipid bilayer would have an emission maximum of 536 nm. The data shown in Figure 5.5 therefore suggest that residue Y151 at the N-terminal end of S5 in KvAP will be close to the glycerol backbone region of the membrane. The decrease in emission maxima from positions 151 to 155 would then indicate a steep change to a more hydrophobic environment, as expected if Y151 was located at the interface. At the C-terminal end of S5 there is a rise in emission wavelength from position 166 to position 174. Since the NBD group at position 174 has an emission maximum of 536.7 nm, this suggests that Pro-174 could be at the interface on the C-terminal side. A location for Pro-174 at the interface would be

consistent with the neighbouring Tyr-173 and Glu-172 residues, since Tyr residues are known to have a preference for the interface and acidic residues have been found to be markers for the interface in a number of membrane proteins (Lee 2003).

Results for quenching of NBD fluorescence by NaI are broadly in agreement with these conclusions (Figure 5.7). Quenching of NBD labelled full length KvAP by NaI is observed to decrease from position 151 to 157, consistent with a location for 151 at the interface. At the C terminal end of the helix an increase in the level of quenching is seen from position 167 to position 175. This implies a gradual approach to the interface, with the level of quenching for NBD at position 174 being very similar to that at position 151, consistent with the interfacial residues being Y151 and P-174. Similar to the pattern of emission maxima (Figure 5.5), residue 173 shows a decrease in quenching, interrupting a rather consistent increase in quenching from position 167. However, comparing the quenching profile for the pore only domain with that for full length KvAP (Figure 5.13b) suggests that the break in the quenching profile for full length KvAP occurs not because quenching is unexpectedly low at position 173 but because it is unexpectedly high at position 172.

Tempo, a hydrophobic molecule, is likely to quench fluorescence largely from the hydrophobic core of the bilayer. For full length KvAP quenching by Tempo increases from position 151 to 157 (Figure 5.8), again consistent with a residue close to Y151 being at the interface. At the C-terminus of the helix, a similar pattern is observed with a steady decrease in quenching from position 166 to residue 175. Again quenching for position 151 is the same as that for position 174; this pattern of quenching is evident in both the full length channel and the pore only mutant (Figure 5.14b).

16-doxyl stearic acid is a free radical which partitions into the lipid phase and quenches fluorescence of lipid exposed NBD (Jittikoon et al. 2007). Interestingly the quenching minimum at the N-terminus of the helix occurs at residue 152 rather than 151 (Figure 5.8) as expected from the NaI (Figure 5.6) and Tempo (Figure

5.7) quenching results, however this result is consistent with the crystal structure of KvAP which suggests that due to the tilt of the S5 helix, residue 152 is in fact further away from the bilayer centre than residue 151. Moving from position 152 towards the middle of the helix there is then an increase in quenching to position 156, consistent with residues 151 and 152 being positioned at or near the interface. As with other quenchers, quenching at position 151 is very similar to that at position 174, agreeing with Y151 and P174 being the interfacial residues.

As shown in Figure 5.10b, emission maxima at the N- and C-terminal ends of S5 are very similar in full length KvAP and in the pore only mutant, and Figures 5.13b, 5.14b and 5.17b show that quenching profiles are also very similar at the N- and C-terminal ends of S5 in full length KvAP and in the pore only mutant. This argues strongly that the pore only domain must have folded correctly, and also have reconstituted correctly into the lipid bilayer, to give a structure the same as that for the pore domain in full length KvAP.

A hydrophobic core for S5 from Tyr-151 to Pro-174 would give a helix of 23 residues. The helix is shown in Figure 5.21 showing the relationship to two possible positions for the glycerol backbone region of the surrounding bilayer, shown by the horizontal lines. The hydrophobic thickness of the bilayer corresponds to the separation between the glycerol groups on the two sides of the lipid bilayer. The separation between the α -carbons of Y151 and P174 defines a hydrophobic thickness of 29 Å (Figure 5.21). A location for Y151 in the glycerol backbone region of the bilayer on the cytoplasmic side is consistent with the position of the charged group of K147 (Figure 5.21). The situation on the extracellular side is less clear, as proline is not a residue that particularly favours the interface. The position of the α -carbon of P174 is similar to that of the hydroxyl group of Y173, but the charged group of E172 would define a hydrophobic surface just 25 Å from that on the cytoplasmic side (Figure 5.21). This thinner bilayer would correspond better to the position of the selectivity filter in KvAP, as shown. The hydrophobic thickness of an undistorted bilayer of di(C18:1)PC is ca 27 Å (Lee 2003) which would match well either of these estimates of KvAP thickness. Of course, there will always be a problem in estimating hydrophobic thicknesses from crystal structures because residues at the ends of the transmembrane α -helices

would be expected to move in the absence of a normal bilayer interface; for example, in a membrane, a simple rotation of E172, Y173 or both could easily bring the carboxyl group of E172 and the –OH group of Y173 into a common plane. Given the location of the selectivity filter in the KvAP structure, the most probable hydrophobic thickness of the protein would seem to be 25 Å (Figure 5.21).

Figure 5.22 relates this information to the Kv1.2-Kv2.1 chimera. Using the sequence alignment shown in Table 5.12, Y151 and P174 in KvAP correspond to G325 and D348 respectively in the chimera. Gly is an unlikely interfacial residue, but the neighbouring E323 is likely to be located with its carboxyl group close to the lipid glycerol backbone region and this would define a surface in good agreement with the locations for charged groups at the ends of the other transmembrane α -helices (Figure 5.22). If D348 were to define the interface on the other side of the membrane, the hydrophobic thickness would be 31 Å and the loops at the top of the selectivity filter would be located within the hydrophobic core of the membrane, which seems unlikely. It is therefore probable that the interface is defined by E346 rather than by D348, giving a thickness of 28 Å and agreeing well with the positions of charged groups at the ends of other other helices (Figure 5.22).

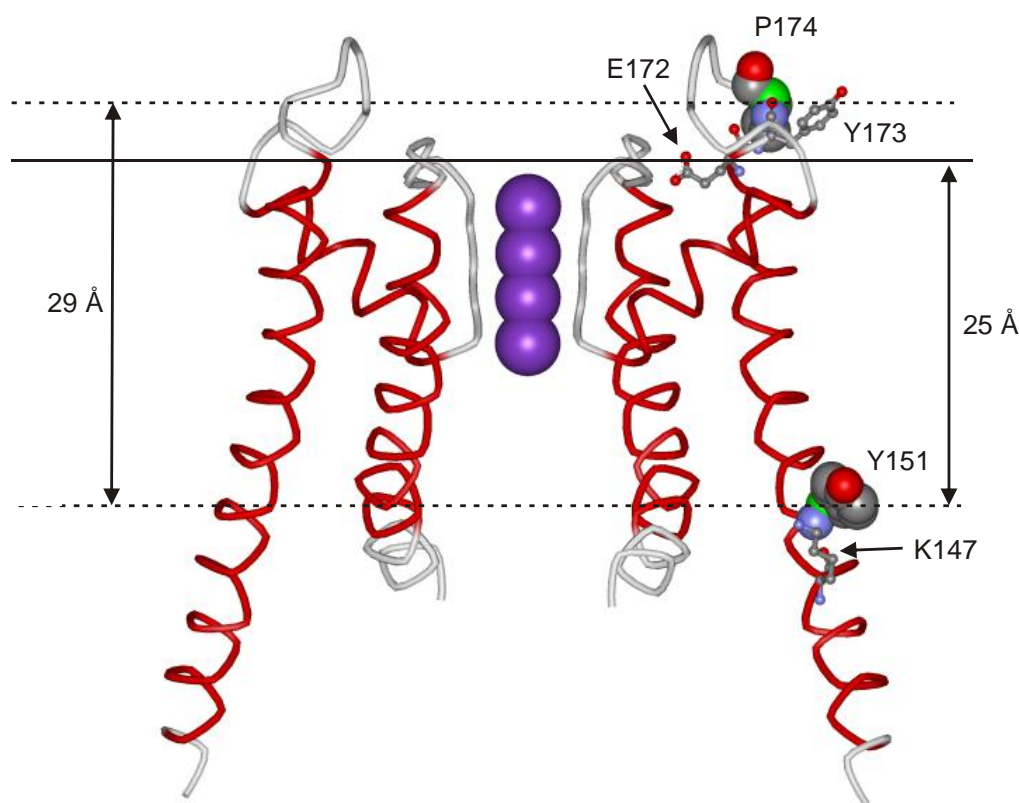


Figure 5.21: The hydrophobic thickness of KvAP. The diagram shows a cross section of the pore domain of KvAP with Y151 and P174 shown in space-fill format, with the α -carbons shown in green. Potassium ions are shown in purple. The separation between the α -carbons defines a hydrophobic thickness of 29 Å, as shown by the horizontal lines. The location of the interface on the cytoplasmic side is confirmed by the position of K147. On the extracellular side, the location of Y173 is consistent with the hydrophobic thickness defined by P174, but the position of E172 suggests a thinner bilayer of hydrophobic thickness 25 Å, and is also more consistent with the location of the selectivity filter. [Coordinates from PDB file 1ORQ], Rendered with WebLab Viewerpro (Molecular Dimensions Inc.)

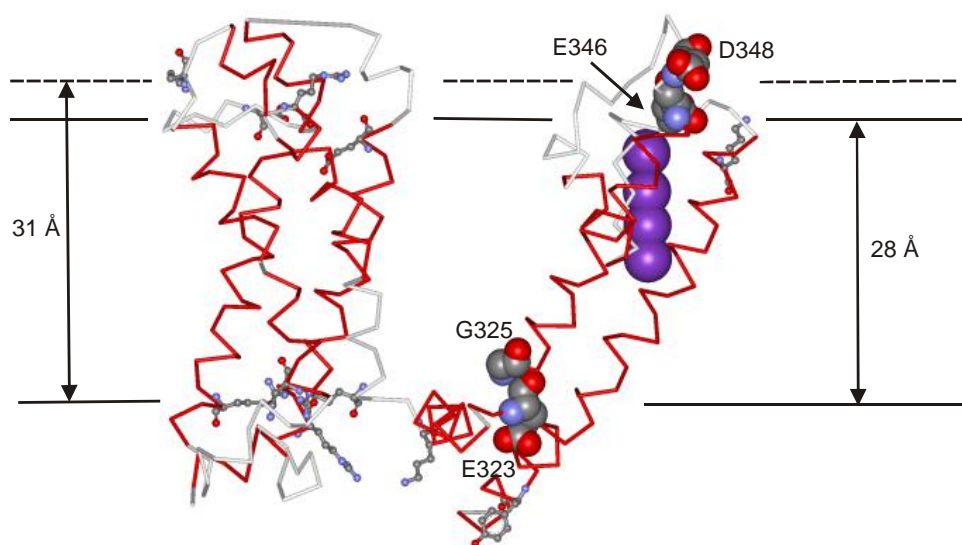


Figure 5.22: The hydrophobic thickness of the Kv1.2-Kv2.1 chimera. The diagram shows one subunit with G325 and D348 shown in space-fill format; also shown in space-fill format are the neighbouring residues E323 and E346. Potassium ions are shown in purple. Charged residues located at the ends of transmembrane α -helices S1-S4 and S6 are shown in ball-and-stick format and help to locate the probable location of the interfaces. Possible locations for the interfaces are shown by the horizontal lines [Coordinates from PDB file 2R9R], Rendered with WebLab Viewerpro (Molecular Dimensions Inc.)

5.4.2 Position of the voltage sensor

Moving along helix S5 from position 151 to the C-terminal end at position 174, the wavelengths for the fluorescence emission maxima first decrease and then increase again, with minimum values towards the middle of the helix (Figure 5.5), as expected for the variation of dielectric constant across a lipid bilayer. The dielectric constant of an aliphatic hydrocarbon is ca. 2, and this is generally taken to be the dielectric constant of the hydrophobic core of a lipid bilayer. The dielectric constant of water is 78 at 25 °C. Thus the dielectric constant must vary very markedly over the lipid headgroup region from a value of 78 a few water molecules out from the lipid headgroup region to a value close to 2 just below the glycerol backbone region. Flewelling and Hubbell (Flewelling and Hubbell 1986) assumed that the dielectric constant varies in a smooth and continuous way over the interface, described by a sigmoidal dependence of dielectric constant over positions in the interface region. They therefore described the dielectric constant of a bilayer by the following expression, giving a trough-like profile across the membrane:

Equation 5.2

$$\varepsilon = \varepsilon_2 + \frac{\varepsilon_1 - \varepsilon_2}{1 + \exp\left(\frac{d - d_0}{\sigma}\right)}$$

Here ε is the dielectric constant at a distance d from the bilayer centre, and ε_1 and ε_2 are the dielectric constants in the bilayer centre (2) and in water (78) respectively. d_0 is the value of d at the point of maximum gradient, corresponding to the point where $\varepsilon = (\varepsilon_1 + \varepsilon_2)/2.0$, and σ is an exponential decay constant which reflects the width of the transition region. This shape profile for the polarity profile across a lipid bilayer has been demonstrated experimentally from ESR measurements with spin-labelled lipids in lipid bilayers by Marsh (Marsh et al. 1982). The ESR experiments by Marsh gave a value for d_0 in a bilayer of di(C18:1)PC of about 13 Å so that the width of the region between the points of maximum gradient is ca 26 Å, very close to the hydrophobic thickness of a bilayer

of di(C18:1)PC which is ca 27 Å. Thus the region of the bilayer defined by the values of d_o corresponds to the hydrophobic core of the bilayer.

The emission spectrum of the NBD group is polarity dependent, the wavelength of maximum fluorescence emission increasing with increasing polarity of the surrounding medium. Figure 5.3 shows the variation of the emission maximum for IANBD in dioxane/water mixtures as a function of the dielectric constant of the mixture: dielectric constants were taken from Akerlof and Short (Akerlof and Short 1936). To provide a numerical description of the NBD/dielectric constant curve, the data in Figure 5.3 were fitted to a double hyperbola using the non-linear least squares routine in SigmaPlot: as shown in Figure 5.23, the data fit well to the equation:

Equation 5.3

$$\lambda_{max} = \frac{536.6 \times \epsilon}{0.04 + \epsilon} + \frac{16.08\epsilon}{40.21 + \epsilon}$$

where ϵ is the dielectric constant.

A combination of equations 5.3 and 5.4 then describes how the emission maximum for an NBD group would be expected to vary with distance across a lipid bilayer. Since the form of the equation is restricted to the hydrocarbon core and glycerol backbone regions of the bilayer, the equation will only apply to NBD residues located in the apolar to moderately apolar regions of the bilayer.

To use these equations to describe the expected fluorescence of the NBD group attached to Cys residues in helix S5 of KvAP, it is necessary to relate residue numbers to position. This was done using the crystal structure of KvAP (Lee et al. 2005). It was assumed that the hydrophobic region of S5 begins at Y151 and distances were measured from the α -carbon of this residue along the bilayer normal. The distance between Y151 and P174, measured along the bilayer normal is ca 29 Å, so that the value for d_o in equation 5.3, the distance from the bilayer centre to the interface, is 14.5 Å.

The experimental data were fitted to equations 5.3 and 5.4 using the distances in Table 5.2, with a value of ϵ_2 fixed at 8.0, so that the emission maximum at position

151 matched the experimental value, with a value for ϵ_1 of 2.0, with the only variable being σ . A fit of the experimental data to equations 5.3 and 5.4 is shown in Figure 5.28, giving a value for σ of 1.88 ± 0.36 Å. This agrees well with the value of σ of 2.2 ± 1.2 Å obtained by Carney et al. (2007) from a study of the variation of Trp emission maxima as a function of location in MscL and with estimates of 1 - 2 Å made by Marsh (Marsh 2001) from an analysis of EPR data.

As can be seen in Figure 5.24 whilst fluorescence emission maxima for some positions lie close to the theoretical profile, many do not. Figure 5.25 and Figure 5.26 show helical wheel and helical net plots for S5 showing that the positions that lie furthest from the theoretical profile fall on one face of S5, corresponding to residues 152, 153, 166, 170 and 171; residue 174 has not been included since the calculated emission spectrum for this interfacial residue will depend very strongly on the dielectric constant chosen for the interfacial region. It is surprising that the data fit so well to this simple model for the polarity profile across the membrane, given that some residues will be in contact with the surrounding lipid bilayer whereas others will be in contact with the rest of the protein. It should be noted however that distances have been measured from the α -carbon of the amino acid residue, and if the NBD group is locked in a cleft in the protein this could result in a location for the NBD group significantly different from that of the α -carbon of the amino acid residue; this argument would suggest that the estimated distances are likely to be most reasonable for a very flexible NBD group where the average position of the NBD group might be similar to that of the α -carbon atom. The emission maxima for the pore only mutant were also fitted to equations 5.3 and 5.4, giving a best fit with a value for σ of 1.71 ± 0.26 Å (Figure 5.27) in close agreement with the value obtained for full length KvAP.

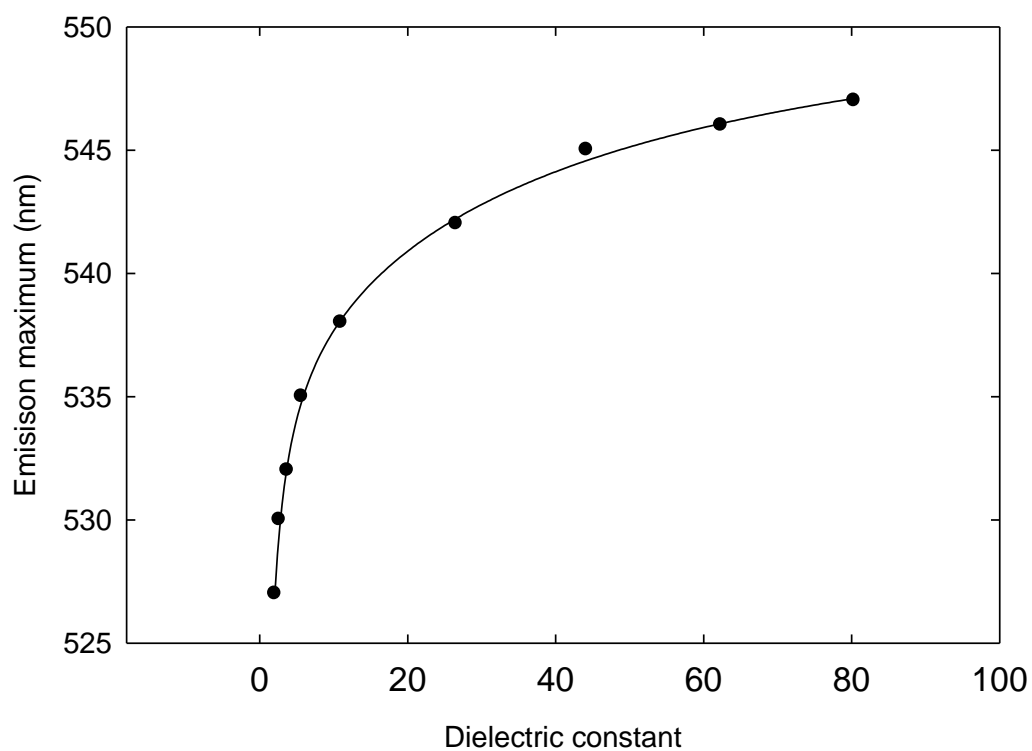


Figure 5.23: Variation of fluorescence emission maximum for NBD with dielectric constant in dioxane/water mixtures. The data were taken from Figure 5.3. The solid line shows the best fit to equation 5.4 as described in the text.

<i>Residue</i>	Distance (Å)
151	0
152	-1.1
153	-0.6
154	2.6
155	4.0
156	2.6
157	5.7
158	7.7
159	7.4
160	7.4
161	10.0
162	12.6
163	12.0
164	13.4
165	16.3
166	16.9
167	16.6
168	19.1
169	21.4
170	21.7
171	22.6
172	24.9
173	26.6
174	29.1

Table 5.2:. Distances between α -carbons of residues in helix S5 of KvAP and that of Y151, measured along the bilayer normal. The data were obtained from the crystal structure of KvAP (PDB accession code 2A0L)

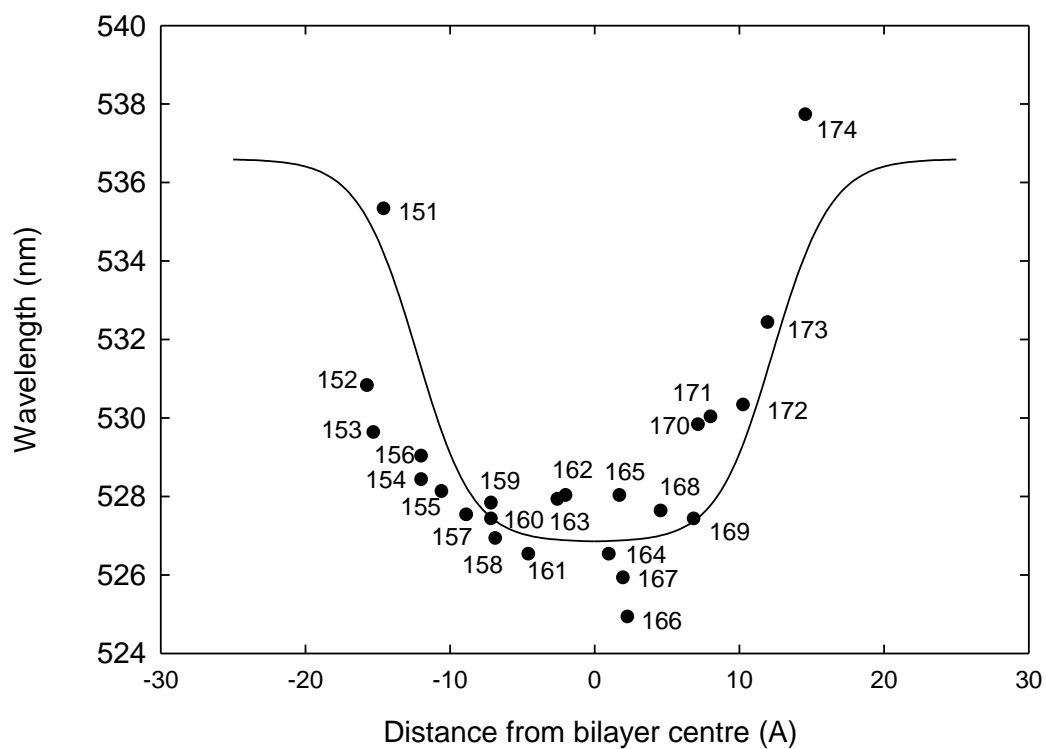


Figure 5.24: Fluorescence emission maxima from NBD labelled KvAP plotted as a function of distance of the residue from the bilayer centre (\AA) as calculated from the KvAP crystal structure of KvAP. The black line shows a fit of the emission maxima to Equation 5.2. Residue positions are given on the figure.

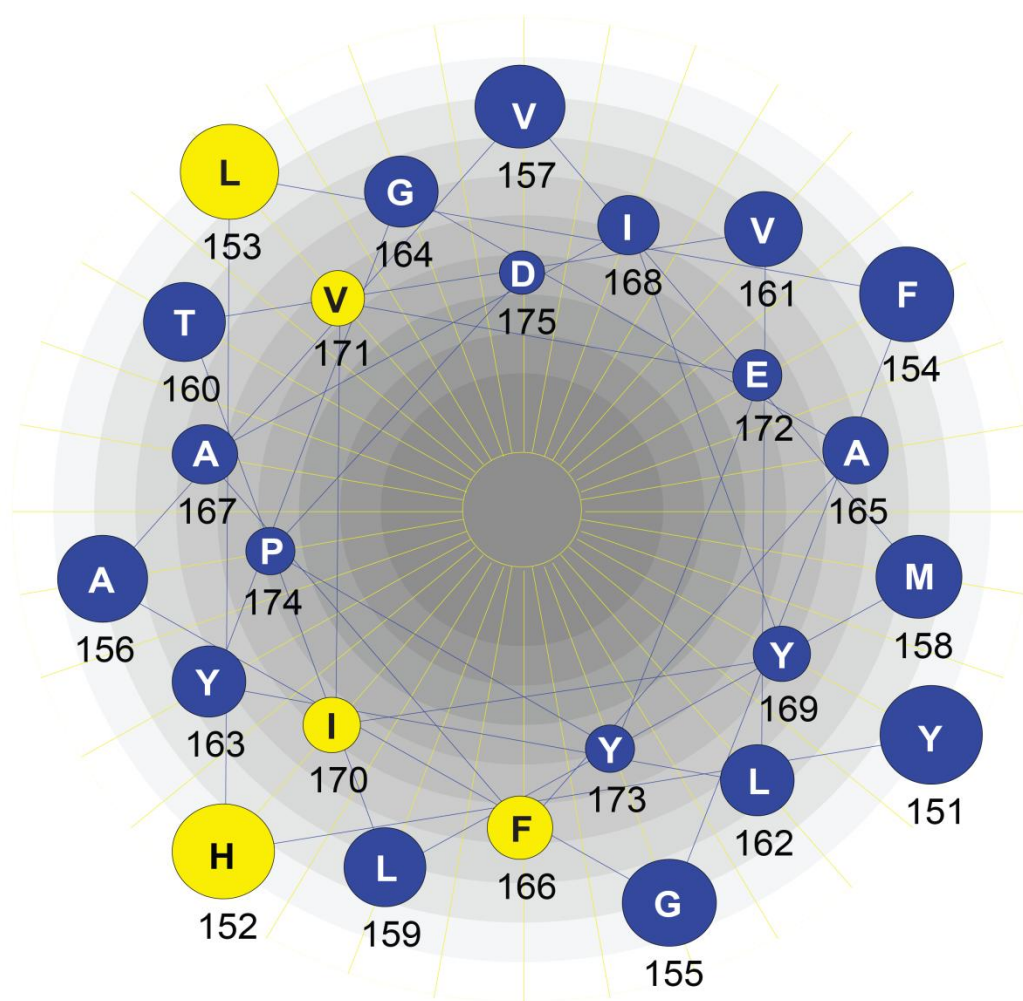


Figure 5.25: Helical wheel of the S5 helix of KvAP showing NBD fluorescence emission maxima, viewed from the N terminus. Residues in yellow represent emission maxima which are furthest from the theoretical profile of NBD emission within the bilayer. Residues are seen to cluster on two opposite faces of the helix. Map drawn using Protean application of Lasergene 8.0 suite

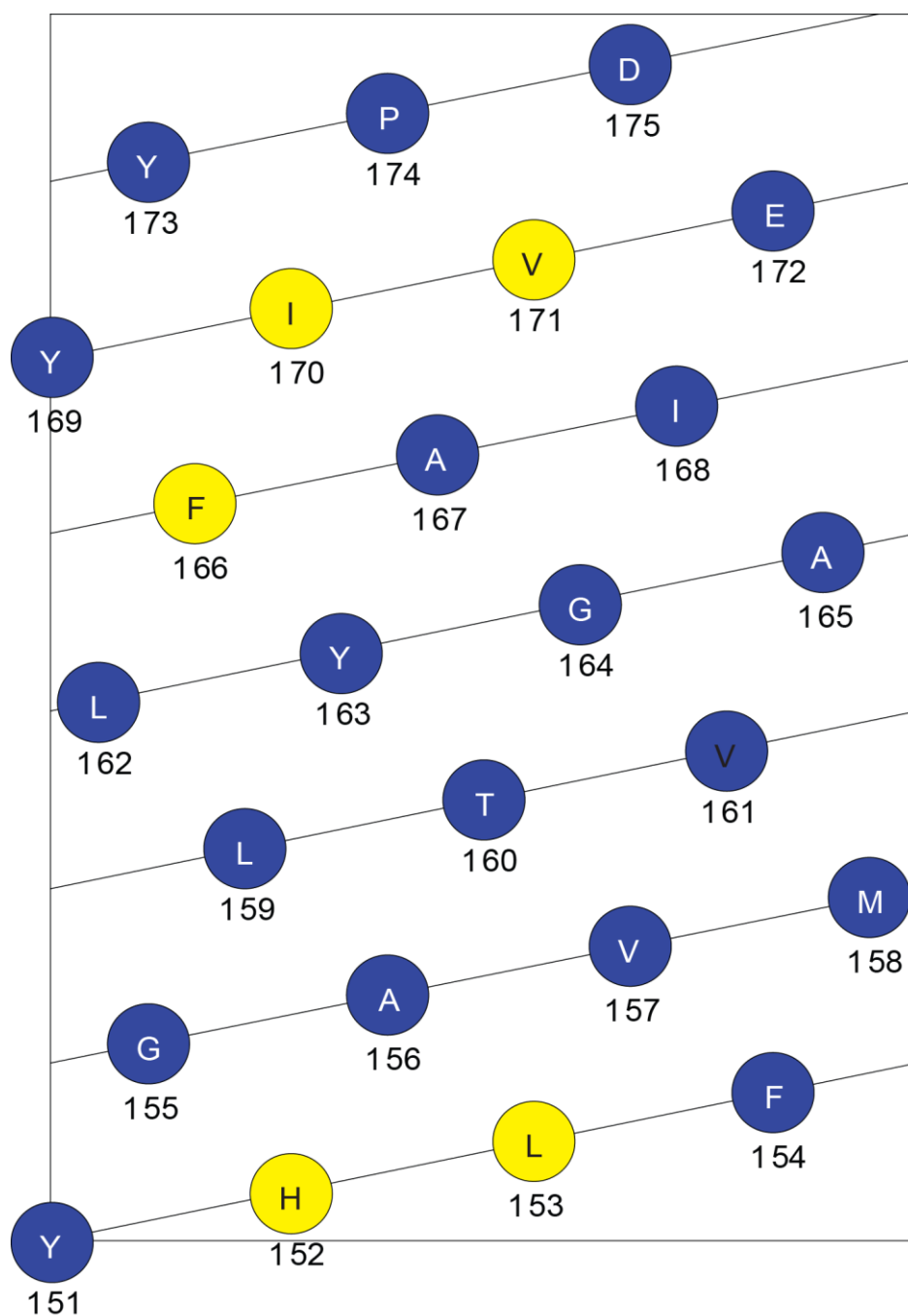


Figure 5.26: Helical net of the S5 helix of KvAP showing NBD fluorescence emission maxima. Residues in yellow represent emission maxima which are furthest from the theoretical profile of NBD emission within the bilayer. Residues are seen to cluster on two opposite faces of the helix. Map drawn using Protean application of Lasergene 8.0 suite

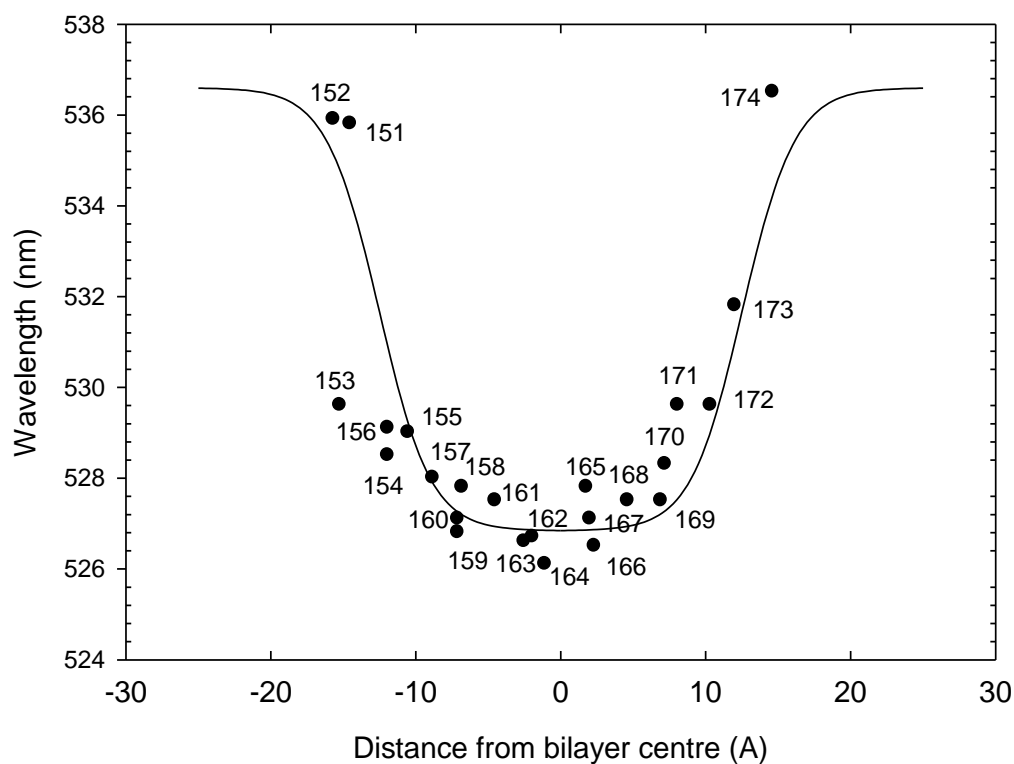


Figure 5.27: Fluorescence emission maxima from the KvAP pore domain only mutant plotted as a function of distance of the residue from the bilayer centre (Å) for helix S5 in the pore only mutant. Distances were calculated from the KvAP crystal structure. The line shows a fit of the emission maxima to Equation 5.3. Residue positions are given on the figure.

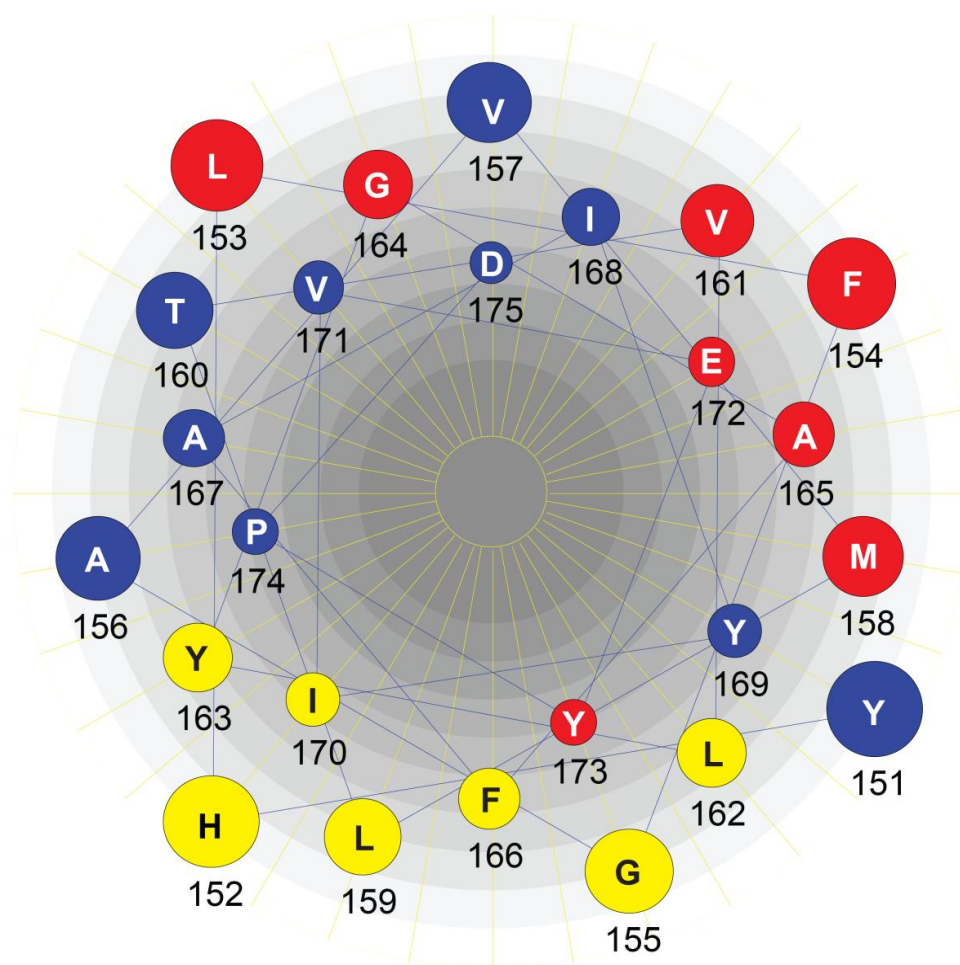


Figure 5.28: Helical wheel of the S5 helix of KvAP showing NBD fluorescence emission maxima, viewed from the N terminus. Residues in yellow represent emission maxima that do not agree with the theoretical emission profile in the presence of the voltage sensor, but do in the absence of the voltage sensor. In red are positions where NBD fluorescence maxima do not fit to the theoretical profile in either the presence or the absence of the voltage sensor. Residues are seen to cluster on two opposite faces of the helix. Map drawn using Protean application of the Lasergene 8.0 suite

Agreement between the experimental emission maxima and the calculated value are slightly better for the pore only mutant than for full length KvAP as is shown in Figure 5.27. In particular, of the five residues 152, 153, 166, 170 and 171 showing the largest deviations between experiment and theory for full length KvAP, three, positions 152, 166 and 170, show smaller deviations for the pore only mutant. This suggests that deviations from theory could occur for those residues in contact with the voltage sensor. Contacts at the various positions in S5 were therefore analysed in terms of the Kv1.2-Kv2.1 chimera structure (Figure 5.29; Table 5.1). As shown in Figure 5.29, one face of helix S5 fits quite snugly against the neighbouring voltage sensor, with other residues being exposed to the central pore or facing the likely location of the surrounding lipid bilayer. In Table 5.1 residues are characterised as either exposed to the putative lipid bilayer, buried in central pore structure, in contact with voltage sensor domain (S1-S4), in contact with the voltage sensor domain and lipid exposed, or in contact with the voltage sensor domain and with the central pore structure. Figure 5.30 illustrates F329, an example of a residue in contact with the voltage sensor domain and lipid exposed, and Figure 5.31 illustrates a residue, S340, in contact with the voltage sensor domain and with the central pore. Figure 5.32 shows residues in S5 making contact with the voltage sensor domain and compares these residues with the corresponding residues in S5 of KvAP.

The analysis shown in Figure 5.28 shows that all positions in full length KvAP exposed to the putative lipid bilayer, whether or not they are also in contact with the voltage sensor (see Table 5.1) show reasonable agreement between experiment and theory and show only small changes on removal of the voltage sensor. At most of the positions buried in the central pore structure agreement between experiment and theory is also good, except at positions 153 and 171; as expected, removal of the voltage sensor domain has little effect on the emission maxima at these positions. However, the remaining three positions where agreement between experiment and theory is poor for full length KvAP, positions 152, 166 and 170, are positions making contact with both the voltage sensor and the central pore structure, and in these cases removal of the pore domain leads to much better agreement between experiment and theory, presumably because these residues are

now at least partly exposed to the lipid bilayer. These three residues have been mapped onto the structure of the Kv1.2-Kv2.1 chimera in Figure 5.33.

These results suggest that there is no water penetration into the space between the voltage sensor and helix S5 since any water penetration would have given a dielectric profile very different from that expected for a simple lipid bilayer. The fact that some positions in S5 show a shift in emission maximum on removal of the voltage sensor suggest that there is significant contact between the voltage sensor and helix S5, as shown in the crystal structure of the Kv1.2-Kv2.1 chimera.

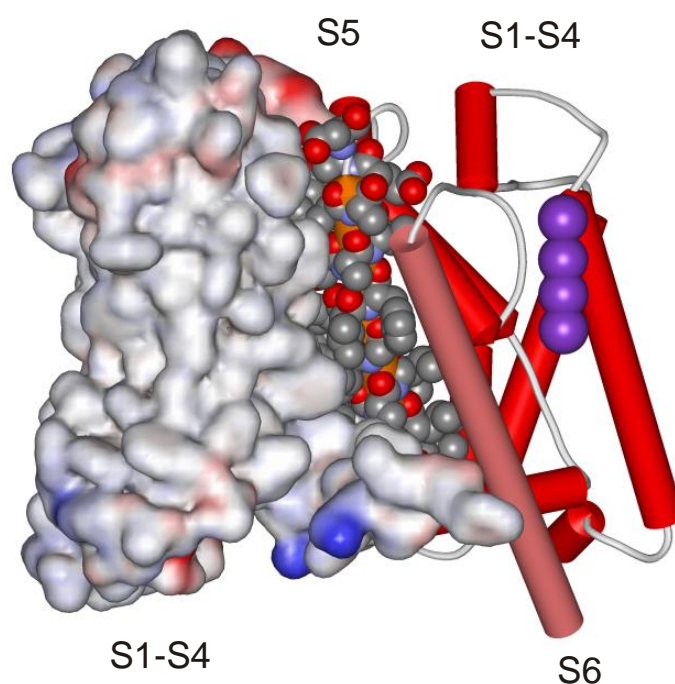


Figure 5.29: The relationship of S5 to the voltage sensor domain in the Kv1.2-Kv2.1 chimera. Helices S1-S4, S5 and S6 are shown for one subunit, with residues in S5 shown in space-fill format. The voltage sensor domain (S1-S4) for the neighbouring subunit is shown as a surface plot. Potassium ions are shown in purple. [Coordinates from PDB file 2R9R], Rendered with WebLab Viewerpro (Molecular Dimensions Inc.)

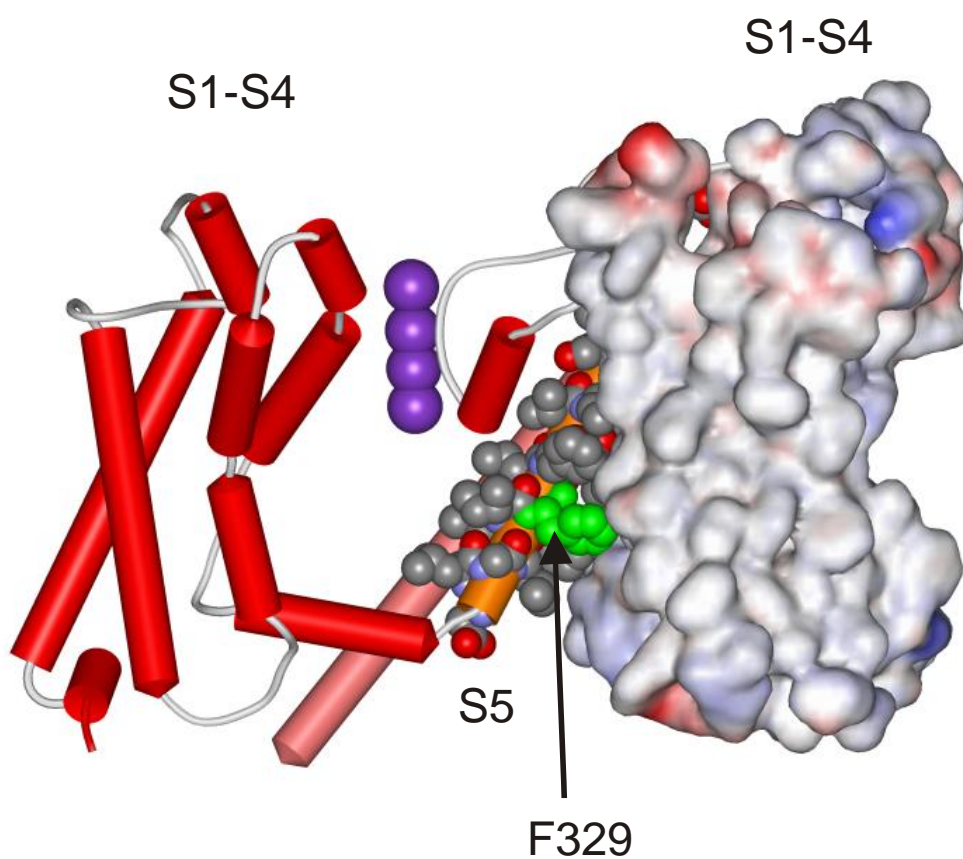


Figure 5.30: A residue, F329, in contact with the voltage sensor and the lipid bilayer. F329 is shown in green. Details as in Figure 5.30, Rendered with WebLab Viewerpro (Molecular Dimensions Inc.)

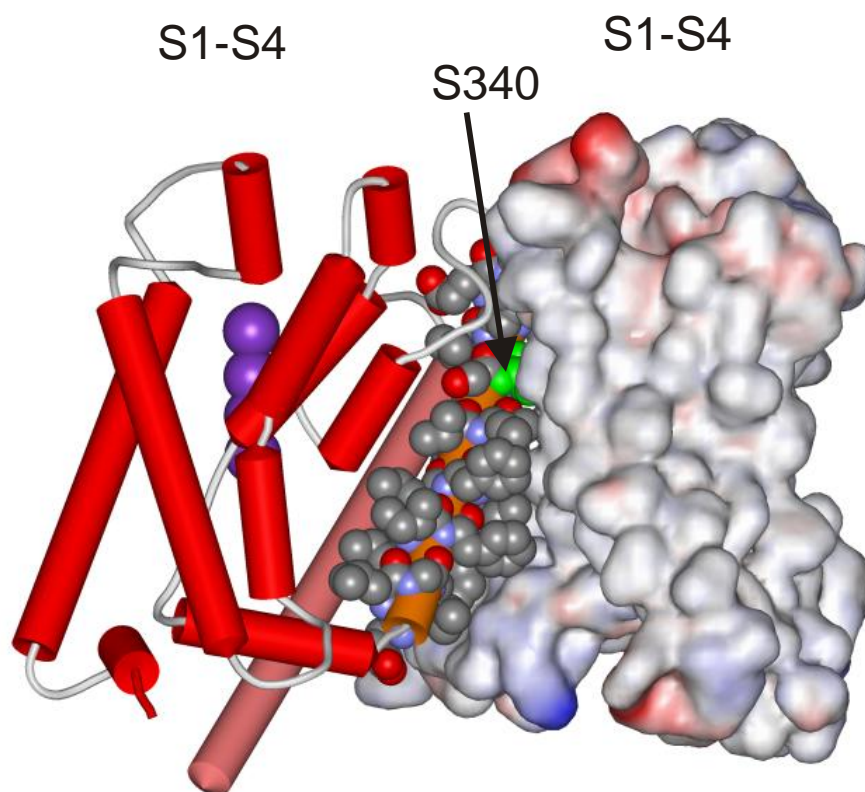


Figure 5.31: A residue, S340, in contact with the voltage sensor and the pore. S340 is shown in green. Details as in Figure 5.30; Rendered with WebLab Viewerpro (Molecular Dimensions Inc.)

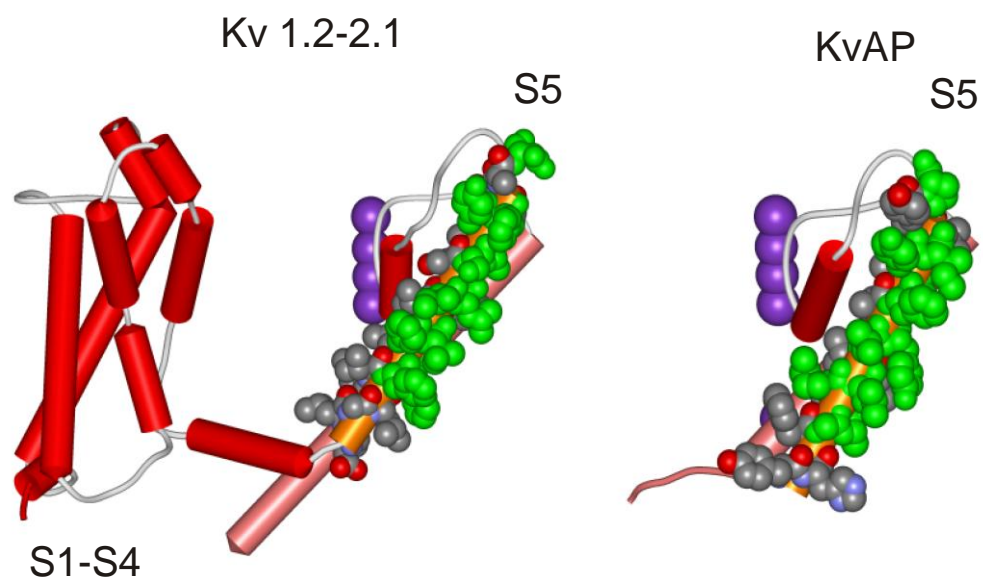


Figure 5.32: Residues making contact with the voltage sensor in the Kv1.2-Kv2.1 chimera and in KvAP. The structure of one subunit is shown for the Kv1.2-Kv2.1 chimera whereas only helices S5-S6 are shown for KvAP. Residues in S5 are shown in space-fill format and those making contact with the voltage sensor are shown in green. Potassium ions are shown in purple. Rendered with WebLab Viewerpro (Molecular Dimensions Inc.) PDB ID's 2R9R and 2A0L

Kv 1.2-2.1

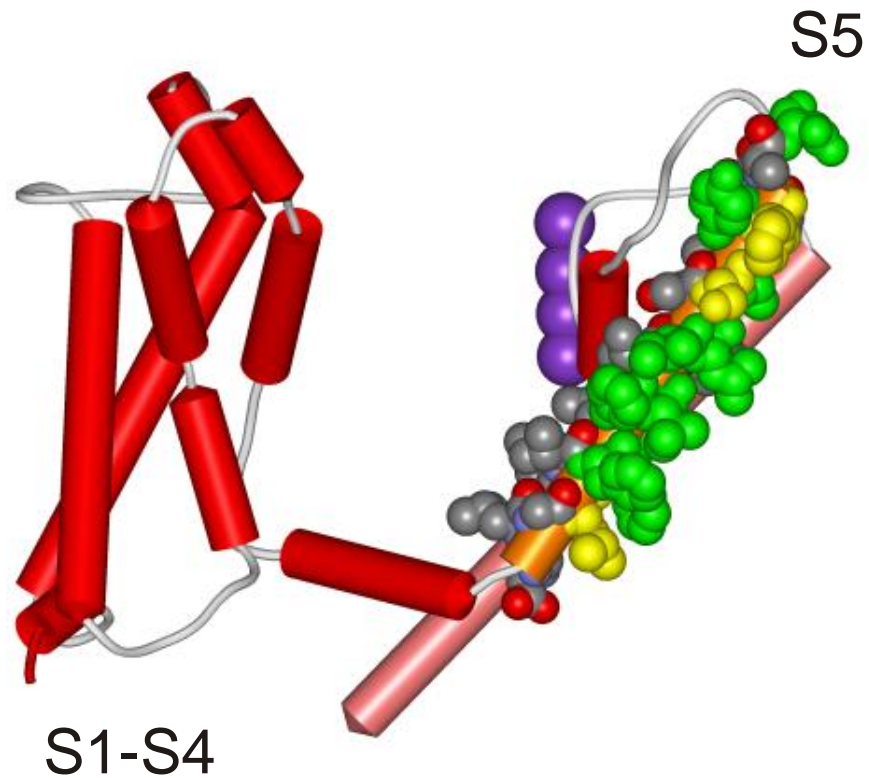


Figure 5.33: Residues making contact with the voltage sensor in the Kv1.2-Kv2.1 chimera. Details of the figure are as in Figure 5.32, Residues in S5 are shown in space-fill format and those making contact with the voltage sensor are shown in green but with residues 152, 166 and 171 shown in yellow. Potassium ions are shown in purple. Rendered with WebLab Viewerpro (Molecular Dimensions Inc.) PDB ID 2R9R

5.4.3 General analysis of quenching data.

The quenching results with NaI were helpful in confirming positions at the ends of S5, but the pattern on quenching observed toward the centre of the membrane are hard to interpret (Figure 5.14b). The profile for NaI quenching resembles a mirror-image of quenching by Tempo (Figure 5.9a), as expected if NaI quenches from the aqueous phase and Tempo quenches from the membrane phase. High levels of quenching by NaI are observed at positions 159 and 163 towards the centre of the membrane (Figure 5.6); these both correspond to positions in contact with the voltage sensor and the lipid bilayer and it is not clear why they should show higher than expected quenching by NaI. There is always a possibility of course that the results follow from some perturbation of the structure induced by the presence of the NBD group.

Levels of quenching by Tempo for full length KvAP are generally high toward the centre of helix S5 (Figure 5.15b), consistent with the marked lipid-exposure of many residues in the helix despite the presence of the voltage sensor. Removal of the voltage sensor leads to increased quenching at positions 155, 162, 163, 169 and 170; these are all positions of contact with the voltage sensor domain suggesting that packing at the S5-voltage sensor interface must be sufficiently tight to keep out the small Tempo molecule. Increased quenching by 16-doxyl stearic acid is also seen at most of these positions on removal of the voltage sensor (Figure 5.18b).

6 Chapter six: Exploring the topology of KvAP using N-(1-Pyrenyl) maleimide

6.1 Introduction

6.1.1 Pyrene fluorescence

Pyrene is a highly fluorescent polycyclic molecule consisting of four fused benzene rings as shown in Figure 6.1a. Pyrene has a high quantum yield (Baba et al. 2009), with a long fluorescence lifetime of 1.6 μ s (Mangle and Topp 1986), which means that it is easily detectable by fluorescence spectroscopy even at low concentrations. Pyrene has an unusual emission spectra compared to many other fluorophores as shown in Figure 6.2, with two large emission peaks at ca 375 nm and 395 nm. This complexity arises from the presence of a number of vibrational energy levels within the excited state of the pyrene fluorophore; emission from these vibrational levels gives rise to vibrational structure in the emission spectrum (Figure 5.1). (Haque et al. 2000).

Another interesting feature of pyrene fluorescence is that when two excited pyrene molecules are located within ca 10Å of each other, an excimer peak appears in the emission spectrum (Sahoo et al. 2000). This is an excited dimer state which exists only when at least one of the two pyrene molecules in close proximity is in the excited state. This excimer exists at a lower energy level than the excited state monomer, and hence the excimer emission peak is observed at around 450 nm.

6.1.2 N-(1-Pyrenyl) maleimide

N-(1-Pyrenyl) maleimide (NPM) is formed by the reaction of pyrene with maleic anhydride and subsequent treatment with acetic anhydride (Weltman et al. 1973). Maleimide is an unsaturated imide which reacts spontaneously with sulphydryls to form a stable sulphur-carbon bond and when attached to pyrene, the maleimide moiety confers onto pyrene the ability to bind sulphydryl groups such as cysteine. NPM is nonfluorescent until it reacts with a cysteine molecule via its maleimide group, upon which it displays similar fluorescence characteristics to pyrene (Weltman et al. 1973). The reaction of NPM with sulphydryls is relatively fast and can be monitored by the increase in fluorescence intensity of pyrene over time (Lux

and Gerard 1981). It has been found however, that in the presence of high concentrations of primary amine groups, such as TRIS buffer or high concentrations of protein, a slower reaction can then occur between the initial adduct and the amine, resulting in intramolecular aminolysis of the succinimido ring. This reaction is characterised by the disappearance of the emission peaks at 376 and 396 and the appearance of two new peaks at 386 and 405 nm. (Wu et al. 1976)

6.1.3 Environmental sensitivity of pyrene

Pyrene is an environmentally sensitive fluorophore; the emission spectrum of pyrene varies with the dielectric constant of the surrounding environment. However, unlike NBD described in Chapter 5, the wavelength at which the two peaks are observed does not change with dielectric constant, but rather the relative intensities of the peaks change (Brahma et al. 2005).

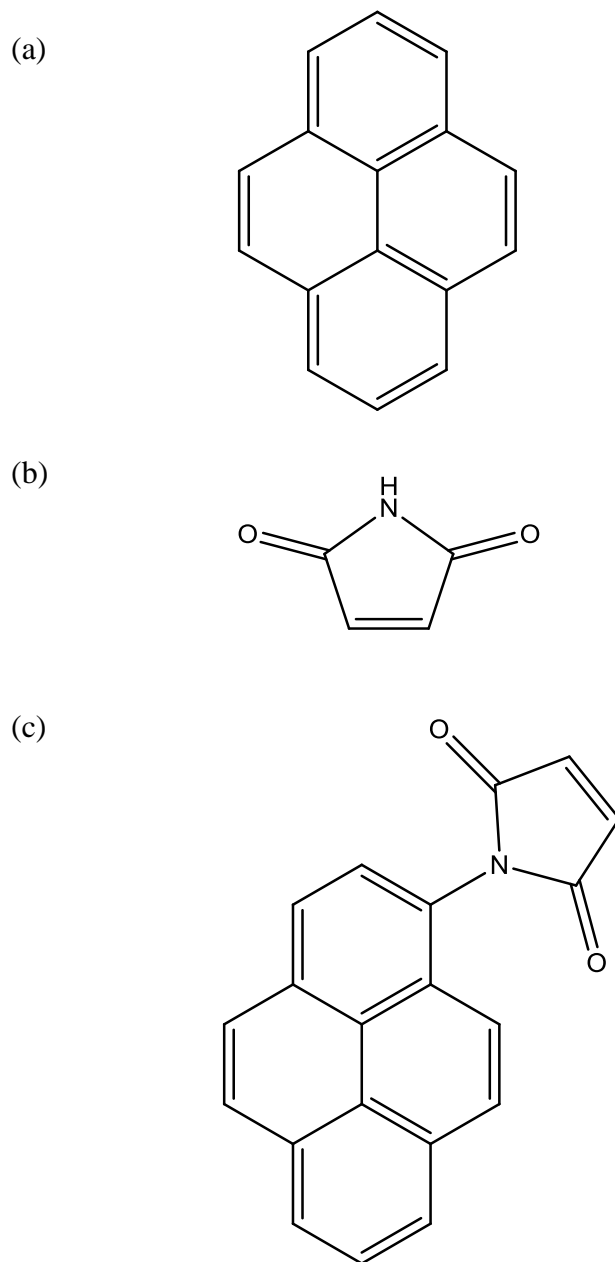


Figure 6.1: (a) Structure of pyrene. (b) The maleimide moiety (c) Pyrene maleimide.

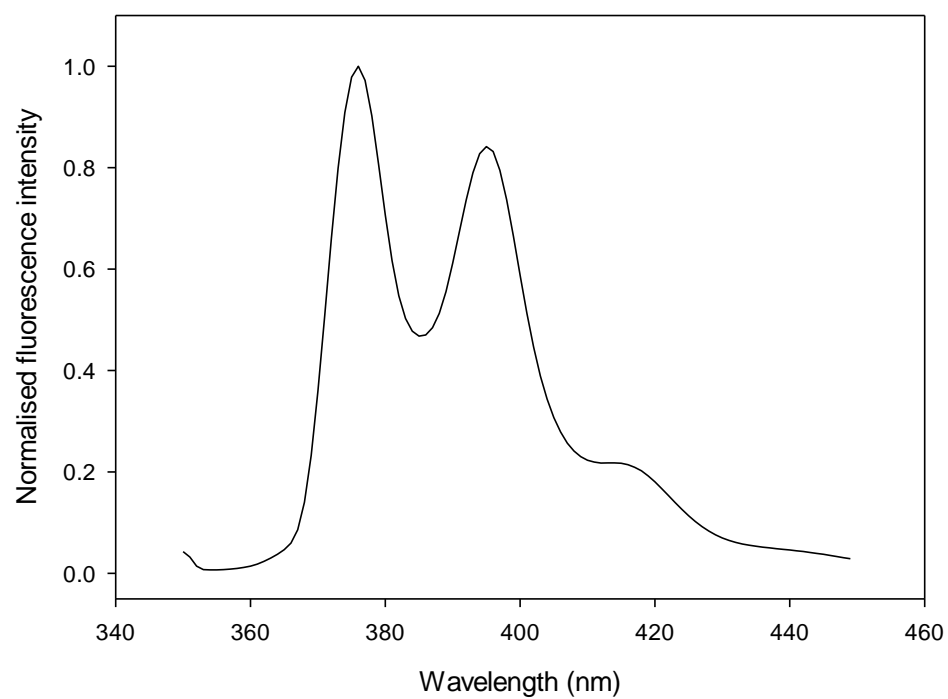


Figure 6.2: Emission spectrum of pyrene maleimide reduced with excess β mercaptoethanol in a 70 % dioxane/30% water mixture.

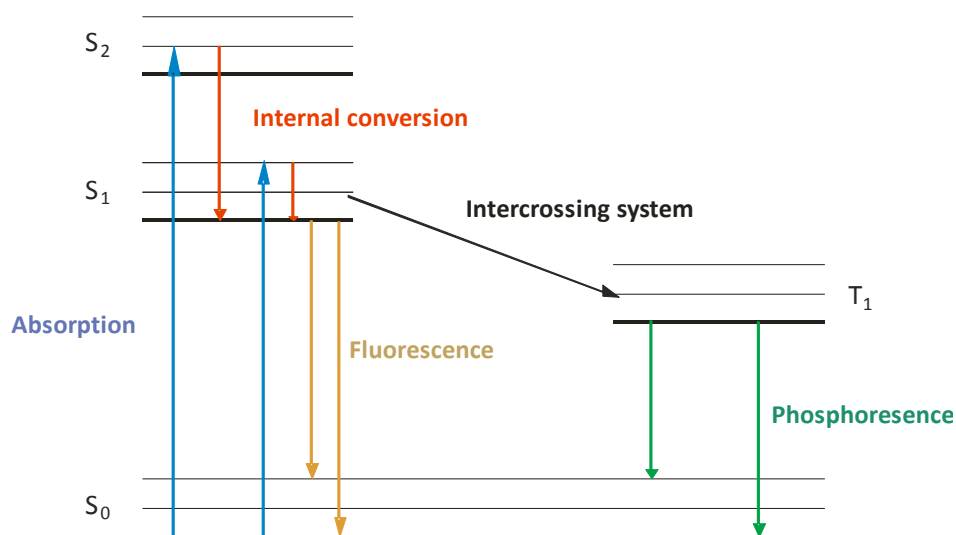


Figure 6.3: Jablonski diagram showing the phenomenon of luminescence. Absorption of light can excite the molecule into the various singlet excited states S_1, S_2 etc. with their associated vibrational levels. Internal conversion usually results in the excited molecule falling into the lowest vibrational level of the S_1 state, from which fluorescence is emitted. However, for pyrene, emission from the various vibrational levels of the excited states gives rise to vibrational structure in the emission spectrum. Inter system crossing into the triplet state T_1 is also possible, giving rise to phosphorescence. Adapted from Lakowicz 2006

6.2 Materials and methods

6.2.1 Methods

6.2.1.1 Preparation of stock lipid

Stock DOPC (Avanti Polar Lipids) was produced as described in section 2.2.4.2

6.2.1.2 Preparation of stock Brominated lipid

Stock brominated dioleoylphosphatidylcholine was prepared from stock DOPC as described in section 2.2.4.3.

6.2.1.3 Preparation of Hepes buffer

Hepes buffer was prepared as described in section 2.2.6.1.

6.2.1.4 Preparation of Potassium cholate solution

Potassium cholate solution was prepared as described in section 2.2.4.1.

6.2.1.5 Preparation of Sephadex

Sephadex G-50 was used to remove free dye from the purified KvAP and was prepared as described in section 2.2.6.2.

6.2.1.6 Labelling of KvAP and mutants with NPM

Purified mutants of KvAP were labelled with NPM as described in section 2.2.6.5.

6.2.1.7 Determination of NPM labelling ratio

In order to determine whether all KvAP had been labelled and whether there was any free NPM in solution, the labelling ratio of NPM was determined as described in section 2.2.6.6.

6.2.1.8 Reconstitution of labelled KvAP into lipid bilayers by dilution

NPM labelled mutants of KvAP were reconstituted into bilayer fragments for fluorescence measurements using the dilution method, as described in section 2.2.4.4.

6.2.1.9 Fluorescence measurements of NPM-labelled KvAP

Fluorescence of NPM labelled KvAP was measured as described in section 2.2.6.8.

6.2.1.10 Fluorescence quenching of NPM from the aqueous phase

Potassium Iodide solution was used to quench NPM fluorescence where the NPM probe was accessible to the aqueous phase, as described in section 2.2.6.9.

6.2.1.11 Fluorescence quenching of NPM from the lipid phase

Brominated phosphatidylcholine and 16-doxyl stearic acid were used to quench NPM fluorescence where the NBD probe was accessible to the lipid phase, as described in section 2.2.6.10 and 2.2.6.11 respectively

6.3 Results

6.3.1 Single cysteine mutants of full length KvAP

6.3.1.1 Labelling efficiency of single cysteine mutant of full length KvAP with NPM

Figure 5.5 and show labelling efficiencies of single cysteine mutants of KvAP with NPM. No labelling is seen to exceed 100 % which shows that the method for removal of free dye is efficient, and it is observed that all labelling is above 90% efficient. Little variation in labelling levels is observed between mutants of full length KvAP.

It has been shown that the relative intensities of the various peaks in the fluorescence emission spectrum of pyrene vary with solvent dielectric constant (Lakowitz 1999). The relative heights of the two peaks in the fluorescence emission spectrum of NPM observed following reaction with NPM were also found to vary with dielectric constant in dioxane/water mixtures (unpublished observations) but the peak height ratios observed for the labelled protein fell outside the range observed for the model compound in dioxane/water mixtures, so that useful information could not be obtained from this analysis.

6.3.1.2 Fluorescence quenching of NPM labelled full length KvAP with iodide

The fluorescence of KvAP labelled with pyrene maleimide was recorded in the presence (F) and absence (F_0) of 0.45 M iodide. Figure 6.5 shows the extent of fluorescence quenching by sodium iodide of residues in the S5 helix labelled with pyrene maleimide. It is apparent that there is a complex pattern of quenching within the bilayer, and that the overall level of quenching of pyrene fluorescence by iodide is greater than the quenching of NBD fluorescence observed in Chapter five. Because pyrene is a highly hydrophobic molecule, it is somewhat surprising to see that quenching is observed even for positions within the core of the bilayer.

Pyrene fluorescence at position 151 experiences one of the highest levels of quenching throughout the helix, consistent with the thesis that residue 151 exists at the hydrophobic interface, and is more exposed to aqueous solution than other

residues. There is then a noticeable decrease in quenching to position 157, which displays a low level of quenching. An interesting anomaly in this otherwise continuous reduction in the levels of quenching is position 155 which displays an F/F_0 value close to that of position 151, indicating a significant exposure to aqueous solution. At the C terminal end of the helix, we observe a continuous increase in quenching from position 168 to position 175, but with only a small increase in quenching between positions 170 and 173 which may be indicative of a lower exposure to aqueous solution than expected for some of those residues. Fluorescence quenching levels are very similar for positions 151 and 174 and 175, consistent with these being the interfacial residues at the N- and C-terminal ends of S5, as suggested in Chapter 5. The quenching profile in the central region of the helix is somewhat more complex. We see unusually high levels of quenching within what would logically be the hydrophobic core of the bilayer at positions 159 and 163, along with position 155 which has already been mentioned, whereas quenching minima are observed at positions 157, 161-162, 166 and 168. The quenching minima at positions 157, 162 and 166 are of similar values, indicating that this region may describe the hydrophobic core of the bilayer. The overall shape of the quenching profile is very similar to that observed for iodide quenching of NBD-labelled KvAPp (Figure 5.6).

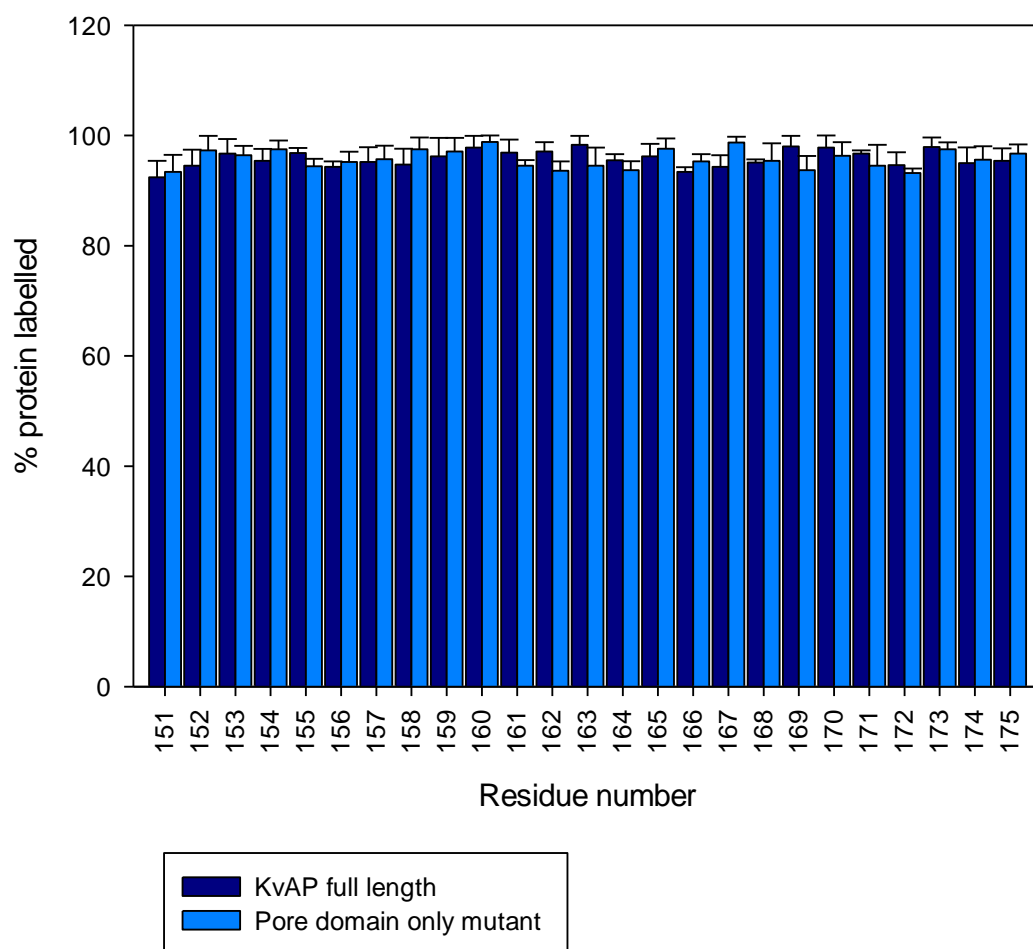


Figure 6.4: Labelling of single cysteine mutants of full length KvAP and the pore domain only mutant with NPM. The bar chart shows the percentage of Cys labelled.

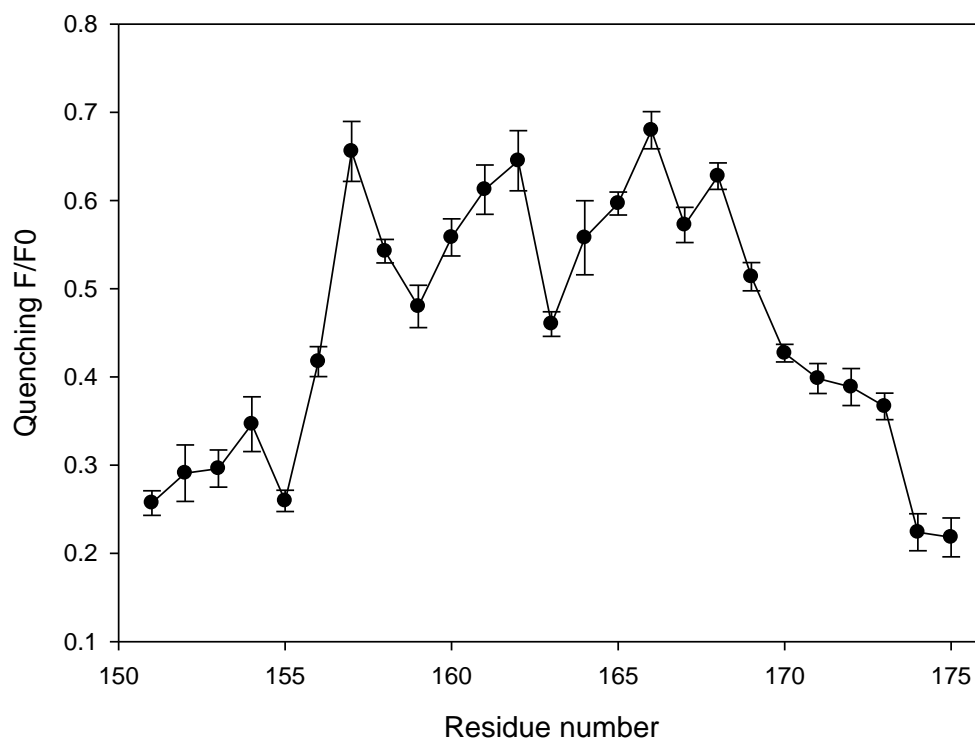


Figure 6.5: F/F_0 values for quenching of NPM-labelled single cysteine mutants of full length KvAP by 0.45 M NaI. F and F_0 correspond to the fluorescence intensities at 392 in the presence and absence of iodide respectively. Error is standard deviation of measurements from three separate reconstitutions for each mutant.

6.3.1.3 Fluorescence quenching of NPM-labelled full length KvAP with 16-doxyl stearic acid

Fluorescence of NPM-labelled KvAP was measured at 392 nm in the presence (F) and absence (F_0) of a 33 mole percent of the spin label 16-doxyl stearic acid. Figure 6.6 shows F/F_0 values for 16-doxyl stearic acid quenching of single cysteine mutants in the S5 helix of full length KvAP. Fluorescence quenching is low at positions 151 and 152 and at positions 174 and 175 again consistent with these being located at the interface at the N- and C-terminal ends of S5 respectively. There is a steep increase in quenching from position 152 to position 156, as expected as the label moves further into the core of the bilayer. At the C terminal end of the helix we observe a rise in quenching from position 166 to 175 again as would be expected on moving from the bilayer core to the interface.

The pattern of quenching for NPM-labelled KvAP is simpler than that observed for NBD-labelled KvAP with a much less extensive pattern of maxima or minima (compare Figures 6.6 and 5.8). The minimum in quenching at position 165 for NPM-labelled KvAP does, however, match a minimum in quenching for NBD-labelled KvAP at the same position.

6.3.1.4 Fluorescence quenching of NPM-labelled full length KvAP with brominated lipid

Figure 6.7 shows F/F_0 values for fluorescence quenching of NPM- labelled KvAP by di(Br₂C18:0)PC , where F is the fluorescence intensity at 392 nm when KvAP is reconstituted into di(Br₂C18:0)PC, and F_0 is the fluorescence intensity when labelled KvAP is reconstituted into di(18:1)PC. Fluorescence quenching by di(Br₂C18:0)PC increases from position 152 to position 157, similar to that seen with 16-doxyl stearic acid (Figure 6.6). This is to be expected as both of these quenching molecules should quench pyrene most efficiently near the core of the membrane. Some differences might, however, have been expected as the quenching bromine atoms are at the 9 and 10 positions of the acyl chains in di(Br₂C18:0)PC whereas the quenching free radical doxyl group in 16-doxyl stearic acid is at position 16 of the acyl chain, which, assuming that the carboxyl group is

located at the interface, would locate the quenching group close to the bilayer centre.

In fact, quenching profiles for di(Br₂C18:0)PC and 16-doxyl stearic acid have a very similar overall shape, presumably a reflection of the considerable disorder and motion in a lipid bilayer. In particular, the similar levels of quenching observed at the two ends of S5 are clear. Maxima and minima in quenching are more pronounced for di(Br₂C18:0)PC than for 16-doxyl stearic acid, but with the maxima and minima occurring at similar positions for the two quenchers. Residues 158-159, 162-163, 165, and 167-168 have lower levels of quenching than might have been expected. Conversely, residues 157, 160, 164 and 166 show particularly high levels of quenching. Di(Br₂C18:0)PC does not quench the fluorescence of the NBD group, and so it is not possible to compare quenching profiles for NPM-labelled and NBD-labelled KvAP with di(Br₂C18:0)PC.

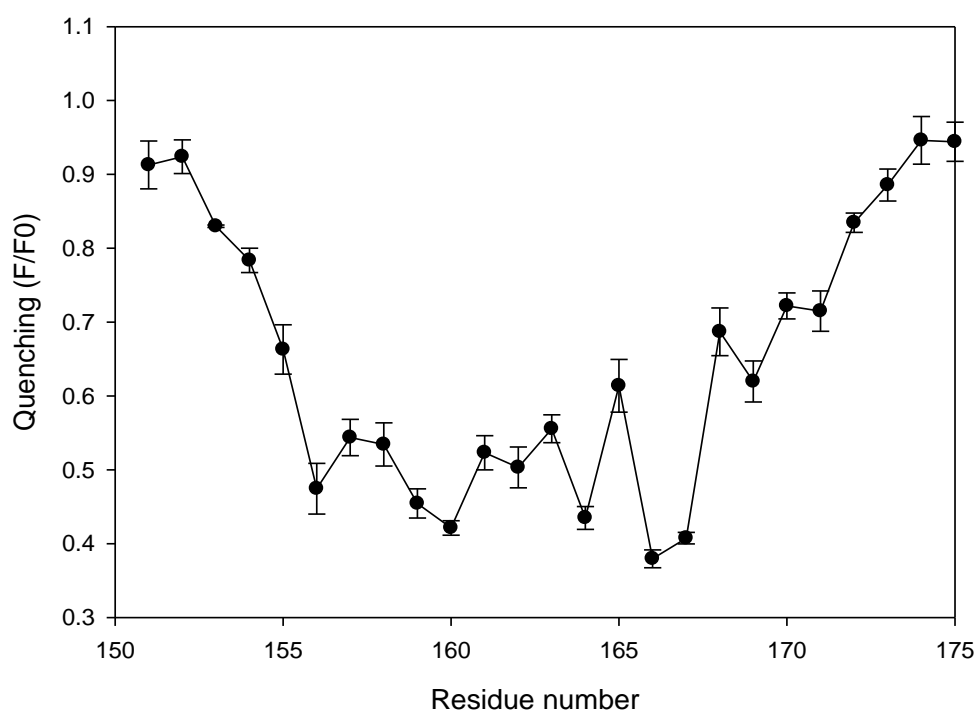


Figure 6.6 F/F_0 values for 16-doxyl stearic acid quenching of NPM-labelled single cysteine mutants of full length KvAP reconstituted into di(18:1)PC, excited at 478 nm at 25°C in Hepes buffer (20 mM Hepes, 150 mM KCl, 1 mM EGTA, pH 7.2) containing 86.6 μ M 16-doxyl stearic acid. The value of F_0 is that in the absence of 16-doxyl stearic acid. Error is standard deviation of measurements from three separate reconstitutions for each mutant.

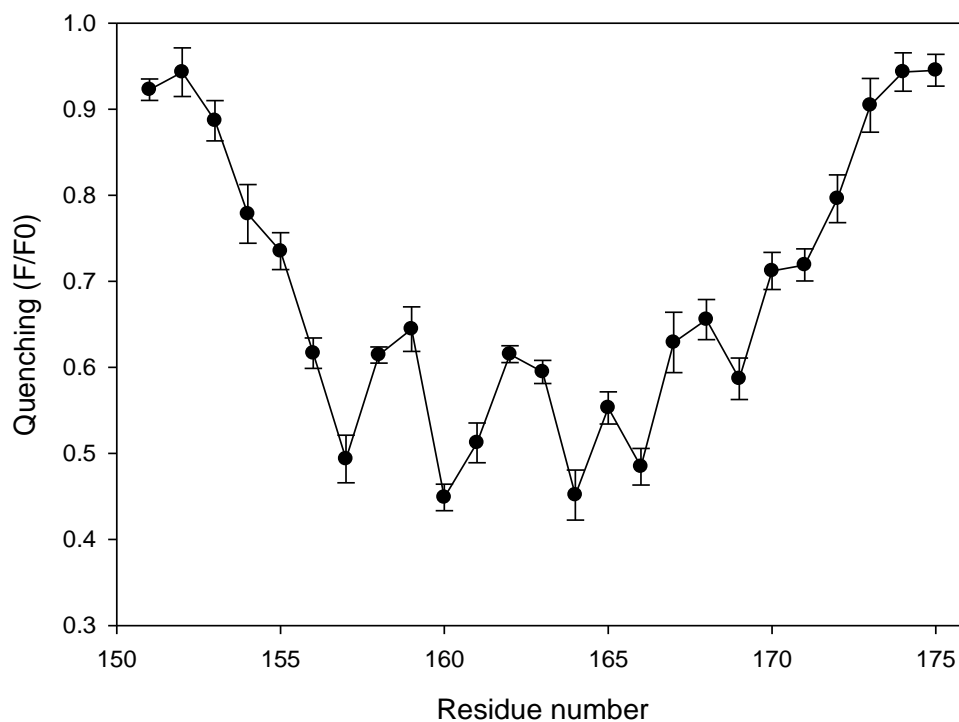


Figure 6.7: F/F_0 values for quenching of NPM-labelled single cysteine mutants of full length KvAP by di($\text{Br}_2\text{C18:0}$)PC in Hepes buffer (20 mM Hepes, 150 mM KCl, 1 mM EGTA, pH 7.0 KOH). F and F_0 correspond to the fluorescence intensity at 392 nm in the presence and absence of di($\text{Br}_2\text{C18:0}$)PC respectively. Error is standard deviation of measurements from three separate reconstitutions for each mutant.

6.3.2 KvAP pore domain only mutant

6.3.2.1 Labelling efficiency of single cysteine mutant of KvAP pore domain only mutant with NPM

Figure 6.4 shows labelling efficiencies of single cysteine mutants of KvAP with NPM and again are high. Little variation in labelling levels is observed between pore domain only mutants.

6.3.2.2 Fluorescence quenching of NPM-labelled KvAP pore domain only mutant with iodide

Figure 6.5Error! Reference source not found. and Figure 6.8a show F/F_0 values for NaI quenching of NPM-labelled pore domain only mutant, where F and F_0 are fluorescence intensities at 392 nm in the presence and absence of 0.45 M iodide respectively. As shown in Figure 6.8b the quenching profile is very similar to that determined for full length KvAP. At the N terminal end of the helix there is a decrease in quenching from position 151 to position 158, with the exception of position 154 which has a lower level of quenching than either of its adjacent residues. This pattern is consistent with a transition into the hydrophobic core of the bilayer, with the related reduction in accessibility to the aqueous medium. A similar pattern is observed at the C terminal end of the helix, where an increase in quenching is seen from position 167 to position 175. This increase is steep between positions 168 and 171, consistent with a sharp increase in dielectric constant, indicative of an approach to the hydrophobic interface of the membrane. As before, if Tyr-151 is located at the interface, the level of quenching associated with this position should be similar to that of a position located at the interface at the C terminal end of the helix, again suggesting that the interface at the C-terminal end corresponds to positions around position 173.

Figure 6.8b shows a comparison of the quenching profiles of the S5 helix in the presence (●) and absence (○) of the voltage sensor domains (VSDs). Although the maxima and minima in the two profiles do not always exactly match, the overall profiles are remarkably similar. The largest differences between the two profiles are observed at the N-terminal end of S5 (positions 151- 155) where lower levels of quenching are observed in the absence of the VSDs than in their presence.

It might have been expected that packing between the VSDs and helix S5 would reduce accessibility to a quencher molecule so that quenching would be lower in the presence of the VSDs. The fact that more quenching by the aqueous quencher I is observed in the presence of the VSDs suggests that the packing of the VSDs with helix S5 is less tight than packing of the lipid bilayer with S5 in the absence of the VSDs. However, a similar effect was not seen for NBD-labelled protein (Figure 5.13b) and the effect is rather small and may not be significant.

Changes in levels of quenching are also observed for central positions in S5, particularly at position 163, although this has the appearance of a shift in the positions corresponding to the maxima and minima (Figure 6.8b). Very similar changes were observed in this central region for NaI quenching of NBD fluorescence (Figure 5.13b). This could, for example, correspond to some small rearrangement of residues in the central part of S5, such as a small rotation, on replacement of a VSD with a lipid bilayer.

6.3.2.3 Fluorescence quenching of NPM labelled KvAP pore domain only mutant with 16-doxyl stearic acid

Figure 6.8a shows levels of quenching of pyrene fluorescence for positions in the S5 helix of single cysteine substitutions of the pore domain only are very similar in the absence or presence of the VSDs (Figure 6.9b).

At the N terminal end of the helix, there is good agreement between both quenching profiles. Position 157 however shows a much lower level of quenching in the absence of the VSDs than in their presence. This is unexpected, especially since the quenching levels of the surrounding residues vary little with and without a VSD. A similar effect was not seen for NBD-labelled protein (Figure 5.17) and so could be an effect due to the presence of the fluorescence labels themselves.

6.3.2.4 Fluorescence quenching of NPM-labelled KvAP pore domain only mutant with brominated lipid

Figure 6.10 show quenching values for NPM-labelled single cysteine mutants of the KvAP pore domain only mutant with di(Br₂C18:0)PC. The quenching profile observed is very similar to that observed with 16-doxyl stearic acid, (Figure 6.9) as

would have been expected since both of these quenchers quench fluorophores within the plane of the membrane. Also as expected the quenching profile with di(Br₂C18:0)PC is very similar in the presence or absence of the VSDs (Figure 6.10b). At the N terminal end of the helix fluorescence quenching increases steadily from position 152 to position 157 and at the C terminus of the helix, the level of quenching decreases from position 166 to position 175, although, in the absence of the VSDs, position 173 shows a higher level of quenching than its neighbouring positions. Within the central region of the helix, the pattern of quenching is quite complex, but again is similar in the absence or presence of the VSDs, except that quenching at position 161 is lower in the absence of the VSDs than in their presence, whereas quenching at positions 162 and 163 is more marked in the absence of the VSDs than in their presence. With 16-doxyl stearic acid slightly greater quenching was also observed at positions 162 and 163 in the absence of the VSDs than in their presence although now quenching at position 161 was the same in the absence or presence of the VSDs (Figure 6.10b). Position 163 showed less quenching by NaI in the absence of the VSDs than in their presence (Figure 6.8b).

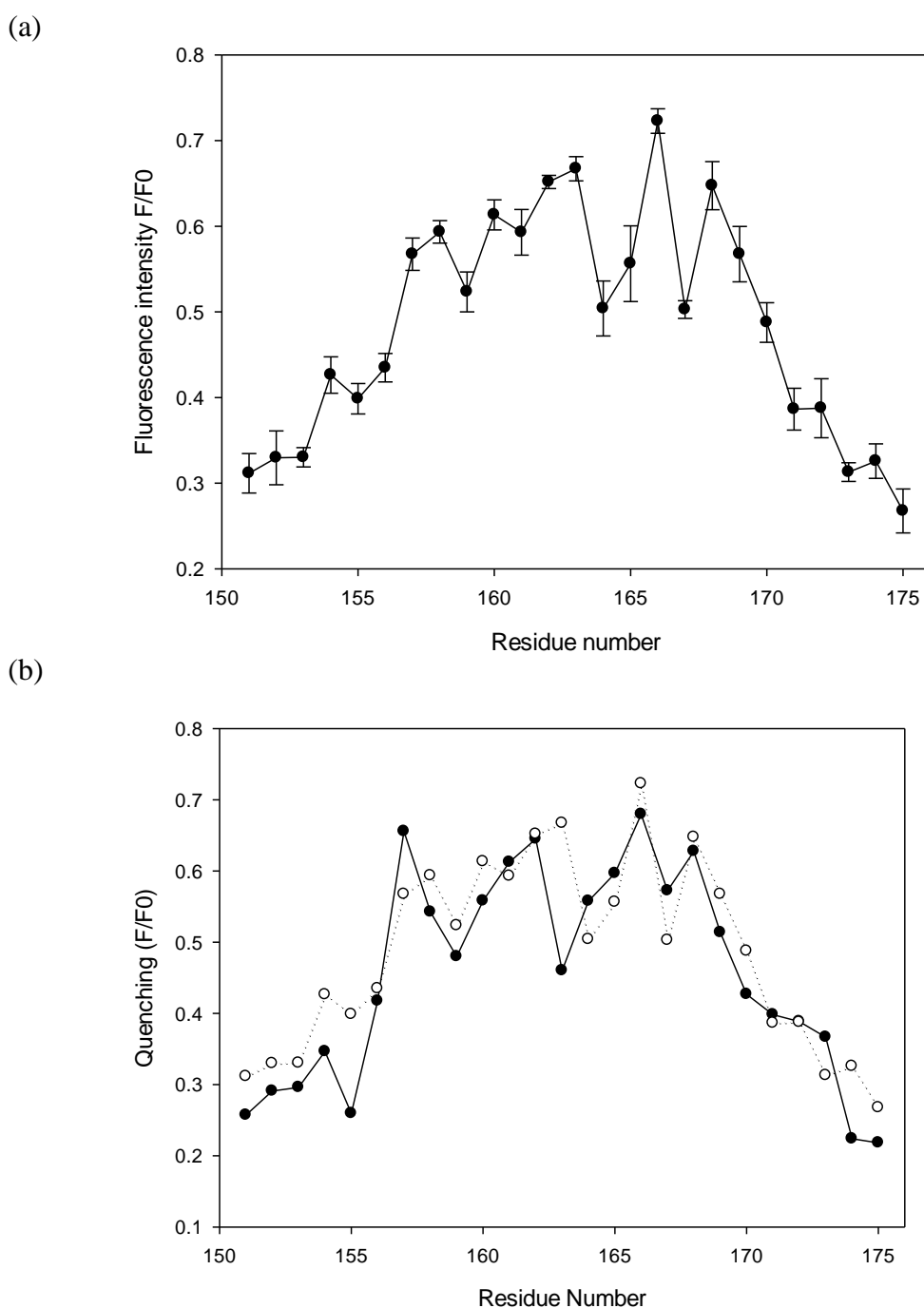


Figure 6.8: (a) F/F_0 values for NaI quenching of NPM-labelled single cysteine mutants of KvAP pore domain only mutant reconstituted into di(18:1)PC, excited at 338 nm at 25°C in Hepes buffer (20 mM Hepes, 0.45 M NaI, 0.45M NaCl, 100 mM $K_2S_2O_3$, 1 mM EGTA pH 7.2). The value of F_0 is that in the absence of NaI. Error is standard deviation of measurements from three separate reconstitutions for each mutant. (b) Comparison of quenching by NaI for NPM-labelled cysteine mutants of full length KvAP (●) and pore domain only mutant (○). Error bars are omitted for clarity.

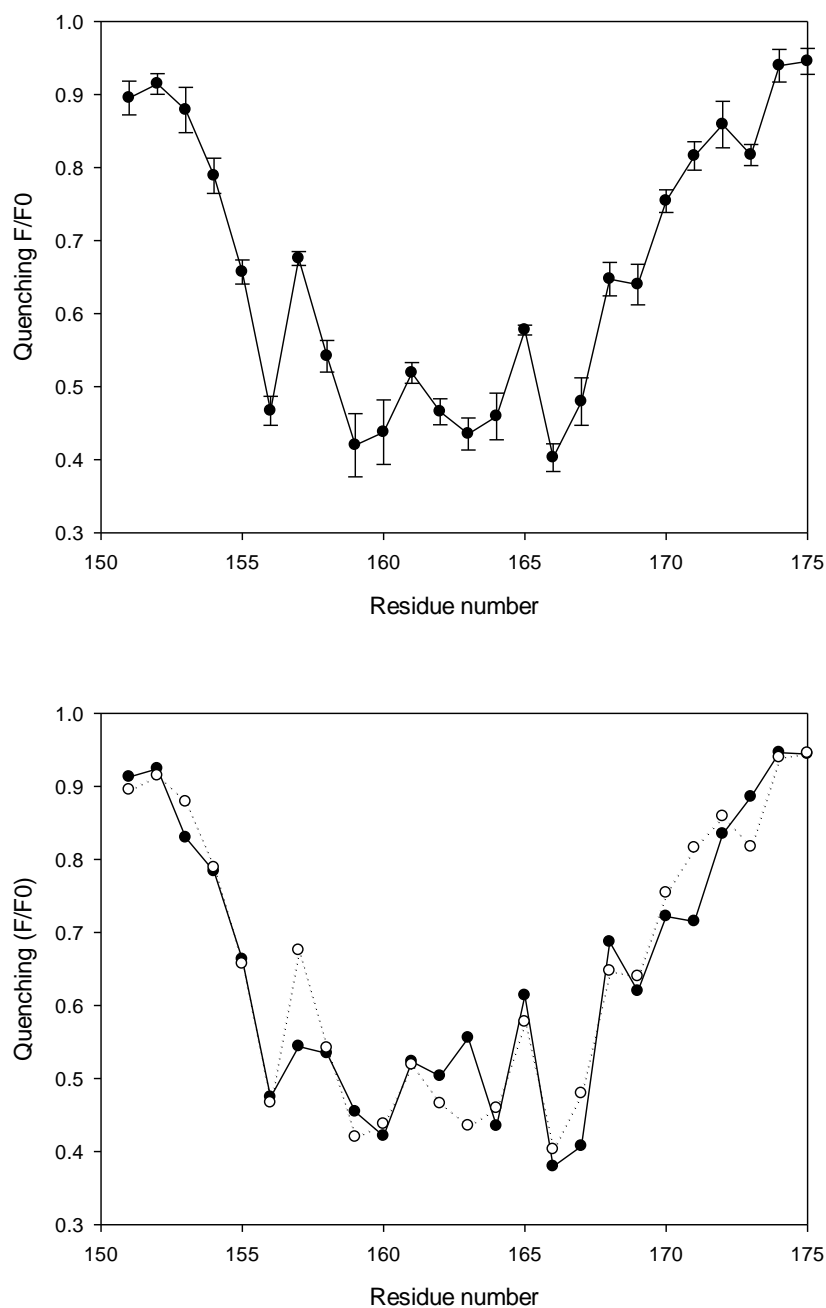


Figure 6.9: (a) F/F_0 values for 16-doxyl stearic acid quenching of NPM-labelled single cysteine mutants of KvAP pore domain only mutant reconstituted into di(18:1)PC, excited at 338 nm at 25°C in Hepes buffer (20 mM Hepes, 150 mM KCl, 1 mM EGTA, pH 7.2) containing 86.6 μ M 16-doxyl stearic acid. F and F_0 correspond to the fluorescence intensity at 392 in the presence and absence quencher. Error is standard deviation of measurements from three separate reconstitutions for each mutant. (b) Comparison of quenching by 16-doxyl stearic acid for NPM labelled cysteine mutants of full length KvAP (●) and pore domain only mutant (○). Error bars are omitted for clarity.

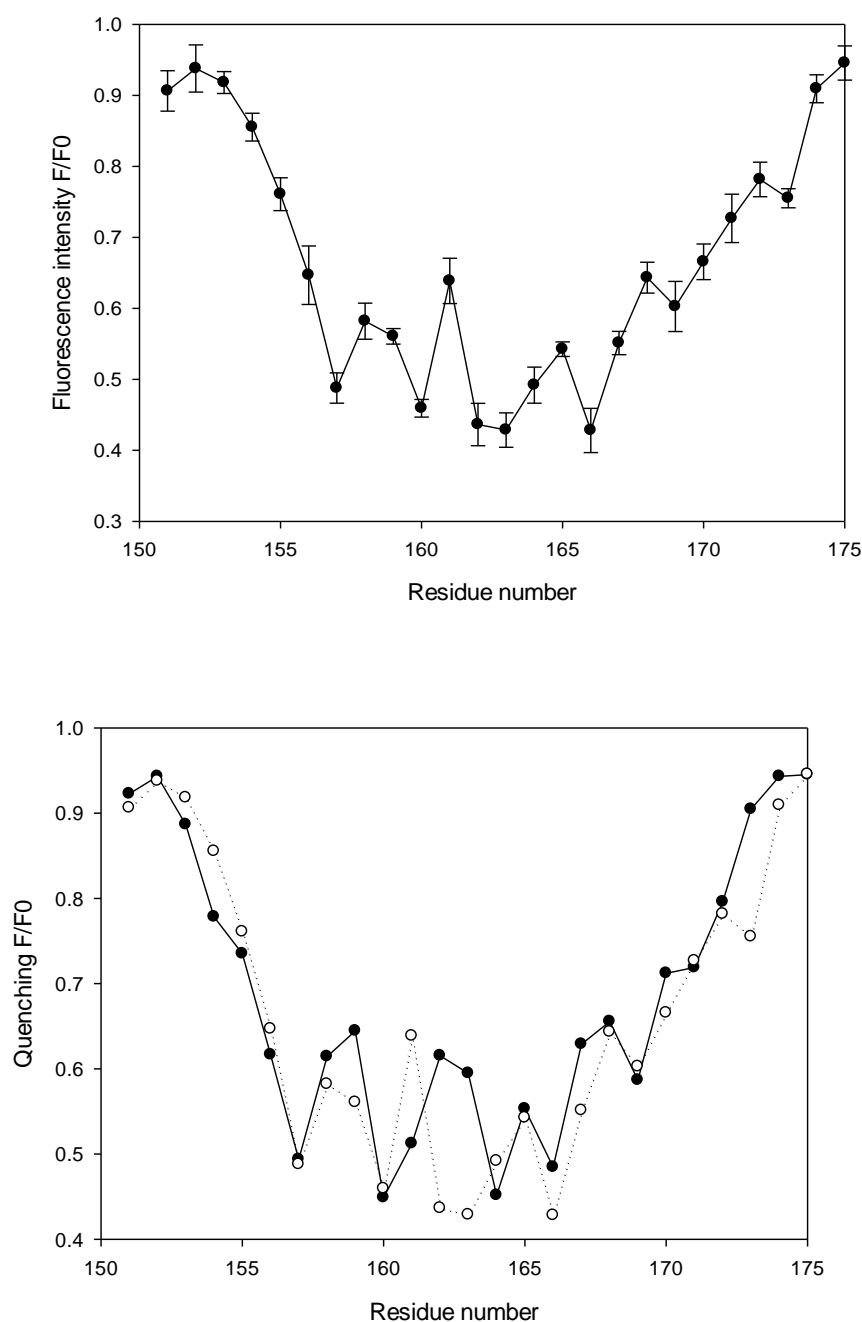


Figure 6.10: (a) F/F_0 values for quenching of NPM-labelled single cysteine mutants of the KvAP pore domain only mutant by di(Br₂C18:0)PC. F and F_0 correspond to the fluorescence intensity at 392 in the presence and absence of di(Br₂C18:0)PC respectively. Error is standard deviation of measurements from three separate reconstitutions for each mutant. (b) Comparison of quenching for NPM-labelled cysteine mutants of full length KvAP (●) and pore domain only mutant (○). Error bars are omitted for clarity.

6.4 Discussion

Mutagenesis and fluorescence labelling of a protein could always cause some small change in the structure of the protein. It is prudent therefore to use more than one fluorescence group where this is possible. The NBD group has the advantage of being very small; the pyrene group is much larger and more hydrophobic. When the two probes give a similar picture it is therefore reasonable to hope that the picture is a real one and not an artefact of the labelling. Pyrene has previously been shown to be highly sensitive to quenching by brominated lipids, spin labels and iodide, so these molecules can be used to assess the exposure of pyrene at specific positions within the S5 helix to the surrounding lipid bilayer. The results obtained here with the NBD and pyrene groups were generally very similar.

6.4.1 The ends of the S5 helix

The quenching results presented here with NPM-labelled KvAP and the pore domain only mutant are in good agreement with the results obtained with NBD-labelled protein described in Chapter 5. As described above, the results with NPM-labelled KvAP suggest that the region of S5 spanning the hydrophobic core of the membrane runs from Tyr-151 on the N-terminal side to Pro-174 or Asp-175 on the C-terminal side. The fact that similar results have been obtained with two very different fluorescence probes gives more confidence in the results.

6.4.2 Position of the voltage sensor

It might have been expected that removal of the VSDs would have resulted in a large change in the quenching properties of NPM-labelled KvAP, but, as with the NBD-labelled protein (Chapter 5), this was generally not the case. Very similar profiles of quenching were obtained in the presence or absence of VSDs, with either an aqueous quencher (Figure 6.8b) or with two membrane-bound quenchers (Figures 6.9b and 6.10b). These results confirm the conclusion of Chapter 5 that replacement of S5-VSDs contacts with S5-lipid bilayer contacts results in only small changes in the environments sensed by residues in S5. This is consistent with the considerable lipid exposure of many of the residues in helix S5 in the Kv1.2-Kv2.1 chimera even in the presence of VSDs; Table 5.1 shows an

alignment of residues in KvAP to the Kv2.1-1.2 chimera, and the characterisation of the exposure of the residues based on the structure of the chimera.

Comparison of NPM fluorescence quenching by NaI in the presence and absence of the voltage sensor is informative (Figure 6.8b). At the N terminal end of S5 we observe a reduction in quenching values for residues 151 to 155 on removal of the VSDs, yet the profile of the quenching does not change markedly, leading to the conclusion that the removal of the voltage sensor has caused a drop in the accessibility of the aqueous solution to these residues. This suggests that the packing of the VSDs with helix S5 is less tight than packing of the lipid bilayer with S5 in the absence of the VSDs but a similar effect was not seen for NBD-labelled protein (Figure 5.13b).

A reduction in quenching by NaI is observed at a number of positions through the S5 helix on removal of the VSDs, such as positions 158, 159 and 160, a pattern which was not observed for NaI quenching of NBD-labelled protein. There is a large reduction in quenching at position 163 upon removal of the voltage sensor, but what is surprising is the relatively high level of quenching observed in the presence of the VSDs since this position would not be expected to be easily accessible to the aqueous solution. A similar, but smaller reduction in quenching is seen at position 166 and 170; Figure 5.27 shows residues 151, 166 and 171, plotted on the KvAP crystal structure. It is apparent that these residues are all on the same face of the helix, facing out from the pore domain, in a position which would be consistent with the possible position of the voltage sensor. The possibility that some of these effects follow from a reorientation of the pyrene group following removal of the VSDs and the accompanying increased exposure of S5 to the lipid bilayer cannot be ruled out.

7 Chapter 7: General discussion

To sense changes in membrane potential the voltage sensing domains (VSD) must contain charges within the core of the membrane that move inward and outward in response to changes in the membrane electric field. These charges are the positively charged residues, normally arginine, but sometimes lysine, found at every third position in the S4 helix; movement of the S4 helix controls whether the channel is open or closed. Crystal structures of voltage-gated K⁺ channels correspond to a state in which the voltage sensors are in their membrane depolarised (positive inside relative to outside) conformation, so that the channel is either in an open, active, or an open, inactivated state, as is seen after a long depolarization of a membrane.

7.1 Mechanism of voltage sensor movement

Since there are no crystal structures showing the position of the closed state of the VSDs relative to the pore, closed state structures have to be deduced indirectly from approaches such as chemical labelling, leading to much controversy (Horn 2005; Tao et al. 2010; Tombola et al. 2006). In earlier models S4 is located at the centre of a helical bundle that is penetrated by large aqueous vestibules leading from the extracellular and intracellular surfaces. Only a small physical movement of S4 would therefore be required to move the charges in S4 from the extracellular aqueous environment into the intracellular aqueous environment; the electric field across the membrane is proposed to be focused over just a few Å rather than over the whole thickness of the lipid bilayer (Tombola et al. 2006). The original crystal structure for KvAP showed, however, that S4 was not buried in a helical bundle but had considerable exposure to the lipid bilayer (Jiang et al. 2003a). This led to the ‘paddle model’ in which S4 and the C-terminal helix of the S3 segment (S3b) formed a compact structure, referred to as a paddle, exposed to the lipid bilayer and moving a large distance (15-20 Å) across the lipid bilayer in response to changes in membrane potential (Jiang et al. 2003b). Subsequent determinations of the structures of voltage gated K⁺ channels which were less distorted than the original KvAP structure led to significant modifications of the paddle model (Long et al. 2007; Tao et al. 2010). The model still proposes that S3b-S4 moves as a unit and that the movement is large (15-20 Å) but now the charges on S4 are not proposed

to move through the hydrophobic environment of the lipid bilayer. Rather the charges on S4 are oriented towards the centre of the four helix (S1-S4) bundle that makes up a VSD with the positively charged residues in the open state located either close to the lipid headgroup region, in an aqueous cleft or vestibule penetrating ca 10 Å below the membrane surface on the extracellular side, or interacting with an acidic residue in S1 (Long et al. 2007). Transition from the open state to the closed state of the channel is proposed to involve a 15 Å ‘downward’ movement of the S3b-S4 paddle relative to the S1 and S2 helices allowing interaction of positive charges on S4 with acidic residues at the N-terminal end of S1. The downward motion of S4 is proposed to push down on the N-terminal end of the S4-S5 linker, exerting a force on the C-terminal end of S6 and causing the channel to close (Long et al. 2007). Since the major contacts between the VSDs and the pore are contacts between S4 and S5 this raises interesting questions about the nature of the S4-S5 interface. Helix-helix interactions in membrane proteins generally show structural specificity, often of the knobs-into-holes type (Curran and Engelman 2003). Specific interactions between S5 and S4 would hinder large-scale sliding of one helix against the other and so it is possible that the interaction surface between S5 and the VSDs is relatively characterless without tight packing of S5 against the VSDs.

In MacKinnon’s model (Long et al. 2007) S3b-S4 moves relative to S1 and S2 to exert a force on the S5-S6 linker. Movement of S4 will only be able to exert a force on the S5-S6 linker if the rest of the VSD is fixed tightly to the central pore. The attachment points between the VSDs and the pore must be quite small since about 66% of the transmembrane surface of each VSD is exposed to lipid (Jogini and Roux 2007) and since the attachment points cannot involve helix S4, the helix in the VSDs that makes most contact with the pore, since S4 is the helix that has to be able to move. The four subunits making up each channel are arranged so that the VSD domain of one subunit is close to helices S5 and S6 of a neighbouring subunit, the major contacts being between helices S4 and S5. However, the crystal structure of the open channel shows that S1 makes a physically tight contact with the pore, although only over a small area, involving the C-terminal end of S1 and the C-terminal ends of S5 and S6 on the extracellular side, and this is suggested to fix the S1-S2 part of the VSD relative to the pore (Long et al. 2007). On the

intracellular side the S4-S5 linker interacts primarily with S6 and could also help to fix the VSDs relative to the pore (Lee et al. 2009). Mutagenesis has shown the importance of the S1-pore interface for channel function (Lee et al. 2009).

The suggestion of these two areas of required close contact between the VSDs and the pore are consistent with experiments showing that VSDs can be swapped between channels (Lee et al. 2009; Lu et al. 2002) as the correct choice of, for example, the S4-S5 linker was required to obtain function (Lu et al. 2002). The major contact between the VSDs and the pore correspond to contacts between the S4 and S5 helices. However, there are very few conserved residues in S5 in the voltage-gated K^+ channels, the requirement being simply that the residues are hydrophobic. Similarly, in S4, apart from the positively charged residues, there are very few conserved residues. This then argues against tight, specific packing of the S4 and S5 helices. This is consistent with the observation that many of the residues in S5 in the Shaker K^+ channel equivalent to the residues in S5 in the Kv1.2-Kv2.1 chimera contacting the VSD (Table 5.6) can be replaced by Trp and other residues with no loss of function (Li-Smerin et al. 2000; Soler-Llavina et al. 2006).

7.2 Exposure of the S5 helix to the lipid bilayer

As well as the considerable exposure of the VSDs to the lipid bilayer, S5 in the central pore also shows considerable exposure to the lipid bilayer. Figure 7.2 shows the pore domain alone of KvAP with one of the S5 helices in space fill format. The relatively loose packing of S5 into the central pore is clear, with tight packing only apparent at the C-terminal end of S5; although the loose packing of S5 could, in principle, be an artefact of the distortions of the KvAP structure, rather similar packing is seen in the Kv1.2-Kv2.1 chimera structure, as detailed below. The observation that the fluorescence emission maxima for NBD located at positions throughout S5 in full length KvAP fit so well to the simple model for the dielectric profile across a lipid bilayer (Chapter 5) is consistent with most residues in S5 being exposed to a 'lipid-like' environment, as is the observation that removal of the VSDs leaves the environment of most residues in S5 unchanged. The fact that the pore domain of KvAP on its own can be expressed, purified and reconstituted into lipid bilayers also argues that the S5-VSD interface can be replaced by a S5-lipid interface with no dramatic effects on the structure or stability of the pore.

Others have shown that the VSDs can also be expressed and reconstituted into lipid bilayers (Krepkiy et al. 2009) so that the VSD-pore interface can be replaced by a VSD-lipid interface again with no dramatic effects on the structure of the VSDs. Minimizing contact between the VSDs and S5 by maximizing the exposure of the VSDs and S5 to the lipid bilayer will help easy movement of S4 relative to the pore. Sliding of S4 up and down against the side of the pore will be easiest if sliding involves simply moving one hydrophobic surface against another. Nevertheless the surface of S5 exposed to the VSD is not particularly smooth and nor is the surface of S4 that contacts the pore (Figure 7.1). There is, however, some suggestion in the structures shown in Figure 7.1 of an angled groove on the surface of S5 matching an angled ridge on S4 (made up of I294, I297, I300 and I303). That could aid sliding of S4 against S5.

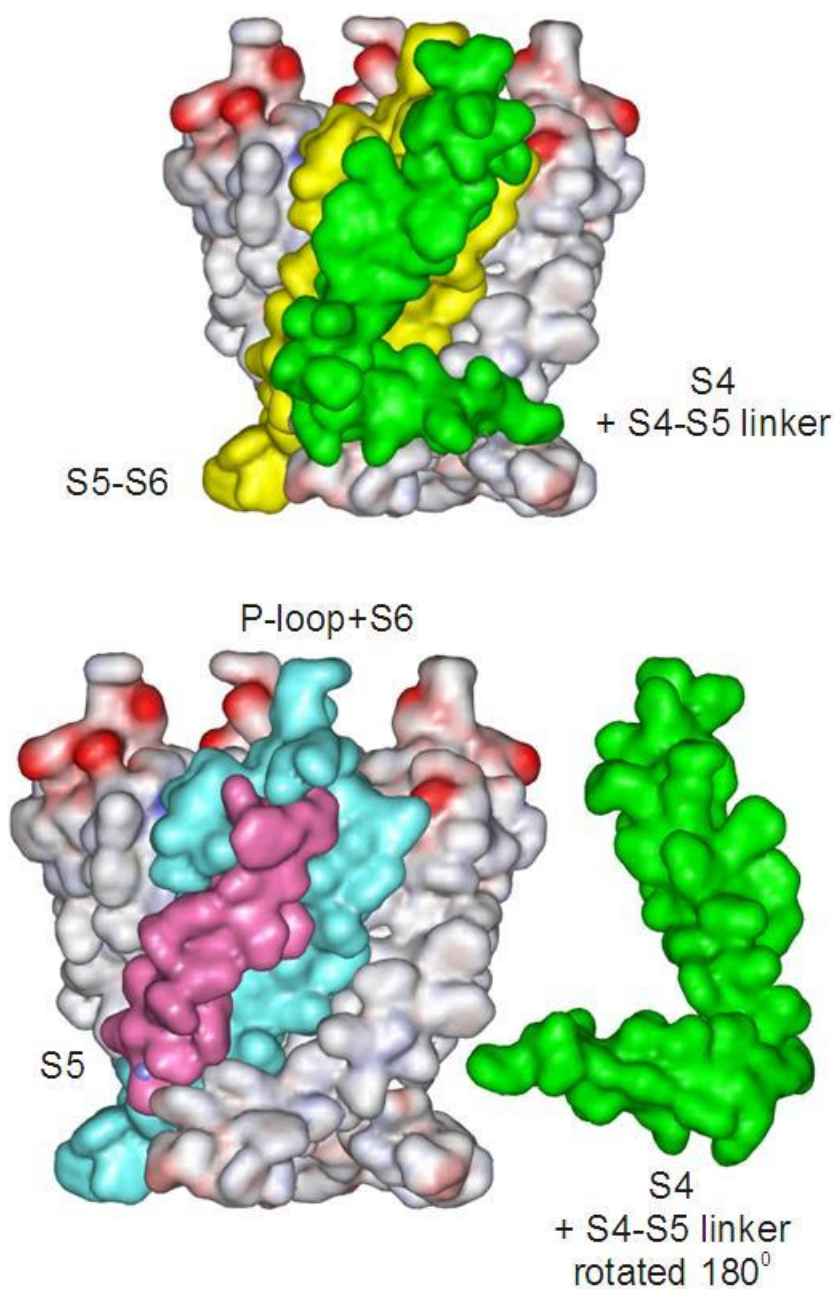


Figure 7.1: The interaction surface between S4 and S5. The central pore is shown in a surface plot coloured by electrostatic charge. The top shows how S4 and the S4-S5 linker, shown in green, sits against the S5-P-loop-S6 surface, shown in yellow. At the bottom, S4 and the S4-S5 linker have been displaced horizontally and rotated through 180° to show the surface normally in contact with the pore; the S5 helix is shown in purple and the P-loop plus S6 are shown in blue. Rendered with WebLab Viewerpro (Molecular Dimensions ltd.), PBD ID 2A0L

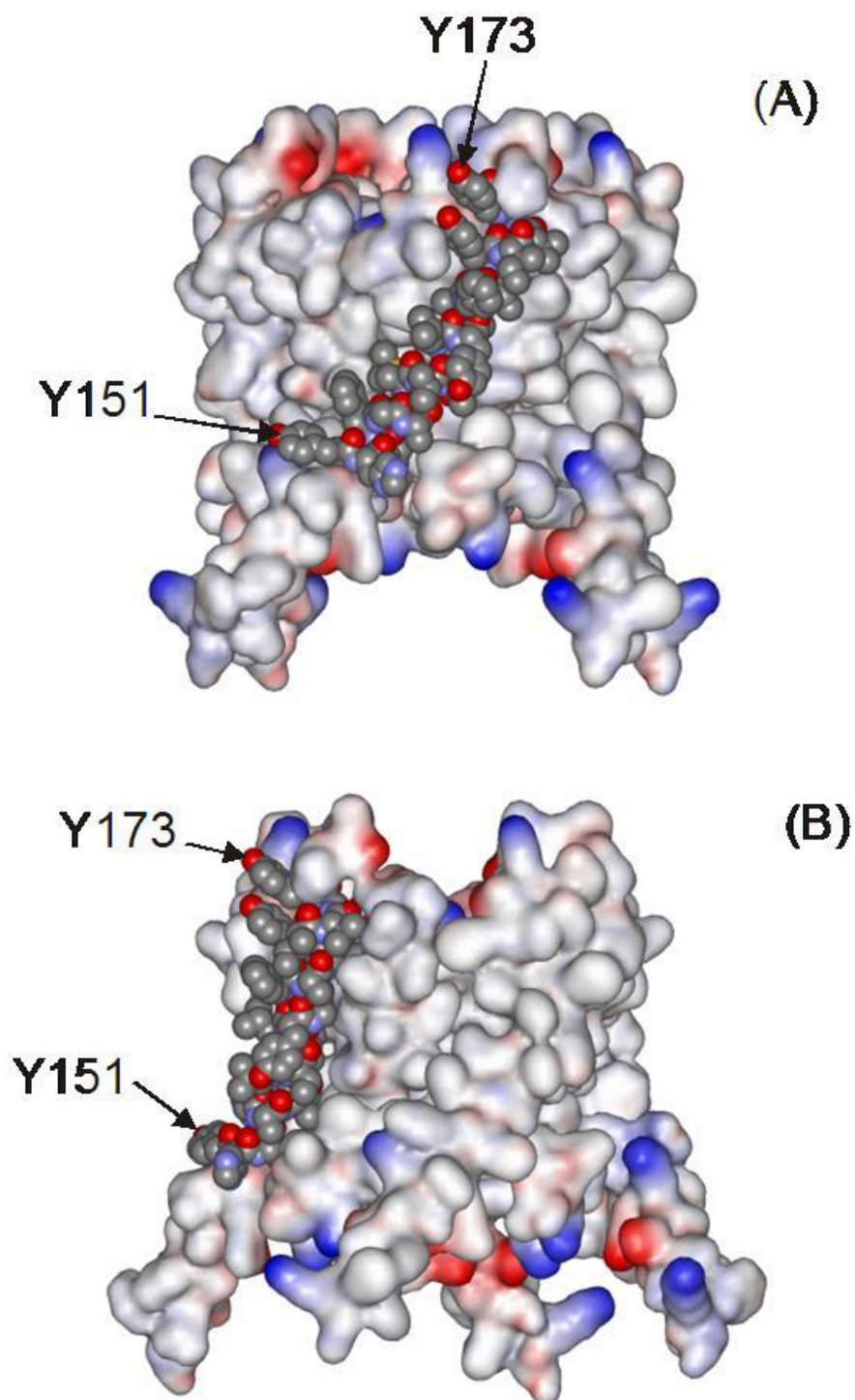


Figure 7.2: Helix S5 in the pore domain of KvAP. A surface plot is shown of the pore domain of KvAP alone, with helix S5 in one of the subunits shown in space fill format. (A) shows how S5 packs into the surface of the pore and (B) shows an edge view, showing the loose packing of the helix with the pore, with tight packing only apparent at the C-terminal end of S5. Rendered with WebLab Viewerpro (Molecular Dimensions ltd.), PBD ID 2A0L

7.3 Proximity of the voltage sensor to the S5 helix

As described in Chapter 5 a few of the positions in S5 show NBD emission spectra that do not agree well with the expectations of a simple dielectric model for the lipid bilayer, and these abnormal positions could be sites for tight packing between S5 and the VSDs. Figure 7.3 shows the interactions between helices S1 and S5 in the chimera: F344 in the Kv1.2-Kv2.1 chimera lies between T184 and F180 in S1 and S340 in S5 also contacts F180. T184 is a highly conserved residue and mutation of either F180 or T184 affects function (Lee et al. 2009). Fluorescence emission maxima for NBD at positions 166 and 170 in KvAP, equivalent to positions 340 and 344 in the Kv1.2-Kv2.1 chimera, shift on removal of the VSD, consistent with the tight packing between S5 and S1 in the VSD in this region shown in Figure 7.3. At the N-terminal end of S5, the fluorescence emission spectrum of NBD at position 152 also shifts on the removal of the voltage sensor. The equivalent residue in the Kv1.2-Kv2.1 chimera, L326, points towards the S4-S5 linker, being closest to G309 in the linker. In KvAP the residue equivalent to G309 is F135, suggesting that contact between the N-terminal end of S5 and the S4-S5 linker could be closer in KvAP than in the Kv1.2-Kv2.1 chimera, which would be consistent with the shift in NBD spectrum at position 152 in KvAP on removal of the VSD. The three positions where NBD fluorescence shifts most on removal of the VSDs and the two positions where the NBD emission is anomalous both in the absence and presence of the VSDs are shown for KvAP in Figure 7.4. This again makes the point that most contact between S5 and the VSDs occurs at the ends of the helix.

7.4 Bilayer thickness around the S5 helix

Since channel opening involves movement of S4 relative to the bilayer normal it is important to know where the bilayer is around the channel and to know whether or not the presence of the channel results in a large change in bilayer thickness. The experiments described in Chapter 5 and 6 suggest that the residues in S5 located in the glycerol backbone regions on the two sides of the lipid bilayer are Tyr-151 and Pro-174. This corresponds to a hydrophobic thickness for the helix, measured along the bilayer normal, of ca 29 Å as defined by the positions of the α -carbons of the

two residues. Since proline is not a residue that would be expected to be enriched at the interface it is possible that the interface at the C-terminal end of S5 is not marked by Pro-174 but, rather, by the carboxyl group of E172; this would give a hydrophobic thickness for S5 of 25 Å. The hydrophobic thickness of an undistorted bilayer of di(C18:1)PC is ca 27 Å (Lee 2003) and so that the hydrophobic thickness of KvAP seems to match well that of the surrounding bilayer. This is expected since the cost of exposing hydrophobic fatty acyl chains or hydrophobic amino acid residues to water is so high (Tanford 1980), the principle of hydrophobic matching. There is no evidence therefore from these experiments for any major distortion of the lipid bilayer around S5 and therefore no evidence for a major change in bilayer thickness around the VSDs, since the VSDs are in close contact with S5. Molecular dynamics simulations of isolated S4 helices have shown that the presence of the multiple arginine residues in S4 results in a very marked thinning of the bilayer around the helix, to allow charge interactions between the arginine residues and the lipid phosphate groups (Bond and Sansom 2007; Freitas et al. 2005). Marked bilayer thinning was also observed around an isolated VSD in molecular dynamics simulations of the distorted VSD domain from the crystal structure of KvAP in which charged residues in S4 were exposed to the lipid bilayer (Bond and Sansom 2007). A neutron diffraction study of an isolated voltage sensor domain in a lipid bilayer detected only small changes in average bilayer thickness, but left open the possibility that changes in the thickness of the bilayer in contact with the VSDs could have been greater (Krepkiy et al. 2009). A molecular dynamics simulation suggested that the thickness of the lipid bilayer decreases by as much as 9 Å close to the voltage sensor, but this conclusion must be treated with caution as the simulation gave a thickness for the unperturbed lipid bilayer about 4 Å thicker than the experimentally determined value (Lee 2009).

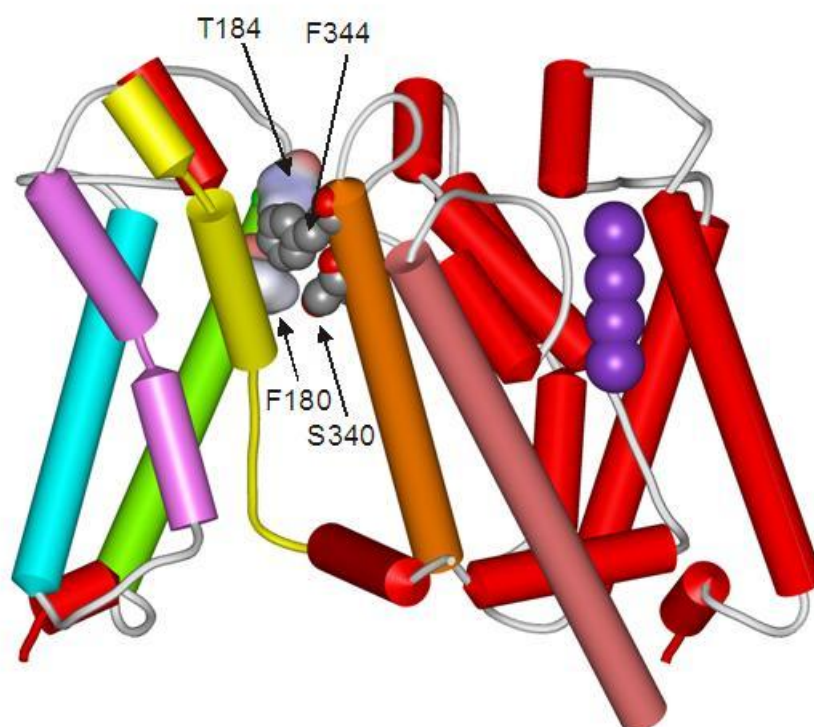


Figure 7.3: Packing of S1 and S5 in the Kv1.2-Kv2.1 chimera. S340 and F344 in S5 are shown in pspace fill format and F180 and T184 in S1 are shown as surface plots. Rendered with WebLab Viewerpro (Molecular Dimensions Ltd.), PBD ID 2R9R

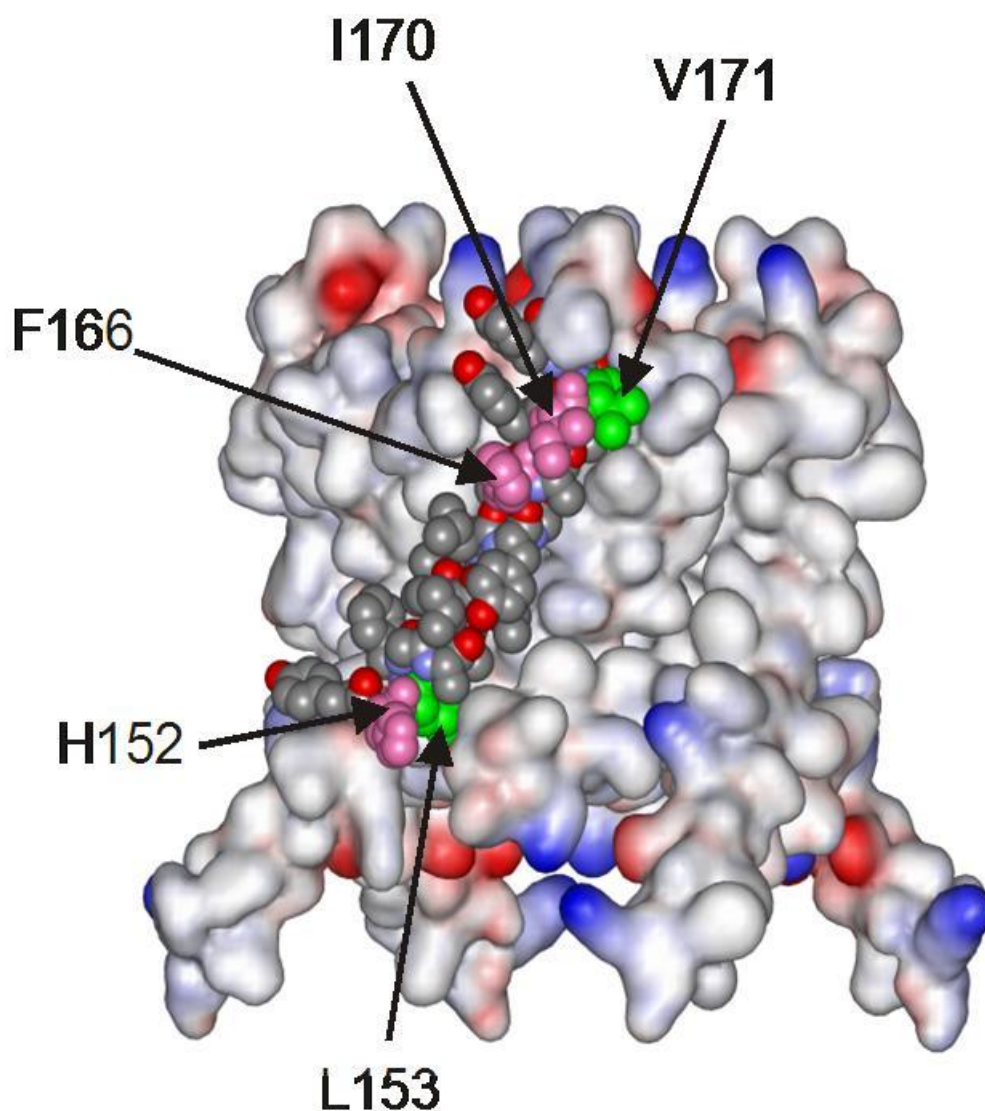


Figure 7.4: Helix S5 coloured for the NBD experiments. The pore domain only of KvAP is shown, with the S5 helix of one subunit shown in space fill format. The two positions where NBD fluorescence emission is anomalous are shown in green, and the three positions where NBD fluorescence shows a large shift on removal of the VSDs are shown in pink. Rendered with WebLab Viewerpro (Molecular Dimensions ltd.), PBD ID 2A0L

7.5 General conclusions and further work

Voltage gated channels are a keenly researched area of membrane science, and as such is a fast moving field. This research sought to explore the proximity and interaction of the voltage sensing domains with the pore domain, and to determine the thickness of the hydrophobic core of the membrane in the locality of the S5 helix.

Much information regarding the interaction of the voltage sensing domains with the pore domain to date has been studied to a large extent with crystallography (Jiang et al 2003, Long et al. 2007, Ruta et al. 2004). It is well understood that the voltage sensing domains are highly flexible structures and are thought to be only loosely attached to pore domain. It therefore follows that the VSD's are likely hugely influenced by the structure of the surrounding membrane; this provides a challenge for crystallography as the experimental technique requires the structure of the membrane to be removed. As described above, and highlighted in table Table 5.1, the fluorescence results widely agree with the crystal structure of potassium channels to date, indicating that despite the apparent flexibility of the voltage sensing domain, the removal of the lipid bilayer may not significantly disrupt the overall structure of the channel, which has a number of interesting implications on the strength of the association of the voltage sensing domain with the pore domain.

As discussed in above, the function of the voltage sensing domains requires the movement of charged residues from one side of the membrane electric field to the other. It is therefore central to the understanding of the mechanism of action of the voltage sensors to understand the local structure of the bilayer. A number of molecular dynamics simulations have undertaken to describe the electric field surrounding the voltage sensing domain, however, none of these have directly calculated the position of the hydrophobic interface at either side of KvAP, but rather, assumed this information from the crystal structure and amino acid distribution (Tombola 2006). The fluorescence data from this study provide a definitive thickness for the hydrophobic core of the membrane and give a position of the hydrophobic interface on the membrane exposed regions of S5. When this is coupled with the endorsement of the crystal structure that this work has also

provided, the position of the hydrophobic interface can therefore be extended onto the adjoining portions of the voltage sensing domain.

A number of questions remain regarding the strength of the interaction of the voltage sensing domain with the pore domain, and the position of the voltage sensors in the closed state of the channel. Fluorescence spectroscopy techniques could be further used to probe the strength of interaction between the voltage sensing domain and the pore domain. The experiments documented above make use of an isolated voltage sensing domain. The Mackinnon group have utilised a similar isolated voltage sensing domain in crystal structures (Jiang et al. 2003) (PDB ID: 1ORQ). The cysteine mutants of the pore domain mutant which have been used in this study could be used to probe the strength of interaction of the pore domain with the voltage sensing domain, as an interaction between these two domains would cause a significant change in any fluorescence signal of a cysteine bound fluorescent molecule. Further mutations could then be undertaken in the S5 helix to probe the effect of the mutation of each residue in the S5 helix on the strength of the Pore-VSD interaction, allowing the identification of key residues in the interaction. This work has hopefully therefore provided important information in the form of experimentally determined parameters for groups using molecular dynamics simulations and will aid in their work.

Further studies on voltage sensing domains, in Kv and other voltage dependent channels will no doubt shed light on the structure and position of the voltage sensing domains in their closed state. At present, this would involve the maintenance of a membrane potential throughout the course of any experiment, in order to hold the VSDs closed. The discovery of a channel which possesses a constitutively closed voltage sensing domain will be the solution to this, and may not be too far away. Given the huge flexibility and instability of the voltage sensor, it follows that there small changes in these domains may lead to their 'inactivation'. These mutants can therefore be studied using structural techniques such as crystallography. The progress which is being made in solid state nuclear magnetic resonance (NMR), in which entire bilayer structures can be studied inclusive of small membrane proteins is extremely positive (Smith 2010). Currently the maximum molecule size for solid state NMR is around 30 kDa (Smith 2010),

however this has increased significantly over that last five years, and as it continues to do so, it is likely that a combination of NMR, crystallography, fluorescence and molecular dynamics will provide significant steps forward in our understanding of voltage gated ion channels.

References

- Accad, M. & Farese, R.V. 1998. Cholesterol homeostasis: a role for oxysterols. *Current Biology*, 8, (17) R601-R604
- Aggarwal, S.K. & MacKinnon, R. 1996. Contribution of the s4 segment to gating charge in the shaker K⁺ channel. *Neuron*, 16, (6) 1169-1177
- Akerlof, G. & Short, O.A. 1936. The dielectric constant of dioxane-water mixtures between 0 and 80 degrees centigrade. *Journal of the American Chemical Society*, 58, (7) 1241-1243
- Alabi, A.A., Bahamonde, M.I., Jung, H.J., Kim, J.I., & Swartz, K.J. 2007. Portability of paddle motif function and pharmacology in voltage sensors. *Nature*, 450, (7168) 370-375
- Alagem, N., Yesylevskyy, S., & Reuveny, E. 2003. The pore helix is involved in stabilizing the open state of inwardly rectifying K⁺ channels. *Biophys.J.*, 85, (1) 300-312
- Albers, S., van de Vossenberg, J., Driessen, A., & Konings, W. 2000. Adaptations of the archeal cell membrane to heat stress. *Frontiers in Bioscience*, 5, 813-820
- Alberts, B., Johnson, A., Lewis, J., & Raff, M. 2007. *Molecular Biology of the Cell*, 5 ed. New York.
- Armstrong, C.M. 1966. Time Course of TEA⁺ induced anomalous rectification in squid giant axons. *The Journal of General Physiology*, 50, (2) 491-503
- Baba, M., Saitoh, M., Kowaka, Y., Taguma, K., Yoshida, K., Semba, Y., Kasahara, S., Yamanaka, T., Ohshima, Y., Hsu, Y.C., & Lin, S.H. 2009. Vibrational and rotational structure and excited-state dynamics of pyrene. *Journal of Chemical Physics*, 131, (22) 224318
- Bane, S.E., Velasquez, J.E., & Robinson, A.S. 2007. Expression and purification of milligram levels of inactive G-protein coupled receptors in E. coli. *Protein Expression and Purification*, 52, (2) 348-355
- Berg, M., Tymoczko, J., & Stryer, L. 2002. *Biochemistry*, 5 ed. New York.
- Berneche, S. & Roux, B. 2003. A microscopic view of ion conduction through the K⁺ channel. *Proceedings of the National Academy of Sciences*, 100, (15) 8644-8648
- Bezannila, F. & Stefani, E. 1998, "Gating currents," *In Methods in Enzymology Ion Channels Part B*, Volume 293 ed. P. M. Conn, ed., Academic Press, pp. 331-352.

- Bixby, K.A., Nanao, M.H., Shen, N.V., Kreusch, A., Bellamy, H., Pfaffinger, P.J., & Choe, S. 1999. Zinc binding and molecular determinants of tetramerization in voltage-gated K⁺ channels. *Nature Structural and Molecular Biology*, 6, (1) 38-43
- Bond, P.J. & Sansom, M.S.P. 2007. Bilayer deformation by the Kv channel voltage sensor domain revealed by self-assembly simulations. *Proceedings of the National Academy of Sciences*, 104, (8) 2631-2636
- Brahma, A., Mandal, C., & Bhattacharyya, D. 2005. Characterization of a dimeric unfolding intermediate of bovine serum albumin under mildly acidic conditions. *Biochimica et Biophysica Acta (BBA) - Proteins & Proteomics*, 1751, (2) 159-169
- Breitwieser, G.E. 1991. G protein-mediated ion channel activation. *Hypertension*, 17, (5) 684-692
- Broomand, A. & Elinder, F. 2008. Large-scale movement within the voltage sensor paddle of a potassium channel - support for a helical-screw motion. *Neuron*, 59, (5) 770-777
- Byrne, B. & Iwata, S. 2002. Membrane protein complexes. *Current Opinion in Structural Biology*, 12, (2) 239-243
- Caffrey, M., Moynihan, D., & Hogan, J. 1991. A database of lipid-phase transition temperatures and enthalpy changes. *Journal of Chemical Information and Computer Sciences*, 31, (2) 275-284
- Campos, F.V., Chanda, B., Roux, B.t., & Bezanilla, F. 2007. Two atomic constraints unambiguously position the S4 segment relative to S1 and S2 segments in the closed state of Shaker K channel. *Proceedings of the National Academy of Sciences*, 104, (19) 7904-7909
- Cantor, R.S. 1997a. Lateral pressures in cell membranes: a mechanism for modulation of protein function. *The Journal of Physical Chemistry B*, 101, (10) 1723-1725
- Cantor, R.S. 1997b. The lateral pressure profile in membranes: a physical mechanism of general anesthesia. *Biochemistry*, 36, (9) 2339-2344
- Cantor, R.S. 1999. Lipid composition and the lateral pressure profile in bilayers. *Biophys.J*, 76, (5) 2625-2639
- Carney, J., East, J.M., & Lee, A.G. 2007. Penetration of lipid chains into transmembrane surfaces of membrane proteins: studies with MscL. *Biophys.J*, 92, (10) 3556-3563
- Cha, A., Snyder, G.E., Selvin, P.R., & Bezanilla, F. 1999. Atomic scale movement of the voltage-sensing region in a potassium channel measured via spectroscopy. *Nature*, 402, (6763) 809-813

- Chakrapani, S., Cuello, L.G., Cortes, D.M., & Perozo, E. 2008. Structural dynamics of an isolated voltage-sensor domain in a lipid bilayer. *Structure*, 16, (3) 398-409
- Chapman, D. 1975. Phase transitions and fluidity characteristics of lipids and cell membranes. *Quarterly Review of Biophysics*, 8, (2) 185-235
- Chattopadhyay, A. 1990. Chemistry and biology of N-(7-nitrobenz-2-oxa-1,3-diazol-4-yl)-labeled lipids: fluorescent probes of biological and model membranes. *Chemistry and Physics of Lipids*, 53, (1) 1-15
- Choe, S. 2002. Potassium channel structures. *Nat.Rev.Neuroscience*, 3, (2) 115-121
- Choi, K.L., Aldrich, R.W., & Yellen, G. 1991. Tetraethylammonium blockade distinguishes two inactivation mechanisms in voltage-activated K⁺ channels. *Proceedings of the National Academy of Sciences*, 88, (12) 5092-5095
- Cohen, A., Ben-Abu, Y., & Zilberberg, N. 2009. Gating the pore of potassium leak channels. *European Biophysics Journal*, 39, (1) 61-73
- Cohen, B.E., Grabe, M., & Jan, L.Y. 2003. Answers and Questions from the KvAP Structures. *Neuron*, 39, (3) 395-400
- Concha, N.O., Head, J.F., Kaetzel, M.A., Dedman, J., & Seaton, B.A. 1993. Rat annexin V crystal structure: Calcium induced conformational changes. *Science*, 261, (5126) 1321-1324
- Cordero-Morales, J.F., Cuello, L.G., Zhao, Y., Jogini, V., Cortes, D.M., & Roux, B. 2006. Molecular determinants of gating at the potassium channel selectivity filter. *Nature Structural and Molecular Biology*, 13, (4) 311-318
- Cuello, L.G., Cortes, D.M., & Perozo, E. 2005. Structural dynamics of the KvAP pore domain lacking the voltage sensing domain. *Biophys.J*, 88, (1) 19A-20A
- Cuello, L.G., Cortes, D.M., & Perozo, E. 2004. Molecular architecture of the KvAP voltage-dependent K⁺ channel in a lipid bilayer. *Science*, 306, (5695) 491-495
- Curran, A.R. & Engelman, D.M. 2003. Sequence motifs, polar interactions and conformational changes in helical membrane proteins. *Current Opinion in Structural Biology*, 13, (4) 412-417
- Damste, J.S.S., Schouten, S., Hopmans, E.C., van Duin, A.C.T., & Geenevasen, J.A.J. 2002. Crenarchaeol: the characteristic core glycerol dibiphytanyl glycerol tetraether membrane lipid of cosmopolitan pelagic crenarchaeota. *Journal of Lipid Research*, 43, (10) 1641-1651
- De Matteis, M.A. & Luini, A. 2008. Exiting the Golgi complex. *Nat.Rev.Mol.Cell Biol.*, 9, (4) 273-284

- De Rosa, M., Gambacorta, A., & Gliozzi, A. 1986. Structure, biosynthesis, and physicochemical properties of archaebacterial lipids. *Microbiology and Molecular Biology Reviews*, 50, (1) 70-80
- Degrip, N., VanOostrum, J., Bovee-Geurts, P.H.M. 1998. Selective detergent-extraction from mixed detergent/lipid/protein micelles, using cyclodextrin inclusion compounds : a novel generic approach for the preparation of proteoliposomes. *Biochemical Journal*, 330, 667-674.
- del Camino, D., Holmgren, M., Liu, Y., & Yellen, G. 2000. Blocker protection in the pore of a voltage-gated K⁺ channel and its structural implications. *Nature*, 403, (6767) 321-325
- del Camino, D. & Yellen, G. 2001. Tight steric closure at the intracellular activation gate of a voltage-gated K⁺ channel. *Neuron*, 32, (4) 649-656
- Derst, C. & Karschin, A. 1998. Review: Evolutionary link between prokaryotic and eukaryotic K⁺ channels. *Journal of Experimental Biology*, 201, (20) 2791b-2799
- Dickey, A. & Faller, R. 2008. Examining the contributions of lipid shape and headgroup charge on bilayer behavior. *Biophys.J.*, 95, (6) 2636-2646
- Doupnik, C.A., Davidson, N., & Lester, H.A. 1995. The inward rectifier potassium channel family. *Current Opinion in Neurobiology*, 5, (3) 268-277
- Doyle, D.A., Cabral, J., Pfuetzner, R.A., Kuo, A., Gulbis, J.M., Cohen, S.L., Chait, B.T., & MacKinnon, R. 1998. The structure of the potassium channel: molecular basis of K⁺ conduction and selectivity. *Science*, 280, (5360) 69-77
- Epand, R.M. 1998. Lipid polymorphism and protein-lipid interactions. *Biochimica et Biophysica Acta (BBA) - Reviews on Biomembranes*, 1376, (3) 353-368
- Ernst, A.M., Contreras, F.X., Bregger, B., & Wieland, F. 2010. Determinants of specificity at the protein-lipid interface in membranes. *FEBS Letters*, 584, (9) 1713-1720
- Fahy, E., Subramaniam, S., Brown, H.A., Glass, C.K., Merrill, A.H., Jr., Murphy, R.C., Raetz, C.R.H., Russell, D.W., Seyama, Y., Shaw, W., Shimizu, T., Spener, F., van Meer, G., VanNieuwenhze, M.S., White, S.H., Witztum, J.L., & Dennis, E.A. 2005. A comprehensive classification system for lipids. *Journal of Lipid Research*, 46, (5) 839-862
- Flewelling, R.F. & Hubbell, W.L. 1986. The membrane dipole potential in a total membrane potential model. Applications to hydrophobic ion interactions with membranes. *Biophys.J.*, 49, (2) 541-552

- Freites, J.A., Tobias, D.J., von, H.G., & White, S.H. 2005. Interface connections of a transmembrane voltage sensor. . *Proceedings of the National Academy of Sciences*, 102, (42) 15059-15064
- Garavito, R.M. & Ferguson-Miller, S. 2001. Detergents as tools in membrane biochemistry. *Journal of Biological Chemistry*, 276: 32403-32406
- Giddings, K.S., Johnson, A.E., & Tweten, R.K. 2003. Redefining cholesterol's role in the mechanism of the cholesterol-dependent cytolysins. *Proceedings of the National Academy of Sciences*, 100, (20) 11315-11320
- Glauner, K.S., Mannuzzu, L.M., Gandhi, C.S., & Isacoff, E.Y. 1999. Spectroscopic mapping of voltage sensor movement in the Shaker potassium channel. *Nature*, 402, (6763) 813-817
- Goldstein, S.A.N., Bockenhauer, D., O'Kelly, I., & Zilberberg, N. 2001. Potassium leak channels and the KCNK family of 2 domain subunits. *Nat.Rev.Neuroscience*, 2, (3) 175-184
- Gorter, E. & Grendel, F. 1925. On bimolecular layers of lipoids on chromocytes of the blood. *The Journal of Experimental Medicine*, 41, (4) 439-443
- Griepnerau B, B.R.A. 2010. The influence of 1-alkanols and external pressure on the lateral pressure profiles of lipid bilayers. *Biophys.J*, 15, (95) 5766-5778
- Grisshammer, R. & Tate, C. 2003. Preface: overexpression of integral membrane proteins. *Biochimica et Biophysica Acta (BBA) - Biomembranes*, 1610, (1) 1
- Grunnet, M., Rasmussen, H.B., Hay-Schmidt, A., & Klaerke, D.A. 2003. The voltage-gated potassium channel subunit, Kv1.3, is expressed in epithelia. *Biochimica et Biophysica Acta (BBA) - Biomembranes*, 1616, (1) 85-94
- Guan, X.L., Souza, C.M., Pichler, H., Dewhurst, G., Schaad, O., Kajiwar, K., Wakabayashi, H., Ivanova, T., Castillon, G.A., Piccolis, M., Abe, F., Loewith, R., Funato, K., Wenk, M.R., & Riezman, H. 2009. Functional interactions between sphingolipids and sterols in biological membranes regulating cell physiology. *Molecular Biology of the Cell*, 20, (7) 2083-2095
- Hanakam, F., Gerisch, G., Lotz, S., Alt, T., & Seelig, A. 1996. Binding of hisactophilin i and ii to lipid membranes is controlled by a pH-dependent myristoyl-histidine switch. *Biochemistry*, 35, (34) 11036-11044
- Hanford, M. & Peebles, T. 2002. Archaeal tetraether lipids. *Applied Biochemistry and Biotechnology*, 97, (1) 45-62
- Haque, M., Ray, S., & Chakrabarti, A. 2000. Polarity estimate of the hydrophobic binding sites in erythroid spectrin: a study by pyrene fluorescence. *Journal of Fluorescence*, 10, (1) 1-6

- Hartzell, H.C. 1988. Regulation of cardiac ion channels by catecholamines, acetylcholine and second messenger systems. *Progress in Biophysics and Molecular Biology*, 52, (3) 165-247
- Hodgkin, A.L. & Huxley, A.F. 1952. A quantitative description of membrane current and its application to conduction and excitation in nerve. *The Journal of Physiology Online*, 117, (4) 500-544
- Honore, E. 2007. The neuronal background K2P channels: focus on TREK1. *Nat.Rev.Neuroscience*, 8, (4) 251-261
- Horn, R. 2005. How ion channels sense membrane potential. *Proceedings of the National Academy of Sciences*, 102, (14) 4929-4930
- Horigome, T. and Sugano, H. 1983. A rapid method for removal of detergents from protein solution. *Analytical biochemistry*, 2, (15) 393-396
- Hoshi, T., Zagotta, W.N., & Aldrich, R.W. 1990. Biophysical and molecular mechanisms of Shaker potassium channel inactivation. *Science*, 250, (4980) 533-538
- Hoshi, T., Zagotta, W.N., & Aldrich, R.W. 1991. Two types of inactivation in Shaker K⁺ channels: Effects of alterations in the carboxy-terminal region. *Neuron*, 7, (4) 547-556
- Jiang, Y., Lee, A., Chen, J.Y., Ruta, V., Cadene, M., Chait, B.T., & MacKinnon, R. 2003a. X-ray structure of a voltage-dependent K⁺ channel. *Nature*, 423, 33-41
- Jiang, Y., Lee, A., Chen, J., Cadene, M., Chait, B.T., & MacKinnon, R. 2002a. Crystal structure and mechanism of a calcium-gated potassium channel. *Nature*, 417, (6888) 515-522
- Jiang, Y., Lee, A., Chen, J., Cadene, M., Chait, B.T., & MacKinnon, R. 2002b. The open pore conformation of potassium channels. *Nature*, 417, (6888) 523-526
- Jiang, Y., Ruta, V., Chen, J., Lee, A., & MacKinnon, R. 2003b. The principle of gating charge movement in a voltage-dependent K⁺ channel. *Nature*, 423, (6935) 42-48
- Jittikoon, J., East J M, & Lee, A.G. 2007. A fluorescence method to define transmembrane alpha helices in membrane proteins: studies with bacterial diacylglycerol kinase. *Biochemistry* 46, (38), 10950-10959
- Jogini, V. & Roux, B. 2007. Dynamics of the Kv1.2 voltage-gated K⁺ channel in a membrane environment. *Biophys.J*, 93, (9) 3070-3082
- Jogini, V. & Roux, B. 2005. Electrostatics of the intracellular vestibule of K⁺ channels. *Journal of Molecular Biology*, 354, (2) 272-288

- Johnson, J.E. & Cornell, R. 1999. Amphitropic proteins: regulation by reversible membrane interactions (Review). *Molecular Membrane Biology*, 16, (3) 217-235
- Khalili-Araghi, F., Jogini, V., Yarov-Yarovoy, V., Tajkhorshid, E., Roux, B., & Schulten, K. 2010. Calculation of the gating charge for the Kv1.2 voltage-activated potassium channel. *Biophys.J*, 98, (10) 2189-2198
- King, G.I. & White, S.H. 1986. Determining bilayer hydrocarbon thickness from neutron diffraction measurements using strip-function models. *Biophys.J*, 49, (5) 1047-1054
- Koga, Y. & Morii, H. 2005. Recent advances in structural research on ether lipids from archaea including comparative and physiological aspects. *Bioscience, Biotechnology and Biochemistry*, 69, (11) 2019-2034
- Korn, S.J. & Trapani, J.G. 2005. Potassium channels. *IEEE transactions on Nanobioscience*, 4, (1) 21-33
- Krepkiy, D., Mihailescu, M., Freites, J.A., Schow, E.V., Worcester, D.L., Gawrisch, K., Tobias, D.J., White, S.H., & Swartz, K.J. 2009a. Structure and hydration of membranes embedded with voltage-sensing domains. *Nature*, 462, (7272) 473-479
- Krepkiy, D., Mihailescu, M., Freites, J.A., Schow, E.V., Worcester, D.L., Gawrisch, K., Tobias, D.J., White, S.H., & Swartz, K.J. 2009b. Structure and hydration of membranes embedded with voltage-sensing domains. *Nature*, 462, (7272) 473-479
- Lakowicz, J.R. 1999. *Principles of fluorescence spectroscopy* Kluwer Academic/Plenum Press, NY.
- Landau, E. & Rosenbusch, J. 1996. Lipidic cubic phases: A novel concept for the crystallization of membrane proteins. *Proceedings of the National Academy of Sciences*, 93, (25) 14532-14535
- Lee, A.G. 2000. Membrane lipids: It's only a phase. *Current Biology*, 10, (10) R377-R380
- Lee, A.G. 2003. Lipid-protein interactions in biological membranes: a structural perspective. *Biochimica et Biophysica Acta (BBA) - Biomembranes*, 1612, (1) 1-40
- Lee, A.G. 2004. How lipids affect the activities of integral membrane proteins. *Biochimica et Biophysica Acta (BBA) - Biomembranes*, 1666, (1-2) 62-87
- Lee, A.G. 2006. Lipid interactions with ion channels. *Future Lipidology*, 1, (1) 103-113
- Lee, A.G. 2009. Structural biology: Highly charged meetings. *Nature*, 462, (7272) 420-421

- Lee, S.Y., Banerjee, A., & MacKinnon, R. 2009. Two separate interfaces between the voltage sensor and pore are required for the function of voltage-dependent K⁺ channels. *PLoS Biol*, 7, (3) e1000047
- Lee, S.Y., Lee, A., Chen, J., & MacKinnon, R. 2005. Structure of the KvAP voltage-dependent K⁺ channel and its dependence on the lipid membrane. *Proceedings of the National Academy of Sciences*, 102, (43) 15441-15446
- Li, B. & Gallin, W. 2004. VKCDB: Voltage-gated potassium channel database. *BMC Bioinformatics*, 5, (1) 3
- Li, Y., Um, S.Y., & McDonald, T.V. 2006. Voltage-gated potassium channels: regulation by accessory subunits. *The Neuroscientist*, 12, (3) 199-210
- Li-Smerin, Y., Hackos, D.H., & Swartz, K.J. 2000. A localized interaction surface for voltage-sensing domains on the pore domain of a K⁺ channel. *Neuron*, 25, (2) 411-423
- Long, S.B., Campbell, E.B., & MacKinnon, R. 2005a. Crystal structure of a mammalian voltage-dependent shaker family K⁺ channel. *Science*, 309, (5736) 897-903
- Long, S.B., Campbell, E.B., & MacKinnon, R. 2005b. Voltage sensor of Kv1.2: structural basis of electromechanical coupling. *Science*, 309, (5736) 903-908
- Long, S.B., Tao, X., Campbell, E.B., & MacKinnon, R. 2007. Atomic structure of a voltage-dependent K⁺ channel in a lipid membrane-like environment. *Nature*, 450, (7168) 376-382
- Loots, E. & Isacoff, E.Y. 1998. Protein rearrangements underlying slow inactivation of the shaker K⁺ channel. *The Journal of General Physiology*, 112, (4) 377-389
- Lotan, R. & Nicholson, G. 1981. *Advanced Cell Biology* New York.
- Lu, Z., Klem, A.M., & Ramu, Y. 2002. Coupling between voltage sensors and activation gate in voltage-gated K⁺ channels. *The Journal of General Physiology*, 120, (5) 663-676
- Ludlum, D.B. 1956. Micelle formation in solutions of some isomeric detergents. *Journal of Physical Chemistry*, 60, (9) 1240-1244
- Lux, B. & Gerard, D. 1981. Reappraisal of the binding processes of N-(3-pyrene)maleimide as a fluorescent probe of proteins. *Journal of Biological Chemistry*, 256, (4) 1767-1771
- Luzhkov, V.B., Nilsson, J., Arhem, P., & Aqvist, J. 2003. Computational modelling of the open-state Kv1.5 ion channel block by bupivacaine. *Biochimica et Biophysica Acta (BBA) - Proteins & Proteomics*, 1652, (1) 35-51
- MacKinnon, R. 2003. Potassium channels. *FEBS Letters*, 555, (1) 62-65

- MacKinnon, R., Cohen, S.L., Kuo, A., Lee, A., & Chait, B.T. 1998. Structural conservation in prokaryotic and eukaryotic potassium channels. *Science*, 280, (5360) 106-109
- Magidovich, E. & Yifrach, O. 2004. Conserved gating hinge in ligand and voltage-dependent K⁺ channels. *Biochemistry*, 43, (42) 13242-13247
- Magleby, K.L. 2003. Gating Mechanism of BK (Slo1) Channels. *The Journal of General Physiology*, 121, (2) 81-96
- Mangle, E.A. & Topp, M.R. 1986. Excited-state dynamics of jet-cooled pyrene and some molecular complexes. *The Journal of Physical Chemistry*, 90, (5) 802-807
- Marassi F.F.S. 2010. Hydration-optimized oriented phospholipid bilayer samples for solid-state NMR structural studies of membrane proteins. *J Magn. Res.* 161, (1) 64-9
- Marius, P., Alvis, S.J., East, J.M., & Lee, A.G. 2005. The interfacial lipid binding site on the potassium channel KcsA is specific for anionic phospholipids. *Biophysical Journal*, 89, (6) 4081-4089
- Marsh, D., Watts, A., Pates, R.D., Uhl, R., Knowles, P.F., & Esmann, M. 1982. ESR spin-label studies of lipid-protein interactions in membranes. *Biophysical Journal*, 37, (1) 265-274
- Marsh, D. 2001. Polarity and permeation profiles in lipid membranes. *Proceedings of the National Academy of Sciences* 98, (14) 7777-7782
- Maurer-Stroh, S. & Eisenhaber, F. 2005. Refinement and prediction of protein prenylation motifs. *Genome Biology*, 6, (6) R55
- Maylie, J., Bond, C.T., Herson, P.S., Lee, W.S., & Adelman, J.P. 2004. Small conductance Ca²⁺-activated K⁺ channels and calmodulin. *The Journal of Physiology*, 554, (2) 255-261
- Mazeres, S., Schram, V., Tocanne, J.F., & Lopez, A. 1996. 7-nitrobenz-2-oxa-1,3-diazole-4-yl-labeled phospholipids in lipid membranes: differences in fluorescence behavior. *Biophysical Journal*, 71, (1) 327-335
- Merrill, A.H. 2002. De Novo Sphingolipid Biosynthesis: a necessary, but dangerous, pathway. *Journal of Biological Chemistry*, 277, (29) 25843-25846
- Miller, C. 2003. A charged view of voltage-gated ion channels. *Nature Structural and Molecular Biology*, 10, (6) 422-424
- Miloshevsky, G.V. & Jordan, P.C. 2007. Open-state conformation of the KcsA K⁺ channel: monte carlo normal mode following simulations. *Structure*, 15, (12) 1654-1662

- Minones, J., Sandez Macho, M., Iribarnegaray, E., & Sanz Pedrero, P. 1981. Phospholipid monolayers. *Colloid & Polymer Science*, 259, (3) 382-390
- Morais-Cabral, J.H., Zhou, Y., & MacKinnon, R. 2001. Energetic optimization of ion conduction rate by the K⁺ selectivity filter. *Nature*, 414, (6859) 37-42
- Mulkidjanian, A.Y., Galperin, M.Y., & Koonin, E.V. 2009. Co-evolution of primordial membranes and membrane proteins. *Trends in Biochemical Sciences*, 34, (4) 206-215
- Muller, D.J., Wu, N., & Palczewski, K. 2008. Vertebrate membrane proteins: structure, function, and insights from biophysical approaches. *Pharmacological Reviews*, 60, (1) 43-78
- Murzin, A.G., Lesk, A.M., & Chothia, C. 1994. Principles determining the structure of β sheet barrels in proteins I. A theoretical analysis. *Journal of Molecular Biology*, 236, (5) 1369-1381
- Neale, E.J., Elliott, D.J.S., Hunter, M., & Sivaprasadarao, A. 2003. Evidence for intersubunit interactions between S4 and S5 transmembrane segments of the shaker potassium channel. *Journal of Biological Chemistry*, 278, (31) 29079-29085
- Neale, E.J., Rong, H., Cockcroft, C.J., & Sivaprasadarao, A. 2007. Mapping the membrane-aqueous border for the voltage-sensing domain of a potassium channel. *Journal of Biological Chemistry*, 282, (52) 37597-37604
- Nelson R.D., Kuan G., Saier M.H., & Montal M. 1999. Modular assembly of voltage-gated channel proteins: a sequence analysis and phylogenetic study. *Journal of Molecular Microbiology and Biotechnology*, 1, 281
- Nichols and, C.G. & Lopatin, A.N. 1997. Inward rectifier potassium channels. *Annual Review of Physiology*, 59, (1) 171-191
- Nichols, C.G. & Lederer, W.J. 1991. Adenosine triphosphate-sensitive potassium channels in the cardiovascular system. *AJP - Heart and Circulatory Physiology*, 261, (6) H1675-H1686
- Nilsson, J., Madeja, M., & Arhem, P. 2003. Local anesthetic block of Kv channels: role of the s6 helix and the S5-S6 linker for bupivacaine action. *Molecular Pharmacology*, 63, (6) 1417-1429
- O'Connor, S., Li, E., Majors, B.S., He, L., Placone, J., Baycin, D., Betenbaugh, M.J., & Hristova, K. 2009. Increased expression of the integral membrane protein ErbB2 in Chinese hamster ovary cells expressing the anti-apoptotic gene Bcl-xL. *Protein Expression and Purification*, 67, (1) 41-47
- O'Leary, T. 2010. Lateral diffusion of lipids in complex biological membranes. *Proceedings of the National Academy of Sciences*, 84, (15) 5231-5235

- Olcese, R., Latorre, R.N., Toro, L., Bezanilla, F., & Stefani, E. 1997. Correlation between charge movement and ionic current during slow inactivation in shaker K⁺ channels. *The Journal of General Physiology*, 110, (5) 579-589
- Parsegian, V.A. 1976. Ion-membrane interactions as structural forces. *Carriers and Channels in Biological Systems*, 264, 161-174
- Pata, V., Ahmed, F., Discher, D.E., & Dan, N. 2004. Membrane solubilization by detergent: resistance conferred by thickness. *Langmuir*, 20, (10) 3888-3893
- Patel, A.B., Khumsupan, P., & Narayanaswami, V. 2010. Pyrene fluorescence analysis offers new insights into the conformation of the lipoprotein-binding domain of human apolipoprotein E. *Biochemistry*, 49, (8) 1766-1775
- Perozo, E., Marien, D., Cortes, & Cuello, L.G. 1999. Structural rearrangements underlying K⁺-channel activation gating. *Science*, 285, (5424) 73-78
- Petersen, F.N.R., Jensen, M.O., & Nielsen, C.H. 2005. Interfacial tryptophan residues: a role for the cation- π effect? *Biophysical Journal*, 89, (6) 3985-3996
- Posson, D.J., Ge, P., Miller, C., Bezanilla, F., & Selvin, P.R. 2005. Small vertical movement of a K⁺ channel voltage sensor measured with luminescence energy transfer. *Nature*, 436, (7052) 848-851
- Powl, A.M., Wright, J.N., East, J.M., & Lee, A.G. 2005. Identification of the hydrophobic thickness of a membrane protein using fluorescence spectroscopy: studies with the mechanosensitive channel MscL. *Biochemistry*, 44, (15) 5713-5721
- Raja, M. 2010. The role of phosphatidic acid and cardiolipin in stability of the tetrameric assembly of potassium channel KcsA. *Journal of Membrane Biology*, 234, (3) 235-240
- Rigaud, J.L., Pitard, B., & Levy, D. 1995. Reconstitution of membrane proteins into liposomes: application to energy-transducing membrane proteins. *Biochimica et Biophysica Acta (BBA) - Bioenergetics*, 1231, (3) 223-246
- Roseman, M.A. 1988. Hydrophobicity of the peptide C=O...H-N hydrogen-bonded group. *Journal of Molecular Biology*, 201, (3) 621-623
- Roux, B. & MacKinnon, R. 1999. The cavity and pore helices in the KcsA K⁺ channel: electrostatic stabilization of monovalent cations. *Science*, 285, (5424) 100-102
- Ruta, V., Chen, J., & MacKinnon, R. 2005. Calibrated measurement of gating-charge arginine displacement in the KvAP voltage-dependent K⁺ channel. *Cell*, 123, (3) 463-475
- Ruta, V. & MacKinnon, R. 2004. Localization of the voltage-sensor toxin receptor on KvAP. *Biochemistry*, 43, (31) 10071-10079

- Sahoo, D., Narayanaswami, V., Kay, C.M., & Ryan, R.O. 2000. Pyrene excimer fluorescence: a spatially sensitive probe to monitor lipid-induced helical rearrangement of apolipophorin III. *Biochemistry*, 39, (22) 6594-6601
- Schoppa, N.E., McCormack, K., Tanouye, M.A., & Sigworth, F.J. 1992. The size of gating charge in wild-type and mutant Shaker potassium channels. *Science*, 255, (5052) 1712-1715
- Schumacher, M.A., Rivard, A.F., Bachinger, H.P., & Adelman, J.P. 2001. Structure of the gating domain of a Ca^{2+} -activated K^+ channel complexed with Ca^{2+} /calmodulin. *Nature*, 410, (6832) 1120-1124
- Sengupta, D., Behera, R.N., Smith, J.C., & Ullmann, G.M. 2005. The alpha helix dipole: screened out? *Structure*, 13, (6) 849-855
- Seoh, S.A., Sigg, D., Papazian, D.M., & Bezanilla, F. 1996. Voltage-sensing residues in the S2 and S4 segments of the Shaker K^+ channel. *Neuron*, 16, (6) 1159-1167
- Shipston, M.J. 2001. Alternative splicing of potassium channels: a dynamic switch of cellular excitability. *Trends in Cell Biology*, 11, (9) 353-358
- Shrivastava, I.H., Peter Tieleman, D., Biggin, P.C., & Sansom, M.S.P. 2002. K^+ versus Na^+ ions in a K^+ channel selectivity filter: A simulation study. *Biophysical Journal*, 83, (2) 633-645
- Simmonds, A.C., East, J.M., Jones, O.T., Rooney, E.K., McWhirter, J., & Lee, A.G. 1982. Annular and non-annular binding sites on the $\text{Ca}^{2+}/\text{Mg}^{2+}$ ATPase. *Biochimica et Biophysica Acta (BBA) - Biomembranes*, 693, (2) 398-406
- Singer, S.J. & Nicolson, G.L. 1972. The fluid mosaic model of the structure of cell membranes. *Science*, 175, (4023) 720-731
- Soler-Llavina, G.J., Chang, T.H., & Swartz, K.J. 2006. Functional interactions at the interface between voltage-sensing and pore domains in the shaker Kv channel. *Neuron*, 52, (4) 623-634
- Sonoda, Y., Newstead, S., Hu, N.J., Alguel, Y., Nji, E., Beis, K., Yashiro, S., Lee, C., Leung, J., Cameron, A.D., Byrne, B., Iwata, S., Drew, D. 2011. Benchmarking membrane protein detergent stability for improving throughput of high-resolution X-ray structures. *Structure*, 19, (1) 17-25
- Stackman, R.W., Hammond, R.S., Linardatos, E., Gerlach, A., Maylie, J., Adelman, J.P., & Tzounopoulos, T. 2002. Small conductance Ca^{2+} -activated K^+ channels modulate synaptic plasticity and memory encoding. *Journal of Neuroscience*, 22, (23) 10163-10171

- Starace, D.M. & Bezanilla, F. 2001. Histidine scanning mutagenesis of basic residues of the s4 segment of the shaker K⁺ channel. *The Journal of General Physiology*, 117, (5) 469-490
- Starace, D.M., Stefani, E., & Bezanilla, F. 1997. Voltage-dependent proton transport by the voltage sensor of the shaker K⁺ channel. *Neuron*, 19, (6) 1319-1327
- Stumpe, S., Schlusser, A., Schleyer, M., & Bakker, E. P. 1996, "K⁺ circulation across the prokaryotic cell membrane: K⁺ uptake systems," *In Handbook of Biological Physics*
- Transport processes in eukaryotic and prokaryotic organisms*, Volume 2 ed. W. N. Konings, ed., North-Holland, pp. 473-499.
- Swartz, K.J. 2004. Opening the gate in potassium channels. *Nature Structural and Molecular Biology*, 11, (6) 499-501
- Swartz, K.J. & MacKinnon, R. 1997a. Hanatoxin modifies the gating of a voltage-dependent K⁺ channel through multiple binding sites. *Neuron*, 18, (4) 665-673
- Swartz, K.J. & MacKinnon, R. 1997b. Mapping the receptor site for hanatoxin, a gating modifier of voltage-dependent K⁺ channels. *Neuron*, 18, (4) 675-682
- Tanford, C.H. 1980. *The Hydrophobic Effect: Formation of Micelles and Biological Membranes* New York, Wiley.
- Tao, X., Lee, A., Limapichat, W., Dougherty, D.A., & MacKinnon, R. 2010. A gating charge transfer center in voltage sensors. *Science*, 328, (5974) 67-73
- Tombola, F., Pathak, M.M., & Isacoff, E.Y. 2006. How does voltage open an ion channel? *Annual Review of Cell and Developmental Biology*, 22, (1) 23-52
- Ungar, D., Bart, A., Haase, W., Kaunzinger, A., Lewitzki, E., Ruiz, T., Reiländer, H., & Michel, H. 2001. Analysis of a putative voltage-gated prokaryotic potassium channel. *European Journal of Biochemistry*, 268, (20) 5386-5396
- Uysal, S., Vasquez, V., Tereshko, V., Esaki, K., Fellouse, F.A., Sidhu, S.S., Koide, S., Perozo, E., & Kossiakoff, A. 2009. Crystal structure of full-length KcsA in its closed conformation. *Proceedings of the National Academy of Sciences*, 106, (16) 6644-6649
- Valiyaveetil, F.I., Zhou, Y., & MacKinnon, R. 2002. Lipids in the structure, folding, and function of the KcsA K⁺ channel. *Biochemistry*, 41, (35) 10771-10777
- Van Voorst, F. & De Kruijff, B. 2000. Role of lipids in the translocation of proteins across membranes. *Biochemical Journal*, 347, (3) 601-612
- Vance, D.E. & Vance, J.E. 2002. *Biochemistry of Lipids, Lipoproteins and Membranes*, 4th Edition, 4 ed.

- Victor, K.G. and. Cafis, D.S. 2001. Location and Dynamics of Basic Peptides at the Membrane Interface: Electron Paramagnetic Resonance Spectroscopy of TetramethylPiperidine-N-Oxyl-4-Amino-4-Carboxylic Acid-Labeled Peptides. *Biophysical Journal*, 81, 2241-2250
- von Heijne, G. 1996. Principles of membrane protein assembly and structure. *Progress in Biophysics and Molecular Biology*, 66, (2) 113-139
- Watts, A., Davoust, J., Marsh, D., & Devaux, P.F. 1981. Distinct states of lipid mobility in bovine rod outer segment membranes Resolution of spin label results. *Biochimica et Biophysica Acta (BBA) - Biomembranes*, 643, (3) 673-676
- Webster, S.M., del Camino, D., Dekker, J.P., & Yellen, G. 2004. Intracellular gate opening in Shaker K⁺ channels defined by high-affinity metal bridges. *Nature*, 428, (6985) 864-868
- Weltman, J.K., Szaro, R.P., Frackelton, A.R., Dowben, R.M., Bunting, J.R., & Cathou, R.E. 1973. N-(3-Pyrene)maleimide: a long lifetime fluorescent sulfhydryl reagent. *Journal of Biological Chemistry*, 248, (9) 3173-3177
- White, S.H. & Wimley, W.C. 2003. Membrane protein folding and stability: physical principles. *Annual Review of Biophysics and Biomolecular Structure*, 28, (1) 319-365
- Wimley, W.C. 2003. The versatile beta-barrel membrane protein. *Current Opinion in Structural Biology*, 13, (4) 404-411
- Wohland, T., Friedrich, K., Hovius, R., & Vogel, H. 1999. Study of ligand-receptor interactions by fluorescence correlation spectroscopy with different fluorophores: evidence that the homopentameric 5-hydroxytryptamine type 3As receptor binds only one ligand. *Biochemistry*, 38, (27) 8671-8681
- Xia, X.M., Fakler, B., Rivard, A., Wayman, G., Johnson-Pais, T., Keen, J.E., Ishii, T., Hirschberg, B., Bond, C.T., Lutsenko, S., Maylie, J., & Adelman, J.P. 1998. Mechanism of calcium gating in small-conductance calcium-activated potassium channels. *Nature*, 395, (6701) 503-507
- Yau, W.M., Wimley, W.C., Gawrisch, K., & White, S.H. 1998. The preference of tryptophan for membrane interfaces. *Biochemistry*, 37, (42) 14713-14718
- Yuen, C.T.K., Davidson, A.R., & Deber, C.M. 2000. Role of aromatic residues at the lipid-water interface in micelle-bound bacteriophage M13 major coat protein. *Biochemistry*, 39, (51) 16155-16162
- Zadek, B., and Nimigean, C.M. 2000. Calcium dependent gating of MthK, a prokaryotic potassium channel. *The Journal of General Physiology*, 127, (6) 73-85.

Zhou, Y., Morais-Cabral, J.H., Kaufman, A., & MacKinnon, R. 2001. Chemistry of ion coordination and hydration revealed by a K⁺ channel-Fab complex at 2.0 Angstrom resolution. *Nature*, 414, (6859) 43-48